UNIVERSITÀ
DEGLI STUDI
DI PADOVA

Head Office: Università degli Studi di Padova

Department of Geosciences

Ph.D. COURSE IN: EARTH SCIENCES

XXX SERIES

DETERIORATION OF CARBONATE ROCKS AND VULNERABILITY OF CULTURAL HERITAGE IN A CHANGING CLIMATE

Coordinator: Prof. Fabrizio Nestola

Supervisor: Prof. Claudio Mazzoli

Co-Supervisor: Prof. Matteo Massironi

Ph.D. student : Silvia Salvini

To Laura,

gone too soon,

never forgotten

Part 3

Deterioration of headstones from the CWGC cemeteries in the Mediterranean area …….. 61

Part 4

Accelerated ageing test of carbonate rocks and their assessment of their recession rates…….. 89

Introduction

The definition of cultural heritage is wide and it includes tangible artifacts (monuments, works of art, buildings, books, artifacts, …) and intangible culture (traditions, folklore, languages…) as well as natural heritage (significant landscape, biodiversity, …). The conservation of cultural heritage is our connection with the past and a moral duty for future generations. The conclusive remarks of the Bruntland Report (1987) stated the birth of the concept of sustainable development[1] and now it is assessed that maintenance planning is the most sustainable conservation strategy for our cultural heritage.

Nowadays, our cultural heritage is endangered because it is made of materials more or less prone to decay. Rock is a more durable building material than wood and mud, so it has been used in anthropic structures since Palaeolithic age. Rock used by man as building material is called (ornamental or dimension) stone.

Stones are subjected to deterioration due to exposure to pollution (emissions from industrial plants, air, vehicular and marine traffic, …), natural environment (rain, wind, frost, …), tourism, etc.

In Italy, stone conservation is a relevant problem because the number of historical cities and towns and of archaeological remains over the entire national territory is extremely high. In the last decades many academic debates have been carried on about the most suitable and sustainable preservation practices necessary in order to maintain this huge amount of monuments and historical centers. In order to develop good conservation and maintenance plans we need to increase our knowledge about the decay of materials and realise reliable projections of future deterioration.

Generally speaking, the historical buildings were built using the rock types locally available and easily workable, consequently the percentage of carbonate rocks (limestones, marbles) among the stone used in the cultural heritage is very high. The rate of carbonate rocks used in built heritage is about 90%[2].

Carbonate rocks were – and still are – preferred because of their aesthetic features, availability and workability, even if their chemical composition makes them more subjected to the environmental impact and prone to decay with respect to the silicate rocks.

In geomorphology studies, degradation phenomena of rocks can be described in terms of change in their surface topography, material loss or surface recession.

Different equations have been drafted over time for describing surface recession but the one by Lipfert (1989) is the most commonly used. This relation considers only a few key factors of decay and refers only to a specific period of time (i.e., year).[3]

$$Loss/m_{rain} = 18.8 + 0.016\,[H^+] + 0{,}18\,(Vd_S * [SO_2] + Vd_N * [HNO_3])/R$$

[1] From Brundtland Report (1987) "Sustainable development is development that meets the needs of the present without compromising the ability of future generations to meet their own needs"

[2] In Italy the use of silicate rocks is less diffuse than in other countries (e.g. Germany, Spain) but there are notable exceptions, such as the sandstones used in the cathedral of Piacenza and the Serena Stone in Florence (Rodolico 1963).

[3] Some authors also tried to apply this equation to predict future limestone recession over long periods of time (Brimblecombe & Grossi, 2009; Sabbioni *et al.*, 2010).

where H^+ is the hydrogen ion concentration, Vd_S and Vd_N are the deposition rates of SO_2 and HNO_3, respectively, $[SO_2]$ and $[HNO_3]$ are SO_2 and HNO_3 concentrations in the atmosphere, and R is the annual precipitation (the $Vd_N*[HNO_3]$ term is often omitted).

The equation reported above completely disregards other environmental factors such as temperature and relative humidity which also have an important effect on deterioration, and textural features of the stone such as grain size and porosity.
The main aim of this study was to understand the effect of petrographic and textural features on the deterioration of carbonate rocks under different environmental conditions. Results have been used to quantify the effect of such stone intrinsic properties on surface recession.
To this aim, research has been organized in three main steps:

1. Selection of a set of carbonate rocks differing for their mineralogy and texture, and detailed characterization of their petrographic and textural features (*Part 1 and 2);*
2. Field survey for the measurement of total stone recession in headstones from different Commonwealth War Graves Commission (a.k.a. CWGC) cemeteries
3. Accelerated ageing tests under monitored environmental conditions on all the selected rocks in order to evaluate the effect of petrographic and textural features on recession rate *(Part 4);*

Regarding the selection of materials, eleven carbonate rock types have been considered among those most frequently used in the built heritage of north-eastern Italy, including the Commonwealth War Graves Commission cemeteries: Vicenza Stone (Nanto and Costozza varieties), Istria Stone, Chiampo Stone (Porfirico and Ondagata varieties), Red and Brown Verona Stone, Pink and White Asiago Stone, Aurisina Stone, Botticino Stone. In addition, Carrara marble has also been selected. This was an important point, considering that most of the previous studies on the recession rate of carbonate rocks were mainly based on measurements performed on marbles, and often on Carrara marble (Meierding 1981, Reddy & Roberts 2005).
The first issue was therefore to characterize all these rock types from a petrographic and textural point of view, using several routine laboratory analytical approaches. More specifically, the following techniques were performed and they allowed defining the texture, mineralogy, chemistry and porosity of the selected rock types: optical microscopy (OM), scanning electron microscopy (SEM), X-ray fluorescence (XRF), X-ray powder diffraction (XRPD), computerized micro-tomography (μ-CT), electron backscattered diffraction (ESBD), densitometry, mercury intrusion porosimetry (MIP). Porosity of the different stones has been determined by comparing results obtained from MIP, m-CT, DIA of BSE images and scanned images of stained thin sections following the method suggested by Grove & Jerram (2011) using ImageJ software package. Average grain size and distribution were determined in thin section separately on domains characterized by different grain size (e.g. micrite, fine-grained sparite, sparite cement, bioclasts) using an optical microscope Zeiss® Axio Scope.A1 coupled with an Axio CamMRC5 linked to a dedicated PC software, and by ESBD.
Regarding the field survey, a number of CWGC cemeteries located in Italy and in Greece were selected in order to represent a wide range of climatic and environmental conditions. Over 3000 measurements of recession were performed on headstones made of different carbonate rocks. In some cases, the possible application of the Structure from Motion (SfM) μ-photogrammetry was evaluated in order to realize a 3D reconstruction of the full headstone. This topic has been presented in a *Technical Note*. The recession rates measured on the headstones were then analysed considering whether stone recession is significantly correlated to lithology, orientation with respect to

geographical coordinates, which influences the exposition to sunlight, climate conditions, and time of exposition, or a combination of these parameters (see *Part 3*). Environmental parameters from the considered localities were collected from the surface climate observing reference networks (mainly ARPA and Hellenic National Meteorological Service) each time selecting data from the nearest measuring station.

Accelerated aging tests have been performed on sets of 22 samples in an environment test chamber Suntest CPS+ (Department of Chemistry, University of Padua) using artificial solutions with composition corresponding to those wetting the cities of Bologna and Stresa (Italy). This consisted of weight measurements using an analytical scale (sensibility 0.0001 g), three-dimensional surface description using a Olympus Lext OLS4000 3D measuring laser microscope (Department of Geosciences, University of Padova) (Figure 1) and a SfM μ-photogrammetry set-up. Surface data were processed using Matlab and ArcMap, in order to model 3-D surface and quantify recession (see *Part 4 and Technical Note*).

Aging experiments showed that grain size is the main textural parameter controlling the surface recession rate in carbonate rocks with negligible amounts of clay minerals. A new equation for evaluating the recession rate has been therefore formulated accordingly, and compared with those from the literature using recession measurements from the CWGC cemeteries.

Such an equation may potentially be used to obtain more reliable projections of stone deterioration for different types of carbonate rocks and update the information contained in the *Atlas of Climate Change* (Sabbioni *et al.* 2010) based on the different IPCC future scenarios of climate change (Fick & Hijimans 2017), thus providing better tools to stakeholders involved in designing maintenance and conservation plans.

Part 1: A petrographic characterization of the carbonate rocks used for the monumental built heritage of north-eastern Italy.

Part 2: Combined multi-analytical approach to the characterization of the pore system in different carbonate rocks.

Part 3: Deterioration of headstones from the CWGC cemeteries in the Mediterranean area

Part 4: Accelerated aging tests on carbonate rocks and assessment of their recession rate.

Technical Note: Photogrammetry as a tool for evaluating stone decay.

Part 1: A petrographic characterization of the carbonate rocks used for the monumental built heritage in northeastern Italy

ABSTRACT

This paper presents the petrographic characterization of some ornamental limestones widely used in the built heritage of northeastern Italy.
Quarry samples of selected materials were studied through Optical Microscopy (OM), Scanning Electron Microscope (SEM), Computerized X-Ray micro-tomography (μ-CT), Electron Backscattered Diffraction (ESBD), X-ray Fluorescence (XRF), X-ray Powder Diffraction (XRPD), and Mercury Intrusion Porosimetry (MIP).
The carbonate building materials considered in this work are the Vicenza Stone, the Carrara Marble, the Verona Stone, the Asiago Stone, the Istria-Orsera Stone, the Aurisina Stone, the Chiampo Stone, and the Botticino Stone, all commonly present in the built environment, especially in the Veneto region. Petrographic and textural features of carbonate rocks strongly influence deterioration rate; the knowledge of these features is therefore essential in the understanding of the deterioration mechanisms and ultimately in the prediction of decay as a function of environmental parameters.

Keywords
Carbonate rocks, petrographic characterization, Veneto region, northeastern Italy, built heritage, grain-size, building materials

1. Introduction

Natural dimension stones are an important resource of raw building material. Restoration and conservation practices often employ dimension stones that are aesthetically similar to the original stones. For doing this good knowledge on stone resources and their characteristics (mineralogy, petrography, historical use, exploitation techniques) is required.
Since the Roman Age, carbonate rocks have been the most diffused dimension stones in the built environment due to their wide availability and ease of work. Starting from the 19th century, the development of motorized technologies for stone processing, granitoid and other silicate rocks, less subjected to weathering than carbonate rocks, conquered an increasing market share.
Transportation costs have always discouraged the commercialization of dimension stones over long distances so that often specific rock types characterize certain cities or specific cultural landscapes (Siegesmund & Snethlage 2014) such as Carrara marble in northern Tuscany, Lecce stone in Salento, Globigerina stone in Malta, a combination of bricks and Verona stones in the Po Valley, etc. (Fig. 1). This represents an important aspect of our cultural heritage that should be safeguarded from excessive contaminations with imported stones, making deterioration issues of local dimension and ornamental stones even more critical. Nowadays, the use of locally available limestones for cladding on modern buildings is growing as designers are considering these materials as part of the local cultural identity and a link between the present and the past.
In the Veneto region, as well as in the whole southern Europe, stones have been widely employed as building and ornamental materials for historical and modern constructions, such as church embellishment, and urban decor (monuments, paving, fountains, façade coverings, etc.).
In this region various stones with suitable characteristics, especially carbonate rocks, crop out and have been quarried in the piedmont belt since antiquity.

In a broader study that aims at carrying out a detailed analysis of the factors influencing deterioration in limestone, a precise identification and characterization of the considered stones through chemical, mineralogical, petrographic and textural analyses is necessary.

Figure 1. *Views of old towns and historical monuments made with locally available stone building materials. From left to right: inside of the Carrara cathedral, totally covered with Carrara marble; street view of Lecce with buildings made of Lecce stone; view of a porch in Florence with columns and details made of Pietra Serena sandstone; town street in Malta with houses and urban paving made of local Globigerina limestone; view of the roofs of Genoa, covered with slate.*

2. The stone materials

The studied lithologies have been chosen among the limestones commonly used in the built heritage of northeastern Italy (Fig. 2). Despite some of them have ambiguous commercial names, they all are sedimentary rocks with the exception of Carrara Marble which is metamorphic.

They differ in textural characteristics such as porosity and grain size, as well as in the content of minor constituents, which may also have a relevant effect on deterioration.

2.1. Vicenza Stone

Vicenza Stone (or soft stone of Vicenza) is a general name of various biocalcarenitic rocks quarried in the Berici Hills, extending for about 20 km south of Vicenza, characterized by light colors with ivory, light grey, straw yellow, warm light brown hues.

This “soft stone” of Berici Hills characterizes the middle Eocene geological formation of “Calcari Nummulitici” and the Oligocene “Calcareniti of Castelgomberto” (Cattaneo et al. 1976, Benchiarin 2007, Cappellaro et al. 2012). They derive their popular local name from their soft texture, which makes them easy to cut and carve, favored by the high porosity and the water content when freshly extracted. Macropores are abundant and the content in large bioclasts is high. The typical weathering forms consist in dissolution and pulverization, accompanied by an often important biological activity; humidity marks and black crusts are often present. Due to its high specific surface determined by

porosity and the presence of thin clay-rich layers containing swelling micas such as montmorillonite, Vicenza stone is liable to deteriorate. For this reason, it has been object of various studies (Marchesini *et al.* 1972, Cattaneo *et al.* 1976, Fassina & Cherido 1985, Ginevra *et al.* 1999, Dalla Libera 2006, Benchiarin 2007, Benchiarin *et al.* 2012, Di Benedetto *et al.* 2012).
In the present research, the Nanto and the Costozza varieties have been considered.

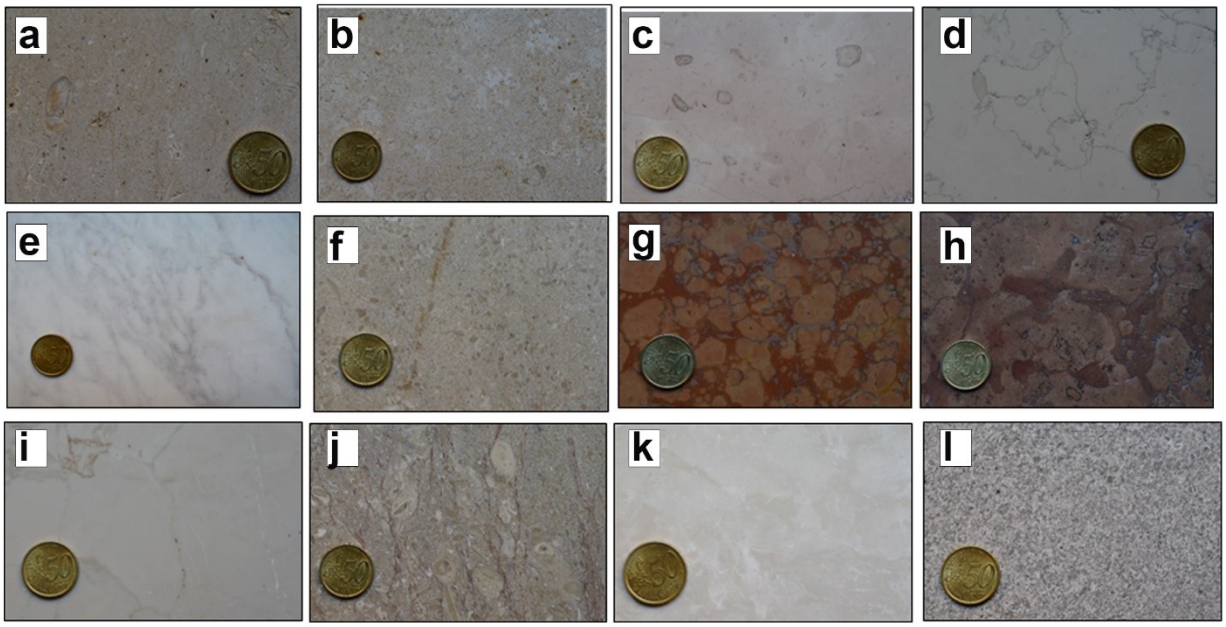

Figure 2. *Photographs of the analyzed rocks, the commercial names of which follow: Nanto stone (a), Vicenza stone (b), Pink Asiago stone (c), White Asiago stone (d), Carrara marble (e), Chiampo Paglierino stone (f), Red Verona stone (g), Brown Verona marble (h), Istrian (Orsera) stone (i), Chiampo Ondagata stone (j), Botticino marble (k), Aurisina stone (l)*

Nanto stone is quarried near Nanto from the layers placed at the bottom of the Calcari Nummulitici Formation (Massari et al. 1976, Benchiarin 2007) and it is also known with the commercial name of "Giallo Dorato" (i.e. Golden Yellow) due to its warm yellowish-brown hue. The texture is characterized by isoriented macrofossils in a golden sand matrix. This limestone is suitable both for internal and external claddings, internal floors and staircases, and every other building component. Thanks to its fire-resistance, it has been traditionally used in fireplaces (Rodolico 1953).
Costozza Stone is the traditional light ivory variety of White Vicenza Stone. It is the result of the sedimentation of innumerable minute fossils, which create its thin and flowery texture; in particular this texture is related to the presence of fossil algae. It is quarried from the stratigraphically higher layers of the Calcareniti di Castelgomberto Formation, which includes back-reef tidal channel deposits of Oligocene age.
White Vicenza stone was largely used in historical masonry and in statuary, as admirably testified by the Olympic Theatre, the Palladian Villas and the Logge of the Palazzo della Ragione in Vicenza, the 78 statues located in Prato della Valle Square in Padua (Braga 2004, Cornale & Rosanò 1994) (Fig. 3). This stone was used in the Mysterious Baths by De Chirico in Milan, and in numerous 20th century buildings, both for internal and external cladding, internal floors and staircases, and other building components.

Figure 3. *Vicenza Stone in the cultural heritage. From top to bottom, from left to right: Loggia Cornaro in Padua (Nanto variety), Church of Saint Lawrence in Vicenza (Nanto variety), Olympic Theatre in Vicenza (Costozza variety), Barbaran da Porto Palace in Vicenza (ground floor in Nanto variety, first floor in Costozza variety), statue at Villa Valmarana ai Nani in Vicenza (Costozza variety), original sculpture decorating the façade of Saint George's oratory, now in the cloister of the Basilica in Padua (Nanto variety), Palazzo della Ragione in Vicenza (Costozza variety), sculptures in Prato della Valle square (Costozza variety).*

2.2.Istria Stone

Istria Stone (in Italian "pietra d'Istria") includes a group of carbonate building stones deposited during the Upper Jurassic (Tithonian) in a shallow platform environment pertaining to the Friuli Platform Domain that crops out in the Croatian Istria peninsula, between Portorož and Pula (Cucchi et al. 1987; Borghi et al. 2015) (Fig. 4). Since the Roman Age these stones have been largely used in the Venetian and Dalmatian architecture (Fig. 5).

This study considered the Orsera (Montraker) variety, a.k.a. Kirmenjak limestone. This stone has a salt white – pale grey color, with compressive strength and density approaching those of marble (Geometrante et al.).

The first documented exploitation of this quarry dates back to the year 568 AD, when the edification of Venice began. In 1307, the Venetian Senate decided that Istria Stone should be the only building material used in Venetian buildings as well as in all the Venetian possessions in southern Italy and Greece. It has been calculated that about 80% of stone employed in Venice buildings derived from Istria region (Dunda & Kujundžić 2004).

Technical features of this stone (table 1), such as high durability, extremely low water content and absorption, high compressive strength, and resistance to Venetian aggressive saline environment, with frequent tidal flooding and subsequent drying, made this stone the ideal building material to be located between the wooden poles of the foundation and the bricks of the walls. In Venice this stone

is used as an efficient barrier against damp raising, by orienting stylolitic layers horizontally. In this way, capillary water paths are interrupted, creating a multilayer humidity barrier (Šimunić Buršić *et al.* 2007; Lazzarini 2012).

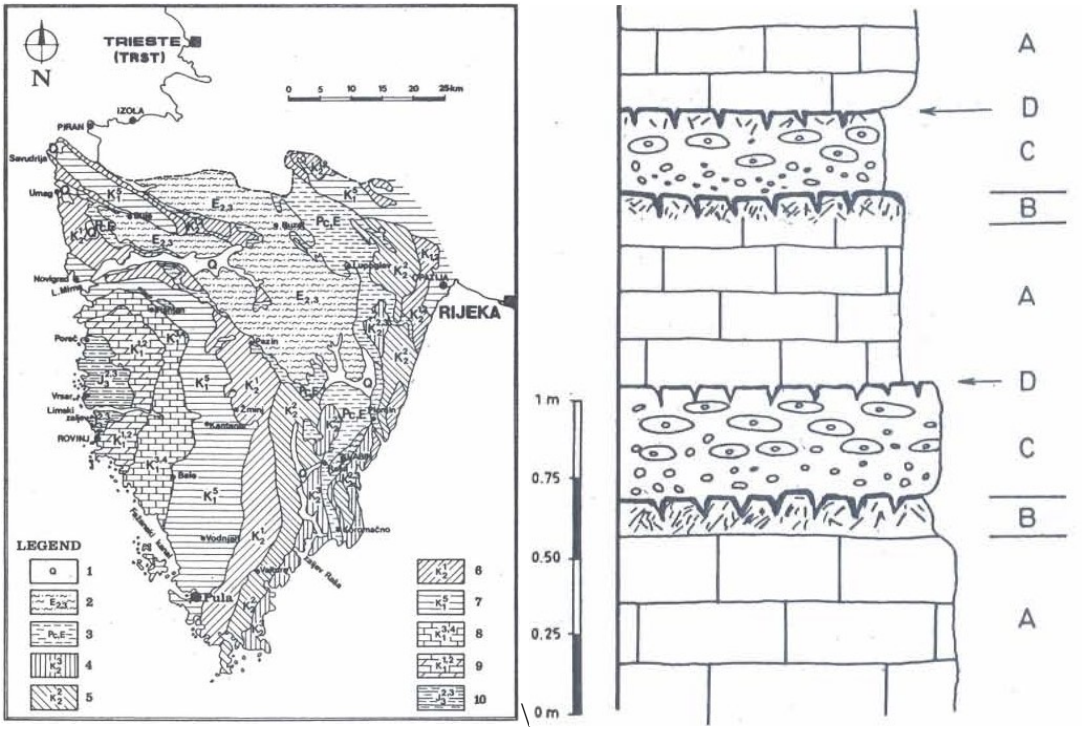

Figure 4. *Left: geological map of Istria, Upper Jurassic formation enhanced. Right: stratigraphic succession of the Kirmenjak quarry, the Orsera stone is quarried from layers A, which are subtidal-lagunal deposits characterized by stylolitic micrite. (after Crnković & Jovičic 2004)*

The coupling of Istria Stone with brick structures is reported also in other areas of the Veneto region but in Verona and Vicenza other limestones prevail. However, some monuments in Venice are all covered with Istria stone like the Rialto Bridge, Ducal Palace, Bridge of Sighs, Santa Lucia train station.

On the one hand, like other compact limestones, Istrian Stone is difficult to carve (even more than marble) because it tends to splinter easily and to present conchoidal fracture, especially when it is worked parallel to the joints. On the other hand, this stone is easily polished (Lazzarini 2012).

Table 1. *Mechanical and physical properties of Orsera, Kirmenjak dimension stone (from Pivko, 2003)*

Compressive strength dry samples, MPa	138.5
Compressive strength water-saturated samples, MPa	113.5
Compressive strength after 25 freeze – thaw cycles, MPa	103.0
Resistance to grinding (Boeheme method), $cm^3/50\ cm^2$	16.1
Density, kg/m^3	2700
Bulk Density, kg/m^3	2677
Porosity, %	0.85
Water absorption at P_{atm}, %	0.77

Orsera limestone was used also in Dubrovnik (Croatia) together with the variety quarried in Vrnik, for the Basilica Euprasiana in Poreč (Croatia), for the traditional "kažun" in the Istrian peninsula, for

the Mausoleum of Theodoric in Ravenna, the Roman Bridge in Rimini, the Cathedral of Fermo, the monument to the Fallen in Ancona, Dante's tomb in Ravenna.

Figure 5. *Orsera-Krimenjak limestone in the cultural heritage. From left to right, from top to bottom: detail of Ducal Palace in Venice, detail of a common Venetian building where the whiteness of Istria stone contrasts with the color of bricks, Mausoleum of Theodoric in Ravenna, Rialto Bridge in Venice, the Balance Stone in Dubrovnik, a traditional kažun in Istria peninsula.*

2.3.Aurisina stone

Aurisina stone pertains to the "Calcari di Aurisina" Formation which is part of the Friuli Platform Domain, made of carbonate platforms deposits and referred to a shallow and warm marine water environment of the Upper Cretaceous (Turonian- lower Senonian). The quarry area is located near Aurisina (Nabrežina), some hundreds metres from the sea coast, about 10 km north of Trieste.

Aurisina Stone is a rock that has been used since Roman times and remains of various architectural elements made of Aurisina are widespread in the Po Valley and Friuli (Bugini & Folli 2014) (Fig.6).

Figure 6. *Aurisina limestone in the cultural heritage. From left to right: Roman headstone nearby Milan, column in Aquileia, Devil's Bridge in Cividale del Friuli, Longobardian Ratchis' Altar in Cividale del Friuli.*

The present-day exploitation embraces three varieties: Fiorito (deformed shells), Granitello (coarse shell fragments, packstone), Roman stone (fine shell fragments, wackestone). This study considered the Granitello variety, which is a light grey limestone with irregular white spots, characterized by the presence of rudists bioclasts.

2.4.Chiampo Stone

The name "Chiampo stone" refers to the compact Nummulitic Limestone Formation (Early to Middle Eocene), which is ~ 30 mt thick and crops out in the Venetian Alpine foothills, more specifically in the area of the eastern Lessini Mountains, along both the flanks of the Chiampo Valley (Papazzoni 1995, Matteucci 2005).

The commercial names Chiampo Marble or Chiampo Stone refer to a varieties of sedimentary rocks with a light brownish-grey-pale pink color. This study considered the Porfirico and Ondagata varieties.

This stone was largely appreciated by the Italian architect Vincenzo Scamozzi because of both its whiteness and granularity (similar to that of Vicenza stone) and the strength of a compact limestone. The Chiampo nember (similar to Ondagata variety) can be perfectly polished even if the stone texture is not uniform as it is often composed of an aggregate of fossil remains, especially nummulites. Currently the most precious type is the light pink one (Pearl / Paglierino variety) with few veins. Chiampo limestone has been used mainly for small decorative elements (stairs, wells) but also for monuments like the monolithic columns in the square "Piazza dei Signori" of Vicenza (Rodolico 1953). In the 1920s-1950s the Chiampo quarries were extensively cultivated due to the construction of various buildings like the 1st World War CWGC cemeteries in Italy, the New Hospital in Milan, the Borsa Palace in Genoa, the Tribunal Palace in Bolzano, the Grande Palace in Livorno, the Baha'i International Archives Building in Haifa (Israel) (Fig.7).

Figure 7. *Chiampo Stone. From left to right, from top to bottom: columns in Piazza dei Signori in Vicenza, Borsa Palace in Genoa, headstones in the 1st World War Cemetry in Bordighera, New "Ospedale Maggiore" in Milan, Grande Palace in Livorno, Tribunal Palace in Bolzano.*

2.5.Red Verona Marble

Red Verona Marble is the commercial name of a sedimentary limestone that pertains to the Rosso Ammonitico Veronese (RAV) Formation (Middle – Late Jurassic) which outcrops in the Lesini Hills

of the Venetian Alpine foothills. It was deposited on the top of a submarine plateau (Trento Platform) where the sedimentation rates were very low (Gaetani 1975, Bosellini & Martinucci 1975, Winterer & Bosellini 1981, Martire et al. 2006). Sometimes, due to its high request, the stone is quarried from the Scaglia Rossa (Fig. 1) formation, which is less precious. It is a red nodular limestone with ammonite molds characterized by the juxtaposition of lighter color nodules and darker matrix rich in clay and crossed by dissolution seams. The grain is fine and the color is variable from red to yellow or white. The presence of molds of ammonites causes frequent discontinuities (Korus 2005, Benchiarin 2007, Borghi et al. 2015).

This type of stone was known by Leonardo da Vinci[4] and it has been also called Veronese marble or Verona Broccatello limestone. It has been widely used as ornamental stone since ancient times (i.e. Roman Arena of Verona). The architecture of the Po Valley is characterized by an extensive use of brick structures, so the Red Verona stone was especially used for interior details like capitals and columns or outside the major cathedrals of Northern Italy as column-bearing lions near the entrance (Fig. 8).[5]

This work considered both the Red and Brown varieties from the Lessini district.

Figure 8. *Red Verona marble in the cultural heritage. From left to right: column bearing lion outside a church in Bergamo, detail of Antelami's Deposition in the Cathedral of Parma, columns in Saint Zeno's cloister.*

2.6.Asiago Stone

Asiago stone comes from the pelagic formation of the Biancone (Majolica Veneta, Lower Cretaceous), a thin-bedded white micritic limestone (Martire 1996). It is similar to Red Verona, but it has pale color and less nodules. This research considered both the Pink and White stone varieties (Fig. 9).

The stone is used for small decorative elements in common buildings of the Veneto Region (window sills, door frames, tiling) but sometimes it is used for "noble purposes" like the new altar in the Basilica of Saint Anthony in Padua where the Pink Asiago is coupled with Orsera stone.

2.7. Botticino Stone

Botticino deposits belong to the Corna Formation of the Lombardian Basin (Upper Triassic – Lower Jurassic), located in the Southern Alps and quarried in the surroundings of Brescia (Rezzato area) (Fig. 10). Botticino stone consists of thickly bedded cream-colored and slightly dolomitic limestone prominently crossed by stylolites. These limestones were deposited in a shallow tropical platform environment and they show a variety of textures ranging from desiccated mudstones to oncoid-bearing floatstones (Schirolli 1997, Borghi et al. 2015, Di Battistini et al. 2005).

[4] "Truovasi nelle montagne di Verona la sua pietra rossa mista di tutti i nichi convertiti in essa pietra."

[5] For the façade coverings of the buildings, white limestone such as Istria stone and Verona limestone, were preferred.

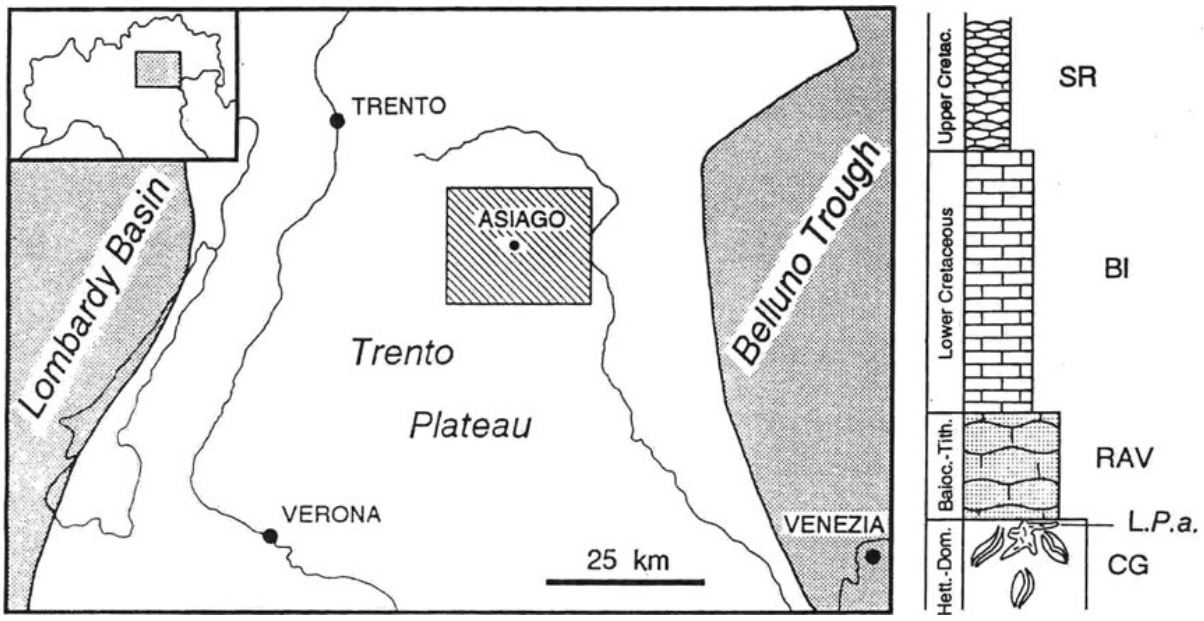

Figure 9. *Jurassic Cretaceous stratigraphic succession on the Asiago Plateau (CG: Calcari Grigi; L.P.a.: Lumachella a Posidonia alpina; RAV: Rosso Ammonitico Veronese; BI: Biancone; SR: Scaglia Rossa). Stratigraphic succession after Martire (1996)*

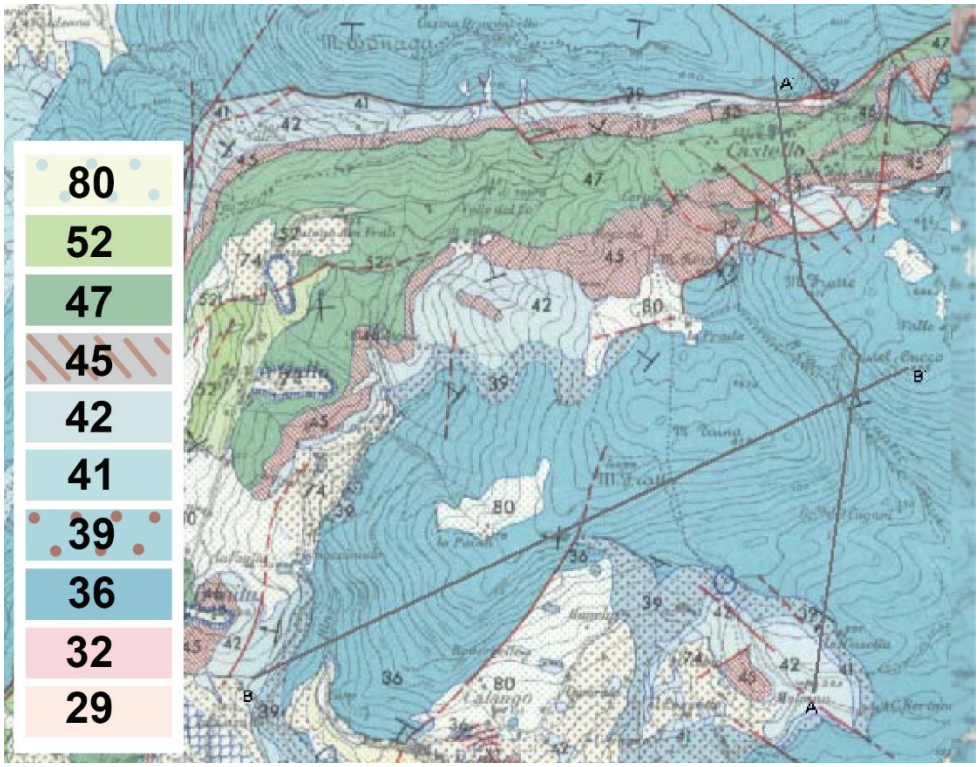

Figure 10. *Geological map of the Corna Formation, in the Lombardian Basin (adapted from Zucchi et al. 2006). The codes identify: 80 - quaternary sediments, 52 - Lombardian Scaglia (SDL), 47 - Maiolica (MAI), 45 - Selcifero Lombardo Group (SM), 42 - Concesio Group (CC), 41 - Medolo group (MD), 39 - Corso, 36 - Corna (COR), 32 - Zu limestone (ZUU), 29 - Dolomia Principale (DPR).*

The stone is mostly quarried from open-pit sites. The studied variety is the Classic Botticino, the most diffuse type. It is a limestone originated from calcareous remnants of algae (Pivko 2003).

Figure 11. *Botticino Stone in the cultural heritage and modern architecture. From top to bottom, from left to right: Vittoriano Monument in Rome, Grand Central Station in New York City, Red Sea Hospital in Jeddah, Roman Temple dedicated to Emperor Vespasian in Brescia, One International Place in Boston, Loggia Palace in Brescia, Chamber of Commerce in Osaka.*

This stone has been used since Roman times, especially in the Brescia area, where the quarries are located. Here Botticino stone was used in the construction of the Roman Temple of the Emperor Vespasian, the Theater, the Church of the Virgin of Miracles, the Loggia Palace, the Cathedral (Clerici & Meda 2005). At the end of 19th century the use of this building stone began to spread in the whole Italy and across the world (Fig. 11): the Vittoriano monument in Rome, the Gare du Nord in Bruxelles, the Arch of Victory in Bolzano, the White House in Washington, the Commercial Italian Bank in Milan, the Grand Central Station and the basement of the Liberty statue in New York, the Chamber of Commerce in Osaka, the Red Sea Hospital in Jeddah, the One International Place in Boston, are all realized using this stone. The main technical features of the Botticino stone are reported in table 2.

Table 2. *Mechanical characteristics of Botticino limestone (Department of Earth Sciences, Parma)*

Compressive strength dry samples, MPa	183
Compressive strength after 25 cycles of freezing and thawing, MPa	164
Real flexural strength under concentrated load	12.7
Flexural strength under concentrated load after freeze-thaw cycle, MPa	12.9
Real density, kg/m^3	2710
Bulk density, kg/m^3	2683
Porosity, %	1.00
Water absorption at P_{atm}, %	0.14

2.8. White Carrara marble

White Carrara marble is the only metamorphic rock considered in this research. Carrara marble has a large number of commercial varieties. These rocks derive from original Mesozoic sequences of the Tuscan Nappe which were metamorphosed under low-grade conditions, and now they outcrop in the Apuan Alps (Carmignani et al. 1978, Meccheri et al. 2007, Borghi et al. 2015) (Fig.12).

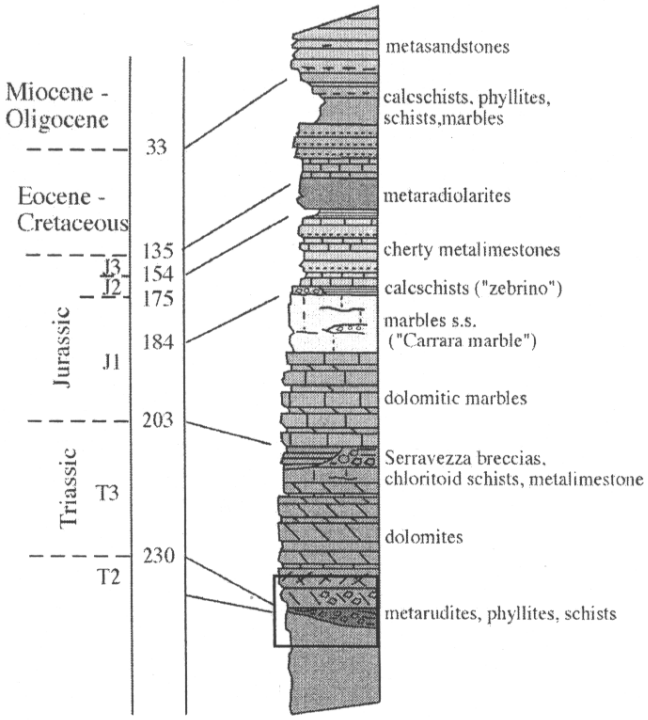

Figura 12. *Stratigraphic succession of the Apuan district*

The Apuan marbles are the most famous Italian marbles. Although they have homogeneous chemical and mineralogical composition, different Apuan white marbles show different behavior when exposed to external environment (Cantisani 2009). Table 3 reports the typical technical features of the Carrara marble.

White marbles have a pearly white color, fine to medium-large grain size; their color is homogeneous or spotted with small patches and gray veins, irregularly distributed and due to microcrystalline pyrite. Although with different ornamentation (grains, stains, veins), most ordinary marbles correspond to the more active platform areas characterized by better growth conditions (oxygenation, clean water, etc.) and by mechanical constraints of minor size. In particular, the white varieties have been largely used, both in the past and nowadays, for building monuments and works of art.

Carrara marble has been extensively used since the Roman Age (Fig. 13). Important monuments of Ancient Rome as well as many Renaissance sculptures are made of this material e.g. the Pantheon, Trajan's and Marcus Aurelius' Columns, Michelangelo's Pietà (1499) and David (1501-1504). The importance of these monuments and the availability of raw material made this stone a primary choice for relevant monuments and buildings all over the world. The Marble Arch in London, sarcophagi of nobles around Europe, the Cathedral of Manila, the Opera House in Oslo, the Finland Hall in Helsinki, the Hindu Temple Prem Mandir in India, Harvard Medical School and various other buildings in the USA and Canada, the fountain Bassin de Madrid in Paris are on the long list of prominent buildings which largely utilized this marble.

Figure 13. *Carrara marble in the cultural heritage and modern architecture. From top to bottom, from left to right: Harvard Medical School in Boston, Sheikh Zayed Mosque in Abu Dhabi, Cathedral of Carrara, Michelangelo's David, Sarcophagus of Saint Queen Hedwig of Poland in Cracow, Finland Hall in Helsinki, Oslo Opera House, temple Prem Mandir in India.*

As other stones, Carrara marble is also largely used in the territories close to the quarry district (i.e. the Apuan district and Tuscany). For example, the Cathedrals of Massa and Carrara as well as the Ducal Palace of Massa are entirely made of Carrara marble, in the whole Tuscany, churches are made of this marble which is often coupled with other building stones. In Italy, the marble was less used in Lombardy because the transportation of stone blocks was possible only by circumnavigating the Italian peninsula until the Po delta.

A summary of the main geological outlines and lithological classification of all the considered rock types is reported in table 3.

Table 3. *Mechanical characteristics of Carrara marble (by CGT-Siena)*

Compressive strength dry samples, MPa	101.4
Real flexural strength under concentrated load	11.6
Flexural strength under concentrated load after 48 freeze-thaw cycle, MPa	9.6
Real density, kg/m^3	2710
Slip resistance (dry)	71
Slip resistance (wet)	33
Porosity, %	0.4
Water absoption at P_{atm}, %	0.12

Table 4. *Summary of principal geological classifications, geological formation of provenance and deposition age of the carbonate rocks considered here. A = Pink Asiago, AU = Aurisina stone, B = Brown Verona Stone, BO = Botticino Stone, C = Chiampo Ondagata, E = White Asiago Stone, M = Carrara Marble, N = Vicenza Stone (Nanto variety), O = Istria Stone (Orsera variety), P = Chiampo Paglierino Stone, V = Vicenza Stone (Costozza variety).*

Sample	Folk classification	Kendall/Folk classification	Dunham classification	Geological Formation	Geological Age
Carrara Marble	---	---	Crystalline carbonate	Tuscan Nappe	Cretaceous
Botticino S.	Dolomitic Micrite	Dolomitic Micrite	Crystalline carbonate	Corna Formation	Upper – Lower Jurassic
Brown Verona S.	Biomicrite	Intramicrite	Wackestone	Rosso Ammonitico Veronese	Middle – Late Jurassic
Red Verona S.	Biomicrite	Intramicrite	Wackestone	Rosso Ammonitico Veronese	Middle – Late Jurassic
Chiampo Paglierino S.	Biomicrite	Intramicrite	Packstone/Grainstone	Nummulitic Limestone	Middle Eocene
Chiampo Ondagata S.	Biomicrite	Intramicrite	Packstone/Grainstone	Nummulitic Limestone	Middle Eocene
White Asiago S.	Biomicrite	Oomicrite	Wackestone	Majolica Veneta	Lower Cretaceous
Pink Asiago S.	Biomicrite	Oomicrite	Wackestone	Majolica Veneta	Lower Cretaceous
Nanto S.	Biomicrite	Biomicrite	Packstone	Nummulitic Limestone	Lower Eocene
Costozza S.	Biomicrite	Biomicrite	Packstone	Calcareniti di Castelgomberto	Oligocene
Aurisina S.	Biomicrite	Biomicrite	Packstone	Trieste Karst Limestone	Cretaceous
Orsera S.	Micrite	Dismicrite	Mudstone	Unity of External Dinarides	Jurassic

3. Analytical methods

Sample slates were made available by quarry companies (Colosio Snc, Grassi Pietre Srl, Euromarmi). Standard uncovered thin sections were prepared and observed under petrographic optical microscope (OM) and scanning electron microscope (SEM).

OM observations were done using a Zeiss® AxioScope.A1 coupled with an AxioCamMRC5 camera connected to a PC running the AxioVision Red 4.8 software package. This equipment was also utilized to determine grain size distribution of the textural elements recognized in thin section.

SEM – BSE images were acquired with a Scanning Electron Microscope CamScan MX 2500 microscope (Department of Geosciences), equipped with a LaB_6 cathode, operating at 20 kV and a working distance (WD) of 20 mm, and an Electron Backscattered Diffraction (EBSD) system. Thin sections required carbon coating before being analyzed. Digital Image Analyses (DIA) of a matrix of 30 x 40 BSE overlapping (25%) images with a resolution of 1280 × 1024 pixels at a magnification of 200X (1 pixel = 0.5 micron) were performed in order to obtain information about sample porosity and pore size distribution (see Part 2 for a detailed description of the pore system in the carbonate rocks considered in this study). Thin section of the marble sample was Syton polished and analyzed by EBSD to determine grain size distribution and compare results with measurements obtained by optical microscopy.

A representative amount of material was separated from each sample and ground in order to perform X-ray Fluorescence (XRF) and X-ray Powder Diffraction (XRPD) analyses.
XRF bulk chemical analyses were conducted with a Philips PW 2400 spectrometer equipped with a 3kW Rh X-Ray tube. Samples were prepared as beads from calcined powder and $Li_2B_4O_7$ with a dilution ratio of 1:10. Geological standards were used for the calibration (Govindaraju 1994). The concentrations of major (SiO_2, TiO_2, Al_2O_3, Fe_2O_3tot, MnO, MgO, CaO, Na_2O, K_2O, P_2O_5) and trace elements (Sc, V, Cr, Co, Ni, Cu, Zn, Ga, Rb, Sr, Y, Zr, Nb, Ba, La, Ce, Nd, Pb, Th, and U) were calculated. Instrumental precision (defined by several measurements performed on the same sample) is within 0.6% relative for major elements, and within 3% relative for trace elements. Detection limits are within 0.01% for major elements Al, Mg and Na, within 0.2% for Si, within 0.005% for Ti, Fe, Mn, Ca, K and P. Limits for trace elements are (in ppm): Sc=5, V=5, Cr=6, Co=3, Ni=3, Cu=3, Zn=3, Ga=5, Rb=3, Sr=3, Y=3, Zr=3, Nb=3, Ba=10, La=10, Ce=10, Nd=10, Pb=5, Th=3, U=3. Loss on ignition (L.O.I.) has been calculated heating a known amount of sample in a furnace at 860°C for about 20 mins, then at 980°C for about 2 hours.
Mineralogical composition was determined by XRPD on a Philips X-Pert PRO diffractometer, in Bragg-Brentano geometry, equipped with a Cu X-ray tube, operating at 40 kV and 40 mA, and a solid-state detector (X'Celerator). The powders (about 1 g) of 12 bulk samples were mounted on a circular sample holder (32 mm Ø). Scans were performed in the range 3° to 80° 2θ with an integrated step size of 0017° 2θ and a counting time of 100 s $step^{-1}$. Identification of minerals, quantification and cell parameter determination were performed using High Score Plus and the ICSD database (PANalytical). A pseudo-Voigt function was employed for fitting the profiles.
Cores (length = 2 cm, diameter = 8 mm) were cut off from fresh samples in order to analyze them through Mercury Intrusion Porosimetry and X-ray Computed micro-Tomography. For more detailed description of the analytical procedure, results and discussion see Part 2.
In this study MIP was performed at the Department of Physics and Earth Sciences of the University of Parma using a PoreMaster 33 system (Quantachrome Instruments®) with the following parameters: sample cell is 1.0 × 3.0 cm in size and 2 cm^3 in volume, pressure range is 0.5–33.000 psi, contact angle (θ) of mercury is 140°, and surface tension (σ) of mercury is 0.48 N/m (480 dyn/cm), pore size range is from 0.0064 to 950 μm. The required value of the dry density of materials was measured through a Ultrapic 1200 picnometer (Quantachrome Instruments®).
Before measurements, samples were dried at 40°C for 24h and then about 2 g (i.e. a little core with diameter of 8 mm and 2 cm long) of material were analyzed.
Computerized X-Ray micro-tomography analyses were performed with a bench-top Skyscan 1172 micro-CT scanner (Bruker®) at the Department of Geosciences, University of Padua.

4. Results

4.1.OM observation and grain size estimation

Synthetic results about the grain size of the different textural elements recognized in thin section are reported in Table 5. Photomicrographs of the main textural elements recognized in the various samples and characterized by different grain size are reported in fig. 14 and 15.

Vicenza Stone (Costozza and Nanto varieties)

According to Dunham (1962) and Folk (1959) Nanto Stone is petrographically classified as a packstone or a biomicrite, respectively. It is characterized by a clastic-organogenic, and grain-supported texture. The matrix is mainly intergranular.

The skeleton is mainly represented by bioclasts, where Nummulites and Assilines are prevalent over red algae and other benthic organisms (bryozoans, echinoderms). Nummulites are composed by isoriented calcite crystals (3-4 μm wide). Skeletal grains of benthic organisms are often micritized, with grain size below 1 μm. In this sample sparite (average grain size = 15 μm) is rare.

As Nanto Stone, Costozza Stone is petrographically classified as a packstone or a biomicrite and it displays a clastic-organogenic grain-supported texture. Large clasts above several mm in length are common. Porosity is high and large pores are more frequent than in Nanto variety. Red algae (*Rhodophyta*) and benthic fossils (bryozoans, echinoderms) prevail over Nummulites and planktonic foraminifera (Miliolids). This suggests that the depositional environment was a lagoon with little water circulation, as also confirmed by the large amounts of matrix, characteristic of stable sediments subjected only to weak currents (Benchiarin 2007).

As in the Nanto Stone, the benthic fossils present in the Vicenza Stone are all micritized, with grain size below 1 μm.

Istria Stone

The texture is compact and micritic and composed by small calcite crystals (3-5 μm), so it can be classified as a micrite or a mudstone (Folk 1959, Dunham 1962). Small pores are very rare.

Veins and cavities are filled with sparite (Ø=40μm).

Aurisina Stone

Petrographically classified as a biomicrite-packstone, Aurisina stone is characterized by *Rudists,* i.e. extinct epiphaunal bivalves (*Hippuritidae* and *Radiolitidae*), the attached left valve of which was a tall, conical-shaped shell, while the right valve became a lid-like cover (Bugini & Folli 2014). Echinoderms are also frequent and partially micritized. Sparry calcite is within the grain size range of 5-10 μm.

Chiampo Stone

Both varieties of Chiampo Stone can be classified as a grain (bioclast) supported packstone or biomicrite. As already reported in literature (Pivko 2003, Bosellini et al. 1967, Borghi et al. 2015) the bioclasts found in this rock are mainly Nummulites and Assilines as in the Vicenza stone. However, their structure is more compact and characterized by a low porosity. Bioclasts (e.g. Nummulites) are constituted by isoriented calcite grains with diameter below 3 μm. Sparite can be found as secondary filling phase within bioclasts forming coarse aggregates with an average grain size of ~40 μm, or as a cement reducing intergranular porosity, with grains of ~25 μm.

Verona Stone

The two varieties of Verona Stone are classified as a biomicrite or wackestone. In both samples, the matrix contains the skeletal remains of marine organisms such as *Calpionellids* up to 80 μm in size (in the Red Verona Stone) and *Ostracods* with a spine shape and dimension of about 1 mm in length and 30 μm thick. These fossils optically behave like monocrystalline individuals. Cement contains clay minerals, sometimes concentrated along specific layers favoring deterioration mechanisms.

Asiago Stone

The two varieties of Asiago Stone, present a matrix composed by ultra-fine micrite. The aspect is similar to that of Verona stone but in these samples fine-grained micritic mud is more abundant and the fossil record comprises only smaller *Calpionellids* individuals of about 45-50 μm in size.

Table 5. *Summary of grain size measurements by Optical Microscope. Values marked with an asterisk have been calculated mediating at least 100 measurements, 1000 in the case of the marble. Sample abbreviation as in Table 4.*

Sample		**Grain size (μm)**	**Notes**
A	Micrite	<0.1-0.3	
	Bioclasts	44*	
	Sparry calcite	1-2, 3-5 inside bioclast	
AU	Micrite	<1	
	Bioclasts	Up to 1000-2000	Often micritized, echinoderms have a monocrystalline behaviour
	Sparry calcite	5-10	
B	Micrite	5-10	
	Fine micrite	1	
	Bioclasts	Ostracods: 30* (thickness) Ooids: 85*	Monocrystalline behaviour
BO	Dolomite	127*	
	Fine micrite	2	
	Micrite	5-10	
C	Micrite	<1	
	Sparry calcite	40* (within bioclast) – 25* (within rock porosity	
	Bioclasts	Up to cm size	Constituted by isoriented calcite grains (<3 μm), central pores filled with sparite
E	Micrite	<0.1-0.3	
	Bioclasts	51*	
	Sparry calcite	1-2, 3-5 within bioclast	
M	Texture	155*	
N	Sparry calcite	15	Rare
	Micrite (Bioclasts)	1-4	<1 μm if they are micritized bioclast; 3-4 μm if they are isoriented
	Bioclasts (Echinoderms)	300-500	Not so many
O	Micrite	3-5	
	Sparry calcite	40*	Inside veins
P	Micrite	<1	
	Sparry calcite	45* (within bioclast)	
	Bioclasts	Up to 2000	
R	Micrite	5-10	
	Fine micrite	1	
	Bioclasts	Ostracods: 30* (thickness) Ooids: 107*	Monocrystalline behaviour
V	Sparry calcite	5-10	
	Bioclasts	500 (Echinoderms) or more	
	Micrite	<1	In micritized bioclasts.

Botticino

Botticino Stone is characterized by large dolomite crystals (127 μm) surrounded by a micritic matrix with grain size between 1 and 10 μm.

Carrara marble

Carrara marble presents a homogeneous texture made of calcite crystals. The grain size of calcite ranges from 10 to 200-300 μm with a mean value of 70 μm.

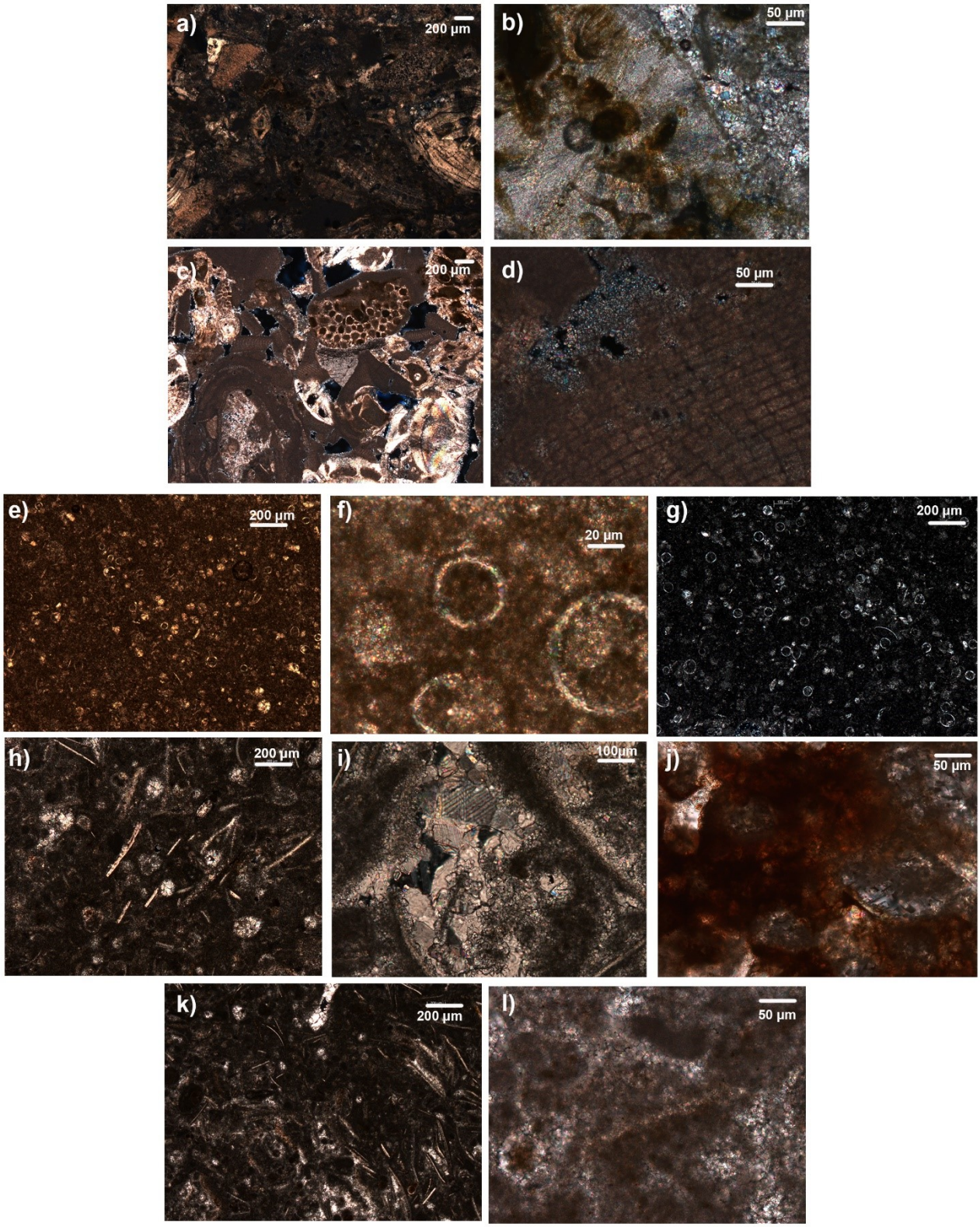

Figure 14. *Photomicrographs of thin section: a) Nanto stone general view (2,5x), b) Nanto stone detail (20x), c) Costozza stone general view (2,5x), d) Costozza stone detail of a micritized fossil (20x), e) Pink Asiago general view (5x), f) Pink Asiago detail (50x), g) White Asiago general view (5x), h) Brown Verona general view (5x), i) Brown Verona detail of sparry calcite inside a bioclast (10x), j) Brown Verona detail of a red vein (20x), k) Red Verona general view(5x), l) Red Verona detail of texture with micrite and fine sparite*

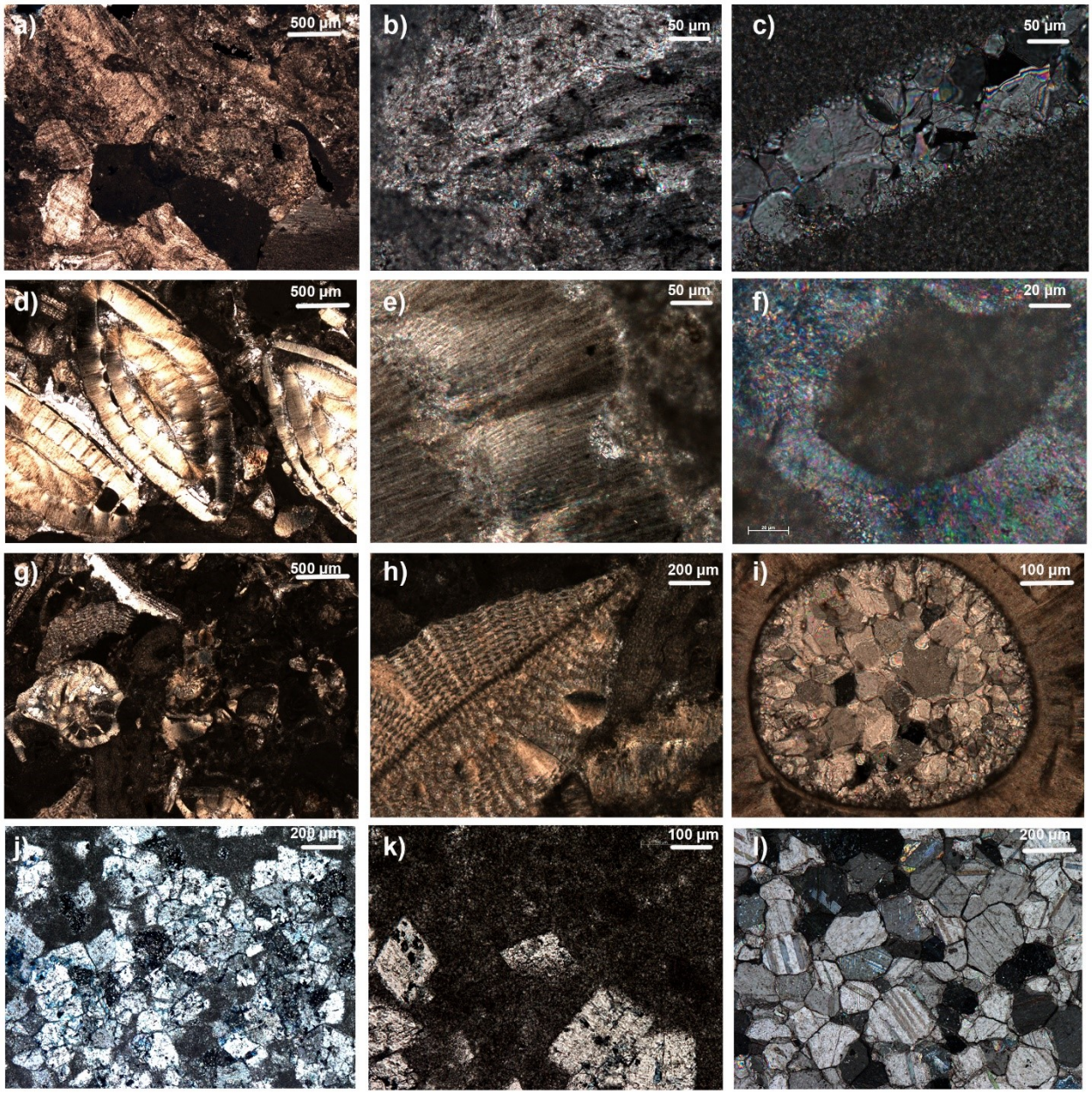

Figure 15. *Photomicrographs of thin section: a) Aurisina stone general view (2,5x), b) Aurisina stone detail of lamellar sparite (20x), c) Orsera stone, detail of vein filled with sparry calcite (20x), d)Chiampo Ondagata general view with large nummulites(2,5x), e) Chiampo Ondagata detail with isotropic micrite texture in nummulite (20x), f) Chiampo Ondagata detail micrite (50x), g) Chiampo Paglierino general view (2,5x), h) Chiampo Paglierino detail with bioclast-echinoderm (5x), i) Chiampo Paglierino detail porosity within bioclast filled with sparry calcite (10x), j) Botticino marble general view (5x), k) Botticino Marble detail of the micritized matrix (10x), l) Carrara marble texture (5x).*

4.2.Electron Backscattered Diffraction (EBSD)

EBSD was performed on a thin section of Carrara marble in order to compare grain size distribution with that obtained by optical microscopy (Fig. 16).

The grain size distribution obtained using these two analytical techniques is very similar, although the average grain size obtained by EBSD results to be significantly lower (~50 µm). This can be explained considering that a larger amount of small crystals can be determined by ESBD, determining a considerable reduction in the estimate of the average grain size.

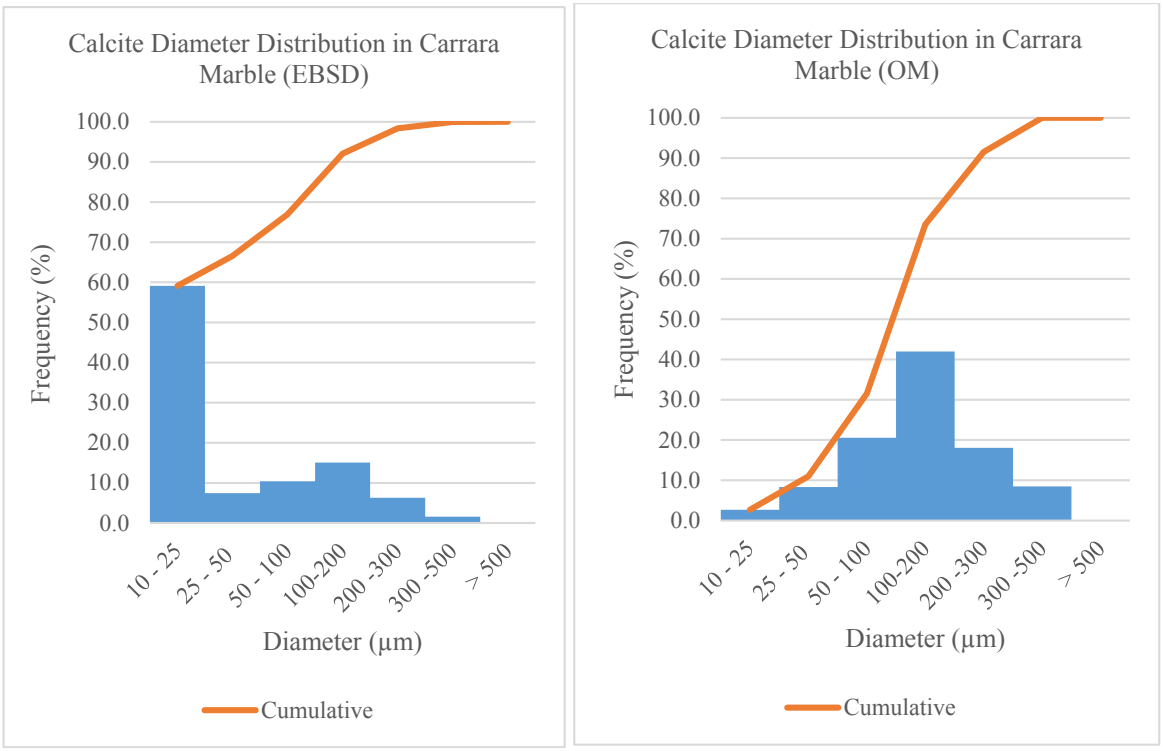

Figure 16. *Charts of the cumulative frequencies of the grain size distribution of Carrara marble measured through EBSD (left) and OM (right)*

4.3.XRPD analyses

Mineral composition was determined by XRPD in order to evaluate the possible influence of different content in minor mineral phases on stone vulnerability to deterioration processes. Results are reported in Table 6. Clearly the main mineral phase is calcite, which is always comprised between 95% and 98%, with the exception of Botticino limestone which shows the typical composition of a dolomitic limestone, with 57% of calcite and 47% of dolomite (Fig. 17).

Analysing the data obtained for the samples of Vicenza stone, Nanto stone (which also is the oldest) has a higher insoluble residue than Costozza stone, as already reported in the literature (Benchiarin 2007). This may be due to the different environmental conditions of deposition and to the different terrigenous contributions at the times of formation of these sediments. The residual fraction of the Nanto stone is composed by illite (5%). This is apparently discordant with the XRD results obtained by Di Benedetto et al. (2012) that shows quartz (1%), clay minerals (1%) and iron oxides as minor phases. Still in the same sample they found a micaceous component in a brownish area, more subjected to weathering originated from freeze-thaw cycles.

As expected, the mineralogical composition of Orsera stone, which is a white and compact limestone is completely calcitic (100% calcite), with minor components below detection limit. Also the Aurisina stone resulted to be completely constituted by calcite. As it concerns the Chiampo stone, both varieties show similar composition, with Calcite between 61 and 66%, Mg-Calcite between 34 and 38%, and traces of Palygorskite M. The presence of these clay minerals can encourage the detachment of bioclasts during freeze-thaw cycles or wet-dry cycles, amplifying deterioration vulnerability.

The two samples of Verona stone (Brown Verona and Red Verona) show a different composition regarding the minor mineral components. The Red variety is basically constituted by calcite only, while Brown variety contains minor mineral phases (quartz and illite) which are sometimes arranged in veins, determining a considerable heterogeneity of the material.

Table 6. *Results of the XRPD analyses. Samples abbreviations as in Table 4.*

Sample	**XRPD**
A	98% Cal, 2% Qtz
AU	100% Cal
B	94% Cal, 4% Ill, 2% Qtz
BO	57% Cal, 43% Dol
C	66% Cal, 34% Mg-Cal, traces Plg M
E	97% Cal, 3% Qtz
M	100% Cal, traces Ms
N	95% Cal, 5% Ill
O	100% Cal
P	61% Cal, 38% Mg-Cal, 1% Plg M
R	100% Cal
V	100% Cal

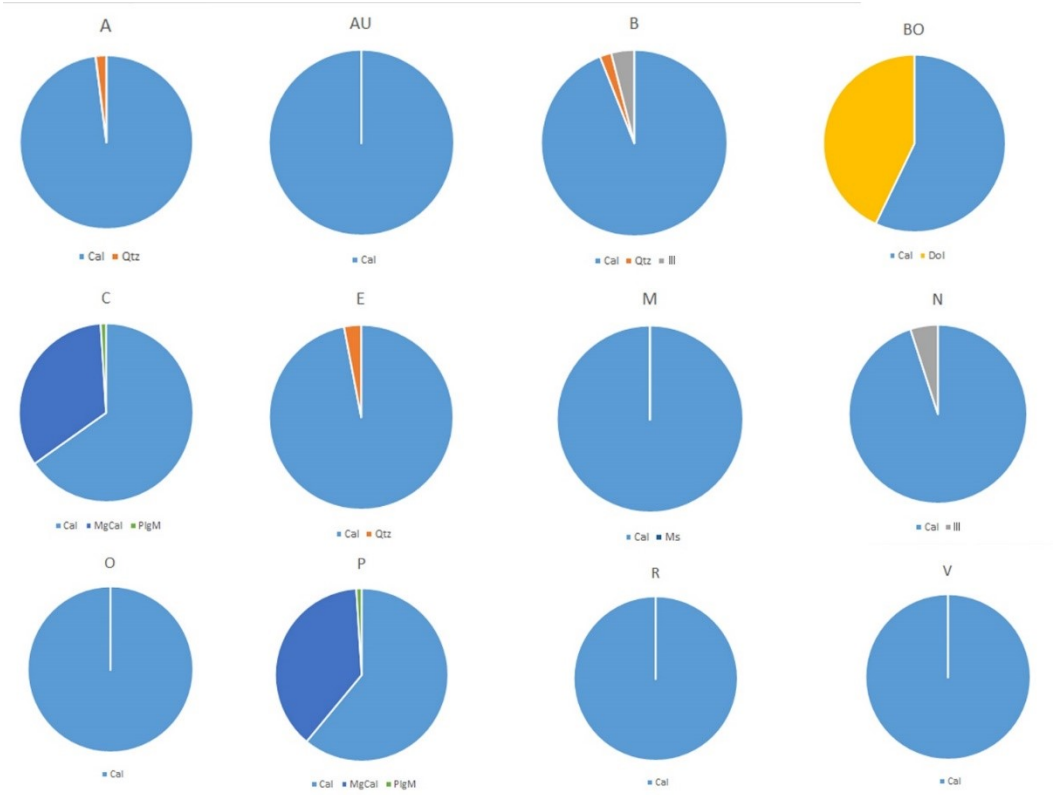

Figure 17. *Charts summarizing the composition of samples as obtained by XRPD. Samples abbreviations as in Table 4.*

Both varieties of the Asiago stone (Pink Asiago and White Asiago) show a small amount of quartz as a minor component (2-3%), significantly lower than Verona marble, which is congruent with the macroscopic texture of Asiago stone, characterized by fainter veins with respect to Verona stone.
As expected, Carrara marble is completely constituted by calcite, with traces of muscovite below detection limit for the XRPD, but recognized in thin section.

4.4.XRF analysis

Typically, high contents of CaO have been reported for all limestones studied here except Botticino limestone which shows a higher MgO concentration (10.07%) while other samples show values below 1%. Both varieties of Chiampo stone (Ondagata and Paglierino) show a higher percentage of MgO that can be explained by the presence of red algae and fossils, which are generally composed of Mg-rich calcite. Regarding Vicenza stone varieties, in the Nanto stone, the concentration of ferric oxides (Fe_2O_3) is higher than in the Costozza one and this explains the warm yellow color of Nanto stone. The presence of SiO_2 and Al_2O_3 is correlated to the presence of illite and quartz. In Nanto stone there is also a slightly higher content in Al_2O_3, MgO, TiO_2, K_2O, Fe_2O_3, Cr and V with respect to Costozza stone, probably due to the presence of a higher amount of illite and other clay minerals. Trace elements may provide information about the paleo-environment (Benchiarin 2007).

Table 7. *Results of XRF analysis. Major elements reported in percentage. Samples abbreviations as in in Table 4.*

Sample	Major Elements (%)										L.O.I.	TOT
	SiO_2	TiO_2	Al_2O_3	Fe_2O_3	MnO	MgO	CaO	Na_2O	K_2O	P_2O_5		
A	1.09	0.01	0.25	0.18	0.03	0.27	54.65	0.01	0.05	0.04	42.85	99.42
AU	0.01	0.01	0.01	0.02	0.01	0.16	56.13	0.01	0.01	0.01	42.97	99.32
B	2.45	0.04	0.72	0.49	0.13	0.30	53.01	0.01	0.13	0.13	42.01	99.44
BO	0.04	0.01	0.06	0.03	0.01	10.07	47.57	0.01	0.01	0.01	41.53	99.33
C	0.35	0.02	0.12	0.12	0.01	0.53	54.70	0.01	0.01	0.03	43.47	99.38
E	1.13	0.01	0.26	0.15	0.02	0.29	54.57	0.01	0.05	0.06	42.78	99.32
M	0.01	0.01	0.05	0.02	0.01	0.83	57.83	0.01	0.01	0.01	40.21	98.99
N	2.66	0.23	0.92	1.18	0.01	0.50	52.11	0.01	0.31	0.04	41.71	99.67
O	0.28	0.01	0.16	0.06	0.01	0.20	55.89	0.01	0.03	0.01	43.17	99.82
P	0.71	0.02	0.18	0.14	0.02	0.57	54.40	0.01	0.01	0.03	43.30	99.39
R	0.42	0.01	0.20	0.18	0.01	0.26	55.26	0.01	0.05	0.07	43.14	99.60
V	0.16	0.01	0.11	0.20	0.01	0.28	55.48	0.01	0.02	0.03	43.25	99.55

Table 8. *Results of XRF analysis. Minor element reported in percentage. Samples abbreviations as in Table 4.*

Sample	Trace elements (ppm)																				
	S	Sc	V	Cr	Co	Ni	Cu	Zn	Ga	Rb	Sr	Y	Zr	Nb	Ba	La	Ce	Nd	Pb	Th	U
A	270	<5	<5	11	3	4	35	34	<5	14	298	19	9	<3	38	22	<10	30	<5	24	<3
AU	129	<5	8	21	<3	<3	31	13	<5	13	676	<3	5	<3	30	<10	<10	15	<5	25	<3
B	451	<5	9	13	27	60	48	47	<5	22	215	33	23	<3	84	41	28	43	<5	31	<3
BO	118	<5	<5	14	<3	<3	36	10	<5	21	174	<3	7	<3	18	<10	<10	25	<5	40	<3
C	445	<5	16	34	<3	<3	31	17	<5	5	476	3	10	<3	25	<10	<10	18	<5	18	6
E	193	<5	<5	17	<3	3	35	47	<5	5	327	19	11	<3	35	<10	12	33	<5	28	<3
M	1428	<5	<5	9	<3	<3	33	28	<5	20	332	<3	8	<3	17	20	20	17	<5	26	<3
N	536	<5	45	56	<3	13	36	34	<5	20	935	6	27	3	40	11	25	34	<5	22	8
O	170	<5	<5	16	<3	<3	29	14	<5	13	196	<3	11	<3	32	<10	<10	25	<5	34	4
P	650	<5	46	47	<3	4	35	18	<5	5	470	5	11	<3	22	<10	<10	26	<5	20	<3
R	461	<5	8	13	<3	3	33	28	<5	6	220	21	13	<3	26	28	<10	43	<5	24	<3
V	391	<5	14	18	<3	4	34	12	<5	22	798	<3	6	<3	26	<10	<10	23	<5	23	4

For example, Sr content is helpful in understanding the origin and diagenesis of carbonates, since dolomitic limestones generally contain less Sr than calcitic limestone. As expected in the Botticino stone this value is low. A relatively high value of Sr/Mg ratio (observed in Asiago stone, Aurisina stone, Vicenza stone) suggest that these stones were deposited in shallow water in the coastal platform domain.

Table 9. *Elaboration of XRF results. Paleo-environmental indicators. Samples abbreviations as in Table 4.*

Sample	Ni/Co	Sr/Mg	V/Ca
A	1.33	1.104	---
AU	---	4.225	0.0001
B	2.22	0.717	0.0002
BO	---	0.017	---
C	---	0.898	0.0003
E	---	1.128	---
M	---	0.400	---
N	---	1.870	0.0009
O	---	0.980	---
P	---	0.825	0.0008
R	---	0.846	0.0001
V	---	2.850	0.0003

Other significant markers are redox-sensitive trace elements (V, Cr, Ni, Co, Zn, Cu), widely used as indicators of paleo-environmental conditions on the sea bed. In particular, the Ni/Co ratio is considered an index of paleo-oxygenation conditions. In our samples, the values of this ratio are always <5, indicating that the sediments were deposited under an oxic water column. Taking into account the relative Ni enrichment of Nanto stone and Brown Verona stone it may be assumed that these groups of rocks were deposited in less oxic conditions than the others. Vanadium may also be used as a paleo-redox proxy. Recent culture experiments on foraminifers have shown that the V/Ca ratio in foraminifer shells (Hastings et al. 1996, Benchiarin 2007) is incorporated in direct proportion to that found in seawater.

4.5.Porosity

Porosity has been evaluated using multiple techniques (see also Part 2 for a detailed discussion): Digital Image Analysis (DIA) of SEM–BSE images, X-Ray Computerized micro-Tomography (micro-CT), Mercury Intrusion Porosimetry (MIP). The total porosity obtained from DIA of SEM – BSE images and micro-CT as well as the open porosity measured through MIP are shown in Table 10. Major discrepancies between micro-CT and the other methods may be explained considering that this analytical technique has a limitation on the minimum detectable pore dimension, which is 4.75 μm for the specific setup used during the acquisition sessions. Because pores smaller than 4.75 μm constitute a relevant fraction of the total porosity, micro-CT data underestimate total porosity. Indeed, the majority of the samples is constituted by pores smaller than 1μm. In the case of the Nanto stone, an apparent incongruence arised from the comparison of the porosity values obtained from MIP and DIA from one side, and micro-CT on the other. This incongruence can be explained considering the pore size distribution which reveals that most of the pores lies below 5 μm.

Table 10. *Summary of density and porosity results obtained through different techniques: DIA of SEM-BSE 200X images, micro-CT, and Mercury Intrusion Porosimetry. Samples abbreviations as in Table 4.*

Sample	SEM (DIA) %>0.5µm	Micro-CT % > 4.75 µm	MIP %>0.006 µm	Density (g/cm^3)
			Open Porosity	
A	0.17	0.28	3.54	2.6881±0.0080
AU	0.62	1.21	4.61	2.7055±0.0075
B	0.03	0.07	0.10	2.7209±0.0056
BO	4.34	1.30	1.73	2.7669±0.0043
C	1.72	1.49	1.04	2.7074±0.0076
E	0.24	1.04	2.22	2.6824±0.0045
M	2.11	0.04	1.00	2.7413±0.0027
N	25.08	8.96	27.18	2.7890±0.0087
O	0.42	1.07	0.40	2.7107±0.0073
P	0.95	0.73	0.36	2.7085±0.0041
R	0.64	0.27	0.26	2.7292±0.0053
V	17.33	13.54	28.52	2.7369±0.0049

Conclusion

The aim of this study was to assess the petrographic, textural and geochemical characteristics of the selected carbonate rocks constituting a large variety of monuments and historical buildings of northeastern Italy. Multiple techniques (OM, ESBD, XRF, XRD, SEM, MIP, micro-CT) have been used in order to assess the mineralogy, chemical composition, grain size and porosity of each rock type considered.

Important information have been collected about the abundance and dimension of bioclasts, the presence of sparitic calcite either in veins or as a cement, and that of micrite, the grain size and the porosity of which have been determined.

The results of this part of the research improved our knowledge on the stone materials employed in the built heritage of northeastern Italy.

References

Benchiarin S. (2007) Carbonate lithotypes employed in historical monuments: quarry materials, deterioration and restoration treatments. PhDThesis, University of Padua.

Benchiarin S., Fassina V., Molin G. (2012) Assessment of conservation treatments on Paduan Nanto Stone monuments. In Proceedings of the 12th Congress on the Deterioration and Conservation of Stone, New York. Unpublished, http://iscs.icomos.org/pdf-files/NewYorkConf/bencetal.pdf

Borghi A., Berra V., D'Atri A., Dino G.A., Gallo L.M., Giacobino E., Martire L., Massaro G., Vaggelli G., Bertok C., Castelli D., Costa E., Ferrando S., Groppo C., Rolfo F. (2015) Stone materials used for monumental buildings in the historical centre of Turin (NW Italy): architectonical survey and petrographical characterization of Via Roma. From Pereira D., Marker B.R., Kramar S., Cooper B.J., Schouenborg B.E. (Eds) Global Heritage Stone: Towards International Recognition of Building and Ornamental Stone, *Geological Society London Special Publications*, **407**, 201-218.

Braga G. (2004) Le pietre naturali da costruzione della città di Padova. Ed Cleup, Padova.

Bosellini A., Martinucci M. (1975) Annegamento delle piattaforme carbonatiche (nota preliminare). *Ann Univ Ferrara (n.s.), Sez. IX, Sc Geol Paleont*, **5-10**,181-193.

Bugini R., Folli L. (2014) The use of "Aurisina limestone" in the Roman architecture (Milan and Lombardy). In: VIII Congresso Nazionale di Archeometria, Scienze e Beni Culturali: stato dell'arte e prospettive, Bologna 5 - 7 Febbraio 2014.

Cantisani E., Pecchioni E., Fratini F., Garzonio C.A., Malesani P., Molli G. (2009) Thermal stress in the Apuan marbles: Relationship between microstructure and petrophysical characteristics. *Int J Rock Mech Min*, **46**, 128-137.

Cappellaro M., Dal Farra A., De Lorenzi Pezzolo A. (2012) DRIFT characterization of the "Soft Stone of the Berici Hills" and first results of a fast method for the classification of its main varieties through Multivariate Analysis. *Sciences at Ca' Foscari*, Venezia, 46-59.

Carmignani L., Giglia G., Klingfield R. (1978) Structural evolution of the Apuane Alps: an example of continental margin deformation. *J Geol,* **86,** 487-504.

Cattaneo A., De Vecchi Gp., Menegazzo Vitturi L. (1976) Le pietre tenere dei Colli Berici. Ed. Soc. cooperativa tip., Padova.

Centro Geotecnologie di Siena (2009) The Tuscan Marble Identities. Ed. Regione Toscana.

Clerici A., Meda A. (2005) Confronto tra le caratteristiche meccaniche di diversi livelli di estrazione del Botticino Classico. *Giornale di Geologia Applicata*, **2**, 307-312.

Cornale P., Rosanò P. Eds. (1994) Le pietre tenere del vicentino: uso e restauro. Ed. Padova.

Crnković B., Jovičić D. (1993) Dimension stone deposits in Croatia. *Rudarsko-geološko-naftni zbornik*, **5**, 139-163.

Cucchi F., Pirini Radrizzani C., Pugliese N. (1987) The carbonete stratigraphic sequence of the Karst of Trieste (Italy). *Memorie Società Geologica Italiana,* **40,** 35-44.

Di Battistini, G., Vernia, L., Zucchi, D., Modena, M., Ronchini, R. (2005) Il marmo Botticino classico. Nuovi dati sulla caratterizzazione fisico-meccanica di questo importante materiale lapideo ornamentale. *L'informatore del marmista*, **44-518,** 25-34.

Di Benedetto C., Cappelletti P., Favaro M., Graziano S.F., Langella A., Calcaterra D., Colella A. (2015) Porosity as key factor in the durability of two historical building stones: Neapolitan Yellow Tuff and Vicenza Stone. *Eng Geol*, **193**, 310-319.

Dunda S., Kujundžić T. (2004) Historical review of exploitation and utilization of stone in Croatia. In Přykril R. (Eds) Proceedings of the Congress "Dimension stone-New Perspectives for a Traditional Building Material. Prague,14-17 June, 29-34.

Dunham, R. J. (1962) Classification of carbonate rocks according to depositional texture. In Ham, W. E. (Eds), Classification of Carbonate Rocks. *American Association of Petroleum Geologists, Memoir,* **1**, 108-121.

Fassina V., Cherido M. (1985) The Nanto stone deterioration and restoration of Loggia Cornaro in Padova. Preprints of the Vth Int. Congr. Deterioration and Conservation of Stone, Lausanne, 313-324.

Folk, R.L. (1959) Practical petrographic classification of limestones. *AAPG BULL*, **43**, 1-38.

Geometrante R., Almesberger D., Rizzo A. (?) Characterization of the State of compression of Pietra d'Istria elements by non - destructive ultrasonic technique http://www.ndt.net/article/wcndt00/papers/idn173/idn173.htm

Ginevra M., Saralli M., Sedea R. (1999) Il bacino estrattivo dei Colli Berici. Assessorato alle politiche per l'ambiente, Regione del Veneto, Giunta Regionale; Quaderno n°1, Venezia.

Govindaraju K. (1994) Compilation of working values and sample description for 383 geostandards. *Geostandards Newsletter*, **18** (Special Issue), 1-158.

Hastings D.W., Emerson S.R., Erez J., Nelson B.K. (1996) Vanadium in foraminiferal calcite. Evaluation of a method to determine paleo-seawater vanadium concentrations. *Geochim Cosmochim Acta*, **60**, 3701-3715.

Lazzarini L. (2012) Pietra d'Istria: quarries, characterization, deterioration of the stone of Venice. In Proceeding of the 12th Congress on the Deterioration and Conservation of Stone, New York. Unpublished, http://iscs.icomos.org/pdf-files/NewYorkConf/lazzarin.pdf

Martire L. (1996) Stratigraphy, facies and synsedimentary tectonics in the Jurassic Rosso Ammonitico Veronese (Altopiano di Asiago, NE Italy). *Facies*, **35-1**, 209.

Martire L., Clari P., Lozar F., Pavia G. (2006) The Rosso Ammonitico Veronese (Middle-Upper Jurassic of the Trento Plateau): a proposal of lithostratigraphic ordering and formalization. *Riv Ital Paleontol S,* **112,** 227-250.

Matteucci R., Russo A. (2005) The Middle Eocene siliceous sponges from Val di Chiampo (Lessini Mountains, northern Italy). *Annali dell'Università di Ferrara, Mus. Sci. Nat*., special volume.

Marchesini B., Biscontin G., Frascati S. (1972) Alterazione delle pietre tenere dei colli Berici. Atti XXVI Congresso A.T.I., Roma, 1-23.

Massari F., Medizza F., Sedea R. (1976) L'evoluzione geologica dell'area euganea tra il Giurese superiore e l'Oligocene inferiore. *Mem Ist Geol Min Univ Padova*, **30**, 174-197.

Meccheri M., Molli G., Conti P., Blasi P., Vaselli L. (2007) Carrara marble (Alpi Apuane, Italy): a geological and economical updated review. *Z Dtsch Ges Geowiss,* **158,** 719-735.

Mietto P. (1988) Aspetti geologici dei Monti Berici. In "I Colli Berici-Natura e Civiltà". Ed. Signum, Vicenza, 13-23.

Papazzoni C. A. (1995) Nummulite biostratigraphy at the Middle/Upper Eocene boundary in the northern Mediterranean area. *Rivista italiana di paleontologia e stratigrafia*. **101 – 1**, 63–80.

Pivko D. (2003) Natural stone in Earth's History. *Acta Geologica Universitatis Comenianae*, **58**, 73-86.

Rodolico F. (1953) Le pietre delle città d'Italia. Ed. Le Monnier, Firenze.

Siegesmund S., Snethlage R. (2014) Stone in Architecture. Ed. Springer, London.

Šimunić Buršić M., Aljinović D., Cancelliere S. (2007) Kirmenjak – Pietra d'Istria: a preliminary investigation of its use in Venetian architectural heritage. *Geol Soc London Spec Publ*, **271**, 63-68.

Schirolli P. (1997) La successione liassica nelle Prealpi Bresciane centro-occidentali (Alpi Meridionali, Italia): stratigrafia, evoluzione paleogeografico-strutturale ed eventi connessi al rifting. *Atti Ticinensi di Scienze della Terra. Serie Speciale*, **6**, 5-137.

Vernia L., Zucchi D., Modena M. (2005) Il marmo Botticino classico - Classic Botticino Marble. *L'informatore del marmista*, **43-515,** 39-47.

Winterer E. L., Bosellini, A. (1981) Subsidence and sedimentation on Jurassic passive continental margin, Southern Alps, Italy. *AAPG Bulletin*, **65-3,** 394-421.

Part 2: Combined multi-analytical approach to the characterization of the pore system in different carbonate rocks

ABSTRACT

Porosity is the main element which correlates building materials and their environment (especially in cases of aggressive weathering, e.g. salt crystallization and freeze-thaw cycles) and, therefore, it is an important parameter to evaluate and predict the durability of stone. Various studies combine different techniques to study porosity for a better estimation, but they are all affected by different instrumental limitations, that give in some cases different results.
In this work twelve different carbonate rocks, differing in composition and grain size and commonly used as building materials in Northern Italy and Tuscany were analyzed using a combined multi-analytical approach. The comparison of results obtained from different analytical methods (mercury intrusion porosimetry, 2D and 3D analysis of SEM-BSE images and micro-computed tomography reconstruction), in defined "overlapping ranges" of porosity allow a realistic reconstruction of porosity, overcoming the specific instrumental limitations and achieving a complete and more realistic knowledge of the pore system of the different building stones.

Highlights

- Porosity of various building materials used in Built Heritage is analyzed

- Results obtained from different techniques are merged together

Keywords

Porosity, Pore system, Carbonate rocks, Combined Techniques, Image analysis, Mercury Intrusion Porosimetry, micro-CT, 2D and 3D digital image reconstruction, pore morphology, pore quantification

1. Introduction

Porosity and pore structure mostly affect the physical and mechanical properties of building materials (Fitzner 1994, Manganelli Del Fa 2002, Winkler 2003).
The pore system, indeed, connects the building material with the environment allowing the circulation of water and of chemical species dissolved in it, responsible for several physical, chemical and biological deterioration processes affecting the durability of stones (Corvo et al. 2010, Di Benedetto et al. 2009). The most important stone deterioration processes with damage dependent on the pore structure of the material subjected to stone decay are: salt cry- and decrystallization cycles (Arnold e Zehnder 1990, Rodriguez-Navarro & Doehne 1999, Scherer 1999, Charola 2000, Doehne 2002, Sawdy & Price 2004, Steiger 2005, Cardell et al. 2008), freeze-thaw cycles (Nicholson & Nicholson 2000, Ruedrich & Siegesmund 2007, Grossi et al. 2007, Ruedrich et al. 2011), and the formation of gypsum crusts (Bugini et al. 2000).
Although porosity often represents a weakness factor especially for the stone decay processes, it also provides some favorable features for their implementation in building construction such as workability and thermal and acoustic insulation (Fitzner 1994, Di Benedetto 2002).
The study of the pore system of building and ornamental stones, as well as that of their composition and texture, is important because it permits to determine their behavior under stressed conditions and,

therefore, to estimate their durability (Benavente et al. 2004). Thus, this also allows the planning of more effective maintenance activities thanks to a better understanding and prediction of the decay processes.

Different pore size classifications are reported in literature (De Quervain 1967, Choquette & Pray 1970, Dubinin 1979, Gregg & Sing 1983, Klopfer 1985, Kodikara et al. 1999). By the typology of materials studied, this work refers to the classification created by De Quervain (1967) and reported by Siegesmund & Dürrast (2011) in which pores are divided into:

- micropores (radius < 5 μm);
- mesopores (radius: 5-200 μm);
- macropores (radius: 200-2000 μm).

As reported in literature, in carbonate rocks, the porosity and pore space distribution is subject to great variation. In metamorphic rocks, interlocking calcite grains of crystalline marble have a pore space of 0.5 % or less (Winkler 1994).

Limestone has a greater water retention than marble due to its greater porosity (Baedecker & Reddy 1993).

Porosity in carbonate rocks results from many processes, both depositional and post-depositional. Several mechanisms appear particularly important in producing or changing porosity and pore size distribution in carbonate rocks. Primary interparticle porosity is formed by the deposition of well-sorted calcareous sand or gravel under the influence of strong currents or waves, or by local production of calcareous sand-sized particles with sufficient rapidity to deposit particle on particle, with little or no interstitial mud. Dissolution of interstitial mud in calcareous sand may produce micro-vuggy secondary porosity resembling interparticle pore space. An initial pore with a primary porosity may be enlarged by dissolution or reduced in volume by cementation to give a secondary porosity, and certain pores may be created solely by secondary diagenetic processes. Simple cementation by calcite, anhydrite or dolomite destroys porosity and pore size. Calcite cement appears to be especially common where the particles are monocrystalline. Primary structures are produced by the formation of a rigid or semi-rigid framework which may be organic or inorganic, and inter-framework pockets may be filled with sediment or, later, with cement (Benchiarin 2007).

Different analytical techniques have been developed for the measurement, description and quantification of pore structures in rocks and porous materials (Anovitz & Cole 2015): digital analysis of SEM-BSE images (Dal Sasso et al. 2014, Coletti et al. 2016), and of photomicrographs and scansions (Grove & Jerram 2011), Mercury Intrusion Porosimetry (MIP) (Leòn y Leòn 1998; Giesche 2006), water absorption (Molina et al., 2015), Nitrogen Adsorption (Rigby et al. 2004, Zong et al. 2015), X-ray Computed micro-Tomography (micro-CT) (Cnudde et al. 2009, Noiriel 2015), Small Angle Neutron Scattering (SANS) (Barbera et al. 2014), NMR microscopy (Rijniers et al. 2005).

Different results can be obtained when using diverse techniques, so several studies combine various techniques for the estimation of stone porosity (Barbera et al. 2014, De Boever et al. 2015). In this work 2D analysis of thin sections through SEM, MIP and 3D reconstruction by micro–CT will be combined and compared by them, in order to determine the pore system and their relative abundance in the sample, following the procedure suggested by Coletti et al. (2016).

This multi-analytical approach method can provide a realistic reconstruction of the pore system.

Materials & Methods

2.1. Sample materials

The studied stone materials were 12 different types of carbonate rocks, frequently used as building materials in historical monuments and constructions of Northern Italy. These stones come from different geological formations outcropping in northeastern Italy and in Tuscany region. The selected rocks were: Vicenza Stone (Nanto and Costozza varieties), Istria Stone, Chiampo Stone (Porfirico and Ondagata varieties), Red and Brown Verona Stone, Pink and White Asiago Stone, Carrara marble, Aurisina Stone, Botticino Stone. Geological classification, chemical-mineralogical-petrographical characteristics are described in detail in Part 1) and here are summarized in Tables 1 and 2.

Table 1. *Summary of classification, geological formation of provenance and geological age of the carbonate rocks considered here. Sample abbreviations are: BO = Botticino, C = Chiampo Ondagata, R= Red Verona Marble, B= Brown Verona Marble, A = Pink Asiago, E= White Asiago, O= Istria, M= Carrara marble, P= Chiampo Paglierino, PE= Chiampo CWGC, AU = Aurisina, N= Nanto, V= Vicenza (Costozza variety).*

Sample	Rock type	Folk classification	Kendall/Folk classification	Dunham classification	Geological Formation	Geological Age
M	Carrara Marble	---	---	Crystalline carbonate	Tuscan Nappe	Cretaceous
BO	Botticino Stone	---	---	Crystalline carbonate	Corna Formation,	Upper – Lower Jurassic
B	Brown Verona S.	Biomicrite	Intramicrite	Wackestone	Rosso Ammonitico Veronese	Middle – Late Jurassic
R	Red Verona S.	Biomicrite	Intramicrite	Wackestone	Rosso Ammonitico Veronese	Middle – Late Jurassic
P	Chiampo Paglierino S.	Biomicrite	Intramicrite	Packstone/Grainstone	Nummulitic Limestone	Middle Eocene
C	Chiampo Ondagata S.	Biomicrite	Intramicrite	Packstone/Grainstone	Nummulitic Limestone,	Middle Eocene
E	White Asiago S.	Biomicrite	Oomicrite	Wackestone	Majolica Veneta	Lower Cretaceous
A	Pink Asiago S.	Biomicrite	Oomicrite	Wackestone	Majolica Veneta	Lower Cretaceous
N	Nanto S.	Biomicrite	Biomicrite	Packstone	Soft Stone of Berici Hills	Lower Eocene
V	Costozza S.	Biomicrite	Biomicrite	Pakstone	Soft Stone of Berici Hills	Lower Eocene
AU	Aurisina S.	Biomicrite	Biomicrite	Packstone	Friuli Platform Domain	Cretaceous
O	Orsera S.	Micrite	Dismicrite	Mudstone	Friuli Platform Domain	Cretaceous

1.2.Analytical techniques

The pore system of limestones was studied combining different techniques to characterize the pore system and overcome their differences and limitations:

1. Mercury Intrusion Porosimetry (MIP) performed at the Department of Chemistry, Life Sciences and Environmental Sustainability, University of Parma, Italy.
2. Digital Image Analysis (DIA) of back-scattered (BSE) images acquired by Scanning Electron Microscopy (SEM), Department of Geosciences, Padua, Italy.
3. X-ray micro-Computed Tomography (micro-CT), Department of Geosciences, Padua, Italy)

Pore size and pore distribution in the range for each technique is different:

1. MIP: 0.006–970 μm.
2. > 0.5 μm (limit of resolution: 0.5 μm = 1 pixel) for DIA of SEM-BSE images
3. > 4.75 μm (limit of resolution: 4.75 μm = 1 pixel) for micro-CT (1 voxel = 107 μm^3)

Table 2. *XRPD and XRF results. Regarding XRF results below are reported only percentage of major elements and Loss on ignition (LOI). Mineral abbreviations: Cal = calcite; Qtz = quartz; Dol = dolomite, Mg-Cal=Mg-Calcite, Ms = muscovite; Ill = Illite; Plg M = palygorskyte M. Percentages obtained with RIR method. Samples abbreviations as in Table 1.*

Sample	**XRPD**	**XRF**											
		SiO_2	**TiO_2**	**Al_2O_3**	**Fe_2O_3**	**MnO**	**MgO**	**CaO**	**Na_2O**	**K_2O**	**P_2O_5**	**L.O.I.**	**TOT**
A	98% Cal, 2% Qtz	1.09	0.01	0.25	0.18	0.03	0.27	54.65	0.01	0.05	0.04	42.85	99.42
AU	100% Cal	0.01	0.01	0.01	0.02	0.01	0.16	56.13	0.01	0.01	0.01	42.97	99.32
B	94% Cal, 4% Ill, 2% Qtz	2.45	0.04	0.72	0.49	0.13	0.30	53.01	0.01	0.13	0.13	42.01	99.44
BO	57% Cal, 43% Dol	0.04	0.01	0.06	0.03	0.01	10.07	47.57	0.01	0.01	0.01	41.53	99.33
C	66% Cal, 34% Mg-Cal, traces Plg M	0.35	0.02	0.12	0.12	0.01	0.53	54.70	0.01	0.01	0.03	43.47	99.38
E	97% Cal, 3% Qtz	1.13	0.01	0.26	0.15	0.02	0.29	54.57	0.01	0.05	0.06	42.78	99.32
M	100% Cal, traces Ms	0.01	0.01	0.05	0.02	0.01	0.83	57.83	0.01	0.01	0.01	40.21	98.99
N	95% Cal, 5% Ill	2.66	0.23	0.92	1.18	0.01	0.50	52.11	0.01	0.31	0.04	41.71	99.67
O	100% Cal	0.28	0.01	0.16	0.06	0.01	0.20	55.89	0.01	0.03	0.01	43.17	99.82
P	61% Cal, 38% Mg-Cal, 1% Plg M	0.71	0.02	0.18	0.14	0.02	0.57	54.40	0.01	0.01	0.03	43.30	99.39
R	100% Cal	0.42	0.01	0.20	0.18	0.01	0.26	55.26	0.01	0.05	0.07	43.14	99.60
V	100% Cal	0.16	0.01	0.11	0.20	0.01	0.28	55.48	0.01	0.02	0.03	43.25	99.55

2.2.1. Digital Image Analysis (DIA) of SEM-BSE Images

SEM-BSE images obtained from the analysis of thin sections are a suitable alternative to traditional optical methods and this is an efficient technique in quantifying the porosity of geo-materials. DIA of SEM – BSE images is a direct technique that permits the measurements of total (close + open) porosity, shape and size of the pores.

The thin sections were described acquiring a matrix of 30 x 40 BSE overlapping (25%) images with a resolution of 1280 × 1024 pixels at a magnification of 200X acquired with a CamScan MX 2500 microscope, equipped with a LaB_6 cathode, operating at 20 kV and working distance (WD) of 20mm. The 1200 images obtained on each thin section, were merged together through a two-step procedure:

- 12 groups of about 100 images were merged by Microsoft ICE Software obtaining 12 images.
- the merged jpg images were then elaborated (manual deblur) and mostly manually stitched together (software used: PS).

Finally, the grey-scale images were segmented, binarised and analised using ImageJ software.

Analysis of pore size is based on the measure of the Feret diameter, defined as the distance between the two parallel planes restricting the object perpendicular to that direction in 2D.

2.2.2. X-Ray micro-Computed Tomography (micro-CT)

Stone sample micro-cores (diameter = 8 mm, length = 20 mm) were analyzed with a bench-top Skyscan 1172 micro-CT scanner (Bruker®) at the Department of Geosciences of the University of Padua.

The scanner is equipped with a Hamamatsu 100/250 microfocus X-ray source, operating at an acceleration voltage of 74 kV and a beam current of 133 μA, with a Hamamatsu C9300 10 megapixel camera (pixel size 8.5 μm) filtered by 0.5 mm Al foil. Projection images were acquired every 0.3° over 360° rotation with exposure time of 2500 ms and camera binning of 2 × 2, averaging 8 frames in vertical random movement mode to minimize noise, and connecting 3 scans to cover the entire vertical length of the cores. The run time for each scan was about 21 h. Cross-section slices were reconstructed from raw projection images with the NRecon software (Bruker®), with application of thermal correction, misalignment compensation, ring artefact reduction and beam hardening correction, yielding voxel edges of 4.75 μm, corresponding to a minimum volume unit (voxel) of ~107 μm^3. Since in micro-CT images grey-scale values are proportional to the X-ray attenuation coefficient, which is a function of the mean atomic number of the specific voxel, porosity was segmented by thresholding tomographic images with the CT-Analyser software (Bruker®), which yielded binary image stacks.

Image quantification involves correctly skeletonising the body of the sample, on the X-ray absorption coefficient contrast, and segmenting the solid by the porous phases.

After segmentation, porosity was calculated as the ratio of the number of voxels of the pores (pore-voxels) to the total volume of interest (VOI) as follows:

$PT=Npv/Npv+Nsv$

where Npv is the number of pore-voxels (white) and Nsv is the number of solid-voxels (black).

Structural thickness is the parameter used to measure pore-size diameters and distribution, and to characterize the three-dimensional (3D) pore structure. It is based on the approach to fit maximal spheres inside the structure, and then set the value of the largest sphere contained in it.

2.2.3. Mercury Intrusion Porosimetry (MIP)

Mercury Intrusion Porosimetry (MIP) is a powerful technique used to evaluate effective open porosity and pore-size distribution, total pore area, average pore diameter, tortuosity (Leon y Leon 1998, Fusi & Martínez-Martínez 2013). Since closed pores are not considered in MIP analysis as they cannot be filled by mercury, the technique is considered an "indirect" method based on the movement of fluids inside the material and it evaluates only interconnected pores.

MIP is based on the principle that a non-wetting liquid, with a contact angle greater than 90°, will intrude capillaries under specific pressure and according to the following Washburn's equation pore volume and size distribution is automatically calculated (Pirard et al. 2002):

$P_{(l)}+P_{(g)}= 4\sigma\cos\theta/2D_p$

where $P_{(l)}$ is the pressure of the liquid (in this case, mercury), $P_{(g)}$ the pressure of the gas in the pores (approximated to 0 atm in initial vacuum conditions), σ the surface tension of the liquid, θ the contact angle of intrusion of the liquid (generally between 135° and 142° for mercury) and D_p is the pore diameter.

MIP have been widely used to analyze the pore structure of materials with pore ranging from 360 to 0,0055 μm.

The technique is still used although the toxicity of mercury. Expensive waste management costs are balanced by using high sensitivity instruments and small samples (about 2 cm^3). In a mercury-free future some porosimetry instruments running with other wetting liquids such as that used by Jena and Gupta (2001) can become normal routine but in this study a reference technique is necessary and consequently the use of MIP is motivated.

In this study MIP was performed at the Department of Physics and Earth Sciences of the University of Parma using a PoreMaster 33 system (Quantachrome Instruments®) with the following parameters: sample cell is 1.0 × 3.0 cm in size and 2 cm^3 in volume, pressure range is 0.5–33.000 psi, contact angle (θ) of mercury is 140°, and surface tension (σ) of mercury is 0.48 N/m (480 dyn/cm), pore size range is from 0.0064 to 950 μm.

Dry density of materials was measured trough a picnometer Ultrapic 1200. The considered value of density was the mean of 10 measures.

Before the measurements, samples were dried at 40°C for 24h and then about 2 g (i.e. a little core with 8 mm diameter and 2 cm length) of material was analyzed. Sample was first degassed and then intruded by mercury, a non-wetting liquid. Since mercury is a non-wetting liquid, it does not spontaneously penetrate pores by capillary action, but it must be forced by external pressure. The required pressure is inversely proportional to the size of the pores. First mercury fills larger pores and then, when the pressure increases, it fills the smaller ones. Assuming a contact angle of 140° and a surface tension of 480 dyne cm^{-1}, a pressure of about 206 MPa is required for mercury to access pores as small as 0.006 μm.

Although MIP is widely used, it has two important limitations: the assumption that pores are perfectly cylindrical in shape, and that mercury moves from larger pores to smaller ones, discarding the opposite case, i.e., pores with the so-called "ink-bottle" morphology. Therefore, mercury enters voids at a pressure determined only by the size of their entry points, and not the true size of the pore itself. In addition, at high intrusion pressures (exceeding 414 MPa) pore structure may be damaged, distorting the pore range distribution with an artificial increase in the small pore fraction.

Permeability (K) of the two samples was also estimated from porosimetry results by using the following equation (Lowell et al., 2004) implemented in the Quantachrome software:

$K=\phi \cdot d2/32$

where ϕ is the total porosity, and d the average pore size.

3. Results – Discussion

3.1. 2D- DIA of 200x SEM – BSE images.

This procedure was based on the results obtained by precedent researches that reported the poor representativness of a single BSE image when dealing with complex and heterogeneous pores, in terms of both pore size and distribution (Coletti et al. 2016).

The values of total porosity, maximum pore diameter and circularity are reported in Table 3. The samples with the highest porosity values are the two varieties of Vicenza Stone: Nanto (N, 25.08%) and Costozza (V, 17.33%). On the other hands the values of total porosity of nodular limestones such as Verona Stone (sample B) and Asiago Stone (sample E) varieties are very low and generally below 0.25%.

Crystalline carbonates have intermediate values: Botticino stone (BO) has 4.34 % of porosity, while Carrara marble has an amount of 2.11% of pores.

All samples show a mean diameter value between 1 and 5 µm (Table 4), suggesting the abundance of micropores (De Quervain 1967, Siegesmund & Dürrast 2014).
Pore shape is generally anisotropic, as suggested by the great difference in the aspect ratio between max Feret diameter and the mean Feret diameter. Sample A present more homogeneous and rounded pores, while others present generally anisotropic shape, in particular the samples N and V. The elongated shape of pores is also confirmed by values of circularity obtained by ImageJ processing data. Indeed, the circularity parameter is expressed as $c=4\pi (A/P^2)$ where A and P are the area and the perimeter of each pore, respectively. This factor falls between 0 (perfectly elongated shape) and 1 (perfectly circular shape). Samples do not show significant differences in circularity parameters among them. All specimens showed a circularity value of 0.17 -0.18 (Table 3) thus implying that the pores have mostly an elongated shape.

Table 3. *Main parameters related to porosity as obtained from 200X SEM-BSE images. Total porosity is expressed as percentage, maximum pore diameter is the max value of the minFeret and it is reported in µm. Samples abbreviations as in Table 1.*

	SEM-BSE (DIA)			
Sample	**%tot > 0.5 µm**	**Ø max (µm)**	**Ø mean (µm)**	**Circularity**
A	0.17	6.801	3.41	0.17
AU	0.62	235.4	1.77	0.17
B	0.03	134.94	3.39	0.18
BO	4.34	607.89	4.29	0.17
C	1.72	112.26	1.39	0.17
E	0.24	319.29	2.43	0.17
M	2.11	233.51	1.70	0.17
N	25.08	2067.75	3.78	0.17
O	0.42	169.91	2.79	0.17
P	0.95	285.78	2.29	0.17
R	0.64	181.81	1.61	0.17
V	17.33	584.17	1.03	0.17

Table 4 reports the distribution of pore size for each range expressed as percentage of porosity, while Table 5 represents the pore distribution expressed as total porosity percentage. In these tables and in Figure 1 it is evident that the highest percentages of pores are in the range 0.5-25 µm for all samples and there is a bimodal distribution with a first peak between 0 and 2 µm, and a second one between 5 and 7 µm. (Table 5)
Samples N and V show highest percentages at bigger ranges of pores (200-250 µm and 250-360 µm). Indeed, more than 50% of the total porosity of the sample N and more than 30% of the sample V (Table 4) is comprised above 250 µm pore-size.

Table 4. *2D- DIA of 200x SEM – BSE images. Pore size distribution range expressed as percentage of total porosity. Samples abbreviations as in Table 1.*

pore range (µm)	A (%)	AU (%)	B (%)	BO (%)	C (%)	E (%)	M (%)	N (%)	O (%)	P (%)	R (%)	V (%)
0.5-5	12.73	48.36	28.54	10.39	78.88	41.55	54.45	5.32	19.92	37.61	51.87	12.15
5 - 25	56.71	34.12	41.53	40.47	17.21	38.10	23.36	12.98	39.64	39.08	27.65	12.14
25-50	5.08	6.85	14.02	20.75	1.13	8.18	5.35	8.64	15.82	9.52	5.48	7.69
50-70	25.47	1.84	3.55	8.15	0.28	4.16	3.66	5.48	7.00	3.81	2.33	5.60
70-100	0.00	2.93	0.84	6.02	0.49	0.00	4.05	6.18	8.67	1.93	5.20	8.44
100-150	0.00	0.95	11.53	5.83	0.19	5.04	5.95	8.49	6.48	2.94	3.17	12.44
150-200	0.00	0.00	0.00	2.30	1.84	0.00	1.17	6.72	2.46	1.84	4.31	11.41
200-250	0.00	4.95	0.00	0.98	0.00	0.00	2.01	5.88	0.00	1.25	0.00	10.26
250-360	0.00	0.00	0.00	5.11	0.00	2.99	0.00	25.07	0.00	2.02	0.00	8.53
>360	0.00	0.00	0.00	0.00	0.00	0.00	0.00	19.47	0.00	0.00	0.00	5.11

Table 5. *2D- DIA of 200X SEM – BSE images. Pore size distribution expressed as total porosity. Samples abbreviations as in Table 1.*

pore range (µm)	A (%)	AU (%)	B (%)	BO (%)	C (%)	E (%)	M (%)	N (%)	O (%)	P (%)	R (%)	V (%)
0.5-5	0.02	0.30	0.01	0.45	1.36	0.10	1.15	1.33	0.08	0.36	0.33	2.11
5-25	0.10	0.21	0.01	1.76	0.30	0.09	0.49	3.25	0.17	0.37	0.18	2.10
25-50	0.01	0.04	0.00	0.90	0.02	0.02	0.11	2.17	0.07	0.09	0.04	1.33
50-70	0.04	0.01	0.01	0.35	0.00	0.01	0.08	1.37	0.03	0.04	0.01	0.97
70-100	0.00	0.02	0.00	0.26	0.01	0.00	0.09	1.55	0.04	0.02	0.03	1.46
100-150	0.00	0.01	0.00	0.25	0.00	0.01	0.13	2.13	0.03	0.03	0.02	2.16
150-200	0.00	0.00	0.00	0.10	0.03	0.00	0.02	1.69	0.01	0.02	0.03	1.98
200-250	0.00	0.03	0.00	0.04	0.00	0.00	0.04	1.47	0.00	0.01	0.00	1.78
250-360	0.00	0.00	0.00	0.22	0.00	0.01	0.00	10.11	0.00	0.02	0.00	3.44
>360	0.00	0.00	0.00	0.00	0.00	0.00	0.00	7.85	0.00	0.00	0.00	2.06

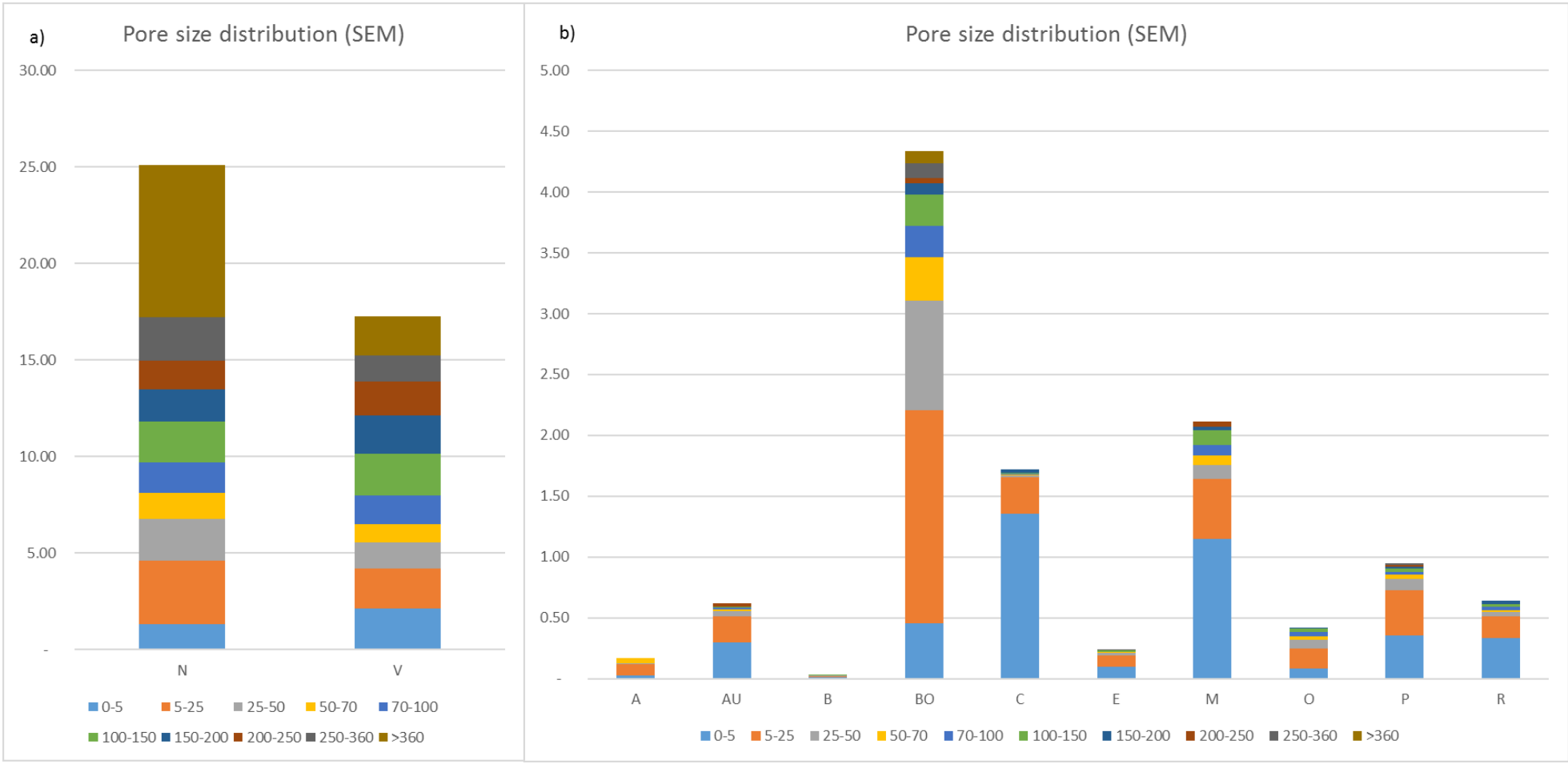

Figure 1. *Pore size distribution obtained from 2D analysis of 200X SEM-BSE images. Samples abbreviations as in Table 1.*

3.2.3D- DIA of micro-CT

The stack of binarised images, obtained for each sample core, was 3D analyzed by CTAn® after reconstructing by NRecon®. Total porosity was lower than that obtained by SEM – BSE images but very similar, with porosity values comprised between 0.25 and 1.5 %. Marbles (BO and M) in this case have smaller porosity than in samples analyzed by 2D DIA, with total values respectively of 1.03 and 0.04% of total porosity. This is probably due to the different threshold limit adopted by the 2D and 3D digital imaging, 0.5 µm for SEM-EBS and 4.75 µm for micro-CT. Observing pore range distribution (Tables 7, 8 and 9), this is confirmed by the most abundance of pores in sizes < 20 µm and the micro-scale that characterizes the pore system of these type of rocks. The highest values are for samples N and V, referring to the Vicenza stones, which have 8.96 ad 13.54% of total porosity, following the same trend already showed in the 2D imaging analysis. Elongated shape of the pores is confirmed, in particular in sample AU, BO, N and V. Indeed, these last have a maximum diameter (Table 6) with a significant discrepancy (with values above 100 µm) with the abundance and distribution of pores in the smallest range (4.75-24 µm) (Table 8, Figure 2).

The Fractal Dimension (FD) is an indicator of the surface complexity of an object and has dimension between 2 and 3. The found values of the analyzed samples fell between 2.36 and 2.86, and they confirm the true fractal behavior of the pore system.

Table 6. *Main porosity parameters as obtained from micro-CT. Ø max is the max value of structural thickness, FD is the fractal dimension. Samples abbreviations as in Table 1.*

	micro-CT		
Sample	**%tot (>4.75 µm)**	**Ø max (µm)**	**FD**
A	0.28	23.72	2.69
AU	1.20	270.42	2.46
B	0.07	71.16	2.36
BO	1.30	147.07	2.63
C	1.50	33.21	2.86
E	1.04	33.21	2.83
M	0.04	33.21	2.28
N	8.96	308.37	2.72
O	1.07	90.14	2.80
P	0.73	33.21	2.80
R	0.27	42.70	2.69
V	13.54	241.95	2.85

Table 7. *Percentage of the pore size distribution obtained with micro-CT analysis. Sample abbreviations as in Table 1.*

Pore size diameter (µm)	A (%)	AU (%)	B (%)	BO (%)	C (%)	E (%)	M (%)	N (%)	O (%)	P (%)	R (%)	V (%)
4.75 - 14.23	99.62	15.40	97.85	64.92	97.21	98.93	99.69	40.79	85.60	97.27	99.68	21.14
14.24 - 23.72	0.37	21.24	1.81	28.64	2.7	1.06	0.30	32.93	12.34	2.73	0.31	26.37
23.73- 33.21	0	14.09	0.05	4.08	0.02	0.00	0.00	9.98	1.55	0.00	0.00	13.08
33.221 -42.70	0	13.05	0.02	1.33	0	0	0	6.08	0.31	0	0.00	11.15
42.71 -52.19	0	9.15	0.05	0.42	0	0	0	3.14	0.09	0	0	7.65
52.20 -61.67	0	6.08	0.07	0.18	0	0	0	1.71	0.04	0	0	4.97
61.68 -71.16	0	5.13	0.15	0.10	0	0	0	1.323	0.03	0	0	4.36
71.17 -<80.65	0	3.57	0	0.09	0	0	0	0.90	0.03	0	0	3.11
80.66 -<90.14	0	2.51	0	0.04	0	0	0	0.62	0.013	0	0	2.13
90.15 -<99.63	0	1.96	0	0.05	0	0	0	0.50	0	0	0	1.63
99.64 -<109.11	0	1.59	0	0.03	0	0	0	0.46	0	0	0	1.19
109.12 -<118.60	0	1.21	0	0.01	0	0	0	0.26	0	0	0	0.83
118.61 -<128.09	0	0.95	0	0.02	0	0	0	0.25	0	0	0	0.63
128.10 -<137.58	0	0.89	0	0.02	0	0	0	0.24	0	0	0	0.45
137.59 -<147.07	0	0.49	0	0.07	0	0	0	0.16	0	0	0	0.30
147.08 -<156.56	0	0.39	0	0	0	0	0	0.15	0	0	0	0.21
156.57 -<166.04	0	0.4	0	0	0	0	0	0.11	0	0	0	0.18
166.05 -<175.53	0	0.24	0	0	0	0	0	0.15	0	0	0	0.13
175.54 -<185.02	0	0.22	0	0	0	0	0	0.08	0	0	0	0.15
185.03 -<194.51	0	0.35	0	0	0	0	0	0.04	0	0	0	0.10
194.52 -<204.00	0	0.15	0	0	0	0	0	0.01	0	0	0	0.07
204.01 -<213.49	0	0.14	0	0	0	0	0	0.02	0	0	0	0.05
213.50 -<223.00	0	0.07	0	0	0	0	0	0.01	0	0	0	0.06
223.01 -<232.47	0	0.05	0	0	0	0	0	0.01	0	0	0	0.02
232.487 -<242.00	0	0.07	0	0	0	0	0	0.01	0	0	0	0.03
241.01 -<251.44	0	0.21	0	0	0	0	0	0.02	0	0	0	0
251.45 -<260.93	0	0.22	0	0	0	0	0	0.05	0	0	0	0
260.94 -<270.41	0	0.21	0	0	0	0	0	0	0	0	0	0

Table 8. *3D- DIA of micro-CT. Total porosity (%) in different pore size distribution ranges. Samples abbreviations as in Table 1.*

Pore diameter (µm)	A (%)	AU (%)	B (%)	BO (%)	C (%)	E (%)	M (%)	N (%)	O (%)	P (%)	R (%)	V (%)
4.75-24	100.00	36.63	99.66	93.56	99.98	100.00	100.00	73.43	97.95	100.00	100.00	47.5%
24-50	0.00	36.29	0.12	5.83	0.02	0.00	0.00	19.41	1.95	0.00	0.01	31.8%
50-70	0.00	11.20	0.22	0.28	0.00	0.00	0.00	3.16	0.06	0.00	0.00	9.3%
70-100	0.00	8.04	0.00	0.18	0.00	0.00	0.00	2.05	0.04	0.00	0.00	6.8%
100-150	0.00	5.13	0.00	0.16	0.00	0.00	0.00	1.30	0.00	0.00	0.00	3.4%
150-200	0.00	1.73	0.00	0.00	0.00	0.00	0.00	0.56	0.00	0.00	0.00	0.8%
200-250	0.00	0.54	0.00	0.00	0.00	0.00	0.00	0.02	0.00	0.00	0.00	0.1%
250-360	0.00	0.43	0.00	0.00	0.00	0.00	0.00	0.06	0.00	0.00	0.00	0.0%

Table 9. *3D-DIA of micro- CT. Pore size distribution range and value of total porosity (%). Samples abbreviations as in Table 1.*

Pore diameter (µm)	A (%)	AU (%)	B (%)	BO (%)	C (%)	E (%)	M (%)	N (%)	O (%)	P (%)	R (%)	V (%)
4,75-24	0.28	0.44	0.07	1.22	1.50	1.04	0.04	2.83	1.05	0.73	0.27	6.43
24-50	0.00	0.44	0.00	0.08	0.00	0.00	0.00	0.75	0.02	0.00	0.00	4.32
50-70	0.00	0.13	0.00	0.00	0.00	0.00	0.00	0.12	0.00	0.00	0.00	1.26
70-100	0.00	0.10	0.00	0.00	0.00	0.00	0.00	0.08	0.00	0.00	0.00	0.93
100-150	0.00	0.06	0.00	0.00	0.00	0.00	0.00	0.05	0.00	0.00	0.00	0.46
150-200	0.00	0.02	0.00	0.00	0.00	0.00	0.00	0.02	0.00	0.00	0.00	0.11
200-250	0.00	0.01	0.00	0.00	0.00	0.00	0.00	0.00	0.00	0.00	0.00	0.02
250-360	0.00	0.01	0.00	0.00	0.00	0.00	0.00	0.00	0.00	0.00	0.00	0.00

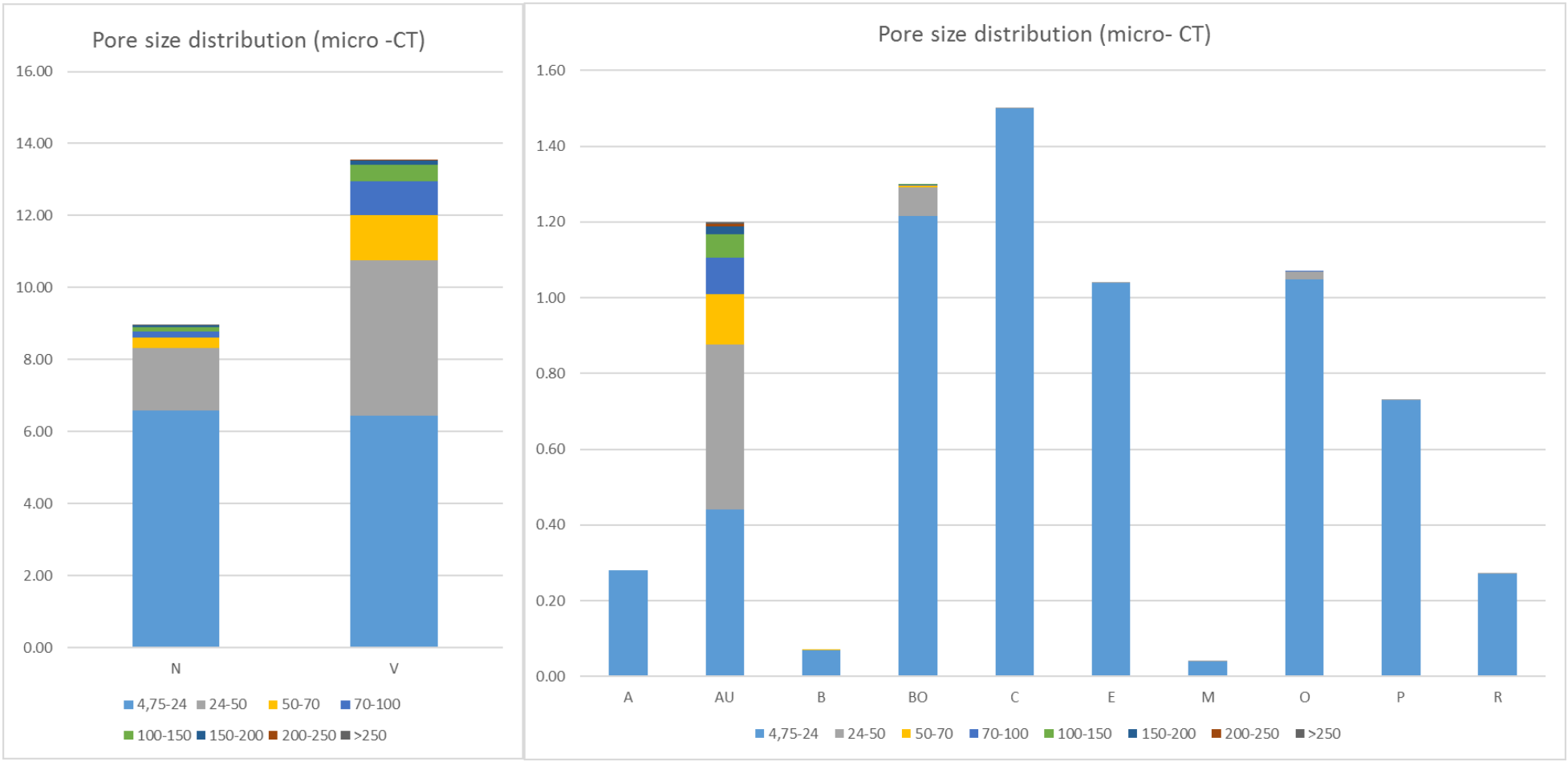

Figure 2. *Pore size distribution obtained from 3D analysis of micro-CT data. Samples abbreviations as in Table 1.*

3.1.Mercury Intrusion Porosimetry

The data, obtained through MIP, are summarized in Table 10. The pore distribution is reported in Tables 11-12 and in Fig. 3. The lowest values are measured in compact and well cemented limestones such as Brown and Red Verona stones (R and B samples, respectively), both Chiampo varieties (C and CV samples), Orsera stone (O sample) and marbles (M and BO samples). Verona and Asiago varieties seemed to be very similar by means of macroscopical analysis and other techniques (see Part 1), but the study of the porosity highlights that the porosity of Asiago limestones (A and E samples) is higher than Verona stone (R and B samples).

MIP curves that correlated porosity with diameter can be seen in Figures 5-7. The distribution is unimodal in all samples. Marbles (sample M and BO) have a critical pore size at 0.11 and 0.14 µm. wackestones and packstones have a narrow peak in a critical pore size between 0.007 and 0.07 µm, except sample O (Orsera Stone) which has his critical pore size at 9.35 µm. The largest percentage of pore, indeed, is found in the range < 0.5 µm, save for the sample O (Tables 11 and 12). Sample N and V show the highest values of porosity (27.17 and 28.52%) and a bimodal distribution of pores with a principal peak at 0.01/0.03 µm and another at 0.10/0.17 µm. This behavior in the two types of the Vicenza Stone, suggest a particular weak behavior under the typical pressures of MIP technique, which could be causes of fractures and damaging of the internal pore system, increasing total porosity and shifting the pore range distribution at a higher pores dimension, invalidating the good pores estimation.

The Figure 3 shows the volume of intruded mercury, that is plotted versus the pressure of mercury intrusion for Asiago stone (sample A). In most rock types, the extrusion curve is horizontal and mercury is completely entrapped in the sample after pressure is decreased. It means that the pores are not highly interconnected and the pore structure is quite tortuous (Barbera et al. 2012).

Bulk and real densities measured by MIP, and integrated by picnometric measurements, are very similar for all samples with values of ~2.70 g/cm^3.

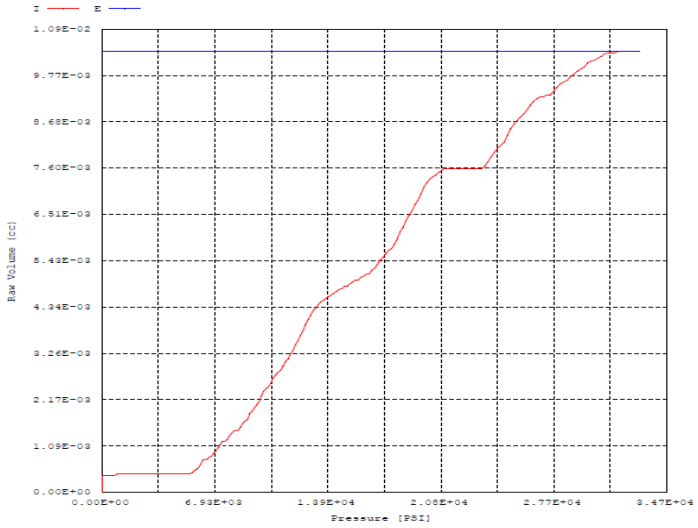

Figure 3. *Mercury intrusion (red) and extrusion (blue) curves for Asiago stone*

Table 10. *Summary of MIP results and density measurements. Samples abbreviations as in Table 1.*

	MIP						Picnometer
Sample	**OP (%)**	**Interparticle Porosity (%)**	**Intraparticle Porosity (%)**	**Ø Max (µm)**	**Bulk Density (g/cm^3)**	**Apparent Density (g/cm^3)**	**Density (g/cm^3)**
A	3.5378	1.2688	2.2690	216.472	2.6879	2.7439	2.6881±0.0080
AU	4.6061	1.0067	3.5994	272.892	2.7054	2.7941	2.7055±0.0075
B	0.0975	0.0970	0.0005	394.038	N/A	N/A	2.7209±0.0056
BO	1.7331	0.4392	1.2939	235.338	N/A	N/A	2.7669±0.0043
C	1.0399	1.0243	0.0156	216.471	2.7075	2.7040	2.7074±0.0076
E	2.2227	0.3916	1.8312	215.562	2.6823	2.7308	2.6824±0.0045
M	1.0004	0.6665	0.3340	215.562	N/A	N/A	2.7413±0.0027
N	27.1772	0.4502	24.6959	371.766	N/A	N/A	2.7890±0.0087
O	0.3929	0.3929	0.0000	211.127	2.7106	2.6978	2.7107±0.0073
P	0.3457	1.0150	0.0321	221.519	N/A	N/A	2.7085±0.0041
R	0.2559	0.1902	0.0657	379.466	2.7307	2.7305	2.7292±0.0053
V	28.5238	15.8084	12.7154	221.519	N/A	N/A	2.7369±0.0049

Table 11. *Mercury intrusion porosimetry. Pore size distribution range. Samples abbreviations as in Table 1.*

Pore diameter (µm)	A (%)	AU (%)	B (%)	BO (%)	C (%)	E (%)	M (%)	N (%)	O (%)	P (%)	R (%)	V (%)
0,0065-0,5	64.00	80.15	0.48	71.71	1.50	81.12	29.76	43.79	0.00	59.76	24.60	46.78
0,5-4,75	0.00	0.00	0.00	3.29	0.00	0.00	4.28	55.59	0.00	1.64	2.08	0.00
4,75-24	0.00	4.51	0.00	0.00	5.97	0.00	7.75	0.09	15.37	5.50	27.47	21.26
24-50	0.00	4.18	0.00	0.00	14.93	0.00	3.88	0.09	9.80	0.00	0.00	22.56
50-70	0.48	2.56	0.00	0.00	2.98	5.21	7.59	0.00	2.11	1.01	0.00	3.42
70-100	3.02	2.64	49.82	0.66	17.63	1.74	6.88	0.00	16.77	4.50	0.00	2.92
100-150	13.69	2.17	7.53	12.49	19.54	4.40	22.57	0.01	14.69	0.00	11.65	2.19
150-200	15.98	0.00	9.04	10.07	31.49	4.80	15.35	0.10	33.57	5.04	6.66	0.87
200-250	2.69	2.85	7.53	1.78	5.96	1.47	1.94	0.00	7.69	0.00	0.00	0.00
250-360	0.00	0.94	25.60	0.00	0.00	0.00	0.00	0.33	0.00	22.55	27.54	0.00

Table 12. *Mercury intrusion porosimetry. Pore size distribution range and value of total porosity (%). Samples abbreviations as in Table 1.*

Pore diameter (µm)	A (%)	AU (%)	B (%)	BO (%)	C (%)	E (%)	M (%)	N (%)	O (%)	P (%)	R (%)	V (%)
0,0065-0,5	2.27	3.695	-	1.24	0.02	1.80	0.30	11.90	-	0.21	0.06	13.34
0,5-4,75	-	-	-	0.06	-	-	0.04	15.11	-	0.01	0.01	-
4,75-24	-	0.208	-	-	0.06	-	0.08	0.02	0.06	0.02	0.07	6.06
24-50	-	0.193	-	-	0.16	-	0.04	0.02	0.04	-	-	6.43
50-70	0.02	0.118	-	-	0.03	0.12	0.08	-	0.01	0.00	-	0.98
70-100	0.11	0.122	0.05	0.01	0.18	0.04	0.07	-	0.07	0.02	-	0.83
100-150	0.48	0.100	0.01	0.22	0.20	0.10	0.23	0.00	0.06	-	0.03	0.62
150-200	0.57	-	0.01	0.17	0.33	0.11	0.15	0.03	0.13	0.02	0.02	0.25
200-250	0.10	0.131	0.01	0.03	0.06	0.03	0.02	-	0.03	-	-	-
250-360	-	0.043	0.02	-	-	-	-	0.09	-	0.08	0.07	-

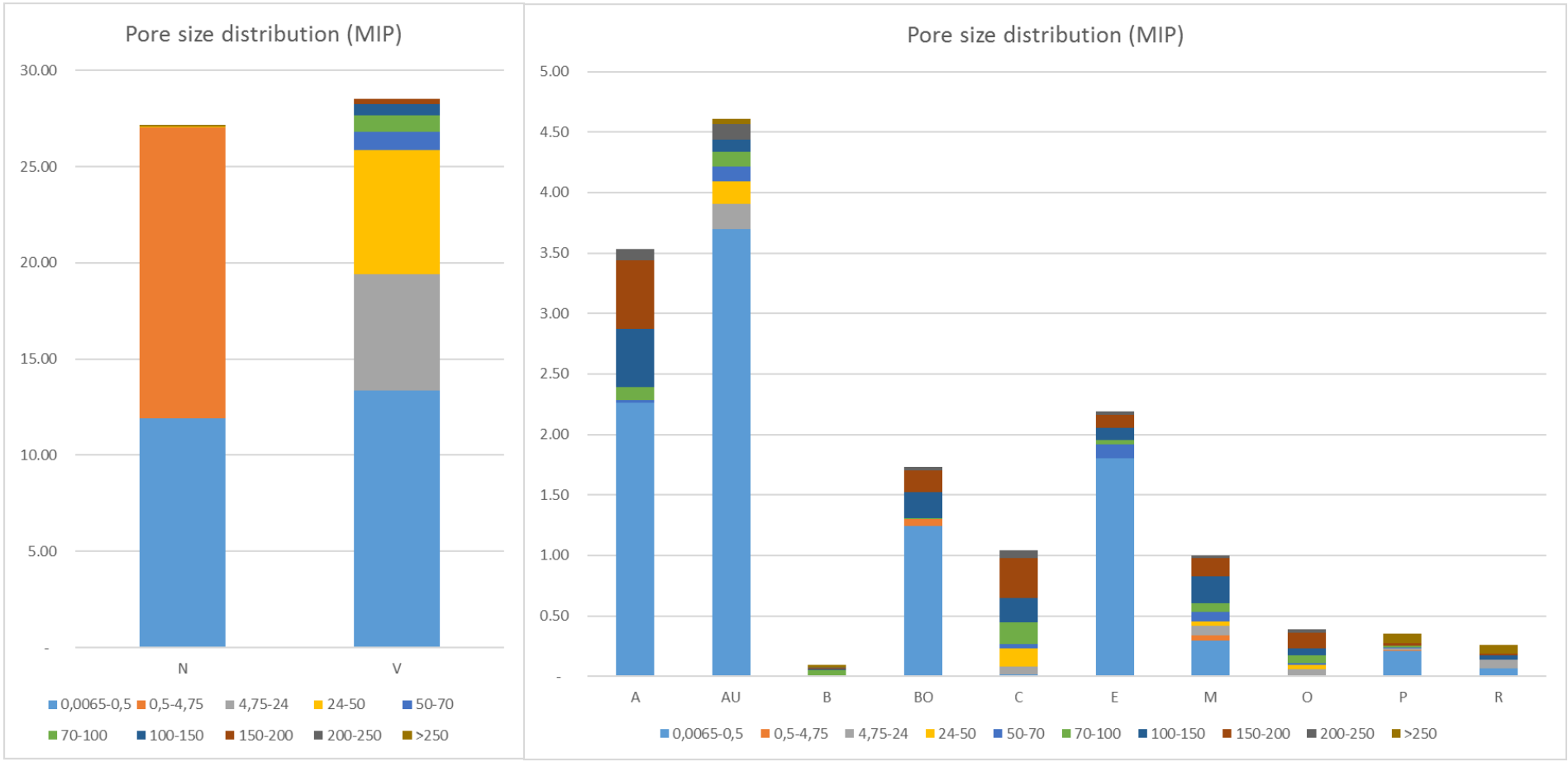

Figure 4. *Pore size distribution obtained from MIP. Samples abbreviations as in Table 1.*

3.5. Comparing techniques: cumulative curves reconstruction

In order to compare results obtained from the various techniques, the porosity fraction pertaining to a different overlapping range was extracted from the pore-size distribution curves of the various techniques used (Coletti et al. 2016).
In our study two overlapping pore ranges were examined:

1) pores between 0.5 and 4.75 μm, giving partial results extrapolated by MIP and DIA of 200x SEM-BSE images
2) pore between 4.75 and 360 μm, giving partial results extrapolated by MIP, micro – CT and DIA of 200x SEM – BSE images.

These results (Table 13) show that these techniques provide different porosity values within the same pore size range but similar pattern of pore-size distribution can be observed. The only discrepancy can be observed in Nanto stone (sample N) values in the 0.5-4.75 μm range. MIP value is higher than SEM. This may be due to the ink-bottle effect which tends to underestimate the real pore size in this range, especially with high porous and fragile materials. As further proof the percentage of porosity measured by SEM in the range 4.75-360 μm is higher than MIP one, still affected by the ink-bottle effect and with a minor accuracy due to the approaching of its upper limit of applicability (Cnudde et al. 2009).

A considerable fraction of the pores assigned by MIP to the interval below 4.75 μm, at least corresponding to the total porosity determined by micro-CT or SEM – BSE images, should be referred to smaller pores fractured and damaged, which increased their sizes. So, the real fraction of pores below 6 μm should correspond to the difference between the total open porosity obtained by MIP and that provided by micro–CT and SEM- BSE images. The fragility of sample N is also observed in micro–CT and SEM- BSE images, where porosity have higher values than in other samples (Table 13). It is probably due to a damaging of the sample during the sample preparation, both in this section, where same crystals detached leaving lacks. Same considerations could be done for sample V, that presents a very similar behavior in micro-CT and SEM-EBS images, and it presents a bimodal pore distribution as sample N in MIP analysis (Tables 11 and 12).
For each sample a cumulative curve of the pore size distribution was obtained by merging the results of the different techniques (Figures 5-7).

Table 13. *Porosity referred to specific ranges obtained with different analytical techniques. Values expressed in percentage. Samples abbreviations as in Table 1.*

Pore range (Ø, μm)	Techniques	**A (%)**	**AU (%)**	**B (%)**	**BO (%)**	**C (%)**	**M (%)**	**N (%)**	**O (%)**	**P (%)**	**R (%)**	**V (%)**	**E (%)**
0.006-0.5	MIP	2.27	3.69	0.01	1.24	0.02	0.30	11.90	0.00	0.21	0.06	13.34	1.80
0.5-4.75	MIP	0.00	0.00	0.00	0.06	0.00	0.04	15.11	0.00	0.01	0.01	0.00	0.00
	SEM-BSE 200x	0.02	0.30	0.01	0.45	1.36	1.15	1.33	0.08	0.36	0.33	2.11	0.10
4.75-360	MIP	1.27	0.92	0.10	0.43	1.02	0.66	0.17	0.39	0.14	0.19	15.18	0.39
	SEM-BSE 200x	0.15	0.32	0.02	3.79	0.36	0.96	15.90	0.34	0.59	0.31	13.12	0.14
	Micro-CT	0.28	1.20	0.07	1.30	1.50	0.04	8.96	1.07	0.73	0.27	13.51	1.04
>360	SEM-BSE 200x	0.00	0.00	0.00	0.10	0.00	0.00	7.85	0.00	0.00	0.00	2.06	0.00

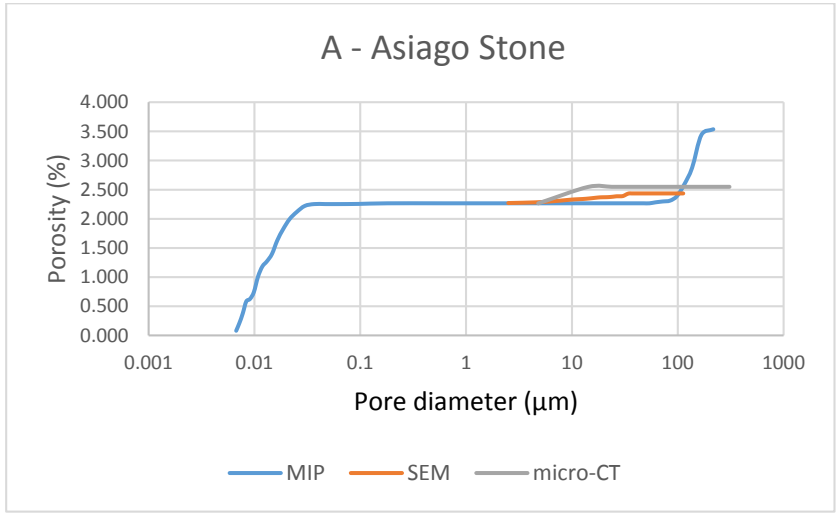

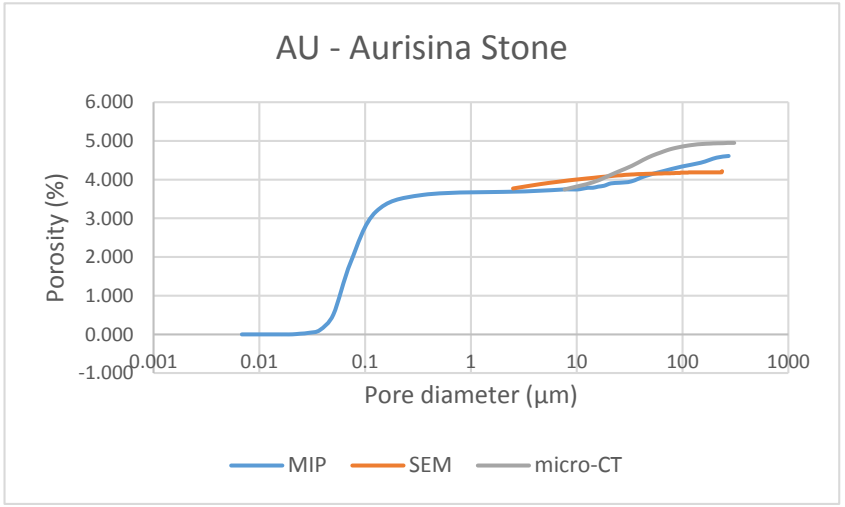

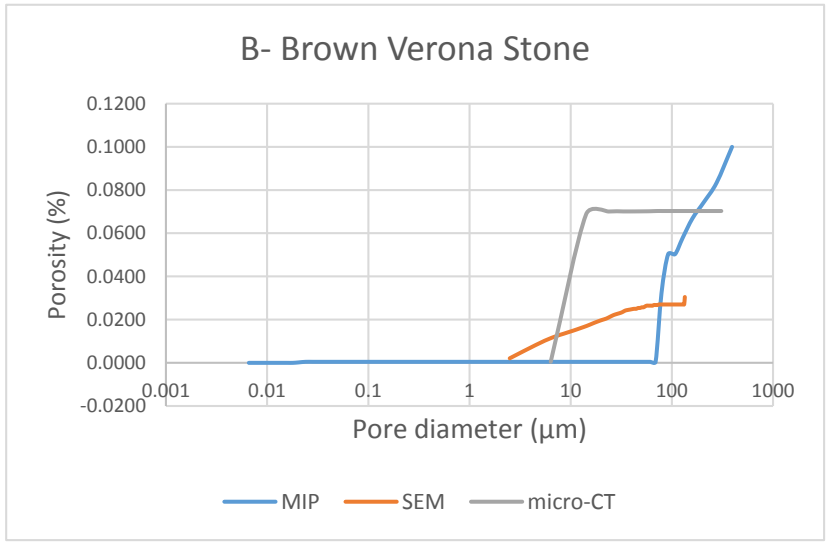

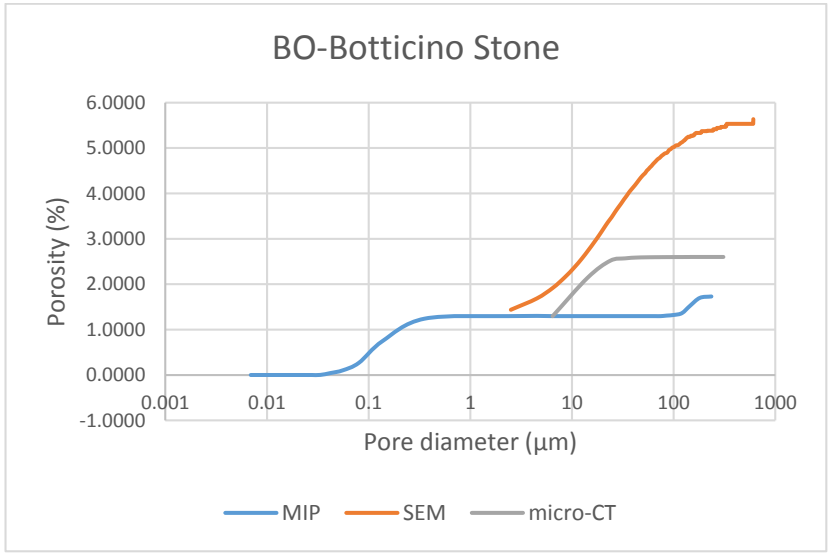

Figure 3. *Cumulative curves of the pore-size distribution*

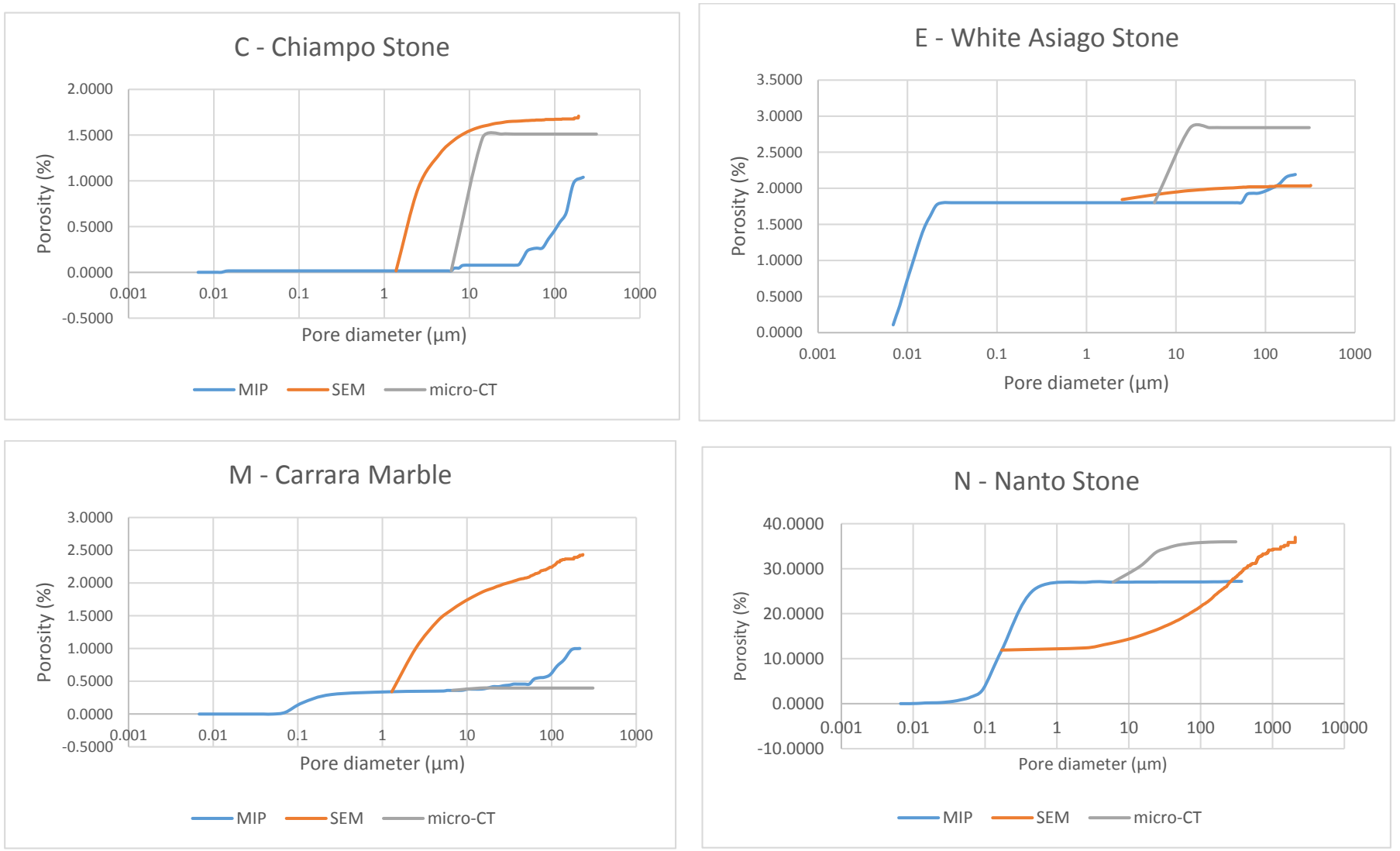

Figure 4. *Cumulative curves of the pore size distribution*

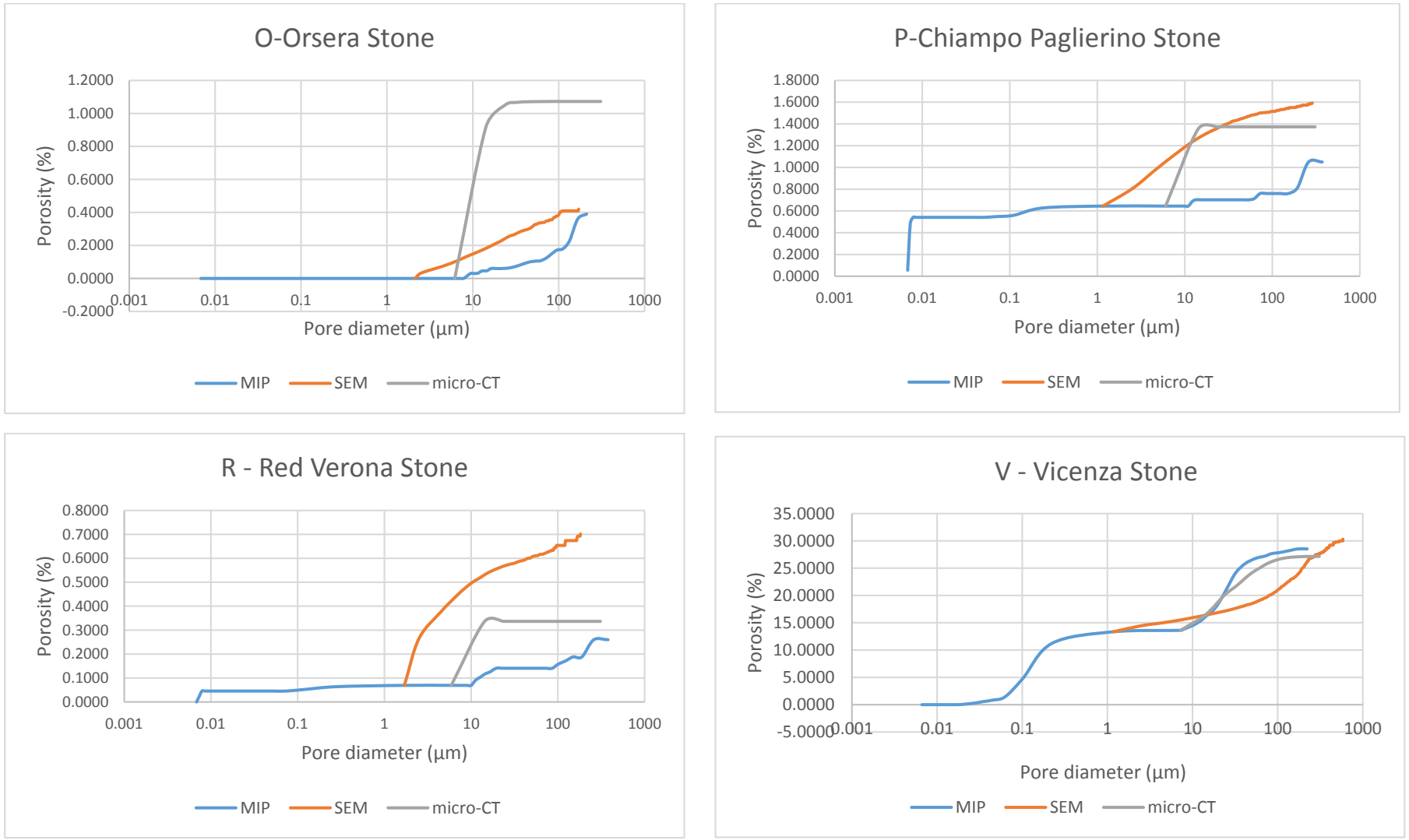

Figure 5. *Cumulative curves of the pore size distribution*

Due to the overlapping pore size ranges between the various methods, the cumulative curves were calculated by defining a specific pore-size cut off as a threshold limit between adjacent techniques. The main curve is the MIP one, the other curves started with the pattern determined by MIP up to 2.5 when it is followed by 2D SEM – BSE images results and up to 4.75 μm when it is followed by micro-CT ones. For Nanto Stone, which results are strongly affected by ink-bottle effect the MIP limit for SEM – BSE curve was set up to 0.5 μm, thus providing a good accordance between the various techniques.

Table 14. *Total porosity obtained by adding the contribution from the various methods. Samples abbreviations as in Table 1.*

	A (%)	AU (%)	B (%)	BO (%)	C (%)	E (%)	M (%)	N (%)	O (%)	P (%)	R (%)	V (%)
MIP	3.54	4.61	0.10	1.73	1.04	2.19	1.00	27.18	0.39	1.05	0.26	28.52
MIP+ SEM	2.44	4.22	0.03	5.64	1.71	2.04	2.43	36.98	0.42	1.59	0.70	30.33
MIP +micro-CT	2.55	4.95	0.07	2.60	1.51	2.84	0.40	35.99	1.07	1.37	0.34	27.15

Conclusion

Porosity data, obtained from mercury intrusion porosimetry, micro–CT, and SEM–BSE have been compared and advantages and disadvantages of these three techniques were discussed.
Due to the fact that micro–CT and MIP measure different pore size ranges, in this work porosity data which were obtained from the combination of different direct (DIA of SEM-BSE and micro-CT images, scans) and indirect (mercury intrusion porosimetry) techniques, were compared and merged together in order to successfully provide a reliable characterization of the pore system in the carbonate rocks considered in this research.
The comparison of cumulative curves and overlapping data highlighted the limitations of the techniques and the advantages of a combining method. Results are very similar in all samples, expect for misinterpretations due to the intrinsic fragility of samples, in which pore system collapsed during their preparation or during the data acquisition. This is the case, in particular, of the Nanto Stone (sample N) and of the Costozza Stone (sample V), in which both total porosity and pore distribution are increased by pore damaging.

SEM and micro-CT are powerful techniques but it could lead to lack of data for samples characterized of abundance of micropores (< 0.5 μm), such as in carbonatic rocks. MIP results alone allow a better good description of pore size description, because the most of samples have porosity gathered under the limit of threshold of digital imaging analyses.
The low percentage of porosity in the other wackstones/packstones confirmed that they are characterized by well-preserved foraminifera with highly cemented and lime micrite, including dewatering and physical compactation, and destroying macro-pores. In addition, most fractures are filled by calcite cement, leaving only the partial-filled calcite fractures and intercrystalline pores with dimensions < 0.5 μm.
Both cementation and compactation have modified and reduced the connectivity of the pore network as demonstred by the presence of a high level of fractal pattern and tortousity. Also crystalline carbonates are characterized by micropores, with a porosity between 0.5 and 3%, because the natural crystals grow and re-arrange during the re-crystallization process due to cemented micropores developed between the grains by pressure.
The combined methods of analysis adopted with the use of the “overlapping ranges” allowed a more realistic description and knowledge of the porosity. In particular, the coupling MIP – microCT, can provide a realistic reconstruction of the pore system in materials characterized by a complex pore structure over a wide pore size distribution.

Aknowledgments

Authors wish to thank Castelli S. (Cam Scan), Barchi L. (MIP analysis), Tauro L. (thin sections) Pasqual D. (XRF analysis), Zorzi F. (XRD), Coletti C. for the precious advices.

References

Anovitz L.M., Cole D.R. (2015) Characterization and analysis of porosity and pore structure. *Rev Mineral Geochem*, **80**, 61–164.

Arnold A., Zehnder K. (1990) Salt weathering on monuments. In: The conservation of monuments in the Mediterranean Basin: the influence of coastal environment and salt spray on limestone and marble. Proceedings of the 1st International Symposium, Bari, 7-10 June 1989. Ed. Grafo, Bari, pp. 31-58.

Baedecker P. A., Reddy M.M. (1993) The Erosion of Carbonate Stone by Acid Rain. *J Chem Educ*, **70- 2**, 104-108.

Barbera G., Barone G., Crupi V., Longo F., Maisano G., Majolino D., Mazzoleni P., Raneri S., Teixeira J., Venuti V. (2014) A multi-technique approach for the determination of the porous structure of building stone. *Eur J Mineral*, **26**, 189–198.

Benchiarin S. (2007) Carbonate lithotypes employed in historical monuments: quarry materials, deterioration and restoration treatments. PhDThesis, University of Padua.

Benavente D., del Cura M. G., Fort R., Ordóñez S. (2004) Durability estimation of porous building stones from pore structure and strength. *Engineering Geology*, **74-1,** 113-127.

Bugini R., Laurenzi Tabasso M., Realini M. (2000) Rate of formation of black crusts on marble. A case study. *J Cult Herit*, **1**, 111-116.

Charola A. E. (2000) Salts in the deterioration of porous materials: an overview. *Journal of the American institute for conservation*, **39-3,** 327-343.

Choquette P.W., Pray L.C. (1970) Nomenclature and classification of porosity in sedimentary carbonates. *Am Assoc Pet Geol Bull*, **54-2**, 207-250.

Coletti C., Cultrone G., Maritan L., Mazzoli C. (2016) Combined multi-analytical approach for study of pore system in bricks: How much porosity is there? *Mat Char*, **121**, 82-92.

Corvo F., Reyes J., Valdes C., Villaseñor F., Cuesta O., Aguilar D., & Quintana P. (2010) Influence of air pollution and humidity on limestone materials degradation in historical buildings located in cities under tropical coastal climates. *Water, air, and soil pollution*, **205,** 359.

Cnudde V., Cwirzen A., Masschaele B., Jacobs P.J.S. (2009) Porosity and microstructure characterization of building stones and concretes. *Eng Geol*, **103**, 76–83.

Dal Sasso G., Maritan L., Salvatori S., Mazzoli C., Artioli G. (2014) Discriminating pottery production by image analysis: a case study of Mesolithic and Neolithic pottery from Al Khiday (Khartoum, Sudan). *Journal of Archaeological Science*, **46**, 125-143.

De Boever W., Derluyn H.D., Van Hoorebeke L., Cnudde V. (2015) Data-fusion of high resolution X-ray CT, SEM and EDS for 3D and pseudo-3D chemical and structural characterization of sandstone. *Micron*, **74**, 15–21.

De Quervain F. (1967) Technische Gesteinskunde. Lehrbücher und Monographien aus dem Gebiete der exakten Wissenschaften. *Mineralogisch-geotechnische Reihe*, **1.**

Di Benedetto C., Cappelletti P., Favaro M., Graziano S.F., Langella A., Calcaterra D., Colella A. (2015) Porosity as key factor in the durability of two historical building stones: Neapolitan Yellow Tuff and Vicenza Stone. *Eng Geol*, **193**, 310-319.

Doehne E. (2002). Salt weathering: a selective review. *Geological society, London, special publications*, *205*(1), 51-64.

Dubinin M. M. (1979) Characterization of porous solids. *Society of Chemical Industry, London*, **1**.

Fitzner B., Basten D. (1994) Gesteinsporosität—Klassifizierung, meßtechnische Erfassung und Bewertung ihrer Verwitterungsrelevanz—Jahresberichte aus dem Forschungsprogramm ‘‘Steinzerfall-Steinkonservierung’’ 1992, Förderprojekt des Bundesministers für Forschung
und Technologie. Ed. Verlag Ernst & Sohn, Berlin.

Fusi N., Martinez-Martinez J. (2013) Mercury porosimetry as a tool for improving quality of micro-CT images in low porosity carbonate rocks. *Eng Geol*, **166**, 272-282.

Galaup S., Liu Y., Cerepi A. (2012) New integrated 2D–3D physical method to evaluate the porosity and microstructure of carbonate and dolomite porous systems. *Micropor Mesopor Mat*, **154**, 175 -186.

Giesche H. (2006) Mercury porosimetry: a general (practical) overview. *Part Part Syst Char*, **23**, 9–19.

Gregg S. J., Sing K. S. (1983) Adsorption, surface area, and porosity. *Berichte der Bunsengesellschaft für physikaliche Chemie*, **86-10**, 957.

Grossi C.M., Brimblecombe P., Harris I. (2007) Predicting long term freeze-thaw risks on Europe built heritage and archaeological sites in a changing climate. *Sci Total Environ*, **377**, 273–281.

Jena A., Gupta K. (2001) An innovative technique for pore structure analysis of fuel cell and battery components using flow porometry. *Journal of Power Sources*, **96-1,** 214-219.

Klopfer H. (1985) Feuchte. In: Lutz P., Jenisch R., Klopfer H. et al. (Eds) Lehrbuch der Bauphysik. Ed. Teubner, Stuttgart.

Kodikara J., Barbour S.L., Fredlund D.G. (1999) Changes in clay structure and behavior due to wetting and drying. In: 8th Australian-New Zealand conference on geomechanics, Australian Geomechanics, Hobart.

León y León C.A. (1998) New perspectives in mercury porosimetry. *Advances in Colloid and Interface Science,* **76**, 341-372.

Lowell R. P., Germanovich L. N. (2004) Hydrothermal processes at mid-ocean ridges: Results from scale analysis and single-pass models. *Mid-Ocean Ridges*, 219-244.

Manganelli del Fà C. (2002) La porosità nei materiali lapidei naturali e artificiali.

Molina E., Benavente D., Sebastian E., Cultrone G. (2015) The influence of rock fabric in the durability of two sandstones used in the Andalusian Architectural Heritage (Montoro and Ronda, Spain). *Eng Geol,* **197**, 67–81.

Moro F., Böhni H. (2002) Ink-Bottle Effect in Mercury Intrusion Porosimetry of Cement-Based Materials. *Journal of Colloid and Interface Science*, **246**, 135-149.

Nicholson D.T. (2001) Pore properties as indicators of breakdown mechanism in experimentally weathered limestones. *Earth Surf Proc Land*, **26**, 819-838.

Noiriel C. (2015) Resolving time-dependent evolution of pore-scale structure, permeability and reactivity using X-ray microtomography. *Rev Mineral Geochem*, **80**, 247–285.

Pirard R., Alié C., Pirard J.P. (2002) Characterization of porous texture of hyperporous materials by mercury porosimetry using densification equation. *Powder Technol*, **128**, 242–247.

Rigby S.P., Fletcher R.S., Riley S.N. (2004) Characterization of porous solids using integrated nitrogen sorption and mercury porosimetry. *Chem Eng Sci*, **59**, 41–51.

Rijniers L.A., Pel L., Huinink H.P., Kopinga K. (2005) Salt crystallization as damage mechanism in porous building materials – a nuclear magnetic resonance study. *Magn Reson Imaging*, **23**, 273-276.

Rodriguez-Navarro C., Doehne E. (1999) Salt weathering: Influence of evaporation rate, supersaturation and crystallization pattern. *Earth Surf Proc Land*, **24**, 191–209.

Ruedrich J., Siegesmund S. (2007) Salt and ice crystallization in porous sandstones. *Env Geol*, **52-2**, 225-249.

Ruedrich J., Kirchner D., Siegesmund S. (2011) Physical weathering of building stones induced by freeze–thaw action: a laboratory long-term study. *Environmental Earth Sciences*, **63**, 1573-1586.

Sawdy A., Price C. (2005) Salt damage at Cleeve Abbey, England. Part II: seasonal variability of salt distribution and implications for sampling strategies. *Journal of cultural heritage*, **6-3,** 269-275.

Scherer G.W. (1999) Crystallization in pores. *Cem Concr Res,* **29**, 1347–1358.

Siegesmund S., Dürrast H. (2011) Physical and mechanical properties of rocks. In S. Siegesmund, R. Snethlage (Eds), Stone in architecture. Properties, durability (4th ed.). Ed. Springer, Berlin, pp. 97-225.

Sing K.S.W., Everett D.H., Haul R.A.W., Moscou L., Pierotti R.A., Rouquérol J., Siemienievska T. (1985) Reporting physisorption data for gas/solid systems with special reference to the determination of surface area and porosity. *Pure Appl Chem*, **57**, 603–619.

Steiger M., Charola A.E. (2011) Weathering and deterioration. In S. Siegesmund, R. Snethlage (Eds), Stone in architecture. Properties, durability (4th ed.). Ed. Springer, Berlin, pp. 227–316.

Steiger M. (2005) Crystal growth in porous materials. The crystallisation pressure of large crystals. *J Cryst Growth*, **282**, 455–469.

Winkler, E. (2013). Stone in architecture: properties, durability. Ed. Springer, Berlin.

Zong Y. Yu X., Zhu M., Lu S. (2015) Characterizing soil pore structure using nitrogen adsorption, mercury intrusion porosimetry, and synchrotron-radiation-based X-ray computed microtomography techniques. *J Soils Sediments*, **15**, 302–312.

Part 3: Deterioration of headstones from the CWGC cemeteries in the Mediterranean area

ABSTRACT

In geomorphological studies stone decay can be expressed in terms of surface recession and, for this reason, various researches have been carried out in order to assess regional or environmental differences in recession values. In this paper we report the results of the field surveys carried out on Chiampo and Botticino headstones made of Chiampo stone and Botticino stone located in various Commonwealth War Graves Commission cemeteries of Italy and Greece.
The over 3000 recession measurements collected have been analyzed in order to understand whether the differences of surface recession of limestones depends on different environmental contexts, orientation of the surfaces and their time of exposition. Rainfall and prevailing winds have also been considered.
Data elaboration found evidences of an evident correlation between major values of recession and prevailing winds.

Keywords
Recession rates, weathering rates, carbonate rocks, stone decay, headstones, base-minus-top method, tombstone thickness

1. Introduction

Human artifacts as well as natural landforms are subjected to weathering and erosion. These slow processes can be consistently accelerated by pollutants agents and a visible damage to building materials can be seen even in few decades. Actually, the decay of stones is due to different deterioration mechanisms depending on specific factors such as climatic conditions or pollutant agents.
Since 1850 ca. air pollution has caused an acceleration of degradation with particular regard to carbonate rocks which are particularly prone to decay originated by dry deposition and acid rain. When the affected material is a component of a Cultural Heritage asset, the damage is not only economic but artistic since the aesthetic value of the artifact can be compromised.
The inorganic and organic compounds generated from air pollution interact with the mineral material by complex physical and chemical interactions thus accelerating the decay of stone (Baedecker & Reddy 1993, Siegsmund & Snethlage 2014). In stone conservation literature, the decay of stone is known with different terms: surface diagenesis, weathering (especially for geomorphologists), deterioration, degradation, stone pathology, … they all mean the changes of rocks and their constituents toward a new equilibrium state when they face a change in the surface environment. Discoloration, structural alteration, chemical precipitation and surface recession are all products of weathering processes (Pope et al. 2002).
The field surveys carried out in this work out aim to measure stone decay of different types of limestone located in various environmental contexts.

1.1.Influence of climate and microenvironmental parameters in stone decay processes

The prevalence of different mechanical and chemical weathering processes in different climatic regions was studied by Brimblecombe (2010) who associated different effects on built structures depending on the diverse climatic areas of the Köppen-Geiger classification where they are located. According to his research, polar and alpine environments are dominated by mechanical processes of rock breakdown, whereas humid tropics are dominated by chemical weathering.

Table 1. *Major climate effects observed on heritage based on the climate areas of the Köppen-Geiger classification (Brimblecombe, 2010).*

Köppen-Geiger classification	**Climate**	**Effects on heritage**
Bwh	Hot arid climate	Dry ground, little vegetation, chance of wind blown sand, extreme thermal stress. Earthen buildings are frequent in this climate and their materials are friable and additionally sensitive to the rare but heavy falls of rains.
Csa	Warm climate with hot summer	Thermal stress on materials exposed to strong insulation. Dry conditions in the summer may minimize fungal attack.
Csbc	Warm fully climate with dry warm summers	Drier condition and lower variation in humidity leads to less salt damage, and some potential for frost weathering. Some potential for thermal stress on materials exposed to strong insulation.
Cfab	Warm fully humid climate with warm to hot summers	Damp conditions and variation in humidity that cause salt damage, occasional freezing events present the potential for frost weathering. Warm and damp conditions can lead to fungal attack.
Dfb	Fully humid snow climate with warm summers	Lower variation in humidity leads to less salt damage, but potential frost weathering.
Dfc	Fully humid snow climate with cool summers	Lower variation in humidity leads to less salt damage, but cold winters conditions mean a high potential for frost weathering in spring and autumn.
E	Polar or montane climate	Conditions so cold that ground may remain frozen. This is a potential problem if temperature increases causing frost heave, because it could disrupt soils and archaeological sites.

In our research the climate zones Cfa and Cfb were considered separately being Cfa the traditional continental climate with hot summers common in the Po Valley and Cfb a climate with less hot summers but colder winters typical of the Apennine regions. In addition, some locations studied in Greece are defined Bsk which is a hot “steppe” climate, intermediate between the desert (Bwh) and the Mediterranean Csa climate.

The cemeteries located in the Alps, often classified Cfb, are affected by longer periods of snow cover, and for this reason we have classified these locations as Cfb-Alps.

However, climate is not sufficient to explain the pattern of stone decay. In conservation science it is common to observe some phenomena on a specific façade of the monuments, i.e. biodeterioration on the northern slides and façades, enhanced thermal stress damage on the southern and western sides.

In addition, the prevailing winds influence the pollutant deposition: for example, if the wind blows from North-West and East the southern side of the analyzed building is more blackened than the other façades (Ponziani et. al. 2012).

1.2.Measuring stone recession rates

Different methods of measurements of stone decay exposed outdoor for long periods of time are reported in literature:

- Photography. This method cannot be used to quantify the surface recession. It consists in a simple qualitative observation using photographic evidences documenting the rates of decay of statuary (Winkler 1977, Amoroso & Fassina 1983).
- Determination of surface recession by measurement of surface reduction of marbles based on the height difference between lead lettering and marble (Dragovich 1991, Dragovich 1995).
- Micrometers (MEM) have been widely used for measuring surface erosion since the seventies (Viles & Trudgill 1984, Moses et al. 1995, Smith et al. 1995, Stephenson & Finlayson 2009). Recent models have a sensibility of 10 μm. It has been used for a long – term monitoring of the erosion of a horizontal surface of the Saint – Paul Cathedral in London (Trudgill et al. 1989, Trudgill et al. 1991, Trudgill et al. 2001, Inkpen 2012a, Inkpen 2012b). Beside the problems of the different measuring devices used in a long-term research, the major flaw of this technique is that it requires the presence of metals studs, fixed on the stone surface, which can be lost throughout time and makes this technique partially invasive.
- Determination of surface recession using calipers. This method, established by Meierding (1981) and subsequently used in various studies (Baer & Berman 1983, Feddema & Meierding 1987, Roberts 2005), compares the top thickness (maximum weathering loss) to base thickness (minimum weathering loss) of tombstones in order to determine surface recession. This method is also known as "base-minus-top" method.
- Run-off experiments. They study the influence of incident (acid) rain and runoff on stone surface (Dolske & Gatz 1985, Reddy 1987, Dolske 1995) . The difference in concentration of Ca^{2+} is considered stone loss. In this case composition of air is estimated from local meteorological network or measured in situ, however these systems do not record all pollutants and impurities. In addition, composition of air is extremely variable and even if the measurements are done for individual rain events, there are still some uncertainties.
- Field monitoring of fresh samples are usually carried out for relatively short periods of time (1-5 years). The extreme variability of environmental compositions makes more difficult the evaluation of the parameters affecting stone decay. Many researches have focused their attention on the field test method in order to observe the decay variability of different stones exposed to the same natural environmental conditions, or that of a certain stone type to different environmental conditions when exposed in different places. Further review about recession measurements is reported in Part 4.

Table 2. *Selected studies about the weathering of limestone used in Cultural Heritage. They cover a variety of contexts and methods (from Pope et al. 2002)*

Study	Location	Context	Method(s)	Lithology
Sharp et al., 1982	London, England	18th C. cathedral	surface recession	limestone
Jaynes and Cooke, 1987	SE England	architecture, various ages	morphology, mass loss	limestone
Mottershead, 1998	Salcombe, England	16th–19th C. architecture	petrography, surface recession	greenschist
Inkpen, 1999	various UK	tombstones	surface recession	marble
Sjöberg, 1994	Sweden	petroglyphs	Schmidt hammer	gneiss
Storemyr, 1997	Nidaros, Norway	13th C. cathedral	morphology, petrography	various
Sellier, 1997	Carnac, France	megaliths	morphology, surface recession	granitic
Delgado Rodriguez, 1994	W. Europe (esp., Portugal, Spain)	megaliths; Medieval and Renaissance architecture	various	granitic
Romão and Rattazzi, 1996	Portugal	megaliths	visual, microscopy	granitic
Pope, 2002	Portugal	prehistoric to modern cultural stone	Schmidt hammer	granite
Emery, 1960	Giza, Egypt	Great Pyramid	debris accumulation	limestone
Gauri et al., 1990	Giza, Egypt	Sphinx	petrography	limestone
Paradise, 1995	Petra, Jordan	Roman theater	surface recession	sandstone
Topal and Doyuran, 1997	Cappadocia, Turkey	Carved bedrock, petroglyphs	structural integrity	tuff
Gauri and Holdren, 1981	Agra, India	Taj Mahal	microscopy, chemical	marble
Van Tilberg, 1990	Easter Island	large statues	conservation methods	basalt
Winkler, 1965	New York, USA	Egyptian obelisk	visual	granitic
Brown and Clifton, 1978	Southwest USA	adobe architecture	visual, structural properties	clay
Petuskey et al., 1995	Southwest USA	Prehistoric (12th C.) ruins	surface recession, microscopy, chemistry	sandstone
Meierding, 1981	various USA	tombstones	inscription legibility	marble
Vogt, 1999	Arizona, USA	tombstones	confocal laser microscope	sandstone
Dragovich, 1981, 1986	Sydney, Australia	tombstones	surface recession	marble
Gorbushina et al., 1993	various	statuary and architecture, lab	microscopy	marble
McGee and Mossotti, 1992	experimental	stone samples	mass loss, gypsum accumulation	marble, limestone
Yerrapragada et al., 1996	experimental	lab and outdoor tests	chemical mass loss and gain, surface recession	marble

2. Locations

2.1.Choice of sites. Why CWGC cemeteries?

The main aim of field surveys is the measurement of stone decay and recession in different environmental contexts. With this perspective is of paramount importance the lithological and geometrical uniformity of the stone of reference and its distribution in the different climatic contexts. All these requirements could have been met by the Commonwealth War Graves Commission (CWGC) cemeteries because they are almost ubiquitous, the headstones have the same shape and they are made up of Botticino or Chiampo stones, with a limited provenience[6]. Hence, these cemeteries are a consistent data source for the measurement of recession rate occurred in the last century in different environmental conditions.

The chief architect of the Commission was responsible for huge areas. For this reason, a great number of cemeteries of the 1st World War located in the Mediterranean area were designed by Sir Robert Lorimer[7] and the original slates are made of Chiampo stone.

[6] For example, Colosio company s.n.c, located in Rezzato (BS) has been the supplier for the Botticino headstones of the CWGC cemeteries since the 1950s.

[7] Sir Robert Lorimer (1864-1929) was a prolific Scottish architect. He designed a lot of CWGC cemeteries in **Italy** (the five cemeteries on the Asiago Plateau, Bordighera British Military Cemetery, Dueville communal cemetery extension, Giavera cemetery and Memorial, Savona Cemetery and Memorial, Montecchio Precalcino communal cemetery extension, CWGC plot inside the Staglieno cemetery in Genoa, Taranto town cemetery extension, Tezze British Cemetery), military cemeteries of **Greece** (Doiran, Karasouli, Kirechoi-Hortakoi, Lahana, Mikra, Lembet Road, Sarigol, Struma), Germany (Cologne cemetery and memorial, Hambourg cemetery, Niederzwehren cemetery, Berlin South Western Front cemetery), the War Memorial cemeteries of Egypt (Alexandria a.k.a Adra, Cairo, Chatby, Ismaila, Kantara, Port Said, Suez, Tel El Kabir), the Naval Memorials in the United Kingdom (Chatam, Plymouth, Portsmouth).

Figure 1. Views of some Commonwealth War Graves Commission (CWGC) cemeteries surveyed in this work. From top to bottom, from left to right: South African cemetery in Castiglione dei Pepoli (BO), CWGC plot in Cremona Town cemetery, panoramic view of Phaleron cemetery in Athens, Mikra cemetery in Thessaloniki (Greece), Hireckoi-Hortakoi cemetery in Thessaloniki (Greece), CWGC plot in Padua Town cemetery, Souda Bay War cemetery in Crete (Greece), CWGC extension of Arquata Scrivia (AL) Communal cemetery, Barenthal British cemetery

In a similar way, Louis de Soissons[8] designed the most important cemeteries of the 2nd World War and began to use the Botticino stone.

2.2. Italy

2.2.1. Padua, Veneto, Italy.

The WW1 cemetery of Padua is a dedicated plot with 25 burials inside the civic Cemetery, the so called "Maggiore". The original Chiampo slates have been all substituted with Botticino ones around 1985. Headstones face south.
WW2 cemetery is located 2 km west of the city center. This cemetery contains 517 graves divided in 6 plots, made of Botticino stone, mostly original. Even plots are NE faced, while odd ones face SW.
Padua is a city in Veneto, sometimes included in the Padua-Venice-Treviso metropolitan area. The clime is classified as Cfa, i.e. the humid subtropical climate, characteristic of Northern Italy, slightly mitigated by the near Adriatic Sea.
Rainfall is significant throughout the year (867 mm), even in the driest month (67mm) the rainfall is substantial. The average temperature is 23.5°C in July and 3.3°C in January. Prevailing winds blow from NE.

2.2.2. Bordighera (IM), Ligury, Italy.

Bordighera British Cemetery is about 200 mt from the sea in a beeline. It is right next to Bordighera Main Communal Cemetery. The site, located on a terraced hill of the Sasso River Valley, was designed by Sir Robert Lorimer. It contains 72 British 1st World War graves mainly made of original Chiampo Stone. The slates are all east facing. This cemetery contains also 12 Austrian graves not considered in this research because they have a different shape.
Bordighera is a small town in the Province of Imperia, located only 20 km away from France. The town is the southernmost of the Ligury region.
The climate is Mediterranean (Csa of Köppen classification) characterized by higher temperatures in winter and milder ones in summer, with a very low humidity rate. The climate can be classified as Csa which in this case is mitigated by Foehn effect since the town is built where the Maritime Alps plunge into the sea. For this reason, mean temperature is 9°C in January, the variation in average temperatures is 14.0°C during the year, snowfalls are extremely rare and exotic plants can easily grow.
Annual rainfall is 810 mm but autumn and winters are much rainier than summers. For example, mean November rainfall is 121 mm while mean July rainfall is only 18 mm. Winds are highly variable, however in spring and summer S and SE winds are prevalent.

2.2.3. Savona, Ligury, Italy.

96 British graves of casualties from Transilvania's shipwreck are located in a dedicated plot of the Zinola monumental cemetery of Savona, which is located 500 meters in a beeline from the Tirreno power plants of Vado Ligure.[9] In addition the port of Vado Ligure is the main Italian port for oil and

[8] Louis Emanuel Jean Guy de Savoie-Carignan de Soissons (1890-1962). He was the Commission's Chief architect for Second World War cemeteries and memorials in Italy, Greece and Australia. He designed almost 50 CWGC cemeteries, among them there are the 2nd World War CWGC cemeteries surveyed in this work (Souda Bay of Crete, Phaleron in Athens, Padua, South African Cemetery in Castiglione dei Pepoli, Bologna, Rome).
[9] Vado Ligure power plants are properties of the Tirreno Power, a company that says "The company pays an enormous amount of attention to observing environmental parameters and has adopted an Environmental Management System that

its derivatives, so there are other two industrial plants in less than 2 km away (Infineum, Exxon group). The slates are all NE faced and they are mostly original, so they are made of Chiampo stone. The plot contains also 8 graves of merchant seamen that are not considered here because the slate shape is uncommon.
The climate of Savona, an important seaport city located 60 km west of Genoa, is Mediterranean (Csa of Köppen classification), and the annual average rainfall is 910 mm.
The average temperature in January is 6.6°C.
The driest month is July with 24 mm, while the rainiest month is October with an average of 126 mm.
Prevailing winds are seasonal: during spring and summer wind blows from S, SE while in autumn and winter it blows from NW.

2.2.4. Dueville (VI), Veneto, Italy.

The CWGC cemetery is an extension of Dueville Communal Cemetery, situated on the road towards Montecchio. All the 133 graves are North East faced and they were all substituted with Botticino slates. The oldest ones are of 30 years old.
Dueville is a small village 12 km north of the city of Vicenza. The climate is warm and temperate (classified as Cfa). There is significant rainfall in Dueville throughout the year (973 mm), the driest (February, 67 mm) and wettest (November, 99 mm) months do not show relevant differences.
In July, the hottest month of the year, the average temperature is 23.6 ° C, while 2.4 ° C is the average temperature of January.
There is no information about the prevailing winds. However, the situation is very similar to that of Vicenza, where the winds blow mostly from SE.

2.2.5. Asiago plateau (VI), Veneto, Italy.

Five different cemeteries are located on the Asiago Plateau where the Battle of Asiago was fought (15-16 June 1918). They are: Boscon, Barenthal, Granezza, Magnaboschi, Cavalletto. These cemeteries are permanently open and quite frequented by history enthusiasts, but due to deep snow falls they are rarely accessible from November to May. These extreme conditions have caused a serious decay.
The Commission has completed the extensive substitution of all the slates (except 7 located in the Boscon cemetery) contained in these cemeteries on the occasion of the Centenary of the Great War, but the oldest Botticino slates date back to 1980 ca.
Barenthal cemetery is located 5 km south of the town of Asiago on a minor, narrow road that loops round from the village of Cesuna to Asiago. On this road there are Barenthal, Granezza and Cavalletto cemeteries. The Barenthal cemetery can be found on the left hand side, after a distance of 1.8 kilometres. It contains 125 First World War burials, nine of them unidentified. Gravestones are NW faced.
Granezza British Cemetery is 9 kilometers south of the town of Asiago in the little municipality of Lusiana. Granezza British Cemetery is on the same road of Barenthal cemetery, at distance of about

has allowed the Vado Ligure, South Torrevaldiga and East Naples plants to obtain ISO 14001 certifications and registration with EMAS (Eco-Management and Audit Scheme), a guarantee of environmental performance research, innovation and excellence". The modernization of the Ligurian power plant was completed in 2009, but the same company has serious legal problems for uncontrolled emissions between 2000-2007. When the plant was of Enel property (from the Sixties up to 2003) the emission situation was awful.

3 km. This cemetery contains 142 First World War burials. The gravestones are SW faced, and they are made of Botticino aged about 10 years old.
Cavalletto cemetery is in open countryside, down the hill from the Rifugio Verdefonte. Mount Cavalletto was the site of an advanced field hospital where urgent cases from the front were treated, as the travel from the mountains to the main hospitals on the plain, was long and difficult. This cemetery contains 100 First World War burials. Some of these graves were brought in after the Armistice from Monte di Sunio British Cemetery. The stone slates face east.
Boscon cemetery lies about 6.5 km south-east of Asiago, in the Monte Lemerle area. It is equidistantly west of Cesuna and south of Canove di Roana. Here are buried 166 First World War servicemen with headstones SW faced.
Magnaboschi: this cemetery is on a slope 2 km south of the village of Cesuna in the Municipality of Roana, next to an Italian war cemetery. It contains 183 gravestone of the First World War, all NW faced.
Asiago plateau is one of the coldest areas in Italy. It is classified as Cfb in Köppen-Geiger climate classification, but the mountain areas are also classified as E. For this reason, I considered these cemeteries, as a separate group, defined Cfb-Alps.
There is no specific information about the prevailing wind but analyzing the data from near localities it can be said that it blows mostly for N or NW.
Asiago has significant rainfall throughout the year (818 mm). The average temperature in July is 17.6°C while the average temperature in January is -2.1°C.

2.2.6. Tezze (TV), Veneto, Italy.

The British Military Cemetery of Tezze lies about 270 meters south of the village of Tezze, near the town cemetery. It contains 356 Commonwealth burials of the servicemen died on the north-east side of the Piave river during the Battle of the Piave in the First World War.
All the slates are SE faced. They have been all substituted quite recently (max 20 years old) and they are all made of Botticino limestones.
Tezze is a village in the Province of Treviso, a large town north of Venice. Tezze is located 8 kilometers east of Susegana, a town on the main road, 24 kilometres north of Treviso.
According to Köppen (1936) the climate of Tezze is classified as Cfa, even if it is milder than the Po Valley. The annual average rainfall is 915 mm, February is the driest month with 59 mm while November is the rainiest one with 94 mm. The average temperature in July, is 23.4 ° C, while 2.3 ° C is the average temperature in January.
There is no information about the prevailing winds. However, the situation is very similar to that of the near localities Miane and Monte Cesen, where the winds blow mostly from SE direction, although during fall, there is a dominance of winds blowing from N-NW.

2.2.7. Giavera del Montello (TV), Veneto, Italy.

Giavera British Cemetery is 1 km from the homonymous village, on the Montello hill.
It contains 417 burials of Commonwealth servicemen who died defending the Piave (Dec. 1917- Mar. 1918) and a memorial which commemorates 150 missing soldiers.
Slates are NE oriented and they are all made of Botticino except one, which is still original (Chiampo, 100 years old).

Giavera is 12 km east of Montebelluna and 20 km west of Conegliano on the S248, the road that joints the two towns.
As Tezze, the climate of Giavera del Montello is classified as Cfa. The rainfall amount is consistent (1009 mm) and it is quite distributed throughout the year. The average temperature of July is of 22.8°C while the average temperature of January is 2.3°C.
As for Tezze, there is no information about the prevailing winds. By the analysis of the statistics of the nearest stations (Vittorio Veneto and Miane), it is possible to suggest that prevailing winds blow from SE.

2.2.8. Cremona, Lombardy, Italy.

The CWGC plot is inside the Communal Cemetery in the back left hand corner and it contains 83 Commonwealth burials of the First World War. All the graves are SW faced. 14 slates are in the original Chiampo Stone (100 years), the others ones have been all substituted with Botticino varieties throughout the years.
Cremona is a city located in the middle of the Po Valley, on the left bank of the Po River.
The climate is classified Cfa, i.e. the humid subtropical climate, distinctive of the Po Valley.
Rainfall is significant throughout the year (810 mm). The average temperature of July is 23.7 °C, while 1.7°C is the average temperature of January.
Prevailing winds have a seasonal behavior, they mostly blow from W-WSW during winters and from E and NE in the other seasons.

2.2.9. Arquata Scrivia (AL), Piedmont, Italy.

This CWGC cemetery is permanently open and it is an extension, on the east side, of the communal cemetery. It was used from December 1917 to March 1920 and it contains 94 Commonwealth burials of the First World War. All the original slates have been substituted with Botticino ones (30 years old). Part of the graves are SE faced while the others are NW faced.
Arquata Scrivia is a little municipality in the Province of Alessandria, on the left bank of the Scrivia river. It is about 100 km southeast of Turin and 35 km southeast of Alessandria.
The climate is classified as Cfb, which is a little colder than Cfa. In fact, snow is frequent in winters. Annual rainfall is substantial (1056mm) and October is the rainiest month (144 mm). The average temperature of July is 21.3°C, while 3.1°C is the average temperature of January.
Prevailing winds have a seasonal behavior. They blow from north all year round, except summers when the prevailing direction is from south.

2.2.10. Castiglione dei Pepoli (BO), Emilia-Romagna, Italy.

The cemetery is at the right edge of the road SP325 entering the town from Bologna. The majority of those buried in this cemetery were South Africans who held positions some 8 kilometres north of Castiglione. The South African cemetery of Castiglione contains 502 Commonwealth burials of the Second World War. The headstones are original and they are about 70 years old. They are made of Botticino stone and they have multiple orientations: N, NW, SE, NE.
Castiglione dei Pepoli is a town in the Province of Bologna in the Appennines region, near the highest point of the road connecting Prato and Bologna. It is about 60 km north of Florence and 60 km south of Bologna.

The climate of Castiglione is classified as Cfb. Its annual rainfall value is 950 mm. The average temperature of July is 20.3°C while 1.4°C is the average temperature of January. The prevailing wind is from South all the year round, however during winter wind blows also from NE and WSW.

2.2.11. Bologna, Emilia-Romagna, Italy.

The War Cemetery lies in the suburb of San Lazzaro (Parco dei Cedri) near the Polish War Cemetery. The cemetery was opened as a garrison cemetery in June 1945 and later, burials were brought into it from the surrounding area. It contains 184 Commonwealth burials of the Second World War, all gravestones are made of Botticino stone and there have been various substitutions.
Bologna is the largest city of the Emilia Romagna region, it is located at the borders of the Po Valley, between Reno and Savena rivers.
The climate of the city is the typical humid subtropical climate of the Po valley (Cfa). The average temperature of July is 24.5°C while 2.3°C is the average temperature of January. The value of the annual rainfall is 774mm, July is the driest month (47mm) while November is the rainiest (92mm). Prevailing wind blows from SSW.

2.2.12. Rome, Lazio, Italy.

Rome War Cemetery lies alongside and within the Aurelian Walls of the ancient city of Rome. Due to frequent theft and vandalism the cemetery is padlocked outside the gardeners working hours. It was opened as a garrison and now it contains 426 Commonwealth burials of the Second World War.
Rome is the capital city of Italy and the metropolitan area counts more than 4 million of inhabitants. Its climate is influenced by the Tyrrhenian Sea and it is classified as Csa.
The annual average rainfall is 798, and there is a strong difference between the average rainfall of the driest month (July, 17 mm) and that of the rainiest one (November, 114mm).
Prevailing winds have a seasonal behavior. They blow from north during winters and falls; from SW and WSW during springs and summers.

2.3.Greece

2.3.1. Athens, Attica, Greece.

The WW1 cemetery of Athens is a little plot within the Pireus English Civil Cemetery (Anastasis Nekrotafeio) located on the western outskirts of Pireus. It contains only 25 graves, east faced and mostly substituted, and thus they are all made of Botticino Stone.
On the contrary, WW2 cemetery of Athens "Phaleron" is situated in the Municipality of Paleo Faliro. The cemetery, which faces the Saronic Gulf, is huge, with 2029 headstones made of Botticino Stone, mostly original and SW faced.
Athens is the largest city of Greece. Its metropolitan area counts almost 4 millions of inhabitants and it includes also the port city of Pireus and Palaio Faliro, at 12 km southwest and 6 km southwest of Athens city center respectively.
Athens presents a borderline Köppen climate classification: Csa-Bsk. The two cemeteries are in different climatic zones due to the dimensions of the Athens metropolitan area. Csa climate prevails in Pireus-Drapetsona area whilst Bsk dominates the Athens Riviera, where Palaio Faliro is situated. In this research Csa-Bsk climate was considered for Pireus and a Bsk for Athens. However, the environmental parameters of the two localities are very similar, so if necessary they could be both considered Bsk.

The annual precipitation of Athens and Pireus is lower than other Greek regions. The yearly precipitation is 397 mm and it is concentrated between the months of October and April. June, July and August are the driest months (5-8 mm of rainfall)
Southern winds prevail all year round in Pireus. In Athens winds have a seasonal behavior: NW winds are typical in winter while SW ones in summer.

2.3.2. Thessaloniki, Greek Macedonia, Greece.

During the First World War the Macedonian – Salonika Front was established in Thessaloniki and the city was the base of the British Salonika Force. In this area the CWGC cemeteries of Lembet Road, Mikra and Kirechkoi-Hortakoi have been surveyed.
Lembet Road military cemetery is the Commonwealth section (1697 graves) located within the Zeitenlik Allied Military cemetery, which is the largest memorial park of Greece. The graves are partly North and partly South faced.
Mikra War military cemetery is situated in the Municipality of Kalamaria, which is still part of the Metropolitan Area of Thessaloniki, between the Dalipi military camp and the Kalamaria Communal Cemetery. It contains 1957 graves (1810 Commonwealth burials, 147 Bulgarian ones), partly NE and partly SW faced.
Kirechkoi-Hortakoi military cemetery is located on the outskirts of Exochi, a village 15 km north east of Thessaloniki, where many hospitals were located. Indeed, most burials of the 588 Commonwealth ones of the WW1 are of soldiers who died of Spanish flu epidemic in Autumn 1918.
The gravestones of the cemeteries of Thessaloniki are made of different materials (Botticino, Chiampo, Portland, etc.).
According to Köppen climate classification Thessaloniki has a Mediterranean climate (Csa) that borders a humid subtropical climate (Cfa), whereas the periphery north of the city shows a semi-arid climate (Bsk).
Winters in Thessaloniki are relatively dry but morning frosts are common. Snowfall are sporadic but occur almost every winter, although the snow cover does not last for more than a few days.
The value of the average annual rainfall is 445 mm. Low precipitations are distributed throughout the year with an average of 21mm in the driest month (August) and a value around 54 mm in the rainiest month (November).
Prevailing winds have a seasonal behavior. Moreover, there are slightly differences between the various cemeteries:

- Mikra (Municipality of Kalamaria): the wind blows from W and WNW during falls and winters and from SW and SSW during springs and summers.
- Lembet Road (city center of Thessaloniki): NW during winter, SSW during spring and summer.
- Kirechkoi Hortakoi (Exochi). Wind information was drafted from the station of Asvestochori, where the wind blows from NW all over the year with some extra blows from NE during winters and from SW during summers.

2.3.3. Souda Bay, Crete, Greece.

The cemetery is in the middle of an olive grove facing the natural harbor of Souda Bay, which was the naval battlefield of the Battle of Crete (May 1941). In this cemetery are now buried 1500 Commonwealth servicemen, half of which are still unidentified.

Souda Bay is located about 5 km east from the old town of Chania (Xania), a city that lies on the north coast of the island.
In Chania the climate is Mediterranean, classified as Csa. The average annual rainfall is 619 mm but the precipitations are concentrated in winter (November 84 mm, December 114 mm, January 122mm, February 93mm) and practically absent during the whole summer (May 12mm, June 3mm, July 1 mm, August 2mm, September 12 mm).
The average temperatures are very mild: 26.1°C in July and 12.2°C in January.
The prevailing wind blows from WNW, but in winters it also blows from NE.

Materials & Methods

2.4.Materials

Different rock types can be found in Commonwealth War Graves Commission cemeteries. In general, specific rock types were used in definite locations and for given periods of time. For example, the Chiampo Perla variety was used in CWGC cemeteries of the 1st World War in Italy, while the Botticino Limestone is typical of 2nd World War Cemeteries and for substitutions after that.[10] The Portland limestone, largely used in the CWGC cemeteries of Great Britain was instead found in Thessaloniki CWGC cemeteries.

Chiampo Stone

The Chiampo stone is the commercial name of the compact 30 mt thick Nummulitic Limestone Formation (Early – Middle Eocene), cropping out in the Venetian Prealps and, more specifically in the area of the eastern Lessini Mountains, along the slopes of the Chiampo Valley.
More in detail the commercial name Chiampo Stone refers to a variety of limestones with a light brownish – grey – pale pink color, quarried in the Lessini district.

Botticino Stone

Botticino deposits belong to the Corna Formation of the Lombardian Basin (Upper Triassic – Lower Jurassic), located in the Southern Alps and quarried in the surroundings of Brescia (Rezzato area). It consists of thickly bedded cream-coloured and slightly dolomitic limestone prominently crossed by stilolites. This limestone was deposited in a shallow tropical platform environment and it shows a variety of textures ranging from desiccated mudstones to oncoid-bearing floatstones (Schirolli 1997, Borghi et al. 2015, Di Battistini et al. 2005).
The variety studied here is the most diffuse Classic Botticino, which consists in a limestone originated from calcareous remnants of algae (Pivko 2003).

Portland Stone

Portland is a porous oolithic limestone (Jurassic) quarried on the Isle of Portland, Dorset, UK.
Portland Limestone consists of over 95% $CaCO_3$, along with small amounts of silica (SiO_2), iron (Fe_2O_3), magnesium oxide (MgO) and alumina (Dubelaar et al. 2003, Searle & Mitchell 2006, Godden 2012).
Probably the Portland varieties used in CWGC cemetery are the Spangle variety (cemeteries of Mikra, Lembet Road) and the whitish Whitbed variety quarried from the Base Bed (cemetery of Exochi).

[10] Botticino and Chiampo Stones have been also analyzed in Part 1 and Part 2.

Portland limestone is used extensively in historic building and structures, especially in the United Kingdom where it has been used since the Roman Age. Significant buildings made of Portland Limestone are Palace of Westminster (1347), St Paul's Cathedral (1700), The British Museum (1753), The Bank of England (1826), the Newton's Cenotaph (1920), UN headquarters, ecc.

A summary of the characteristics of the stones studied in this research is reported in Table 3.

Table 3. *Characteristics of the stone types surveyed: geological classification and formation and age, porosity, density. Botticino and Chiampo data are from Part 1 and 2. Portland data are derived from the scientific literature.*

Sample	Classification	Geological Formation	Geological Age	Porosity (MIP) %	Density (g/cm^3)	XRPD
Botticino	Dolomitic micrite	Corna Formation	Upper-Lower Jurassic	1.73%	2.74	57% Cal, 43% Dol
Chiampo	Biomicrite/ Grainstone	Nummulitic Limestone	Middle Eocene	0.84%	2.71	66% Cal, 34% Mg Cal, traces Plg M
Portland	Biomicrite/ Wackestone	Cherty Series	Jurassic	21.4%	2.4	95% -98% Cal, 2-5 % others

2.5.Methods

The base-minus-top method is a quite simple method (Roberts 2005, Reddy and Roberts 2005) which was improved in this study sticking to the following points:

- Collection of recession rate was made by using digital calipers (Sylvac ®) connected to a smartphone running a dedicated App Sylvac
- Digital calipers used have a sensitivity: 0.01 mm = 10 µm (i.e. more precise than those reported in literature).
- In order to have a robust methodology every slab has been measured at its corners for three times. The recession for every side of the slate has been derived by subtracting the average thickness value of the top from the average base thickness (Fig.2).

It is worth noting that methods based on the deep of lettering are not possible in these cemeteries because the CWGC proceeds with the re-engraving when the readability of the letters does not fully satisfy their standards.

Figure 2. *Placement of calipers for recession measurements. In the left a base measurement, always trying to avoid the chipping caused by gardeners), on the right a top measurement, where it is also visible the smartphone recording the measurements through the Sylvac App, which collects the values via Bluetooth®.*

In some cemeteries, I had also the chance of applying an innovative approach by capturing images of the entire headstone and realize 3D reconstructions through Structure from Motion μ-photogrammetry. This technique requires a long time of acquisition (about 2 hours) and elaboration (about 1 day). Although the final resolution is quite satisfactory (sensibility ~ 50 μm), it is still not comparable with digital caliper measurements (10 μm); therefore, by now it is not yet applicable as an alternative technique in the analysis of stone recession. Detailed description of the SfM approach is reported in Part 5.

Data collected in the field have been integrated within QuantumGIS software in collaboration with the School of Specialization for Architectural and Landscape Heritage (SSBAP, University of Genova).

2.6. A major issue: gravestone dating

During the investigations, the determination of the age of the headstones was not an easy task to accomplish because the CWGC's substitution practice was not systematically accompanied by a proper record.

As a general rule, Chiampo stone was used in the First World War cemeteries of Italy and Greece, while Botticino limestone was used in the Second World War ones, as well as in most of the following substitutions operated when headstone readability deteriorated below the required standards.

Theoretically, it could be even interesting to have slates of various ages and not all dated 1918 or 1945-50. Unfortunately, the CWGC have kept the records of the changed slates only in the last five years. So further hints regarding the date of substitution were searched in invoices archives of the principal CWGC furnisher for the Mediterranean area[11] or interviewing the gardeners of the Commission. In addition, a detailed visual – manual investigation of slates has been carried on since particular kind of stone working has been used in a specific range of time (see Fig. 3).

Figure 3. *Example of characteristic stone working observed in CWGC cemeteries. On the left an original Chiampo slate with its typical working on the side. On the right, a Botticino slate where are visible the guide marks for engraving letters (this is a characteristic that can be found only in the Botticino slates made before 1968).*

[11] Colosio company, located in Rezzato (BS)

Table 4. *Climatic data for the locations surveyed. Obtained from local meteorological networks (ARPA, Helleniki National Meteo Service), and various climate services (https://en.climate-data.org/, https://www.windfinder.com, https://solargis.info/, http://www.degreedays.net/)*

Location	**Climate zone**	**Tmax July (°C)**	**Tmin Jan. (°C)**	**Mean Tmax July(°C)**	**Mean Tmax Jan. (°C)**	**Annual Rainfall (mm)**	**Rain Jan (mm)**	**Rain Jul (mm)**	**Prevailing Winds[12]**	**Solar radiation (KWh/m^2)**	**Degree day (°C)**
Padua	Cfa	29.3	0.6	23.5	3.3	867	62	67	NE	1395	2383
Bordighera	Csa	27.3	5.5	23.1	9.1	810	61	18	S, SE (ss)	1483	1057
Savona	Csa	27.7	3.0	23.1	6.6	910	84	24	NW(fw); S,SE(ss)	1369	1481
Dueville	Cfa	29.1	-0.5	23.6	2.4	973	69	71	SE	1384	2401
Giavera del Montello	Cfa	28.5	-1.7	22.8	2.3	1009	63	77	SE	1365	2468
Tezze	Cfa	28.8	-0.6	23.4	2.3	915	60	68	SE; N, NW (f)	1371	2351
Asiago Plateau	Cfb/Alps	23.1	-5.4	17.6	-2.1	818	36	90	N, NW	1290[13]	4163
Cremona	Cfa	29.6	-2.0	23.7	1.2	810	54	55	E,NE; W, WSW(w)	1423	2389
Arquata Scrivia	Cfb	26.0	0.3	21.3	3.1	1056	80	42	N; S(su)	1415	2664
Bologna	Cfa	30.3	-0.6	24.5	2.3	774	48	47	SSW	1436	2259
Castiglione dei Pepoli	Cfb	25.2	-0.9	20.3	1.4	950	72	45	S; NE, SSW (w)	1408	2876
Rome	Csa	30.6	3.8	24.4	7.7	798	79	17	N (fw); W, WSW (ss)	1598	1085
Athens[14]	Bsk -Csa	33.3	6.3	27.9	9.5	397	52	5	NW(fw); SW(ss)	1730	477
Thessaloniki[15]	Csa-Cfa-Bsk	32.5	1.5	26.5	5.2	445	37	26	NW(fw); SW (ss)	1580[16]	1057
Souda Bay - Chania	Csa	29.1	9.7	26.1	12.2	619	122	1	WNW; NE (w)	1812	318

[12] Sometimes prevailing winds are not the same in the different seasons. Here are the abbreviations used for the seasons: (f) for fall, (w) for winter, (fw) fall and winter, (sp) spring, (su) summer, (ss) spring and summer

[13] Solar data are slight different for the various cemeteries, even if some of them are often in the shade (Cavalletto). Barenthal 1305 KWh/m^2, Granezza 1287 KWh/m^2, Cavalletto 1300 KWh/m^2, Boscon 1296 KWh/m^2, Magnaboschi KWh/m^2.

[14] The two cemeteries located in Athens are located in two different climatic zones: Phaleron Cemetery is on the Riviera, which is classified as Bsk while the British cemetery in Pireus is located in a Csa-Bsk area.

[15] Thessaloniki has a borderline climate classification. The single cemeteries pertain to different climatic zones. Mikra Cemetery is in a Bsk climate area, Kireckoi-Hortackoi has a Cfa Climate, and the Lembet Road cemetery is in the city center of Thessaloniki, that can be considered as a Csa-Bsk area.

[16] Solar data in Thessaloniki are different for the various cemeteries. Mikra 1576 KWh/m^2, Lembet Road 1589 KWh/m^2, Kirechkoi-Hortakoi 1572 KWh/m^2.

3. Results

Climatic data of the locations studied are reported in Table 4. In this table is also reported the Köppen climate classification, which is an important parameter in studies about the decay of cultural heritage materials (Brimblecombe 2010) and the Degree Day, which is a factor largely used by architects and professionals for energy-related calculations.

3.1.Recession data

During the past two years, 11157 graves have been surveyed collecting measures with a digital caliper (sensitivity = 0.01 mm) of 3321 gravestones widespread in 23 cemeteries of the Commonwealth War Graves Commission (CWGC) cemeteries of Italy and Greece.
Synthetic results of the collected data are shown in Table 5.

Table 5. *Synthetic results of mean recession rates collected in CWGC cemeteries of Italy and Greece. Mean recession is the mean value of the whole slate, recession R is the mean of the recession rates collected on the right side of the slate, while recession L is the mean of the recession rates collected on the left side of the slates. Recession data marked with * are referred to cemetery with slates showing multiple orientation within the same cemetery.*

	Surveyed	**Measured**	**Mean Rec (mm)**	**Mean Rec. R (mm)**	**Mean Rec. L (mm)**	**GPS location (Lat, Long)**
Italy						
Bordighera (IM)	72	72	-0.34	-0.34 (N)	-0.33 (S)	43.78544, 7.678263
Savona	96	96	-0.79	-0.74 (NW)	-0.76 (SE)	44.284061, 8.437221
Padova WW1	25	25	-0.22	-0.26 (E)	-0.24 (W)	45.414675, 11.85133
Padova WW2	517	517	-0.78	-0.75 *	-0.81*	45.421618, 11.839925
Arquata Scrivia (AL)	96	62	-0.25	-0.24 *	-0.27*	44.695505, 8.876009
Dueville (VI)	135	135	-0.28	-0.19 (NW)	-0.37(SE)	45.63984, 11.54823
Cremona	83	83	-0.52	-0.55(E)	-0.48(W)	45.144245, 10.023314
Asiago Plateau - Cavalletto	100	96	-0.31	-0.33 (N)	-0.29(S)	45.799845, 11.510324
Asiago Plateau - Boscon	164	33	-0.20	-0.43 (SE)	0.03(NW)	45.837037, 11.481528
Asiago Plateau - Barenthal	125	46	-0.09	0.03 (SW)	-0.09(NE)	45.841193, 11.523371
Asiago Plateau- Granezza	142	88	-0.29	-0.42(SE)	-0.15(NW)	45.808267, 11.531417
Asiago Plateau-Magnaboschi	182	73	-0.05	-0.11(SE)	0.00(NW)	45.825734, 11.460714
Tezze (TV)	355	140	-0.38	-0.27(NE)	-0.48(SW)	45.814565, 12.348272
Giavera del Montello (TV)	417	66	-0.40	-0.28(NW)	-0.52(SE)	45.803000, 12.164500
Castiglione dei Pepoli	502	253	-0.53	0.46 *	0.60*	44.144465, 11.161432
Bologna	184	100	-0.68	-0.56*	-0.81*	44.474610, 11.399785
Roma	432	172	-0.90	-0.74(NE)	-1.06(SW)	41.87502, 12.477238
Greece						
Thessaloniki - Lembet	1694	110	-0.34	-0.20 *	-0.49*	40.654427, 22.933681
Thessaloniki - Mikra	1957	289	-0.53	-0.56*	-0.50*	40.578343, 22.964289
Thessaloniki – Exochi	663	81	-0.53	-0.34(SW)	-0.72(NE)	40.625806, 23.049228
Athens - Pireus	24	24	-0.57	-0.64(N)	-0.51(S)	37.955550, 23.624308
Suda Bay - Crete	1563	360	-0.24	-0.16(N)	-0.32(S)	35.500109, 24.061208
Athens - Phaleron	2029	400	-0.67	-0.59(SE)	-0.76(NW)	37.917914, 23.705464
TOT	**11157**	**3321**				

Table 6. *Summary of the principal information about the gravestones of the studied cemeteries.*

	Predominant Material	**Orientation**	**Predominant Age**
Italy			
Bordighera (IM)	Chiampo	E/W	100 years
Savona	Chiampo	NE/SW	100 years
Padova WW1	Botticino	N/S	30 years
Padova WW2	Botticino	NE/SW	70 years
Arquata Scrivia (AL)	Botticino	NW/SE	30 years max
Dueville (VI)	Botticino	NE/SW	20 years max
Cremona	Mix Chiampo – Botticino	N/S	100 years (Chiampo), 30 years max (Botticino)
Asiago Plateau - Cavalletto	Botticino	E/W	20 years max
Asiago Plateau - Boscon	Chiampo, Botticino	NE/SW	100 years (Chiampo) 5 years max (Botticino)
Asiago Plateau - Barenthal	Botticino	NW/SE	5 years max
Asiago Plateau- Granezza	Botticino	NE/SW	10 years max
Asiago Platea- Magnaboschi	Botticino	NE/SW	10 years max
Tezze (TV)	Botticino	NW/SE	20 years max
Giavera del Montello (TV)	Botticino	NE/SW	20 years max
Castiglione dei Pepoli	Botticino	N/S; NE/SW; NW/SE	70 years
Bologna	Botticino	NW/SE	Variable age (many substitutions)
Roma	Botticino	NW/SE	Variable age (many substitutions)
Greece			
Thessaloniki – Lembet Road	Chiampo, Botticino, Portland	N/S	100 years (Chiampo) 30 years max (Botticino) 70 years (Portland)
Thessaloniki - Mikra	Chiampo, Botticino, Portland	NE/SW	100 years (Chiampo) 30 years max (Botticino) 70 years (Portland)
Thessaloniki – Exochi	Mix*	NW/SE	Portland (70 y.), Variable age[17]
Athens - Pireus	Botticino	E/W	Variable age
Suda Bay - Crete	Botticino	E/W	70 years
Athens - Phaleron	Botticino	NE/SW	70 years

[17] Probably the stone used for substitutions in this cemetery was not only Botticino (I suspect the use of Aurisina-Nabresina one). In addition, the original slates are not in Chiampo stone. However, the CWGC cannot give us sure information about which stone was used in specific periods. Due to the various uncertainties about this cemetery, few recession data from this cemetery have been used in the elaboration discussed in paragraph 4.2 of this Part.

In Table 6 are summarized essential information about the studied cemeteries which are predominant material, slate orientation and predominant age.
From the data summarized in Table 5 and 6 it is possible to note some macroscopic differences in the recession rates of the same type of stone exposed for the same period of time in the same climate with slight different environment such as the Chiampo Stone in Savona (Csa - polluted) and Bordighera (Csa-rural), and the Botticino stone in Athens (Bsk –urban) and Crete (Csa – rural). However, most of the differences cannot be appreciated at a first glance. Many gravestones in the same cemeteries are made with different materials being of different ages, or they are differently orientated even within the same cemetery (and thus left recession data and right recession data sometimes need to be separated or inverted in order to analyze them correctly).
These major problems lead to the design of a data elaboration process, where the whole database of recession rate measurements was analyzed in order to understand whether stone recession is significantly correlated to lithology, orientation (which influences the exposition to sunlight and prevailing winds), climate conditions and time of exposition. Figure 3 shows four possibilities of data elaboration that will be further explained.

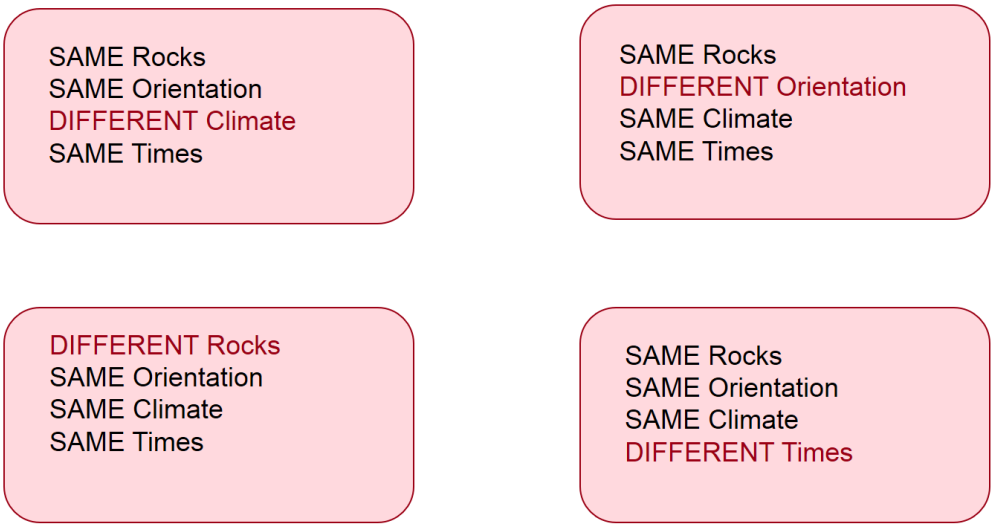

Figure 4. *Scheme summarizing the various possible correlations of the different parameters analyzed, in recession analysis.*

The climate was defined on the basis of the Köppen-Geiger classification. The orientation of the slates is that reported in Table 6. In data analysis, the various left and right recession have been considered on the basis of orientation of the specific side of the slate (see Fig.4).
In a first moment data elaboration was focused on the study of the behavior of different climate zones where the different cemeteries were located and the influence of the orientation of slates with respect to the geographical coordinates.
Results obtained didn't show a precise pattern and their interpretation has been mainly hypothetic. However, when studying the recession of gravestones differently orientated with respect to geographical conditions in various localities (Castiglione) it was observed a major recession on the SE side of the slates. After some other tests, it became clear that a major SE recession wasn't predominant because Padua showed a major recession on the NW side and finally Cremona was perfectly equal in both side. Finally, studying also the prevailing winds it became evident a connection between higher recession values on the slides more exposed to the prevailing winds.

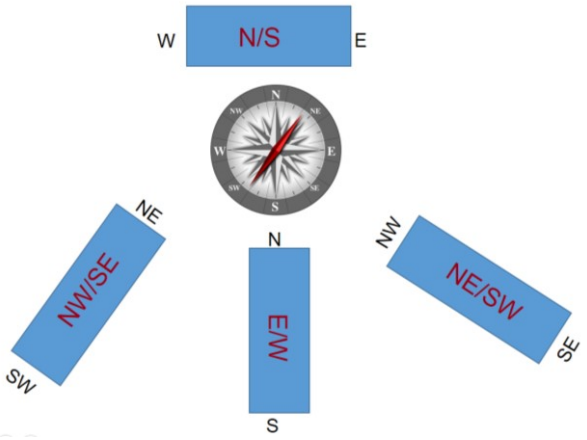

Figure 5. *Scheme about the orientation of the headstones and the effective orientation of the measured slides. For example: a headstone that face E has the right measurement of recession that faces south and the left one that faces north while a headstone that faces west has the right measurement of recession that faces north and the left one that faces south.*

Below are reported the most significant cases analyzed in order to understand whether stone recession is significantly correlated to lithology, orientation with respect to the geographical coordinates, climate conditions and time of exposition. Most cases are explained with the orientation of the headstone with respect to prevailing winds. It is worth remember that wind is not a decay factor like pollution but it is a vector for the wind-driven rainfall. Consequently, the stone surfaces are differently exposed to the action of dissolution of the rain.

3.1.1. Influence of climate

The influence of climate was evaluated by comparing headstones of the same rock type having the same orientation with respect to the geographic conditions and age (figure 5). Below are the studied cases:

- Botticino stone, aged 70 years and NE/SW faced, exposed in different climate zones Bsk, Cfb and Cfa with recession data coming from Athens, Castiglione and Padua War Cemetery (Table 7). Castiglione dei Pepoli and Padua have slightly higher recession values that can be correlated with a higher rainfall. The little difference between Castiglione and Padua can be attributed to a higher polluted environment of the urban environment of Padua.
  However, it seems to be a correlation between the recession rates and the prevailing winds. Indeed, the higher recession rate on the SE side of the gravestones in Castiglione can be correlated with the prevailing wind, which blows from S during all year round. For the same reason, the higher recession on the NW side of the gravestones located in Padua are correlated with the NW wind, which blows mostly during fall and winter, i.e. the period where are concentrated the major rainfall events.
- Botticino stone, with a N/S orientation exposed for 30 years in different climatic zones: Cfa (plot inside the Maggiore cemetery in Padua), Csa-Bsk (Lembet Road – Thessaloniki) (Table 8). These gravestones have been dated basing on oral testimoniances and visual inspections. Due to the large discordance, probably Padua gravestones are not 30 years old but it is impossible to establish a correct date. However, it is still worth notice that the recession in Thessaloniki is strictly dependent from the prevailing wind (Table 8).

- The influence of climate on Chiampo stones was assessed on gravestones NE/SW oriented, exposed for 100 years in different climate zones with data coming from Boscon-Asiago (Cfb-Alps), Cremona (Cfa), Savona (Csa) and Kalamaria (Bsk) are reported in Table 9. Chiampo results are not fully concordant with those found with Botticino stone.
  Kalamaria, Savona and Cremona are similar and quite related to the prevalent wind. In Cremona, headstones are perpendicular to the prevalent wind and so the recession is uniform. In Boscon, located on the Asiago Plateau (where there is also a high rainfall value), the values found are very low. This could be due to poor statistics as it was possible to measure only 6 headstones made of Chiampo in the whole Asiago area where 713 graves were surveyed. In addition, the humidity of the Boscon area favors the formation of crusts, a decay phenomenon which tends to elide the effect of the recession.

Table 7. *Influence of climate. Botticino stone aged 70 years, NW/SE faced, located in different climate zones.*

Climate		**NW**	**SE**	**Rainfall**	**Winds**
Bsk	Athens	-0.78	-0.60	397	NW(fw); SW(ss)
Cfb	Castiglione dei Pepoli	-0.62	-0.83	950	S; NE, SSW (w)
Cfa	Padua	-0.84	-0.72	810	NE

Table 8. *Influence of climate. Botticino stone aged 30 years, N/S faced, located in different climate zones.*

Climate		E	W	Rainfall	Winds
Csa-Bsk	Thessaloniki	-0.70	-1.31	445	(w) NW; (ss) SSW
Cfa	Padova	-0.22	-0.26	810	NE

Table 9. *Influence of climate. Chiampo stone aged 100, NW/SE faced, located in different climate zones.*

Climate		**NW**	**SE**	**Rainfall**	**Winds**
Cfb-Alps	Boscon (Asiago)	0.29	-0.45	818	N, NW
Cfa	Cremona	-0.80	-0.82	810	E, NE; (w) W, WSW
Csa	Savona	-0.79	-0.74	910	NW(fw); S, SE(ss)
Bsk	Kalamaria	-1.24	-0.99	445	W, WNW (fw); SW, SSW(ss)

3.1.2. Influence of orientation

Another important parameter was the orientation. In this phase, gravestones made of the same type of rock, exposed in the same climate, for the same time, but having a different orientation have been analyzed. The most interesting case studies were the followings:

- The cemetery of Castiglione dei Pepoli, in the Appennines Mountains, where the gravestones have different orientation within the same cemetery (Table 10). SW and NW recession are the highest values and they pertain to a plot almost always in shade. Regarding the other orientations, they seem to depend slightly on the prevailing winds (NE is the highest value, which also is the predominant direction of the winter winds).

- Chiampo Stone, located in the same Mediterranean climate with different orientations in Savona (NE/SW) and Bordighera (E/W). These data must be carefully considered because Savona graves are located in a high polluted environment due to the presence of Tirreno Power Plants less than 1 km away. However, in Savona data are also strictly related to the prevailing winds (Table 11).
  In Bordighera winds are very variable and even if they blow mostly from south they do not seem to have a great influence on decay, probably because the cemetery is sheltered by the hills located nearby.

Table 10. *Influence of orientation. Botticino stone, aged 70 years old, in a Cfb climate, with different orientations.*

E	NE	NW	W	SW	SE	Rainfall	Wind
-0.62	-0.51	-0.59	-0.42	-0.44	-0.81	950	S; NE,SSW (w)

Table 11. *Influence of orientation. Chiampo stone aged 100 years old, in Csa climate, with different orientations.*

N	NW	SE	S
-0.34	-0.79	-0.74	-0.33
Bordighera	**Savona**	**Savona**	**Bordighera**

Due to the lack of other interesting cases, for the following example the Bsk climate and the Csa-Bsk climate of the two cemeteries of Thessaloniki, i.e. Lembet Road and Mikra, have been considered together. Consequently, I have had the opportunity of analyzing Chiampo Stone (Table 12) and Portland Stone (Table 13) with different orientations.
The two cemeteries are also subjected to the same prevailing winds, and this explains the higher values for the western and north-western sides. The higher values obtained for Chiampo stone in the Mikra cemetery could be then related to the unsheltered environment, without trees or high walls nearby.
With this reasoning, the value for Portland obtained in Mikra is lower than that expected (i.e. Portland is very subjected to stone decay due to the presence of clay content) but this is probably due to the poor statistics (only 29 measurements were collected for Portland stone in this location).

Table 12. *Influence of orientation. Chiampo Stone aged 100 years old, in Csa-Bsk (Lembet) and Bsk (Mikra) climate, with different orientations.*

E	W	SE	NW
-0.58	-0.98	-0.82	-1.24
Lembet	**Lembet**	**Mikra**	**Mikra**

Table 1. *Influence of orientation. Portland stone aged 60-70 years old, in Csa-Bsk (Lembet) and Bsk (Mikra) climates, with different orientations.*

E	W	SE	NW
-0.49	-1.09	-0.45	-0.50
Lembet	**Lembet**	**Mikra**	**Mikra**

3.1.3. Influence of the exposition time

When analyzing the influence of the exposition time, the same rocks exposed in the same climate and with the same orientation were considered. In this part it wasn't possible to analyze neither Chiampo stone nor Portland stone, because this rocks were used in a specific period of time. Consequently, they have the same age.
However, it was possible to analyze various cases regarding the Botticino stone:

- Gravestones NE/SW oriented, with different ages in the same climate (Bsk) located in Athens (70 -20 – 10 – 3 years old) and in Mikra-Kalamaria (1-5-10-15 years old). In this table are showed the recession value obtained from Botticino headstone, NE/SW faced, exposed in arid climate for different years ranging from 1 to 70. As expected recession values increase with time, and a major recession in SE orientation has been observed.

Table 2. *Influence of orientation. Botticino stone, Bsk climate, NE/SW oriented.*

		Orientation	
	Years	**NW**	**SE**
Kalamaria	1	-0.01	-0.04
Athens	3	-0.26	-0.23
Kalamaria	5	-0.24	-0.13
Athens, Kalamaria	10	-0.51	-0.97
Kalamaria	15	-0.42	-0.71
Athens	20	-0.46	-0.59
Athens	70	-0.81	-0.59

3.1.4. Influence of the rock type

This analysis would permit to analyze different lithologies exposed in various climates for the same period of time, thus allowing to assess if the recession is also controlled by the rock properties.
Unfortunately, this correlation is almost always not practicable because different rock types were generally used in different periods, therefore they always have different ages. However, from a 1987 report of the CWGC, it seems that Portland was used for substitutions in the First World War cemeteries of Mikra and Lembet in Thessaloniki.
The dates of the substitutions are not available but considering that the original slates were made of Chiampo and the recent substitutions are made in Botticino, these data were analyzed making the assumption that the age of Portland is 70 years old, i.e. the same of original Botticino slates in the Second World War cemeteries.
For this reason, there is one possibility of comparison between Portland and Botticino exposed in a Bsk climate (Athens Phaleron and Kalamaria) for 70 years and NE/SW oriented. In addition, also the winds have the same behavior with respect to the orientation of the slates in the two cemeteries.

Table 15. *Data analysis: influence of rock type. Comparison between Portland and Botticino*

	SE	NW		Rainfall	Winds
Portland	-0.45	-0.50	(Kalamaria)	445	W, WNW(fw); SW, SSW (ss)
Botticino	-0.60	-0.79	(Athens)	397	NW(fw); SW(ss)

These results are not those expected because Portland stone is expected to decay faster due to the various studies in the scientific literature describing this soft limestone. This could be due to:

- Poor statistics for Portland stone. Here are considered only 20 Portland slates from Kalamaria while Botticino slates from Athens are about 200.
- The age of Portland was estimated but it is not sure because CWGG has not kept a reliable record, so it could be inexact.
- Athens pollution is higher than Thessaloniki and the cemetery is near the sea and thus subjected to the marine aerosols, especially when the SW and SSW winds blows. These conditions clearly lead to a faster decay and consequently a higher recession rate.

3.1.5. A note on the standard deviation error

Every gravestone had been measured three times, so every recession measurement considered in this work is the average of three measures (Table 16). Recession is the difference between the average top minus the average basis. In this table it is worth notice that the standard deviation error of the three measurements is very low.

Table 16. *Example of measurements. Grave III_C1 of Bologna. R is the Right side while L is the Left one. The geographical orientations have been added during the data elaboration.*

	Base_R	St.Dev Base_R	Top_R	St.Dev. Top_R	Rec._R	Base_L	St. Dev Base_L	Top_L	St.Dev. Top_L	Rec_L
Meas. 1	81.99		81.19			82.74		81.56		
Meas. 2	82.00		81.19			82.75		81.56		
Meas. 3	82.03		81.20			82.75		81.57		
Average	**82.01**	**0.02**	**81.19**	**0.01**	-0.81	**82.75**	**0.01**	**81.56**	**0.01**	-1.18

The values of the standard deviation error of the recession measurements obtained for the Castiglione cemetery (all slates are made of Botticino and they have the same age), are very high, and they seem to elide the differences between among the recession recorded on the various orientations (Table 17.

Table 17. *Standard deviation error of the recession values collected in the South African cemetery of Castiglione dei Pepoli (BO).*

E	dev.st	NE	dev.st	NW	dev.st	W	dev.st	SW	dev.st	SE	dev.st
-0.62	0.83	-0.51	0.96	-0.59	0.91	-0.42	0.87	-0.44	-0.44	-0.81	0.99

However, during the measurements, it has become more and more evident that also some new slates presented high or even positive recession values although the expected values should be close to zero. This means that there is a thickness variability linked to the realization of the headstones themselves, whose surfaces are not always perfectly parallel. Indeed, a variability of the primary thickness is expected due to modern cutting machines having errors of about 1 mm. For this reason, the values of recession of about 350 recent headstones, expected to be close to zero had been analyzed without distinguishing climate, orientation and rock typology (Tables 18, 19). It resulted that when dealing with a large number of slates (in our case 358 measurements of 5 years old slate and 232 measurements of 1 year slates) the average recession value converges on the average value of the significant recession. In fact, for these slates the average value of recession is close to zero and this suggests a random error which affects the data dispersion but not the average value of the recession rate.

Table 38. *Analysis of the measurements of the recession rates of gravestones aged 5 years old maximum. Mean of 358 measurements. A= standard deviation of the standard deviations of the measurements of the base thickness on the right side, B= standard deviation of the standard deviations of the measurements of the top thickness on the right side, C= standard deviation of the standard deviations of the measurements of the base thickness on the left side, D= standard deviation of the standard deviations of the measurements of the top thickness on the left side*

A	B	**Rec_R**	Dev. St. Rec _R	C	D	**Rec_L**	Dev. St Rec_L	**Mean Rec.**	Dev. St. Mean Rec.
0.03	0.04	-0.25	0.59	0.02	0.02	-0.21	0.69	-0.23	0.58

Table 49. *Analyisis of the measurements of the recession rates of gravestones aged 1 years old. Mean of 232 measurements. A, B, C, D as in Table 18.*

A	B	**Rec_R**	Dev. St. Rec _R	C	D	**Rec_L**	Dev. St Rec_L	**Mean Rec.**	Dev. St. Mean Rec.
0.03	0.02	-0.23	0.48	0.02	0.02	-0.10	0.48	-0.16	0.43

In addition, the standard deviations of the standard deviations of the single measures are very low and it means that the three measures are very precise.
In conclusion, relying on a large number of measurements, the average values are significant, although they are still characterized by a high standard deviation values.
The problem of dispersion wasn't never underlined in the scientific literature. It was cited by some authors (Roberts 2005) but was attributed to the variability of stone shape or to the way of measuring of different operators.
This adds uncertainty to all those recession equations that are based on the measure of recession of tombstones. How many measures did they collect? How many gravestones did they considered? How much consistent was the standard deviation error of their measures? And how much was the total dispersion?

4. Conclusion

In this paper are summarized the results of the field surveys carried out on headstones made of different rock materials and located in various Commonwealth War Graves Commission cemeteries of Italy and Greece.
Over 3000 recession measurements have been collected and analyzed in order to understand whether the differences of surface recession depend on environmental context, slate orientation with respect to the geographical coordinates and time of exposition. Rainfall and prevailing winds have been also considered. The values of the recession rates are often influenced by rainfall amount and pollution (e.g. Savona). However, the research reported here shows a clear influence of the direction of the prevailing wind on stone recession. Indeed, the recession of stone presented a higher recession on the side exposed to prevailing wind, i.e. that more subjected to the dissolution operated by the wind-driven rainfall.
An interesting prosecution of this research should be that of elaborating more deeply the correlation between winds and recession rates, although the quantification of the velocity and intensity of winds should be interpolated for most localities.
Due to the unreported substitutions made by CWGC throughout the years it was not possible to compare extensively different lithologies exposed at the same environmental conditions.

For this reason, the following part of the research, described in the Part 4, is going to focus the possible correlation between stone recession of different kind of carbonate rocks in controlled environmental conditions in order to identify a textural parameter characteristic of the stone material, that influences the recession velocity of dissolution for the different kind of limestones.

Acknowledgments
Authors show gratitude to the CWGC organization for authorizing the field surveys in their cemeteries, ARPA network and Elleniki National Meteo Service for providing meteorological data. Silvia Salvini would like also to thanks the CWGC gardeners met during the surveys for the information given and their kind hospitality, a special acknowledgement to Claudia Castelli, CWGC responsible for Northern Italy area for the precious information and help.

References

Amoroso G.G., Fassina V. (1983) Stone decay and conservation. Ed. Elsevier, Amsterdam.

Baedecker P.A., Reddy M.M. (1993) The Erosion of Carbonate Stone by Acid Rain. *J Chem Educ*, **70**, 2, 104-108.

Baer N. S., Berman S. M. (1983) Marble tombstone in national cemeteries as indicators of stone damage: general methods. *J Air Pollut Control Assoc*, **83**.

Brimblecombe P. (2010) Heritage climatology. In: Proceedings of the Ravello International Workshop 14-16 maggio 2009 and Strasbourg European Master – Doctorate Course 7-11 Settembre 2009. Ed. Edipuglia, Bari.

Borghi A., Berra V., D'Atri A., Dino G.A., Gallo L.M., Giacobino E., Martire L., Massaro G., Vaggelli G., Bertok C., Castelli D., Costa E., Ferrando S., Groppo C., Rolfo F. (2015) Stone materials used for monumental building in the historical centre of Turin (NW Italy): architectonical survey and petrographical characterization of Via Roma. In: Pereira D., Marker B.R., Kramar S., Cooper B.J., Schouenborg B.E. (Eds) Global Heritage Stone: Towards International Recognition of Building and Ornamental Stone. *Geological Society London Special Publications*, **407**, 201-218.

Dragovich D. (1981) Weathering rates on marble tombstones at a Sydney cemetery. Institute for the Rate of decay of marble in laboratory and outdoor exposure. *J Mater Civil Eng,* **1-2,** 73-85.

Dragovich D. (1987) Measuring stone wheathering in cities: surface reduction on marble monuments. *Environ Geol Water S,* **9,** 139-142.

Dragovich D. (1991) Marble weathering in an Industrial Environment, Eastern Australia. *Environ Geol Water S*, **17-2**, 127-132.

Dolske D.A. (1995) Deposition of atmospheric polluants to monuments, statues and buildings. *Sci Tot Env*, **167**, 15–31.

Dolske D. A., Gatz D.F. (1985) A field intercomparison of methods for the measurement of particle and gas dry deposition. *J Geophys Res*, **90-D1**, 2076.

Dubelaar C. W., Engering S., Van Hees R. P. J., Lorenz H. G., Koch R. (2003) Lithofacies and petrophysical properties of Portland Base Bed and Portland Whit Bed limestone as related to durability. *Heron,* **48-3**, 221-229.

Feddema J., Meierding T. (1987) Marble weathering and air pollution in Philadelphia. *Atmos Environ,* **21-1,** 143-157.

Godden M. (2015) Portland's Quarries and its Stone.

Inkpen R. J., Jackson J. (2000) Contrasting weathering rates in coastal, urban and rural areas in Southern Britain: preliminary investigation using gravestones. *Earth Surface Processes and Landforms*, **25**, 229-238.

Inkpen R.J., Viles H., Moses C., Baily B. (2012a) Modelling the impact of changing atmospheric pollution levels on limestone erosion rates in central London, 1980-2010. *Atm Env*, **61**, 476-481.

Inkpen R.J., Viles H., Moses C., Baily B., Collier C., Trudgill S.T., Cooke R.U. (2012b) Thirty years of erosion and declining atmospheric pollution at St Paul's Cathedral, London. *Atm Env*, **62**, 521-529.

Köppen W (1936) Das geographische System der Klimate. In: Köppen W, Geiger R (Eds) Handbuch der Klimatologie. Ed. Gebrüder Borntraeger, Berlin, pp. 1−44

Meierding T.C. (1981) Marble tombstone weathering rates: a transect of the United States. *Physical Geography*, **2**-1, 1-18.

Moses C.A. (1996) Methods for assessing stone decay mechanisms in polluted and 'clean' environments, Northern Ireland. In: B.J. Smith, P.A. Warke (Eds), Processes of Urban Stone Decay. Ed. Donhead, 212–227.

Pivko D. (2003) Natural stone in Earth's History. *Acta Geologica Universitatis Comenianae*, **58**, 73-86.

Pomerantz A., Sigmund E., Song Y.Q. (2007) Spatial heterogenity lenght scales in carbonate rocks, *Applied Magnetic Resonance*, **32**, 221.

Ponziani D., Ferrero E., Apollonia L., Migliorini S. (2012) Effect of temperature and humidity excursions and wind exposure on the arch of Augustus in Aosta. *Journal of Cultural Heritage*, **13**, 462-468.

Pope G.A., Meierding T.C., Paradise T.R. (2002) Geomorphology's role in the study of weathering of cultural stone. *Geomorphology*, **47,** 211-225.

Reddy M. (1987) Acid-rain damage to carbonate stone: a preliminary quantitative assessment based on the aqueous geochemistry of rainfall runoff.

Reddy S.M., Roberts S.M. (2005) Surface-recession weathering of marble tombstones: new field data and constraints. *GSA*, **390**, 27-37.

Roberts S.M. (2005) Surface-recession weathering of marble tombstones: new field data and constraints, *GSA*, **390**, 27-37.

Schirolli P. (1997) La successione liassica nelle Prealpi Bresciane centro-occidentali (Alpi Meridionali, Italia): stratigrafia, evoluzione paleogeografico-strutturale ed eventi connessi al rifting. *Atti Ticinensi di Scienze della Terra. Serie Speciale*, **6**, 5-137.

Searle D.E., Mitchell D.J. (2007) The effect of coal and diesel particulates on the weathering loss of Portland Limestone in an urban environment. *Sci Tot Envir*, **370**, 207-223.

Siegesmund S., Snethlage R. (2014) Stone in Architecture. Ed. Springer, Berlin

Smith D.I., Greenaway M.A., Moses C., Spate A.P., 1995. Limestone weathering in eastern Australia. Part 1: erosion rates. *Earth Surface Processes and Landforms*, **20**, 451-463.

Stephenson W.J., Finlayson B.L. (2009) Measuring erosion with the micro-erosion meter and contributions to understanding landform evolution. *Earth Science Reviews*, **95,** 53-62.

Trudgill S.T., Viles H.A., Inkpen R.J., Cooke R.U. (1989) Remeasurement of weathering rates, St Paul's Cathedral, London. *Earth Surface Processes & Landforms*, **14**, 175-196.

Trudgill S.T., Viles H.A., Cooke R.U., Inkpen R.J., Heathwaite A.L., Houston J., (1991) Trends in stone weathering and atmospheric pollution at St Paul's Cathedral, London, 1980-1990. *Atm Env*, **25A**, 2851- 2853.

Trudgill S.T., Viles H.A., Inkpen R.J., Moses C.A., Gosling W., Yates T., Collier P., Smith D.I., Cooke, R.U. (2001) Twenty-year weathering remeasurements at St Paul's Cathedral, London. *Earth Surface Processes and Landforms*, **26**, 1129-1142.

Viles H.A., Trudgill S.T. (1984) Long term remeasurement of micro-erosion meter rates, Aldabra Atoll, Indian Ocean. *Earth Surface Processes and Landforms*, **9**, 89-94.

Weiss S., Siegesmund S., Fuller E. R. Jr. (2002) Thermal tresses and microcracking in calcite and dolomite marbles via finite element modelling. *Geological Society London Special Publications*, **205**, 89-102.

Part 4: Accelerated ageing tests on carbonate stones and assessment of their recession rate

ABSTRACT

Water affects stone materials mainly as rainwater, which is a solution variable in chemical composition and pH due to various external factors like pollution, environment, seasonality, etc.
In this study samples of carbonate stones differing in their textural features and mineral composition have been subjected to accelerated ageing tests in an environmental test chamber simulating the wetting effect of rainwater using two different water compositions corresponding to those of the Italian cities of Bologna (pH ~ 7) and Stresa (pH ~ 6).
Bulk stone recession was evaluated considering sample weight loss as a function of the number of wetting cycles. Direct measurements of recession were performed by Confocal Microscopy (CM) and Structure from Motion (SfM) micro-photogrammetry, which allowed 3D surface reconstruction of the stone surface and evaluation of differential recession as a function of calcite grain size. Linear recession measurements allowed the definition of stone-specific phenomenological coefficients to be applied to recession rate estimates obtained from the currently available recession equations for carbonate rocks. The effect of grain size on stone recession have been also discussed and quantified.
This work represents a pilot study in the identification of a rapid and efficient methodological approach able to determine the recession rate of a specific carbonate rock type in a given environment, in order to provide reliable estimates of future stone deterioration under specific environmental conditions from expected climate scenarios.

Highlights
Study on recession rates of carbonate rocks under controlled environmental conditions.
Innovative and accurate measurements of linear stone recession and correlation with textural features of the rock.
Determination of stone-specific phenomenological coefficients for carbonate rocks, to be applied to currently available recession rate equations.

Keywords
Stone recession rate, accelerated ageing tests, rainwater simulation, confocal microscopy, calcite grain size, carbonate rocks

1. Introduction

Water is a first-order cause of stone damage because it can interact in different ways with the stone material causing different patterns of stone decay. Various chemical and physical processes due to the direct or indirect presence of water in its solid, liquid and gaseous states are treated in numerous studies. The most relevant of these processes on stone decay are:

- *Ice crystallization.* Crystallization of ice is an important deterioration factor affecting building stone materials (Camuffo 1995, Altindag et al. 2004, Hall 2004). Although damage is generally considered as the result of the hydraulic pressure caused by the volume expansion of water during freezing, experiments on freezing organic liquids with negative crystallization volume change (Beaudoin & MacInnis 1974) show that the main cause of volume increase during freezing is the crystallization pressure (see Scherer & Valenza 2004, for a review). In heritage management the

number of freezing events is an index of probable damage that seems particularly appropriate (Sabbioni et al. 2010).

- *Salt crystallization.* During confined crystallization within a porous medium, salt exerts a pressure against the constraining pore walls inducing stone expansion and damage. The specific species of salt crystallizing, the super-saturation condition of the solution, the relative humidity in relation to salt deliquescence, will control damage effectiveness of salt crystallization. In addition, the range and frequency of thermo-hygrometric cycles also have a strong impact on salt damage as high super-saturation conditions can be reached through heavy evaporation and/or strong cooling of a saturated solution (Zehnder & Arnold 1989, Rossi Manaresi & Tucci 1991, Benavente et al. 1999, Scherer 1999, 2004, Flatt, 2002; see Steiger 2005a, 2005b, for a review). Stone deterioration related to marine aerosols may produce peculiar degradation patterns with respect to salt transport via capillary rise due to the different paths of solution penetration into the pore system, the surface distribution of hygroscopic salts on the stone surface and the effect on water condensation and retention within the pore system (Moropoulou et al. 1995, Zezza & Macri 1995, Torfs et al. 1997, Chabas et al. 2001, Cardell et al. 2003).
- *Vapor condensation and evaporation.* Cyclical condensation of vapor and evaporation subject the rock to hydric expansion and may significantly contribute to transport of pollutants within the pore system, which are responsible for many deterioration processes. For this reason, the frequency of condensation/evaporation cycles in micropores is sometimes used as an index of stone vulnerability (Camuffo 1984; Camuffo & Sturaro 2001). Nonetheless, condensed water has a weak action on stone surface if compared to rainwater induced recession (Zendri et al. 2001).
- *Biodeterioration.* The intensity of this deterioration process is strongly influenced by the presence of water on the stone surface and within the pore system, and mediated by other important factors such as mineralogy, porosity and permeability of stone, exposure to direct sunlight radiation, orientation with respect to geographical coordinates, pollutant concentration in air and rainwater (see Wakefield & Jones 1998, Warscheid & Braams 2000, Zanardini et al. 2000, Urzi et al. 2001, and Lisci et al. 2003, for a review).
- *Dissolution by interaction with rainwater.* It is a complex process enhanced by the introduction in the atmosphere of anthropogenic pollutants from different sources connected to power plants, domestic heating, automobile and airplane transportation, which progressively increase the atmospheric concentration of inorganic and organic compounds in the form of gases, aerosols and particulate matter, thus producing rainwater acidification. The potential threat of acid rain on cultural heritage assets, especially those made of carbonate rocks, is widely studied in the literature and it is a major concern in conservation science. (Camuffo 1992, Baedecker & Reddy 1993, Bravo et al. 1998, Marquardt et al. 2001, Singh & Agraval 2007, Reis et al. 2012). Yet, we are far from a satisfactory understanding of the interaction among the different parameters controlling stone recession, therefore our ability in predicting trends of future decay is still too weak to be reliably used by stakeholders and decision makers.

1.1. Chemistry of rain affecting carbonate stone decay

Various studies about the characterization of the chemical composition of precipitation assessed that the composition of rainwater is almost never the same from site to site, or even in different moments during a single rain event (Charlson & Rodhe 1982, Dikaiakos et al. 1990, Zilio Grandi & Szpyrkowicz 1991, Samara et al. 1992). Indeed, the composition of rainwater depends on many

factors such as composition of air, dissolved pollutants, wind, physical environmental parameters, type and regime of the precipitation event, season, ...

When a carbonate rock is exposed to rainwater, different chemical reactions can take place (Cardell-Fernàndez et al. 2002, Bonazza et al. 2009, Franzoni & Sassoni 2011):

- *Dissolution in clean rain or 'karst effect'.* The carbonate stone reacts with carbonic acid, derived from dissolved atmospheric CO_2, which determines the natural acidity of rainwater. Precipitation in equilibrium with atmospheric CO_2 has a pH of 5.65 (Lal Gauri & Holdren Jr 1981, Lipfert 1989, Baedecker & Reddy 1993);
- *Acid rain effect: the acceleration of dissolution processes.* Acid precipitation is mainly determined by diluted acid species such as H_2SO_4 and HNO_3 of anthropogenic origin, mainly derived from the combustion of fossil fuels. In this case, additional Ca^{2+} ions are lost from the carbonate stone. Extreme acid rain is responsible not only of marble and limestone deterioration but also of vegetation damage, ocean and fresh water basins acidification;
- *Dry deposition.* Acidic species such as SO_2 and NO_x may come into contact with the stone surface via dry deposition. In the presence of water adsorbed to pore surface or capillary water, after oxidation and reaction with Ca^{2+} released by calcite, soluble salts are formed. These particles, having a higher solubility than the stone material, are then removed in solution from the stone surface, especially when relative humidity is above their deliquescence limit (Dolske 1995, Searle & Mitchell, 2006).

In presence of water atmospheric SO_2 reacts with $CaCO_3$ to form calcium sulfide, which is then oxidized in the presence of a catalyst to calcium sulfate ($CaSO_4 \cdot 2H_2O$, gypsum). This chemical reaction is a common stone decay pattern: in sheltered areas we can often observe black crusts while in areas directly exposed to rainfall the stone remains white (Mc Gee & Mossotti 1992, Fassina et al. 2002, Sabbioni et al. 2003, Grossi et al. 2006), suggesting that rainwater runoff and dissolution processes dominate deterioration, and the main pattern observed is stone surface recession.

1.2. Pollutants

Compounds such as SO_2, SO_3, NO_x, O_3, Cl_2 and organic oxidants are present in the atmosphere as impurities (pollutants). Their emission is mostly connected to human activities as they are present as impurities in fossil fuels (Brimblecombe 1996), which are the main source of energy for goods and human mobility, industrial plants and domestic heating. They readily interact with the minerals through complex physical and chemical interactions thus accelerating stone decay. Despite numerous initiatives have being undertaken by institutions in order to reduce pollutant emissions from industrial plants and vehicles, almost nothing has been done to reduce those generated by aircraft and ships, and the continuous increase of the number of vehicles worldwide, partially neutralized these efforts. The widespread distribution of vehicles and the extremely small size of the particles emitted spread the phenomenon of air pollution even over areas generally considered uncontaminated.

The intensity of air pollution reflects the quantity of total suspended matter. The number and size of particles decrease with height but increase with rising relative humidity.

Aerosols with size ranging from molecules to raindrops usually settle with rain and react with stone materials in aqueous solution. Particle in the size range from 10^{-2} to 10 microns appear to be the most efficient in determining stone decay. They include the larger molecular compounds, such as corrosive sulfates. While small quantities of sulfate, nitrate, and chloride are supplied by natural sources, the majority is introduced in the atmosphere by automotive and industrial sources (Varotsos et al. 2009).

In addition to NO_x and SO_2, the combustion of fossil fuels produces large quantities of CO_2, CO, soot and polycyclic aromatic hydrocarbons, especially during incomplete combustion (Brimblecombe 1996). Gaseous components partially dissolve in rainwater increasing its acidity, while rain droplets capture soot and larger molecules during precipitation and bring them to the ground or stone surface. During dry periods, these particles accumulate on surfaces by dry fallout and contribute to the formation of grey and black crusts, often cemented by gypsum or other salts. Indeed, the black crusts and crumbling stone on marble structures in industrialized regions are mainly composed of calcium sulfate, nitrates and organic particles (Lal Gauri & Holdren Jr 1981).
In the last decades, various researches determined the nature of the atmospheric particulate[18] and observed its effect on human health (Giugliano et al. 2005, Lonati et al. 2005). However, although these little particles are extremely harmful for the population, their effects on monuments are less critical than those related to the above mentioned gaseous compounds (Esbert et al. 2001).

1.3. Damage functions for the recession of carbonate rocks

Degradation phenomena of stone materials can be quantified by considering changes in their surface topography, loss of material or surface recession. The effect of environmental parameters such as concentration of pollutants in the atmosphere, rainfall and temperature are described in term of damage functions, usually using linear or multiple regression techniques, against measured erosional losses.
Several studies tried to assess the contribution of the different processes to the overall stone decay or estimate average weathering rate. Consequently, numerous equations have been drafted throughout time for describing surface recession or loss of material. Among them, the Lipfert's equation (Lipfert 1989b) is the most commonly used:

$$\frac{\text{loss (µm)}}{\text{rain (m)}} = 18.8 + 0.016[\mathrm{H^+}] + 0.18\,(Vd_S * [\mathrm{SO_2}] + Vd_N * [\mathrm{HNO_3}])/\mathrm{R}$$

where H^+ is the concentration of hydrogen ions, Vd_S and Vd_N are the deposition velocities of SO_2 and HNO_3, respectively, $[SO_2]$ and $[HNO_3]$ are SO_2 and HNO_3 concentrations in the atmosphere, and R is the annual precipitation. The Vd_N*$[HNO_3]$ term is often omitted, assuming that its contribution to recession rate is negligible compared to that of the Vd_S*$[SO_2]$ one. The intercept value of 18.8 derives from the solubility of calcite in equilibrium with 330 ppm CO_2 in the atmosphere.
This relation returns an average (generally annual) recession rate based on average values of the considered parameters over the entire period of interest, which are related to few deterioration mechanisms only: the karst effect, the acid rain effect and the dry deposition effect of gaseous components.
The Lipfert's function has been taken under consideration to quantify the annual surface recession of carbonate stone, due to the effects of clean rain, acid rain and dry deposition of pollutants (Bonazza 2009a). Some authors also tried to apply this equation to predict future limestone recession over long periods of time (Brimblecombe & Grossi 2009; Sabbioni et al. 2010), under different IPCC scenarios

[18] Atmospheric aerosol particles, also known as particulate matter (PM) are microscopic solid or liquid particulate matter suspended in Earth's atmosphere. The most diffuse particles are coarse, with a diameter between 2.5 and 10 µm (PM_{10}) and fine particle with a diameter of 2.5 µm or less ($PM_{2.5}$).

of climate change in Europe (Bonazza et al. 2009a). These formulas have been used to predict patterns of erosion rates for heritage materials within urban areas and across wide regions (e.g. Brimblecombe & Grossi 2008; Grossi et al. 2008). Other authors rearranged Lipfert's damage function in order to reconstruct past atmospheric SO_2 pollution levels from recession rate measurements (Inkpen 2013). A similar equation has been proposed by Reddy et al. (1985) to evaluate the annual surface recession normalized to annual rainfall:

$$\frac{\text{loss (µm)}}{\text{rain (m)}} = 4.88 + 0.0015\ \text{H}^+ + 0.069\ \text{SO}_2$$

where SO_2 corresponds to the concentration of this gas in the atmosphere, expressed as $\mu g/m^3$, while $[H^+]$ is the concentration of hydrogen ions in rainwater, expressed as $\mu eq/m^2yr$. The ionic concentration expressed in this way can be tricky. Therefore, in order to express recession rate in $\mu m/m_{rain}\ yr^{-1}$, SO_2 in $\mu g/m^3$ and ion concentration in mmol/L, this equation can be rearranged in the following manner:

$$\frac{\text{loss (µm)}}{\text{rain (m)}} = 4.88 + 150\frac{[\text{H}^+]}{R} + 0.069\text{SO}_2$$

Another recession equation available in the literature is that designed by Baedecker (1990) based on the tests designed in the frame of the US National Acid Precipitation Assessment Program (NAPAP), and based on the combined effect of temperature and concentration of hydrogen ions on material loss:

$$\frac{\text{mmol Ca}^{2+}}{\text{L}} = 0.16\ [1.0 - 0.015\ \text{T} + 0.0000922\ T^2]/0.683 + 0.49\ [\text{H}^+]$$

where T is the temperature in °C and $[H^+]$ is the concentration of hydrogen ions expressed in mmol/L. Expressing the material loss in mmol/L of Ca^{2+} ions is not so immediate. For this reason, Delalieux et al. (2002) modified the mathematical formulation of this damage function in order to express material loss as a linear recession measured in µm:

$$\frac{\text{loss (µm)}}{\text{rain (m)}} = 9.4 * [1.0 - 0.015\text{T} + 0.000092\ \text{T}^2] + 20\ [\text{H}^+].$$

A further equation that is worth mentioning is that proposed by Webb et al. (1992). This expression considers the influence of various pollutant agents expressed in ppb per day, rainfall expressed in mm per day, and acid ionic concentration in mol/m^2 on weight loss of material per unit surface:

$$g/m^2 = -0.162 + 0.0058\text{SO}_2 + 0.0666\ \text{R} + 638\ \text{acid} - 0.026\ \text{NO}_2 + 0.0155\ \text{NO} + 0.0007\text{O}_3$$

This equation has been adjusted by Delalieux et al. (2002) in order to express carbonate loss in linear surface recession (µm) using a general density value for limestone (2500 kg/m^3), and transforming daily values in average annual ones:

$$\frac{\text{loss (µm)}}{\text{rain (m)}} = \frac{150}{\text{R}} * (-0.16 + 0.0020\ SO_2 + 0.18\ \text{R} + 1.7[\ H^+] * \text{R} - 0.0013\ NO_2 + 0.0086\ \text{NO} + 0.0003\ O_3).$$

In this new formulation, the concentration of SO_2, NO_2, NO and O_3 are expressed in µg/m^3, [H^+] concentration in mmol/L, R (rainfall) in m/yr.

Kucera and Fitz (1995) derived their equation based on run-off tests, which lasted 4 years.

Below is their formulation of the total loss after 4 years expressed in g/m^2:

$$\frac{\text{g}}{\text{m}^2} = 34.4 + 5.96\ [\text{TOW}] * SO_2 + 388\ \text{R}*[H^+]$$

where TOW is the time of wetting (period of time when the relative humidity is higher than 80% and the temperature is above 0 °C), SO_2 is the concentration of SO_2 in the air expressed as µg/m^3, [H^+] is the concentration in hydrogen ions expressed in mg/L, and R is rainfall expressed in m/yr. Also in this case the expression can be rearranged in order to represent parameters with the same units as in the others previously described (Delalieux et al. 2002):

$$\frac{\text{loss (µm)}}{\text{rain (m)}} = \frac{0.1}{\text{R}}*(34+6.0[\text{TOW}]*SO_2+390\ [H^+]*\text{R})$$

Kucera and his research group investigated the effect of contemporaneous occurrence of different pollutants on materials including cultural heritage in the frame of international exposure programs such as the International Cooperative Programs (ICPs) of the United Nations Economic Commission for Europe (UN/UCE) reported in Tidblad et al. (2001). They eventually modeled multi-pollutant impact on different materials under the MULTI-ASSESS Project (2007) for assessing threshold levels of pollutants for the cultural heritage, and they proposed a damage function for carbonate rocks (Kucera et al. 2007) where annual surface recession is expressed as follows:

$$\text{loss (µm)} = 3.95+0.0059\ SO_2*RH_{60}+0.054\ \text{R}\ [H^+]+0.078\ HNO_3*RH_{60}+0.0258\ PM_{10}$$

where concentration of SO_2, HNO_3 and PM_{10} are expressed in µg/m^3, [H^+] is expressed in mg/L with possible values in the range 0.0006-0.13, RH_{60} is the measured relative humidity when this value is above 60% (if RH value is below 60%, a null value is assigned), and R is the annual rainfall in mm.

A further attempt to describe stone damage is described in Delalieux et al. (2002). These authors derived the following equation:

$$\frac{\text{loss (µm)}}{\text{rain (m)}} = \frac{0.015}{\text{R}}*(\text{-}29+590\text{R}+800\ [H^+]*\text{R}+5300\ [SO_4^{2-}]*\text{R}+5.5\ SO_2)$$

where R is the rainfall expressed in m/yr, SO_2 is the concentration of sulfur oxide in the atmosphere (µg/m^3), while [H^+] and [SO_4^{2-}] are ionic concentrations in rainwater, expressed in mmol/L and R is rainfall expressed in m/yr.

Lan et al. (2005) accounted for the effect of stone exposition to sheltered and unsheltered environments after a number of field exposure experiments. They obtained the following damage function in sheltered areas:

$$\text{loss } (\mu\text{m}) = (0.00111\ \text{RH}^*\text{SO}_2)^* t^{0.784}$$

whereas in unsheltered areas recession resulted to be described by the following expression:

$$\text{loss } (\mu\text{m}) = (0.00233\ \text{RH}^*\text{SO}_2)^*\ t + 0.00309\ \text{R}$$

where loss is expressed in μm, R is the total rainfall (mm), *t* is the exposure period in years, SO_2 is the concentration of sulfur dioxide expressed in ppb, RH is the average relative humidity (%). It is evident that the influence of direct rain is taken into account.

Livingston (2016) applied an aqueous geochemical modeling approach to determine the effect of acid rain runoff and dry deposition on carbonate dissolution. He then calculated the acid neutralization path in the pH range 3.5-6 and the effect of dry deposition, describing material loss in terms of amount of Ca^{2+} ion released by the material applying the electroneutrality condition between the solution chemistry of rainfall and runoff:

$$\Delta Ca^{2+} = \Delta SO_4^{2-} + 0.5\ \Delta N_3^- + 0.5\ \Delta(Cl^- - Na^+) + 0.5\ \Delta Alk + \Delta Organics.$$

Livingston (2016) concluded that dry deposition has the potential to contribute nearly by an order of magnitude more to carbonate dissolution with respect to wet acid neutralization. He also observed that SO_4^{2-} was by far the dominant contributor to the pH reduction of rainfall considering a dataset collected in New York City in the early 1980s, with an important contribution of organic acids. Their impact is considered increasingly relevant, considering the progressive declining values of SO_2 in Western Europe and Northern America. Unfortunately, the effect contribution of organic acids was only indirectly assessed in Livingston (2016) assuming that the considerably positive Ca^{2+} unbalance is totally caused by their presence in rainwater.

It is therefore clear from present day models of surface erosion for carbonate rocks that they rely exclusively on environmental factors including air pollution, water composition, atmospheric CO_2 concentration, rainfall and temperature. These models tend generally to underestimate the rate of surface erosion in historical buildings, which is sometimes 2-3 times greater (for example, long term observation studies on the St. Paul's Cathedral in London by Inkpen et al. 2012a, 2012b). Therefore, the prediction of stone decay and damage to heritage urgently require improvement on our knowledge in this research field by refining recession models for carbonate rocks, considering additional factors, which have a first order effect on deterioration, such as petrographic and textural features of the rock. Grain size, porosity, pore-size distribution, mineralogy (e.g. content in clay minerals, sulfurs, etc.) also affect surface recession rate. A careful evaluation of these features is therefore essential to understand and quantitatively model differences in recession rate of stones exposed to the same environmental conditions, or heterogeneity in the recession rate of a given stone material.

1.4. Simulations of rainwater and use of environmental test chambers.

The extreme variability of rainwater composition makes more difficult the evaluation of the parameters affecting stone decay. Many researches have focused their attention on the field test method in order to observe the decay variability of different stones exposed to the same natural environmental conditions, or that of a certain stone type to different environmental conditions when exposed in different places (Comite et al. 2017). Sometimes these studies only considered the analysis

of stone decay or material loss, in other cases runoff water composition was also determined and correlated to recession rate.

However, field tests have various issues to be considered:

- Rate of stone decay is relatively slow if compared to the standard times required by a scientific research project to achieve final results; therefore, most of these types of experiments are carried on for few years. Under these constraints, surface changes are generally so small that their quantification in terms of environmental parameters is affected by considerable errors, hence the method is hardly applicable to the reliable prediction of long term surface recession;
- Realistic exposition tests should be designed for much longer periods, at least 10 years, in order to assess meaningful recession estimates. Such long time series of erosion measurements under monitored environmental conditions are extremely rare in the literature, and the case described in Inkpen et al. (2012a, 2012b) represents a unique series of recession measurements at St. Paul's Cathedral in London lasted thirty years;
- Although field tests have the advantage to submit stones to real outdoor environmental conditions, results on stone recession obtained at a specific site are hardly applicable elsewhere. Indeed, real situations are often extremely complex (various sources of pollution, orientation with respect to the geographical coordinates, extreme acid rain events, wind-blown dust, wind-blown marine aerosols, temperature and RH regime, volcanoes, etc.) and the specific combination of deterioration factors is hardly similar in two different localities unless in terms of generic climate conditions, which may determine which of the possible acting deterioration mechanisms tent to prevail (Kottek et al. 2006; Brimblecombe 2010);

For this reason, some authors tried to reduce the number of variables, for example simplifying the composition of rainwater. Baedecker & Reddy (1993) sprayed a solution prepared using deionized water acidified with sulfuric acid over slabs of marble and limestone, and runoff water collected and analyzed. Thornbush & Viles (2007) placed limestones in plastic bottles filled with solutions containing variable concentrations of H_2CO_3, maintained at constant temperature for 25 days and evaluated weight loss.

Herngren et al. (2005) suggested a procedure to reproduce as closely as possible the chemical characteristics of natural rainfall to be used in indoor experiments, starting from deionized water and adding sulfuric acid for controlling pH, common salt for simulating the electrical conductivity and methanol for imitating the concentration of dissolved organic carbon. Herngren et al. (2005) also designed a rainfall simulator in order to simulate natural runoff on slightly inclined slab surfaces and homogeneous water supply to the different areas of sample surface.

The effect of specific environmental parameters can be also assessed using environmental test chambers. This practice is particular diffused in conservation science for testing the decay of materials and conservation products under specified environmental conditions (Melo et al. 1999, Dal Bianco et al. 2008, Salvini et al. 2012). They are generally designed to control few environmental parameters such as temperature and relative humidity, and they often work using purified water. It is therefore possible to impose variation cycles or extreme conditions of such parameters and to test material resistance or protection efficiency on stone materials under controlled environmental conditions.

Other environmental test chambers are specifically designed for specific stone test methods such as the determination of resistance to aging by SO_2 action in presence of humidity or by salt mist, or for determining the effect of the UV radiation on materials, simulating the exposition to the solar radiation, especially for new products used in conservation (Vacchiano et al. 2007).

1.5. Measurements of stone recession

Different methods of measurements of stone decay exposed outdoor for long periods of time have been reported in the literature. These include the comparison of photographs taken at different times (Winkler 1977, Amoroso & Fassina 1983), the difference in elevation at subsequent measurements with respect to a reference surface using micrometers (Trudgill et al. 1989, Inkpen 2012a, 2012b), the determination of surface recession of slabs or headstones using calipers (Meierding 1981, Baer & Berman 1983, Feddema & Meierding 1987, Roberts 2005), the determination of surface recession by measuring the height difference between lead lettering and marble surface (Dragovich 1991), the amount of Ca^{2+} ions removed from the surface during runoff experiments (Reddy 1988, Delalieux et al. 2002). Further details on these different methods have been discussed in Part 3.

Large discrepancies arose when damage functions have been tested against long-term (over decadal) direct recession measurements (Inkpen et al. 2012a, 2012b). Differences between dose-response functions and measurements of stone erosion, and non-linear response of recession rate to environmental changes (e.g. reduction of SO_2 concentration in the urban atmosphere) have been often observed, and discussed in terms of measurement effects, such as the edge effect on stone tablets, differences in weathering effects over flat vs. rough surfaces (Moses 1996), problems to monitor erosion on stone tablets using micro-erosion meter (MEM) systems (Inkpen 1989), or in terms of differences in the erosional processes on the building surface, such as the topography effect connected to the formation of *rillenkarren* (Lundberg & Ginés 2009) modifying superficial runoff and consequently influencing saturation levels, the effect of biological activity (Viles et al. 2008; Viles 2011), and the memory effect connected to the reactivation of salts (Cooke 1989).
Also accounting for these possible effects, Inkpen et al. (2012a; 2012b) found that dose-response models provided unacceptable underestimation of the surface erosion rate in the St. Paul's Cathedral in London compared to their 30-year MEM-measurements, revealing the unsuitability of available dose-response models in predicting surface recession rates, at least to their case study. Furthermore, some additional factors should be considered and included in the damage and dose-response functions, in order to obtain reliable predictions of the recession rate. Among them, petrographic and textural features of the rock may have a first-order effect on deterioration. Therefore, accelerated aging tests have been conducted on a set of carbonate rocks differing for their textural features (e.g. calcite grain-size from fine-grained micrite to coarse sparitic calcite, porosity) and abundance in secondary mineral phases). Tests consisted in cyclically immerging stone specimens in two different types of water artificially prepared in a way to match those of the town of Bologna, with pH ~ 7, and Stresa, with pH ~ 6. Bulk stone recession was then measured evaluating weight loss, while detailed assessment of recession on the different stone fractions with different grain-size was precisely determined using a confocal measuring laser microscope with a nominal sub-micrometrical precision.

2. Materials and methods

2.1.Materials analyzed

Regarding the selection of materials to be subjected to accelerated aging tests, eleven carbonate rock types have been considered among those most frequently used in the built environment of north-eastern Italy, including the Commonwealth War Graves Commission cemeteries: Vicenza Stone

(Nanto and Costozza varieties), Istria Stone, Chiampo Stone (Porfirico and Ondagata varieties), Red and Brown Verona Stone, Pink and White Asiago Stone, Aurisina Stone, Botticino Stone (Table 1). In addition, Carrara marble has also been selected. This was an important point, considering that most of previous studies on recession rate of carbonate rocks are mainly based on measurements performed on marbles, and often on Carrara marble (Meierding 1981, Reddy & Roberts 2005).

Table 1. *Summary of principal lithological classification, geological formation and age of the carbonate rocks considered in this research.*

Sample	Folk classification	Kendall/Folk classification	Dunham classification	Geological Formation	Geological Age
Carrara Marble	---	---	Crystalline carbonate	Tuscan Nappe	Cretaceous
Botticino Stone	Dolomitic Micrite	Dolomitic Micrite	Crystalline carbonate	Corna Formation	Upper – Lower Jurassic
Brown Verona S.	Biomicrite	Intramicrite	Wackestone	Rosso Ammonitico Veronese	Middle – Late Jurassic
Red Verona S.	Biomicrite	Intramicrite	Wackestone	Rosso Ammonitico Veronese	Middle – Late Jurassic
Chiampo Paglierino S.	Biomicrite	Intramicrite	Packstone/Grainstone	Nummulitic Limestone	Middle Eocene
Chiampo Ondagata S.	Biomicrite	Intramicrite	Packstone/Grainstone	Nummulitic Limestone	Middle Eocene
Pink Asiago S.	Biomicrite	Oomicrite	Wackestone	Majolica Veneta	Lower Cretaceous
Nanto S.	Biomicrite	Biomicrite	Packstone	Nummulitic Limestone	Lower Eocene
Costozza S.	Biomicrite	Biomicrite	Packstone	Calcareniti di Castelgomberto	Oligocene
Aurisina S.	Biomicrite	Biomicrite	Packstone	Trieste Karst Limestone	Cretaceous
Orsera S.	Micrite	Dismicrite	Mudstone	Unity of External Dinarides	Jurassic

Besides their common occurrence in the built heritage, a large range of petrographic and textural features also characterize these rocks, in terms of content of minor mineralogical constituents, mainly clay minerals and dolomite, porosity and pore-size distribution, and grain size of calcite. The careful evaluation of these features is therefore essential to understand and quantitatively model differences in recession rate of stones exposed to the same environmental conditions, or heterogeneity in the recession rate of a given stone material in portions differing for any of the characteristics mentioned above.

2.2. Laboratory analysis

Standard uncovered thin sections have been prepared by cutting a piece from the main stone samples using a slide cutting station. Before fixing the samples to the glass, pieces were vacuum soaked with epoxy resin (Araldite 2020) previously colored with a specific deep blue powder dye. Other unstained and uncovered standard thin sections were also prepared from each of the samples.

Thin sections were observed using a Zeiss® Axio Scope.A1 optical microscope (OM) coupled with an Axio CamMRC5 (Department of Geosciences, Padova) in order to determine their petrographic and textural features. Further investigation was performed using a CamScan MX 2500 scanning

electron microscope (SEM) (Department of Geosciences), equipped with a LaB6 cathode, operating at 20 kV and a working distance (WD) of 20 mm. With this equipment, 30 x 40 matrixes of backscattered electron (BSE) 1280 × 1024 pixels images were acquired at a magnification of 200X (1 pixel corresponding to 0.5 microns) with an overlapping of 25%. Digital Image Analysis (DIA) allowed obtaining information on the sample porosity and pore structure.
A representative aliquot of each sample was ground and analyzed by X-ray Fluorescence (XRF) and X-ray Powder Diffraction (XRPD) at the Institute of Geosciences and Earth Resources (IGG-CNR, Padua).
The chemical composition was determined by X-Ray Fluorescence (XRF) spectroscopy using a Philips PW 2400 spectrometer equipped with a 3kW Rh X-Ray tube, while the mineralogical composition of the studied samples was identified using a PANalytical θ-θ diffractometer equipped with a Cu X-ray tube operating at 40 kV and 40 mA, a sample spinner, a Ni filter and a solid-state detector (X'Celerator).

Figure 6. *Preparation of the samples in order to be subjected to the accelerated aging tests. View of the samples after the final lapping or polishing stage (a); preparation of reference surface: cutting washers (b), polishing (c-d), view of a set of a sample after attachment to the metal washers to be used as reference surface and final polishing, ready for the accelerated aging tests.*

Cores (length=2 cm, diameter= 8 mm) were then drilled from the samples in order to perform Mercury Intrusion Porosimetry (MIP) and X-ray computed micro-tomography (micro-CT).

2.3. The preparation of the samples for the accelerated ageing tests

Sets of 22 specimens (dimension: ≈ 2 x 2 x 1 cm) have been prepared in order to be subjected to accelerated aging tests in an environmental test chamber (Fig.1).
Stainless steel washers were cut in two halves, attached to the opposite sides of each specimen with Araldite 2020 and lapped or polished to the stone surface. These metal parts are resistant to decay, and therefore they may be used as reference quote (Fig.1b-c-d) in the evaluation of stone recession. Each set of 22 specimens comprised 2 samples of the chosen 11 rock types, one sample finished by lapping on sandpaper with a grit of 1200, and the another polished with a grit of 4000 and high gloss finished with a final polishing using a Syton machine. The reason for preparing these two different superficial finishing patterns is that we intended to verify whether initial surface features affect recession under the same environmental conditions, considering that a lapped surface most commonly represents the surface pattern of a stone stab, while a high glossy polishing significantly reduces initial specific surface of the rock, with possible effects on the first stages of rainwater attack.

2.4. The artificial rainwater used for the aging tests

Accelerating aging tests consisted in a sequence of immersion and emersion cycles within two different solutions artificially prepared in order to be as similar as possible to rainwater wetting the city of Bologna (Panettiere et al. 2000), with a pH ~ 7, and Stresa (Rogora et al. 2004), with a pH ~ 6. The ionic concentration of these two types of water are reported in Table 2. The necessary ions were introduced in the form of compounds: $CaCO_3$, $CaCl_2$, KCO_3, Na_2SO_4, $Mg(OH)_2$, H_2SO_4(96%), NaCl, $CaSO_4$, $MgSO_4 \cdot 7H_2O$, $[NH_4]_2SO_4$, $[NH_4]NO_3$, KNO_3, NH_3(21%), HNO_3(98%).

Table 2. *Composition of the two types of water used for the accelerated aging test. Concentration values exposed here are in mmol/45 l, which is the total volume of water prepared to be located within the environmental test chamber used.*

	Na^+	K^+	Mg^{2+}	Ca^{2+}	Cl^-	SO_4^{2-}	HCO_3^-	NH_4^+	NO_3^-	H^+
Bologna	*1.575*	*0.495*	*0.540*	*3.465*	*1.755*	*1.575*	*4.23*	*--*	*--*	*--*
Stresa	*0.810*	*0.135*	*0.360*	*2.88*	*0.405*	*3.69*	*1.89*	*2.34*	*1.80*	*0.675*

2.5. The environmental test chamber

Aging tests have been performed using a benchtop Suntest CPS$^+$ Xenon exposure system (Department of Chemical Sciences, Padua University) equipped with a Xenon Arc Lamp and an immersion system to completely cover specimens with water. This equipment can contain 45 liters of water and it permits the study of water influence on decay (Fig.2a-b). The system is also equipped with a parabolic reflector redirecting the radiation emitted by the xenon lamp in all directions in order to uniformly radiate the samples, a photodiode, designed to measure the total radiation to which the samples are exposed, and a ventilation system, which is essential to maintain internal temperature of the chamber to the preset value.
The samples were subjected to a total of 240 cycles under dry (emersion phase) or wet (immersion phase) conditions.
Each aging cycle consisted of two different phases: the first phase, lasting 60 minutes, consisted in the immersion of specimens in a water kept at a constant temperature of 25°C, with basal standard temperature of 40°C and irradiation of the Xenon lamp of 300 W/m^2; the second phase, lasting 180 minutes, consisted in the emersion and drying of the samples under a UV light (500 W/m^2) with basal standard temperature of 70°C. Experimental parameters are also summarized in table 3.

Figure 7. *Filling of the climatic chamber (Department of Geosciences) and samples inside.*

Table 3. *Environmental test chamber parameters for the accelerated aging cycles performed.*

Phase	**$T_{(water)}$**	**$T_{(ref\ surf)}$**	**Irradiation**	**Time**
Immersion	25°C	40°C	300 W/m^2	60 min.
Emersion	No water	70°C	500 W/m^2	180 min.

2.6. Recession measurements

Material loss of the different specimens has been evaluated after 54, 141, and 240 cycles with respect to the original stone surface. Stone surface recession has been evaluated in different ways. The first one consisted in the measurement of the weight loss of the sample using an analytical scale (accuracy 0.0001 g). Weight loss was then converted to volume loss dividing by stone density and then to linear recession dividing volume loss by the external surface measured using a caliper.

The second method consisted in the three-dimensional surface description using an Olympus Lext OLS4000 confocal laser microscope (Department of Geosciences, University of Padova). For each sample a matrix of 6x6 scans was acquired at a magnification of 200x. Each scan consist of a number of acquisition layers merged by the software, the number of which strongly depends on the surficial roughness of the samples and affects total acquisition time. As an example, for the marble about 40 layers were required, determining an acquisition time of about 30 minutes in fine mode for the whole matrix, while for the Nanto and Aurisina stones 180 layers were necessary, determining an acquisition time of about 90 minutes or higher. Each acquisition resulted in a surface topographic map of the sample with a vertical submicrometric resolution. For each sample four different topographic maps were produced, one before the attack and one after each set of aging cycles. These data were then exported as *.csv files and processed by the Matlab® software package in order to generate point clouds to be successively imported in ArcMap® computer program. This software allowed building a reference surface for each of the topographic maps taking the metal altitude as a reference. Recession in each specific point or area of interest was then obtained by difference from the reference surfaces. An attempt to obtain a measurement of the recession has been also done by Structure from Motion (SfM) μ-photogrammetry. Collected images were elaborated with Agisoft Photoscan® software package to produce 3D models of the stone surface with a nominal resolution of about 5 microns. Further details are explained in the Technical Note.

3. Results

3.1. Petrographic and textural characterization

Laboratory analysis were performed on portions of fresh quarry samples in order to determine petrographic and textural features. The results obtained by XRPD on the mineral composition of the different samples considered and by XRF on the bulk chemical composition are summarized in Table 4. Table 5 reports the data relative to the porosity determined by different techniques while table 6 reports the results relative to the grain size measurements obtained from the analyses made with the optical microscope in thin section. A more detailed discussion about the sample materials and laboratory analyses performed is reported in Part 1 and Part 2.

Table 4. *Results of the laboratory analyses carried out through XRPD and XRF. Mineral abbreviations: Cal = calcite; Qtz = quartz; Dol = dolomite, Mg-Cal=Mg-Calcite, Ms = muscovite; Ill = Illite; Plg M = palygorskyte M. Percentages obtained with RIR method. A= Pink Asiago Stone, AU=Aurisina Stone, B=Brown Verona Stone, BO= Botticino Stone, C=Chiampo Ondagata Stone, M=Carrara Marble, N= Vicenza Stone (Nanto Variety), O=Istria Stone (Orsera variey), P=Chiampo Paglierino Stone, V = Vicenza Stone (Costozza Variety).*

Sample	XRPD	XRF (only %, traces elements are not showed here)											
		SiO_2	TiO_2	Al_2O_3	Fe_2O_3	MnO	MgO	CaO	Na_2O	K_2O	P_2O_5	L.O.I.	TOT
A	98% Cal, 2% Qtz	1.09	0.01	0.25	0.18	0.03	0.27	54.65	0.01	0.05	0.04	42.85	99.42
AU	100% Cal	0.01	0.01	0.01	0.02	0.01	0.16	56.13	0.01	0.01	0.01	42.97	99.32
B	94% Cal, 4% Ill, 2% Qtz	2.45	0.04	0.72	0.49	0.13	0.30	53.01	0.01	0.13	0.13	42.01	99.44
BO	57% Cal, 43% Dol	0.04	0.01	0.06	0.03	0.01	10.07	47.57	0.01	0.01	0.01	41.53	99.33
C	66% Cal, 34% Mg-Cal, traces Plg M	0.35	0.02	0.12	0.12	0.01	0.53	54.70	0.01	0.01	0.03	43.47	99.38
M	100% Cal, traces Ms	0.01	0.01	0.05	0.02	0.01	0.83	57.83	0.01	0.01	0.01	40.21	98.99
N	95% Cal, 5% Ill	2.66	0.23	0.92	1.18	0.01	0.50	52.11	0.01	0.31	0.04	41.71	99.67
O	100% Cal	0.28	0.01	0.16	0.06	0.01	0.20	55.89	0.01	0.03	0.01	43.17	99.82
P	61% Cal, 38% Mg-Cal, 1% Plg M	0.71	0.02	0.18	0.14	0.02	0.57	54.40	0.01	0.01	0.03	43.30	99.39
R	100% Cal	0.42	0.01	0.20	0.18	0.01	0.26	55.26	0.01	0.05	0.07	43.14	99.60
V	100% Cal	0.16	0.01	0.11	0.20	0.01	0.28	55.48	0.01	0.02	0.03	43.25	99.55

Table 5. *Summary of laboratory analysis about porosity. Samples abbreviations as in Table 4.*

Sample	SEM (DIA)		Porosity (MIP)		Porosity (m-CT)		Density
	%tot > 5 µm	Ø max (µm)	%tot > 0.006 µm	Ø max (µm)	%tot > 5 µm	Ø max (µm)	
A	0.17	6.80	3.53	216.47	0.28	23.72	2.6881±0.0080
AU	0.62	235.40	4.61	272.89	1.20	270.41	2.7055±0.0075
B	0.03	134.94	0.10	4.04	0.07	71.16	2.7209±0.0056
BO	4.34	607.89	1.73	235.34	1.30	147.07	2.7669±0.0043
C	1.72	112.26	1.04	216.47	1.49	33.21	2.7074±0.0076
M	2.11	233.51	1.00	215.56	0.03	33.21	2.7413±0.0027
N	25.08	2067.75	27.18	371.77	8.98	308.37	2.7890±0.0087
O	0.42	169.91	0.40	211.13	1.07	90.14	2.7107±0.0073
P	0.95	285.78	0.34	221.52	0.73	33.21	2.7085±0.0041
R	0.64	181.81	0.25	379.47	0.27	42.70	2.7292±0.0053
V	17.33	584.17	28.52	221.52	13.54	241.95	2.7369±0.0049

Table 6. *Grain size of the different portions recognized and measured in thin section for the different samples. Values marked with asterisk have been calculated mediating at least 100 measures, 1000 in the case of marble. Samples*

Sample		**Grain size (μm)**	**Notes**
A	Micrite	<0.1-0.3	
	Bioclasts	44*	
	Sparry calcite	1-2, 3-5 inside bioclast	
AU	Micrite	<1	
	Bioclasts	Up to 1000-2000	Often micritized, echinoderms have a monocrystalline behaviour
	Sparry calcite	5-10	
B	Micrite	5-10	
	Fine micrite	1	
	Bioclasts	Ostracods: 30* (thickness) Ooids: 85*	Monocrystalline behaviour
BO	Dolomite	127*	
	Fine micrite	2	
	Micrite	5-10	
C	Micrite	<1	
	Sparry calcite	40* (within bioclast) – 25* (within rock porosity	
	Bioclasts	Up to cm size	Constituted by isoriented calcite grains (<3 μm), central pores filled with sparite
M	Texture	155*	
N	Sparry calcite	15	Rare
	Micrite (Bioclasts)	1-4	<1 μm if they are micritized bioclast; 3-4 μm if they are isoriented
	Bioclasts (Echinoderms)	300-500	Not so many
O	Micrite	3-5	
	Sparry calcite	40*	Inside veins
P	Micrite	<1	
	Sparry calcite	45* (within bioclast)	
	Bioclasts	Up to 2000	
R	Micrite	5-10	
	Fine micrite	1	
	Bioclasts	Ostracods: 30* (thickness) Ooids: 107*	Monocrystalline behaviour
V	Sparry calcite	5-10	
	Bioclasts	500 (Echiderms) or more	
	Micrite	<1	In micritized fossils.

3.2. Sample recession based on weight measurements

After 54, 141 and 240 aging cycles, samples were dried and weighted. Weight loss was calculated by difference from the weight of the sample measured before the aging experiment (Table 7). Weight loss was converted into volume loss dividing by stone density, and then to linear recession dividing by the sample area calculated from the sample dimensions as measured with a caliper (accuracy 0.001

mm). Recession values expressed in micron are reported in Table 8. Fig. 3 shows the recession values as a function of the number of aging cycles.

Considering that most of the data from literature that contributed to the calibration of the recession rate functions derive from recession measurements of marbles, the recession value of Carrara Marble after 240 aging cycles may be used to assess the corresponding rainfall. For this reason, chamber parameters and average values of the concentration of pollutants in the atmosphere of the town of Padova were considered to apply the different recession functions from the literature. In particular, the following parameters have been used: atmospheric SO_2, NO_2 and O_3 concentration of 4.5 $\mu g/m^3$, 40 $\mu g/m^3$, and 185 $\mu g/m^3$, respectively (average annual data provided by ARPAV); deposition velocity of SO_2 and NO_2 of 0.3 cm/s and 0.1 cm/s, respectively (Lipfert 1989b); a pH = 6 and SO_4^{2-} concentration of 0.082 mmol/L for the Stresa water and a pH = 7 and SO_4^{2-} concentration of 0.035 mmol/L for the Bologna water; a time of wetness (TOW) of 0.6; and a temperature of 25°C. Imposing a rainfall of 1 m, which is approximately the annual rainfall of numerous cities in northern Italy, recession was calculated using Reddy et al. (1985), Lipfert (1989a), Baedecker (1990), Webb et al. (1992), Kucera and Fitz (1995) and Delalieux et al (2002). Lipfert's equation provided the highest recession values (19.76 μm for both the waters) while Reddy's, Baedecker's, Webb's and Kucera's ones provided similar values, all between 4.9 μm and 6.4 μm. On the contrary, Delalieux's equation provided different estimates for the two different waters: 15.32 μm for the Stresa water, 11.57 μm for the Bologna water. These values are in perfect agreements with the recession measured in the Carrara Marble after 240 aging cycles in Stresa water (17.4 μm) and in Bologna water (11.1 μm), suggesting that 240 cycles in our experimental conditions correspond to a rainfall of about 1 m.

The first important observation is that all samples display different recession after aging cycles in the two different waters. In particular, those immerged in the Stresa water always show higher values of the total recession. This is clearly correlated to the different pH of the two waters, which is lower for the Stresa one (pH ~ 6) and higher for the Bologna one (pH ~ 7).

A second important observation is that different samples display significantly different recession values. As an example, we may compare the recession of Carrara Marble, which is characterized by rather homogeneous coarse grains and low porosity, with that of Orsera Stone, which is a micritic limestone also characterized by homogeneous grain size and low porosity. The latter is clearly higher, about 20-50% more than that of Carrara Marble. Considering recession of the Aurisina Stone, which is characterized by a relatively coarse grain size, although significantly lower than Carrara Marble, intermediate recession rates have been observed. This is a clear evidence of the influence of the grain size on recession rate. In the case of Botticino Stone, the calcitic part of which is mainly characterized by fine grained and coarser micrite, we observed a recession value similar to that of marble, apparently in contrast with previous observations. Nonetheless, we have to consider that these recession values are averaged over the entire surface exposed to decay.

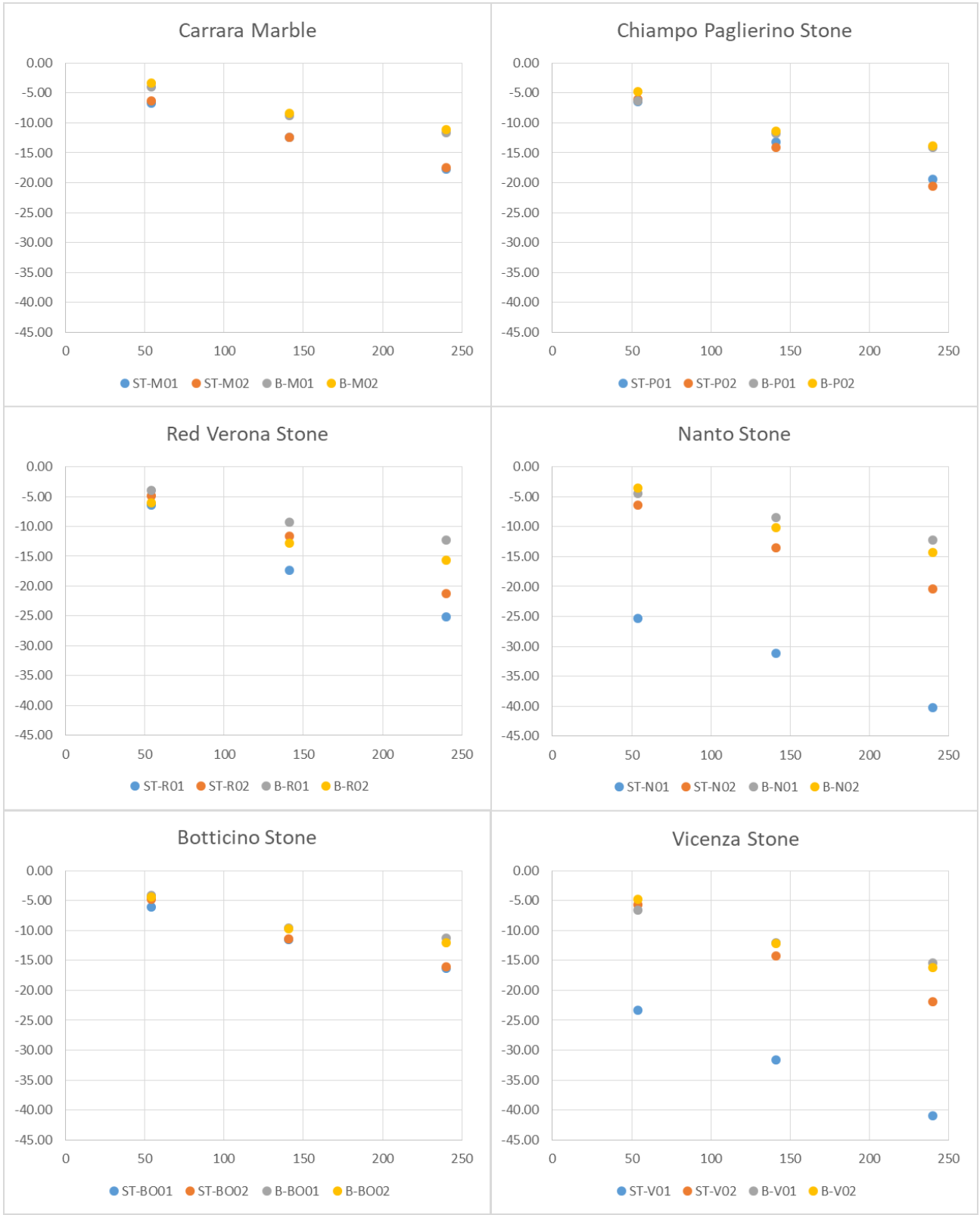

Figure 8. *Recession as a function of the number of aging cycles. Samples with label starting with ST (blue and orange symbols) and B (grey and yellow symbols) are those exposed to the rainwater of Stresa and Bologna, respectively. Labels ending with 01 and 02 refer to highly glossy polished samples and lapped samples, respectively.*

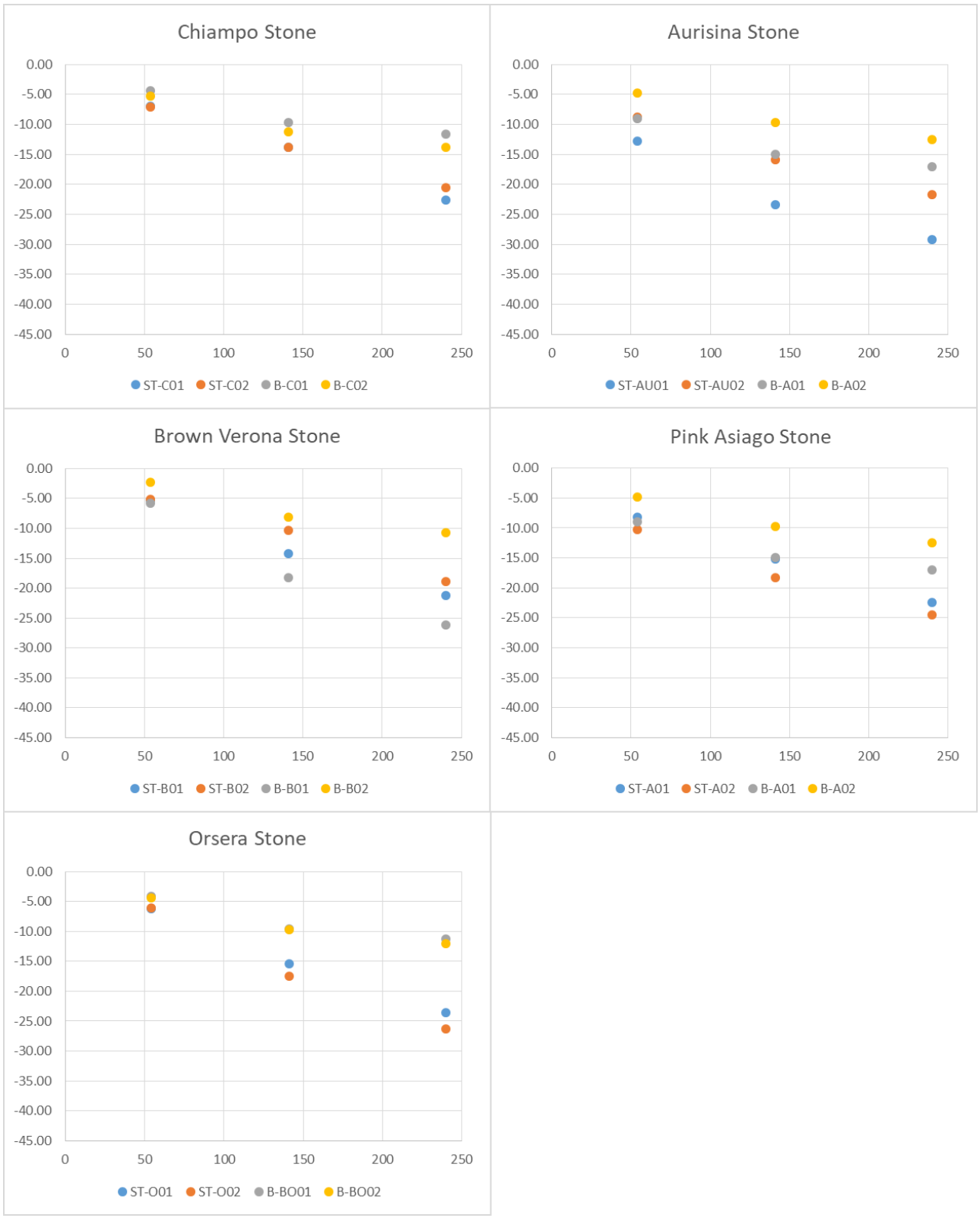

Figure 9. *(continue).*

Table 7. *Weight loss (expressed in grams) of the samples subjected to accelerated ageing in Bologna (pH = 7) and Stresa water (pH=6) after 54, 141 and 240 cycles. Samples abbreviations as in Table 4. 01=polished sample, 02=lapped sample.*

	Bologna			Stresa		
Samples	**T=54**	**T=141**	**T=240**	**T=54**	**T=141**	**T=240**
A-01	-0.0246	-0.0409	-0.0466	-0.0233	-0.0428	-0.0635
A-02	-0.0139	-0.0281	-0.0360	-0.0270	-0.0481	-0.0645
AU-01	-0.0172	-0.0333	-0.0439	-0.0393	-0.0721	-0.0903
AU-02	-0.0114	-0.0297	-0.0384	-0.0292	-0.0532	-0.0724
B-01	-0.0188	-0.0596	-0.0855	-0.0193	-0.0526	-0.0783
B-02	-0.0069	-0.0250	-0.0327	-0.0149	-0.0300	-0.0549
BO-01	-0.0153	-0.0357	-0.0422	-0.0268	-0.0504	-0.0715
BO-02	-0.0145	-0.0321	-0.0401	-0.0153	-0.0358	-0.0509
C-01	-0.0139	-0.0308	-0.0371	-0.0214	-0.0427	-0.0703
C-02	-0.0150	-0.0319	-0.0395	-0.0209	-0.0406	-0.0606
M-01	-0.0150	-0.0326	-0.0430	-0.0229	-0.0426	-0.0607
M-02	-0.0106	-0.0270	-0.0359	-0.0202	-0.0394	-0.0552
N-01	-0.0128	-0.0246	-0.0356	-0.0251	-0.0431	-0.0709
N-02	-0.0118	-0.0343	-0.0480	-0.0205	-0.0431	-0.0653
O-01	-0.0099	-0.0316	-0.0410	-0.0164	-0.0408	-0.0621
O-02	-0.0254	-0.0535	-0.0636	-0.0177	-0.0513	-0.0770
P-01	-0.0189	-0.0349	-0.0419	-0.0189	-0.0382	-0.0563
P-02	-0.0154	-0.0363	-0.0445	-0.0185	-0.0431	-0.0631
R-01	-0.0115	-0.0271	-0.0356	-0.0226	-0.0616	-0.0891
R-02	-0.0229	-0.0487	-0.0594	-0.0138	-0.0330	-0.0606
V-01	-0.0178	-0.0328	-0.0418	-0.0232	-0.0446	-0.0687
V-02	-0.0140	-0.0357	-0.0472	-0.0133	-0.0333	-0.0513

Table 8. *Recession values estimated from weight loss. Values expressed in μm. Samples abbreviations as in Table 4.*

Sample	**BOLOGNA**						**STRESA**					
	Polished			**Lapped**			**Polished**			**Lapped**		
A	-8.97	-14.92	-17.0	-4.81	-9.72	-12.5	-8.24	-15.14	-22.5	-10.28	-18.31	-24,6
AU	-4.63	-8.96	-11.8	-3.35	-8.72	-11.3	-12.7	-23.37	-29.3	-8.73	-15.91	-21.7
B	-5.75	-18.22	-26.1	-2.25	-8.17	-10.7	-5.23	-14.24	-21.2	-5.13	-10.32	-18.9
BO	-4.09	-9.54	-11.3	-4.37	-9.68	-12.1	-6.11	-11.49	-16.3	-4.84	-11.33	-16.1
C	-4.36	-9.66	-11.6	-5.26	-11.18	-13.8	-6.89	-13.75	-22.6	-7.10	-13.80	-20.6
M	-4.05	-8.79	-11.6	-3.29	-8.37	-11.1	-6.68	-12.43	-17.7	-6.38	-12.44	-17.4
N	-4.39	-8.44	-12.2	-3.50	-10.19	-14.3	-8.14	-13.98	-23.0	-6.40	-13.46	-20.4
O	-3.40	-10.87	-14.1	-8.05	-16.96	-20.2	-6.22	-15.47	-23.6	-6.06	-17.55	-26.3
P	-6.38	-11.78	-14.1	-4.80	-11.31	-13.9	-6.50	-13.13	-19.3	-6.05	-14.09	-20.6
R	-3.96	-9.33	-12.3	-6.03	-12.83	-15.7	-6.38	-17.40	-25.2	-4.84	-11.58	-21.3
V	-6.54	-12.05	-15.4	-4.79	-12.22	-16.2	-8.98	-17.26	-26.6	-5.68	-14.21	-21.9
Cycles	**54**	**141**	**240**	**54**	**141**	**240**	**54**	**141**	**240**	**54**	**141**	**240**

Considering that Botticino Stone contains about 46% in dolomite, which is much less soluble than calcite, the linear recession of the calcitic portion of the surface must be significantly higher. Indeed, measurements by confocal microscopy confirm such an idea.

A third systematic trend in stone recession arise when observing samples containing clay minerals. For example, Nanto Stone, Red and Brown Verona Stones, three limestones that have a small but relevant percentage of clay minerals, display the highest recession rates, showing that also the presence of these easily expanding minerals significantly contribute to the total recession of the stone. In addition, the highly glossy polished sample of the Brown Verona Stone (B) showed a significant drift from linearity when exposed to Bologna water between 54 and 141 cycles. This can be explained with a sudden loss of material, considering that the Brown Verona Stone is a nodular limestone, with clay minerals often localized along specific thin layers and subjected to selective erosion during drying-thawing cycles.

Table 9. *Accelerated aging tests of highly glossy polished samples in Bologna water after 240 cycles. Recession values are estimated from weight measurement, and ordered from lower to higher. N value is the ratio between the recession of the stone of interest and that of Carrara Marble. Samples abbreviations as in Table 4.*

	Polished surface	**N value**
BO	-11.3	0.97
C	-11.6	1.00
M	-11.6	1.00
AU	-11.8	1.02
N	-12.2	1.05
R	-12.3	1.06
O	-14.1	1.22
P	-14.1	1.22
V	-15.4	1.33
A	-17.00	1.47
B	-26.1	2.25

Table 10. *Accelerated aging tests of lapped samples in Bologna water after 240 cycles. Recession values are estimated from weight measurement, and ordered from lower to higher. N value is the ratio between the recession of the stone of interest and that of Carrara Marble. Samples abbreviations as in Table 4.*

	Recession	**N value**
B	-10.7	0.96
M	-11.1	1.00
AU	-11.3	1.02
BO	-12.1	1.09
A	-12.5	1.13
C	-13.8	1.24
P	-13.9	1.25
N	-14.3	1.29
R	-15.7	1.41
V	-16.2	1.46
O	-20.2	1.82

As concerns the surface preparation, highly glossy polished and lapped surfaces show different recession under the same aging conditions. However, these differences are not systematic, suggesting that surface working has a minor effect on the overall recession rate.
In tables 9, 10, 11 and 12, the recession estimates obtained from weight loss measurements are reported and ordered from the lowest to the highest. All these values are correlated to the recession measured for the Carrara Marble, providing a phenomenological coefficient N, which is a measure of the different behavior of a given limestone with respect to Carrara Marble, including therefore the effect of different grain size of the calcite crystals, and that of the presence of clay minerals.

Table 11. *Accelerated aging tests of highly glossy polished samples in Stresa water after 240 cycles. Recession values are estimated from weight measurement, and ordered from lower to higher. N value is the ratio between the recession of the stone of interest and that of Carrara Marble. Samples abbreviations as in Table 4.*

	Polished	**N value**
BO	-16.3	0.92
M	-17.7	1.00
P	-19.3	1.09
B	-21.2	1.20
A	-22.5	1.27
C	-22.6	1.28
O	-23	1.30
R	-23.6	1.33
AU	-25.2	1.42
N	-26.6	1.50
V	-29.3	1.66

Table 12. *Accelerated aging tests of lapped samples in Stresa water after 240 cycles. Recession values are estimated from weight measurement, and ordered from lower to higher. N value is the ratio between the recession of the stone of interest and that of Carrara Marble. Samples abbreviations as in Table 4.*

	Recession	**N value**
BO	-16.1	0.93
M	-17.4	0.92
B	-18.9	1.00
N	-20.4	1.08
C	-20.6	1.09
P	-20.6	1.09
R	-21.3	1.13
AU	-21.7	1.15
V	-21.9	1.16
A	-24.6	1.30
O	-26.3	1.39

3.3. Sample recession based on micro-photogrammetry

A considerable effort was dedicated to the design of different setups in order to perform microphotogrammetry of the samples subjected to accelerated aging.

Although in many cases shades and color tones are satisfactory (see Fig. 4), and space resolution can potentially reach 3 µm/pixel, the estimation of surface topography always resulted too noisy precluding up to now the possibility of applying this technique to the analysis of stone surface recession. Further details about this method can be found in the Technical Note.

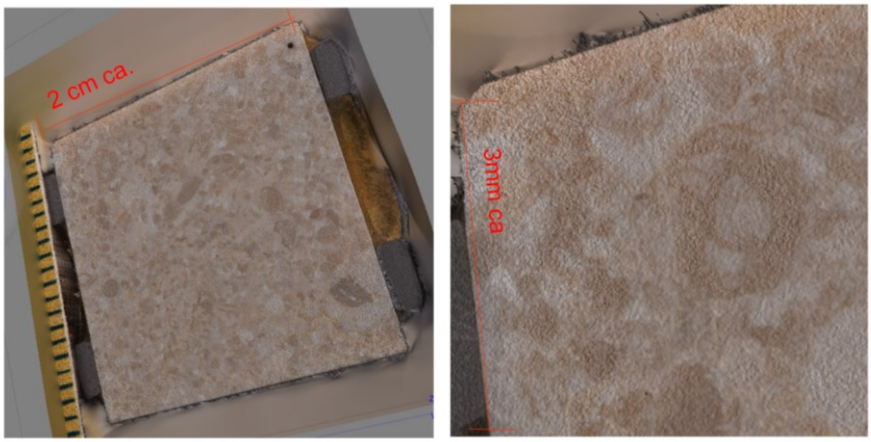

Figure 10. *Details of micro-photogrammetry performed on a Chiampo Paglierino sample with a lapped surface after 240 aging tests in Stresa water.*

3.4. Sample recession based on confocal laser microscopy

Confocal laser microscope analyses were performed in order to precisely determine surface topography and measure differential recession within the same sample when characterized by different portions differing for their grain size of the calcite crystals. Topographic surface of a specific area on each sample was measured after 54, 140 and 240 cycles, and compared to the portion of the same surface acquired before the aging tests. The scanned areas have a real dimension of approximately 2.5 x 2.5 mm.

In Figures 5 and 6 the two examples of Chiampo Paglierino stone and Botticino stone are presented, respectively, with the images referred to the unweathered lapped surface (to the left) and the same surface after 240 aging cycles (to the right). Differences in the lateral inclination of the sample surface from an acquisition to another was corrected referring surface quotes to a reference surface built in contact to the metal washers (far slightly elevated side in the images), and parallel to the stone surface.

In the case of Chiampo Paglierino stone, evolution of the stone surface with aging clearly shows a clear differential recession of bioclasts, which result progressively more elevated with respect to the surrounding fine-grained micrite, and sparitic calcite in veins or along bioclast rims (deep red on the right side of Fig. 5b). In the case of Botticino stone (fig. 6), dolomite crystals result progressively more elevated with respect to the surrounding micrite and coarse-grained micrite. They showed average recession values < 3 µm after 240 aging cycles, while fine-grained micrite and coarse-grained micrite displayed a recession of about 33 µm and 29 µm, respectively, under the effect of the Stresa water. Furthermore, the average recession values have been measured, avoiding sparitic calcite in the selection of the areas of interest. These average recession values are almost perfectly in agreement with the linear recession estimated from weight loss measurements (Table 13), with the exception of

Orsera Stone, for which an average recession of 29.12 µm was calculated in confocal microscopy against a recession based on weight loss of 14.3 µm.
Surface analysis in confocal microscopy successfully allowed to measure differential recession rates for texturally different portions of stone (Table 14). As a general observation, coarse-grained sparitic calcite showed recession values in average half of those obtained for fine-grained micrite, fine-grained micrite recedes slightly more than coarse grained micrite, and bioclast recession falls within a relatively large interval of values, comprised between those measured for the coarse grained micrite and the sparitic calcite. These results therefore clearly show the direct control of grain size on the recession rate. As concerns the effect of porosity on the total loss of material, our experiments did not show relevant correlation with this parameter. It seems therefore that grain size of calcite dominates recession rate, with significant additional weight loss in samples containing clay minerals, at least under our experimental conditions. If the average grain size of the texturally different parts (e.g. fine-grained micrite, coarse micrite, bioclasts, sparitic calcite) are plotted against the relative average recession (Fig. 7), control of grain size on recession is even more clear. The different intercepts of the two equations reported in Fig. 7, derived from the linear regression of the data therein plotted, accounts for the different composition (and therefore pH) of the two waters, with Stresa water being more aggressive then Bologna one. Instead, slope coefficient accounts for the contribution of grain size to the recession rate.

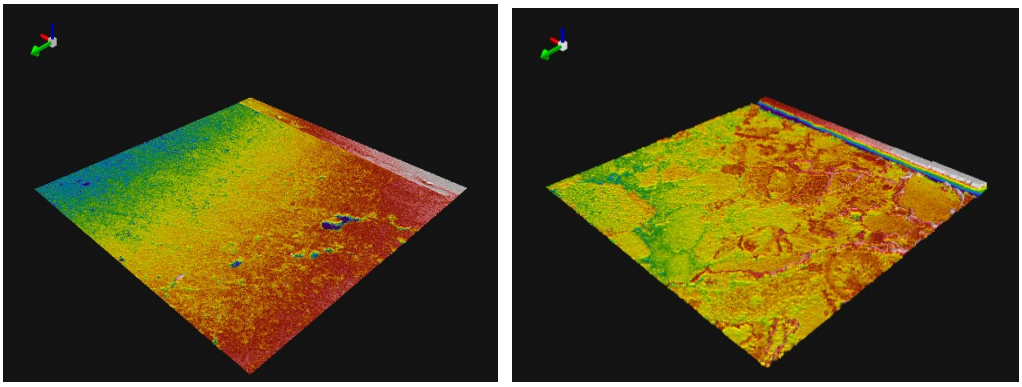

Figure 11. *Example of 3D surface model for a sample of Chiampo Paglierino Stone (P02) before aging (a) and after 240 aging cycles in Stresa water (b).*

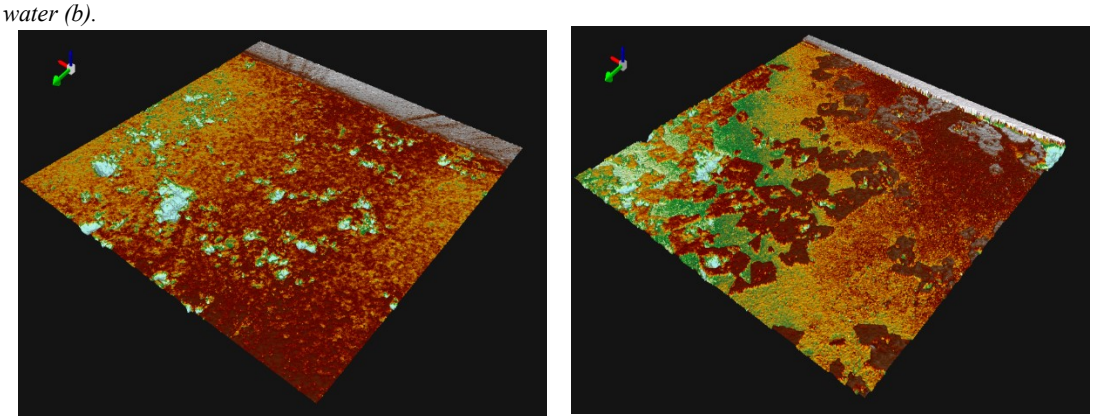

Figure 12. *Example of 3D surface model for a sample of Botticino Stone (P02) before aging (a) and after 240 aging cycles in Stresa water (b).*

Table 13. *Comparison between recession values obtained from weight measurements and by confocal microscope. Samples abbreviations as in Table 4.*

Samples	***Bologna***		***Stresa***	
	Weight	Confocal mic.	Weight	Confocal mic.
A	-10.7		-16.1	
AU	-11.1		-17.4	
B	-11.3		-18.9	
BO	-12.1	-15.97	-20.4	-31.34
C	-12.5	-16.84	-20.6	
M	-13.8	-13.03	-20.6	-26.12
N	-13.9	-14.29	-21.3	
O	-14.3	-29.12	-21.7	-31.41
P	-15.7	-15.19	-21.9	-32.26
R	-16.2		-24.6	
V	-20.2		-26.3	

Table 14. *Summary of the recession values (in µm) measured through the elaboration of the 3D model. Samples abbreviations as in Table 4.*

Sample	**Fine micrite**		**Coarse grained micrite**		**Sparry calcite / Coarse calcite**		**Bioclasts**		**Dolomite**	
	Bologna	Stresa	Bologna	Stresa	Bologna	Stresa	Bologna	Stresa	Bologna	Stresa
BO	-17.23	-33.00	-14.33	-29.01	--	--	-17.22	--	-2.33	-0.50
C	-21.24		-18.21		-8.82		-18.09		--	--
M	--	--	--	--	-13.03	-26.12	--	--	--	--
N	-20.36		-10.67		-5.73		-13.06		--	--
O	-33.61	-35.51	--	--	-7.02	-19.16	--	--	--	--
P	-21.54	-40.02	-17.42	--	-10.51	-13.07	-13.64	-30.23	--	--
Mean	**-22.80**	**-36.18**	**-15.16**	**-29.01**	**-8.02**	**-16.12**	**-14.98**	**-30.23**	**-2.33**	**-0.50**

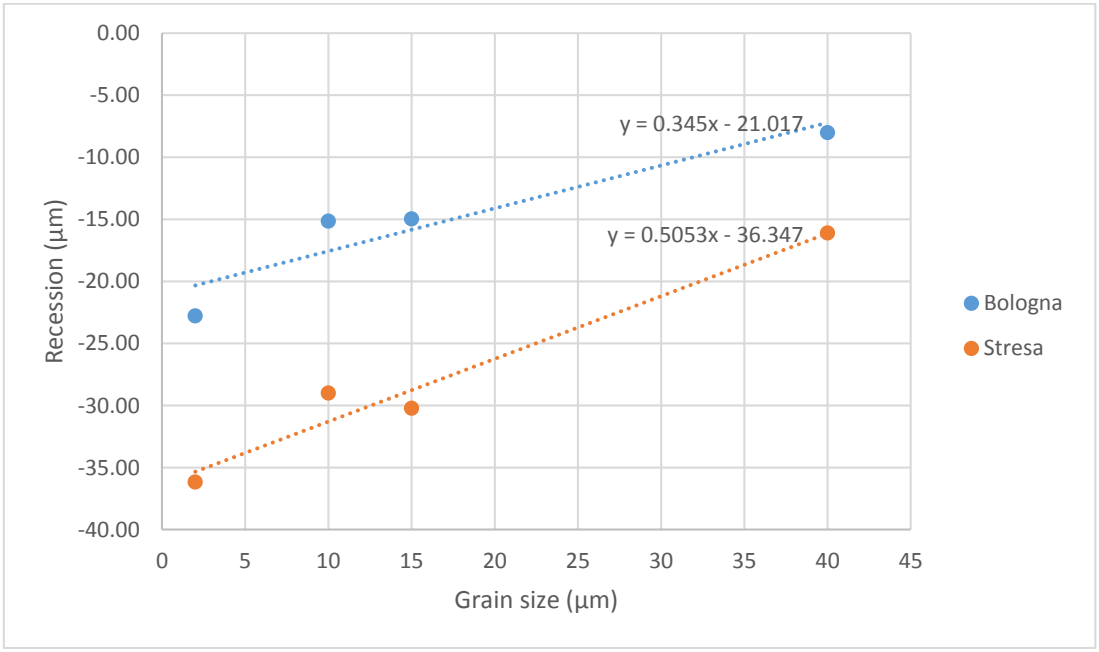

Figure 8. *Correlation between the average grain size of the different textural elements of the considered samples and the relative average recession measured after 240 aging cycles under the Stresa and Bologna waters, respectively.*

4. Discussion

Considering that a number of parameters such as grain size, heterogeneity in grain size distribution and content in clay minerals, the determination of a phenomenological N coefficient which accounts for the global effects of all these parameters, and possibly also for porosity, can be calculated and used to obtain more reliable projections of stone deterioration for different types of carbonate rocks. Table 16 reports the suggested N coefficients for the different stones here considered. The main textural features are also reported, as well as other rock types which share the same characteristics, for which the same N coefficient could be applied.

In Table 6, N coefficients have been applied to recession values estimated using the equation of Reddy et al. (1985) and results were compared to recession measurements from the literature. The same N coefficient calculated for Nanto stone (1.5) has been applied to Portland limestone using recession data obtained by Honeyborne & Price (1977) from stone exposed to highly polluted areas (London) and rural areas in the UK countryside, and by Weber (1985) from a porous limestone exposed in an urban environment (Vienna). Both these rock types display similar textural features to the Nanto Stone in terms of grain size of calcite, presence of bioclasts, porosity and content in clay minerals. The relative lower average recession values of the Botticino stone (N value = 0.95) with respect to Carrara marble, depends on its content in dolomite, the dissolution coefficient of which is much lower than that of calcite. The Indiana limestone investigated by Reddy et al. (1985) has similar characteristics; therefore, the same N coefficient could be applied to this rock type. The N value calculated for Chiampo stone is about 1.15, because of its compact texture and low porosity. These features are similar to a compact limestones studied by Weber (1985), and exposed to the same urban environment (Vienna) as the porous one cited before. Therefore, the same N value of 1.15 could suite to this stone. The comparison of the measured recession rates for these carbonate rocks and the corrected recession rate obtained using the proposed N coefficients, is satisfactory indicating that this coefficient is sufficiently adapt to account for the different textural and petrographic features influencing recession rate of stones even when exposed to the same environmental conditions.

Table 15. *Suggested N values for various carbonate rocks based on the results presented in this study. These values are also applicable to other stones characterized by similar mineralogical composition, texture and grain size.*

Sample	Geological classification	N value	Porosity	Notes	Also suggested for:
Carrara Marble	Crystalline carbonate	1.00	Low	Grain size = ≈100 μm	Naxos, Paros, Aghia Marina, Pentelico
Botticino S.	Dolomitic Micrite/ Cryst. carbonate	0.95	Low	Cal 57%, Dol 43%	Indiana limestone
Verona S.	Biomicrite Wackestone	1.25-1.80	Very Low	High heterogeneity, nodular limestone	Rouge du Roi, Tardos (Hungary), Adneter (Austria), Moneasa (Romania) Rouge Languedoc?,
Pink Asiago S.	Oomicrite/ Wackestone	1.30	Very Low		
Chiampo S.	Biomicrite/ Grainstone	1.15	Low		Beige of Missolonghi
Vicenza S.	Biomicrite/ Packstone	1.5	High	Micritized fossils, clay components, heterogeneity	Portland, Lecce?, Noto?
Aurisina S.	Biomicrite/ Packstone	1.10-1.20	Medium	Micritized fossils	
Orsera S.	Micrite/	1.3	Low	Small grain size: 3 μm	

	Mudstone				

Table 16. *Application of N coefficients to the recession estimates obtained using the equation of Reddy et al. (1985), and comparison with measured recession rates (in μm). HP77: Honeyborne & Price (1977); R85: Reddy et al. (1985); W85: Weber (1985).*

Ref.	Location	Material	Measured recession	SO_2 ($\mu g/m^3$)	Rainfall (m/yr)	$[H^+]$ (mmol/L)	Recession (R85)	Corrected rec. value	N value
HP77	London	Portland	50.0	140	1	0.15	37.06	55.59	1.5
HP77	Rural, U.K.	Portland	17.0	30	1	0.015	9.22	13.83	1.5
R85	East U.S.	Indiana Limestone	7.0	20	1	0.015	8.53	8.10	0.95
W85	Vienna	Porous Limestone	26.5	70	1	0.055	17.98	26.97	1.5
W85	Vienna	Compact Limestone	20.1	70	1	0.055	17.98	20.68	1.15
W85	Vienna	Marble	18.0	70	1	0.055	17.98	17.98	1.0

5. Conclusion

Considering that recession rate estimates derived from available equations are not sufficiently reliable when applied to limestones, an experimental investigation was conducted to determine the possible correlations between stone recession of different types of carbonate rocks and petrographic and textural features by a series of aging tests under controlled environmental conditions.

A set of different carbonate stones have been subjected to accelerated aging in an environmental test chamber simulating the effect of the rain wetting the two Italian cities of Bologna (pH ~ 7) and Stresa (pH ~ 6).

Stone recession was calculated on the basis of material weight loss and measured by confocal microscopy, and positively correlated to grain size of calcite and content in clay minerals, while the effect of porosity seemed to be less relevant. Despite the different recession rate determined by differences in water composition, the influence of grain size tend to provide similar correlation coefficients (see equations in Fig. 7) suggesting that there is a constant effect of grain size on recession rate, independently from the contribution of environmental parameters. In addition, certain rock types may contain significant amounts of clay minerals which enhance material loss during water runoff. These two observations justify the derivation of specific phenomenological coefficients (N) and their application to carbonate rocks with similar textural and mineralogical features. The effect of porosity, which resulted unclear in the present research, will be also included in such a phenomenological coefficient. The analytical setup here presented can be also considered as a guideline to the determination of such phenomenological coefficients for carbonate rocks the textural features of which do not match those of the stones here considered. Furthermore, such rock types could be also exposed to different water compositions in order to better understand stone response to specific environmental conditions characteristic of a given area under study, and reliably predict future stone recession under those specific conditions.

References

Amoroso G.G., Fassina V. (1983) Stone decay and conservation. Ed. Elsevier, Amsterdam.

Altindag R., Alyildiz I.S., Onargan T. (2004) Mechanical property degradation of ignimbrite subjected to recurrent freeze-thaw cycles. *Int J Rock Mech Mining Sci*, **41**, 1023-1028.

Baedecker, P. A. (1990) Effects of acidic deposition on materials.

Baedecker P.A., Reddy M.M. (1993) The Erosion of Carbonate Stone by Acid Rain. *J Chem Educ*, **70**, 2, 104-108.

Baer N. S., Berman S. M. (1983) Marble tombstone in national cemeteries as indicators of stone damage: general methods. *J Air Pollut. Control Assoc*, **83**.

Beaudoin J.J., MacInnis C. (1974) The mechanism of frost damage in hardened cement paste. *Cem Concr Res*, **4**, 139–147.

Benavente D., García del Cura M.A., Fort R., Ordóñez S. (1999) Thermodynamic modelling of changes induced by salt pressure crystallisation in porous media of stone. *J Cryst Growth*, **204**,168-78.

Bonazza A., Messina P., Sabbioni C., Grossi C.M., Brimblecombe P. (2009) Mapping the impact of climate change on surface recession of carbonate buildings in Europe, *Sci Tot Env*, **407**, 2039-2050.

Bravo H.A., Soto R.A., Saavedra R.M.I., Torres R.J., Granada L.M.M., Sánchez P.A. (1998) Acid rain in Mexico case: Maya monuments. *Transations on Ecology and the Environments*, **21**, 661-674.

Brimblecombe P. (1996) *Air composition and chemistry*. Cambridge University Press.

Brimblecombe P., Grossi C.M. (2008) Millennium long recession of limestones facades in London, *Env Geol*, **56**, 463-471.

Brimblecombe P., Grossi C.M. (2009) Millennium long damage to building materials in London, *Sci Tot Env*, **407**, 1354 -1361.

Camuffo D. (1984) Condensation-evaporation cycles in pore and capillary systems according to the Kelvin model. *Water Air Soil Poll*, **21-1**, 151-159.

Camuffo D. (1992) Acid Rain and Deterioration of Monuments: How Old Is the Phenomenon? *Atm Env*, **26B**, 241-247.

Camuffo D. (1995) Physical weathering of stones, *Sci Tot Env*, **167**, 1-14.

Camuffo D., Sturaro G. (2001) The climate of Rome and its action on monument decay. *Clim Res*, **16**, 145-155.

Cardell-Fernández C., Vleugels G., Torfs K., Van Grieken R. (2002) The processes dominating Ca dissolution of limestone when exposed to ambient atmospheric conditions as determined by comparing dissolution models. *Env Geol*, **43-1,** 160-171.

Cardell C., Delalieux F., Roumpopoulos K., Moropoulou A., Auger F., Van Grieken R. (2003) Salt-induced decay in calcareous stone monuments and buildings in a marine environment in SW France. *Constr Build Mater*, **17**, 165-179.

Chabas A., Jeannette D. (2001) Weathering of marbles and granites in marine environment: petrophysical properties and special role of atmospheric salts. *Environ Geol*, **40-3**, 359 –68.

Charlson R.J., Rodhe H. (1982) Factors controlling the acidity of natural rainwater. *Nature,* **295,** 683-685.

Dikaiakos J. G., Tsitouris C. G., Siskos P. A., Melissos D. A., Nastos, P. (1990) Rainwater composition in Athens, Greece. *Atm Env B. Urban Atmosphere*, **24-1,** 171-176.

Cooke R.U. (1989) Geomorphological contribution to acid rain research: studies of stone weathering. *Geographical Journal*, **155**, 361-366.

Dal Bianco B., Bertoncello R., Bouquillon A., Dran J., Milanese R., Roehrs S., Sada C., Salomon J., Voltolina S. (2008) Investigation on sol-gel silica coatings for the protection of ancient glass: interaction with glass surface and protection efficiency. *J Non-Cryst Solids*, **354**, 2983-2992.

Delalieux F., Cardell-Fernandez C., Torfs K., Vleugels G., Van Grieken R. (2002) Damage functions and mechanism equations derived from limestone weathering in field exposure. *Water, Air, & Soil Pollution*, **139-1,** 75-94.

Dolske D. A. (1995) Deposition of atmospheric pollutants to monuments, statues, and buildings. *Sci Tot Env*, **167(1-3),** 15-31.

Dragovich D. (1991) Marble weathering in an Industrial Environment, Eastern Australia, *Environ Geol Water S*, **17 -2**, 127-132.

Dunham R. J. (1962) Classification of carbonate rocks according to depositional textures.

Esbert R. M., Dıaz-Pache F., Grossi C. M., Alonso F. J., Ordaz J. (2001) Airborne particulate matter around the Cathedral of Burgos (Castilla y León, Spain). *Atm Env*, **35(2)**, 441-452.

Fassina V., Favaro M., Naccari A. (2002) Principal decay patterns on Venetian monuments. *Geol Soc London, Special Publications*, **205**, 381-391.

Feddema J., Meierding T. (1987) Marble weathering and air pollution in Philadelphia. *Atmos Environ,* **21-1,** 143-157.

Flatt R.J. (2002) Salt damage in porous materials: how high supersaturations are generated, *J Cryst Growth*, **242**, 435-454.

Folk R.L. (1959) Practical petrographic classification of limestones. *AAPG BULL*, **43**, 1-38.

Franzoni E., Sassoni E. (2011). Correlation between microstructural characteristics and weight loss of natural stones exposed to simulated acid rain. *Sci Tot Env*, **412**, 278-285.

Giugliano M., Lonati G., Butelli P., Romele L., Tardivo R., Grosso M. (2005) Fine particulate (PM2.5–PM1) at urban sites with different traffic exposure. *Atm Env*, **39**, 2421–2431.

Grandi F. Z., Szpyrkowicz L. (1991) Sampling and analysis of rain: methods and results of the Venice regional network. *Fresenius' journal of analytical chemistry*, **341-10,** 625-630.

Grossi C.M., Brimblecombe P., Bonazza A., Sabbioni C., Zamagni J. (2006) Sulfate and carbon compounds in black crusts from the Cathedral of Milan and Tower of London. In: Proceeding of the International HWC – Conference, 21-24 June 2006. Ed.CRC Press, Madrid.

Grossi C.M., Bonazza A., Brimblecomble P., Harris I., Sabbioni C. (2008) Predicting twenty-first century recession of architectural limestone in European cities. *Env Geol*, **56**, 455-461.

Hall K. (2004) Evidence for freeze-thaw events and their implications for rock weathering in northern Canada. *Earth Surf Process Landforms*, **29**, 43–57.

Herngren, L., Goonetilleke, A., Sukpum, R., Silva, D. D. (2005) Rainfall simulation as a tool for urban water quality research. *Environmental Engineering Science*, **22-3,** 378-383.

Honeyborne, D. B., & Price, C. A. (1977). Air pollution and the decay of limestone. *BRE note*, **117.**

Inkpen R.J. (1989). Stone decay and atmospheric pollution in a transect across southern Britain. Unpublished PhD thesis, University of London.

Inkpen R. J., Viles H., Moses C., Baily B. (2012a) Modelling the impact of changing atmospheric pollution levels on limestone erosion rates in central London, 1980-2010. *Atm En*, **61**, 476-481.

Inkpen R.J., Viles H., Moses C., Baily B., Collier C., Trudgill S.T., Cooke R.U. (2012b) Thirty years of erosion and declining atmospheric pollution at St Paul's Cathedral, London. *Atm Env*, **62**, 521-529.

Kucera V., Fitz S. (1995) Direct and indirect air pollution effects on materials including cultural monuments. *Water Air Soil Poll,* **85,** 153-165.

Kucera V., Tidblad J., Kreislova K., Knotkova D, Faller M., Reiss R., Snethlage R., Yates T., Henriksen J., Schreiner M., Melcher M., Ferm M., Lefèvre R.-A., Kobus J. (2007) UN/ECE ICP Materials Dose-response functions for the multi pollutant situation, Acid Rain – Deposition to Recovery, 249-258.

Lal Gauri K., Holdren Jr. G.C. (1981) Pollutant effects on stone monuments. *Env Sci Tech*, 386-390.

Lan T. T. N., Thoa N. T. P., Nishimura R., Tsujino Y., Yokoi M., Maeda, Y. (2005). New model for the sulfation of marble by dry deposition Sheltered marble—the indicator of air pollution by sulfur dioxide. *Atm Env*, **39-5,** 913-920.

Lipfert F.W. (1989) Atmospheric damage to calcareous stones: comparison and reconciliation of recent experimental findings. *Atm Env*, **23**, 415-429.

Lisci, M., Monte, M., Pacini, E. (2003) Lichens and higher plants on stone: a review. *Inter Biodet Biodegr*, **51-1,** 1-17.

Livingston R.A., Baer N.S. (1990) Use of tombstones in investigation of deterioration of stone monument. *Environ Geol Water S,* **16-1,** 83-90.

Lonati G., Giugliano M., Butelli P., Romele L., Tardivo R. (2005) Major chemical components of PM2.5 in Milan (Italy). *Atm Env*, **39**, 1925–1934.

Lundberg J., Ginés A. (2009) Rillenkarren, 185-210.

Marquardt W., Brüggemann E., Auel R., Herrmann H., Möller D. (2001) Trends of pollution in rain over East Germany caused by changing emissions. *Tellus*, **53B**, 529-545.

McGee E. S., Mossotti V. G. (1992) Gypsum accumulation on carbonate stone. *Atm Env B. Urban Atmosphere*, **26(2)**, 249-253.

Meierding T.C. (1981) Marble tombstone weathering rates: a transect of the United States. *Phys Geogr*, **2-1**, 1-18.

Melo M.J., Bracci S., Camaiti M., Chiantore O., Piacenti P. (1999) Photodegradation of acrylic resins used in the conservation of stone. *Polymer degradation and Stability*, **66**, 23-30.

Moropoulou A., Theoulakis P., Chrysophakis T. (1995) Correlation between stone weathering and environmental factors in marine atmosphere. *Atm Env*, **29-8**, 895-903.

Moses C.A. (1996) Methods for assessing stone decay mechanisms in polluted and 'clean' environments, Northern Ireland. In: Smith B.J., Warke P.A. (Eds), Processes of Urban Stone Decay. Ed. Donhead, pp. 212-227.

MULTI-ASSESS (2007) Model for Multi-pollutant Impact and Assessment of Threshold Levels for Cultural Heritage. Deliverable 02.

Panettiere P., Cortecci G., Dinelli E., Bencini A., Guidi M. (2000) Chemistry and sulfur isotopic composition of precipitation at Bologna, Italy. *App Geoch*, **15**, 1455-1467.

Reddy M.M. (1988) Acid rain damage to carbonate stone: A quantitative assesment based on the aqueous geochemistry of rainfall runoff from stone. *Earth Surf Processes*, **13,** 335-354.

Reddy S.M., Roberts S.M. (2005) Surface-recession weathering of marble tombstones: new field data and constraints. *GSA*, **390**, 27-37.

Reddy M.M., Sherwood S., Doe B. (1985) Limestone and marble dissolution by acid rain. 5th Int. Congress on Conservation and Deterioration of Stone, Lausanne, 517-526.

Reis S., Grennfelt P., Klimont Z., Amann M., ApSimon H., Hettelingh J. P., ... & Spranger T. (2012). From acid rain to climate change. *Science*, **338,** 1153-1154.

Roberts S.M. (2005) Surface-recession weathering of marble tombstones: new field data and constraints. *GSA*, **390**, 27-37.

Rogora M., Mosello R., Marchetto A. (2004) Long-terms trends in the chemistry of atmospheric deposition in Northwestern Italy: the role of increasing Saharian dust deposition. *Tellus*, **56B,** 426-434.

Rossi-Manaresi R., Tucci A. (1991) Pore structure and the disruptive or cementing effect of salt crystallisation in various types of stone. *Stud Conserv*, **36**, 53-58.

Sabbioni C., Ghedini N., Bonazza A. (2003) Organic anions in damage layers on monuments and buildings. *Atm Env*, **37-9**, 1261-1269.

Sabbioni C., Brimblecombe P., Cassar M. (Eds) (2010) The Atlas of Climate Change Impact on European Cultural Heritage. Ed. Anthem Press, London.

Salvini S., Sacchi B., Frediani P. (2012) Study of protectives obtained from natural resources for the conservation of stone. Proceedings Scienza e Beni Culturali Bressanone, 833-843.

Samara C., Tsitouridou R., Balafoutis C. (1992) Chemical composition of rain in Thessaloniki, Greece, in relation to meteorological conditions. *Atm Env B. Urban Atmosphere*, **26-3,** 359-367.

Scherer G.W. (1999) Crystallization in pores. *Cem Concr Res,* **29**, 1347–1358.

Scherer G.W. (2004) Stress from crystallization of salt. *Cem Concr Res*, **34-9**, 1613–24.

Scherer G.W., Valenza J.J. (2004) Mechanisms of frost damage. In: Young F., Skalny J. (Eds) Materials science of concrete VII. The American Ceramic Society, Westerville, 209–246.

Searle D.E., Mitchell D.J. (2007) The effect of coal and diesel particulates on the weathering loss of Portland Limestone in an urban environment. *Sci Tot Envir*, **370**, 207-223.

Singh A., Agrawal M. (2007) Acid rain and its ecological consequences. *Journal of Environmental Biology*, **29-1,** 15.

Steiger M. (2005a) Crystal growth in porous materials I: the crystallization pressure of large crystals. *J Cryst Growth*, **282**, 455–469.

Steiger M (2005b) Crystal growth in porous materials II: influence of crystal size on the crystallization pressure. *J Cryst Growth*, **282**, 470–481.

Tidblad J., Kucera V., Mikhailov A.A., Henriksen J., Kreislova K., Yates T. (2001) UN ECE ICP materials: dose-response functions on dry and wet acid deposition effects over 8 years of exposure. Water, Air, Soil Pollution, **130**, 1457–1462.

Thornbush M. J., Viles H. A. (2007) Simulation of the dissolution of weathered versus unweathered limestone in carbonic acid solutions of varying strength. *Earth Surface Processes and Landforms*, **32-6,** 841-852.

Torfs K., Van Grieken R. (1997) Chemical relations between atmospheric aerosols, deposition and stone decay layers on historic buildings at the Mediterranean coast. *Atm Env*, **31**, 2179-2192.

Trudgill S.T., Viles H.A., Inkpen R.J., Cooke R.U. (1989) Remeasurement of weathering rates, St Paul's Cathedral, London. *Earth Surface Proc Land*, **14**, 175-196

Vacchiano C.D., Incarnato L., Scarfato P., Acierno D. (2008) Conservation of tuff-stone with polimeric resins. *Constr Build Mater*, **22**, 855-865

Varotsos C., Tzanis C., Cracknell A. (2009) The enhanced deterioration of the cultural heritage monuments due to air pollution. *Env Sci Poll Res*, **16**, 590-592.

Viles H.A. (2011) Microbial geomorphology: a neglected link between life and landscape. *Geomorphology*, **129**, 167-182

Viles H.A., Naylor L.A., Carter N.E.A., Chaput D. (2008) Biogeomorphological disturbance regimes: progress in linking ecological and geomorphological systems. *Earth Surf Proc Landf*, **29**, 1473–1485

Urzì C., Brusetti L., Salamone P., Sorlini C., Stackebrandt E., Daffonchio D. (2001) Biodiversity of Geodermatophilaceae isolated from altered stones and monuments in the Mediterranean basin. *Environ Microbiol*, **3-7,** 471-479.

Wakefield R.D., Jones M.S. (1998) An introduction to stone colonizing micro-organisms and biodeterioration of building stone. *Q J Eng Geol*, **31**, 301-313.

Warscheid T., Braams J. (2000) Biodeterioration of stone: a review. *Int Biodeter Biodegr*, **46**, 343-368.

Webb A.H., Bawden R.J., Busby A.K., Hopkins J.N. (1992) Studies on the effects of air pollution on limestone degradation in Great Britain. *Atmos Environ,* **26B,** 165-181.

Weber, J. (1985) Natural and artificial weathering of Austrian building stones due to air pollution. In: Ve congres international sur l'alteration et la conservation de la pierre. Actes. Vth international congress on

deterioration and conservation of stone. Proceedings, Lausanne, 25-27September 1985. Ed. Presses polytechniques romandes, Lausanne, pp. 527-535.

Winkler E.M. (1982) Decay of stone monuments & Buildings :the Role of Acid Rain. *Technology and Conservation*, 32-36.

Winkler E.M. (1987) Weathering and weathering rates of natural stone. *Environ Geol Water Sci*, **9**, 85–92.

Zanardini E., Abbruscato P., Ghedini N., Realini M., Sorlini C. (2000) Influence of atmospheric pollutants on the biodeterioration of stone. *Int Biodeter Biodegr*, **45,** 35-42.

Zehnder K., Arnold A. (1989) Crystal growth in salt efflorescence. *J Crystal Growth*, **97**,513–521.

Zendri E., Biscontin G., Kosmidis P. (2001) Effects of condensed water on limestone surfaces in a marine environment. *J Cult Herit*, **2-4**, 283-289.

Zezza F., Macrì F. (1995) Marine aerosol and stone decay. *Sci Tot Env*, 167, 123-143.

Technical note:

Photogrammetry as a tool for evaluating stone decay

ABSTRACT

The documentation and 3D representation of Cultural Heritage artefacts are important both for operative and archiving reasons. In this paper we employ Structure from Motion (SfM) μ-photogrammetry some innovative methodologies that have been employed to support the study of stone decay. In particular, we tested this technique using two different approaches: i) 3D model of objects located outdoor, ii) 3D surface model of small objects before and after accelerating aging tests.
The results reported are encouraging, indicating that this completely non-invasive technique can represent a powerful tool in the description of surface morphology and in the studies of stone decay.

Keywords: μ-photogrammetry, surface recession, carbonate rocks, surface morphology, ultra-close range photogrammetry

Highlights

1. Introduction

In Cultural Heritage studies 3D graphical representation of the artefacts is becoming more and more essential. Indeed, 3D digital methods are often more accurate and faster than manual measurements of complex objects. These methods make possible the documentation of endangered Cultural Heritage due to decay, natural hazard or human action. In addition, the collection of the precise relief of the originals is fundamental for future substitutions (see Yilmaz et al. 2007 for a review). Finally, these methods can also be used for the valorisation of cultural heritage by using innovative media together with the augmented reality experiences.
During the last decades, various techniques have been developed for 3D acquisition of Cultural Heritage: Laser Targeting Scanner (LTS), photogrammetric reconstruction from tourist photos and panoramic images, Structure from Motion (SfM) microphotogrammetry and ultra close range microphotogrammetry.

Even if common methods like the Laser Targeting Systems (LTS) have been continuously improved reaching unprecedented resolution down to 1 mm, they are not sufficient for the study of material decay during time and the description of surface morphology. This because the measurements of the recession rates require a resolution down to 1 micron.
For this reason, in this research we applied photogrammetric techniques following to different approaches:

- On site approach by Structure from motion (SfM) micro-photogrammetry, performed on gravestones made of limestone, with a completely portable instrumentation.

- Laboratory approach by ultra-close range photogrammetry, carried out on little stone samples, in order to reach down to 1 mm of resolution.

2. On situ SfM µ-photogrammetry

SfM has a sensibility of 10-100 µm and it is helpful also for the study of decay phenomena and surface morphology (Tiano et al. 2008). In addition, cameras allowing this technique are high portable and less expensive than LTS.

2.1.Materials

Different gravestone located in Commonwealth War Graves Commission(CWGC) Cemeteries of Italy and Greece have been acquired through SfM – microphotogrammetry.
The chosen headstones presented medium decay and no surrounding vegetation:

- Padua (Italy). Gravestone III.E.10, cemetery of Second World War, Via della Biscia. The slate is made of Botticino marble, a compact white-yellowish limestone. This gravestone has been exposed for about 70 years
- Thessaloniki (Greece). Gravestones n° 375 and n° 945, cemetery of Lembet. The slates are made of Botticino of two different ages
- Gravestone n°1937 of the cemetery of Kalamaria. It is made of Portland stone, a high porous limestone
- Asiago (Italy). Gravestone I.D.3, cemetery of Cavalletto. This slate is not original, it is made of Botticino and it is of about 5 years.
- Castiglione dei Pepoli (Italy). Gravestone II.G.1, made of Botticino marble, a compact white-yellowish limestone. This gravestone has been exposed for about 70 years
- Bordighera (Italy). Gravestone III.A.10. This stone has been exposed for about 100 years and it is made of Chiampo stone, a compact fossiliferous limestone.

Table 1. *Summary of analyzed gravestones.*

Grave	**Place**	**Material**	**Age**	**Climate**	**Environment**	**N° Photos**
III.E.10	Padua	Botticino	70 years	Cfa	Urban/Periferic	594
N°1937	Thessaloniki (Kalamaria)	Portland	70 years	Bsk	Urban/Periferic	477
N°375	Thessaloniki (Lembet)	Botticino	≈ 30 years	Csa-Bsk	Urban	567
N°945	Thessaloniki (Lembet)	Botticino	≈ 10 years	Csa-Bsk	Urban	561
II.G.1	Castiglione dei Pepoli	Botticino	70 years	Cfb	Mountain	791
I.D.3	Asiago - Cavalletto	Botticino	≈ 10 years	Cfb-Alps	Mountain	831
III.A.10	Bordighera	Chiampo	100 years	Csa	Marine	787

2.2. Method

An APS-C Reflex camera (Nikon D-300, equipped with a 24-85mm F/2.4-4 lens) set at 50 mm focal length was used. All hardware is battery operated and can be used on sites without any electrical source and a special holding rack has been designed in order to minimize focusing error. For a slate of classical dimensions of about 76x38x7.6 cm, about 600 shots (*.nef and *.jpg) have been taken.
The working distance was about 50 cm and the camera had to be hold perpendicular to the object, a better precision has been reached with the holding rack which minimize focusing error. However, with the autofocus systems in dotation of the modern reflex cameras, photographic experience and a firm grip it is even possible to capture the images freehand saving time.
The illumination in outdoor contexts could be a critical factor as it can interfere on the reliability of the chromatic change evaluations (Tiano et al. 2008). Even if in our research, the colour was not a paramount parameter, all the possible precautions were taken to avoid light issues (preferring cloudy days for the acquisition or shadowing the slate with a sheet or an umbrella.
Data processing for 3D model production was carried out by using the Agisoft Photoscan software.
Acquired *jpg photographs elaborated with this software allowed us to obtain 3D models with resolution of about 25 μm (Figure 1).
Although the Photoscan function "batch process" can be used to let the PC work overnight, it is strongly suggested to align the images first. This is a quite quick working step (about 1 hour for 600 images) and the preliminary point cloud allow to assess if the images are perfectly aligned. If so, the points outside the surface of interest need to be cleared, otherwise in the following steps (dense cloud, mesh) the software is going to reconstruct unnecessary parts of the environment surrounding the object of interest. If the alignment is not successful, it is possible to detect which images were not aligned (e.g. out of focus images or images out of the sample). Only if the alignment is successful, it is possible to batch the process of the following two steps (building dense cloud, generate mesh) which usually take a lot of time (a whole day for 600 files).

2.3. Results

The resolution of the DEMs obtained from the data elaboration of the *jpeg files is up to 25 – 50 μm. The final file size of each DEM is about 2-4 GB.
In the Figures 1-2-3, the details of three gravestones, made with different materials are showed.
In Figure 1, there are various captures of the 3 D model of a grave in Botticino limestone. It is possible to see aspects of the stone morphology like the bioclasts typical of this limestone, the surficial cracks and the lichens encrustations.
In Figure 2 different details of a Portland headstone are showed, the reconstruction is very realistic and the large fossils characterizing this kind of carbonate rock are clearly visible as well as the typical erosion and exfoliating decay pattern.
Finally, in Figure 3 some views of the 3D model of a Chiampo headstones are reported. It is worth noting the meticulous representation of the stone working on the slate side. In addition, it is possible to observe the ultra realistic shades and colors that can be obtained with this technique.

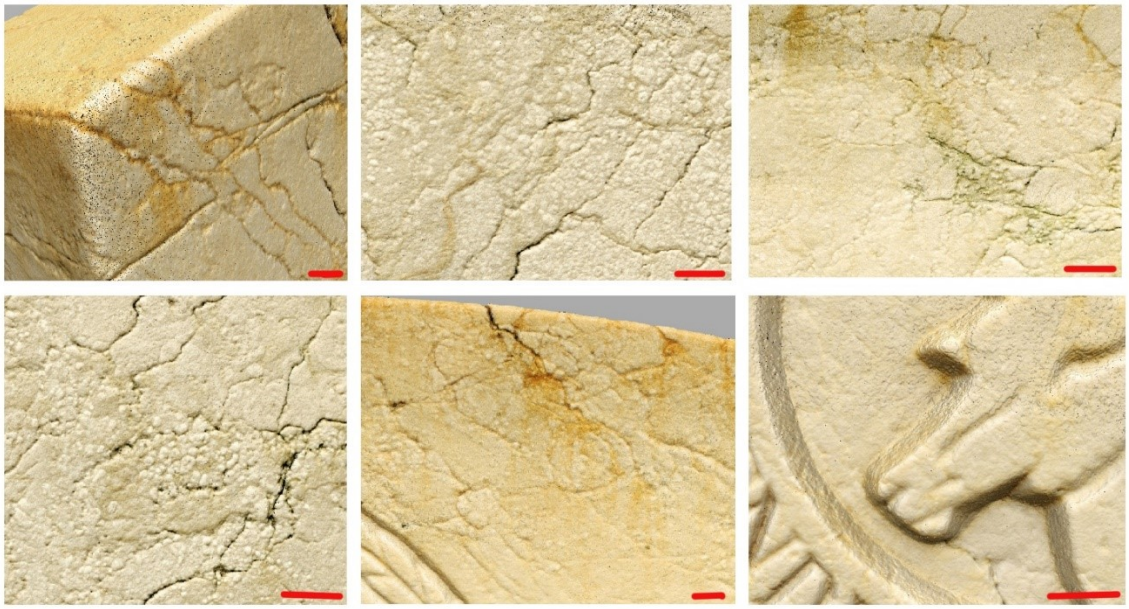

Figure 1. *Details of the 3D model of the III.E.10 grave of the Padua War Cemetery. This headstone is made of Botticino and it is aged 70 years. The red line stands for the unit of 1 cm. We can see many cracks, typical decay pattern of a Botticino limestone when subjected to ice crystallization. In the top left view are visible some micro-organisms and lichens.*

Figure 13. *Details of the 3D model of the grave n° 1937 of the Mikra Military cemetery located in Kalamaria (Thessaloniki metropolitan area). This headstone is made of Portland stone and it is aged about 70 years. The red line stands for the unit of 1 cm.*

Figure 3. *Details of the 3D model of the grave III.A.10 of the Bordighera British cemetery. This headstone is made of Chiampo stone and it is aged about 100 years. The red line stands for the unit of 1 cm.*

These tests confirmed that Structure from Motion µ-photogrammetry is an innovative technique in the study of decay of carbonate rocks. It makes possible the identification of small-scale heterogenicities which are more prone to recession (here we can see a different dissolution between fossils, bio-clasts and carbonate matrix). It was tried a determination of the surface recession value but a resolution of 25 microns/pixel it is not sufficient to estimate the differential recession between bioclasts and the surrounding weaker matrix.

3. Ultra close range µ-photogrammetry

This second experimental approach extremely deepen the concept of photogrammetry and different set-ups with a laboratory equipment have been tested in order to perform a detailed photogrammetry of small samples.

In particular, two sets of 22 stone samples were subjected to accelerated ageing in a climatic chamber (chapter 4), and there was a need of trying to deeply study the change in the morphology of sample and to measure their recession in order to evaluate the decay throughout the accelerated ageing cycles. The reproducibility of the acquisition was an essential condition for this experiment because data acquired at different times had to be compared.

3.1.Materials

The samples of different carbonate stones had a dimension of ≈ 2 x 2 x 1 cm and they were equipped with stainless steel washers that were attached to the opposite sides of the samples with Araldite 2020. As described in Part 4, each set of 22 samples comprise 2 samples for each of the 11 different rock types considered, one sample just finished by lapping and the other one polished.

3.2.Methods

Samples were positioned on a moving stack.
Various set-ups were tested, using a traditional Nikon Flash:

A. Nikon D300 equipped with a 65 mm lens
B. Nikon D300 equipped with a 55 mm lens and an additional macro lens
C. Nikon D3200 equipped with a 55 mm lens and an additional macro lens
D. Nikon D3200 equipped with a microscope lens 4x mounted with an adaptor ring on the 200 mm lens
E. Nikon D3200 equipped with a Canon 65 mm lens mounted on a photographic bellow (step=1)
F. Nikon D3200 equipped with a Canon 65 mm lens mounted on a photographic bellow (step=2)
G. Nikon D3200 equipped with Canon 65mm lens set at F/11 aperture mounted on photographic bellow (step=3)
H. Nikon D3200 equipped with a Canon 65 mm lens mounted on a photographic bellow (step=8)

In Table 2 are summarized the resolution obtained from these set ups and the related major issues.

Table 5. *Summary of the various set-ups tested. Abbreviations as in the bullet list described above.*

Set up	**Photo resolution**	**DEM**	**Notes**
A	5,4 µm/pixel	≈20 µm/pixel	DEM built from the medium dense cloud
B	6 µm/pixel	n.d.	Point cloud already showed unnatural curve
C	3 µm/pixel	n.d	Point cloud already showed unnatural curve
D	n.d.	n.d.	This set up completely failed. Many attempts but the alignment was never reached, not even partially
E	2.5 µm/pixel	10 µm/pixel	DEM built from the medium dense cloud
F	2 µm/pixel	3 µm/pixel	DEM built from the high dense cloud
G	1.8 µm/pixel	2.5 µm/pixel	DEM built from the high dense cloud
H	1 µm/pixel	2.1 µm/pixel	DEM built from the high dense cloud. Unfortunately, the model shows a slight unnatural curve.

3.3.Results

Regarding the set-up H, it was elaborated also a DEM from the ultra-high dense cloud (resolution was 1.5 µm/pixel). However, it required much more time (about 300%, 16 hours) than the DEM built from the high cloud. For this reason, the slight difference in resolution does not motivate the time loss.

The G (see Figure 4) set up was the most promising one. So, about 150-200 photos were taken for every sample, requiring about 40 minutes of shooting for each one of them.
Sample with a polished surface encountered various difficulties because their surface reflected the light of the flash, especially on metal surfaces and on Carrara marble. After various attempts, this technique was performed only on lapped samples. However this is not a problem, as almost all the stone surfaces of the cultural heritage exposed outdoor is not polished.

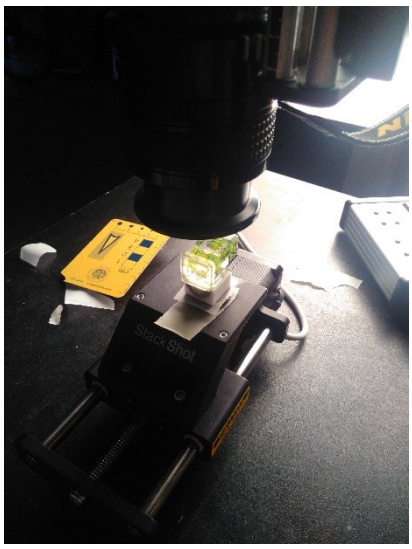

Figure 4. *Experimental set up G, used for acquisition of the images.*

The most common issue, shown in figure 5 and particularly relevant with uniform samples, is the alignment which can take up to 10 -15 minutes for each sample and often fails. We were however able to assess that the misalignment can be caused by images which captured very little portions of the sample border or were unsuccessfully acquired. Indeed, it might happen that the same point cannot be present in several images because the sample moved on the stack (i.e. in Carrara marble or Orsera stone capturing about 200 images of a 4 cm^2 area is clearly not an easy task). However, the software is able to mark not aligned images.

Figure 5. *Sample of Orsera stone with lapped surface. Elaboration of the point cloud. On the left the result of the initial alignment, which was very difficult also because this stone has a uniform surface. On the right the successful alignment of the point cloud after the merging of two separate chunks of aligned images.*

In this way it is possible to separate the images into two chunks, one with the images already aligned and one with the images still not aligned. Afterwards, a new alignment can be realized only with the second chunk and then a merge of the two chunks can be performed. This procedure often resolved the alignment issues (see Figure 5).

Figure 6. *Details of the 3D models of two lapped samples at the end of the accelerated aging test: a sample of Orsera stone is on the left, while a sample of Brown Verona stone is on the right.*

Due to the technical difficulties encountered during the elaboration and comparison of the previous files, other methods were also tried with the aim of finding a good resolution with minor effort. In particular we firstly adopted an instrumental set up (see Figure 7) with a D300 Nikon camera equipped with a 65 mm Canon macro lens, the sample was positioned on a rotating stage and illuminated by a professional laboratory flash. About 20 photos with different orientations were taken but the resulting point cloud were very messy so this method wasn't successful.

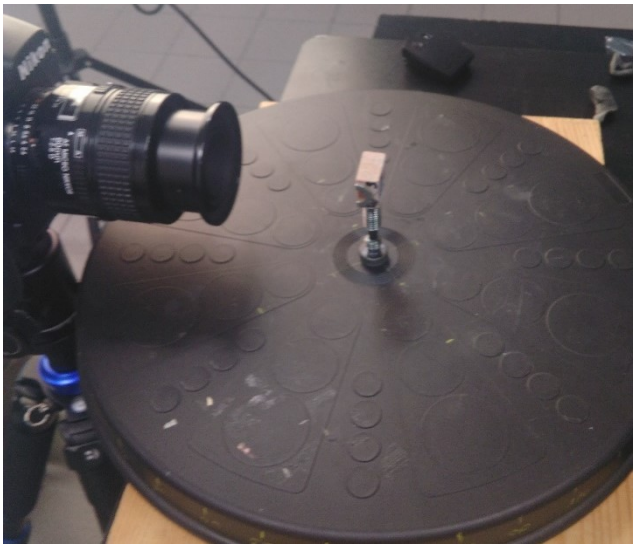

Figure 7. *Experimental set up for a quick 3D acquisition of the sample surface. Unfortunately, this method was unsuccessful.*

Finally, a camera Nikon D3400 coupled with 60 mm Nikon lens was fixed to a holding rack in order to capture photographs from above, trying to frame the entire sample in the image. The sample was positioned on a plain surface and slithered in order to capture different view of the same surface with minimal differences. About 20 images were captured on every sample.

The 20 images allowed us to quickly create a dense cloud in ultra-resolution and the related mesh. Thus, the lower resolution of the image (about 7 µm) is compensated by the velocity of the elaboration. Indeed, in this case the complete elaboration required about 4-6 hour, an affordable time if compared to the entire days needed with the other set ups (Table 2).
The final resolution of the DEM is about 5 µm, which is excellent for the qualitative study of decay and surface topography. However, there are still some uncertainties for using this technique as a tool for measuring the surface recession for experimental aged samples. For example, in the experiment carried out in Part 3 the higher recession values were around 30-40 µm. Due to the noise of the model (about 2-3 pixel) and the little values this method needs to be furtherly implemented.
Below are reported some images of the results obtained with this successful set-up.

Figure 14. *Detail of the 3D model of the Red Verona stone with lapped surface, after 240 aging cycles*

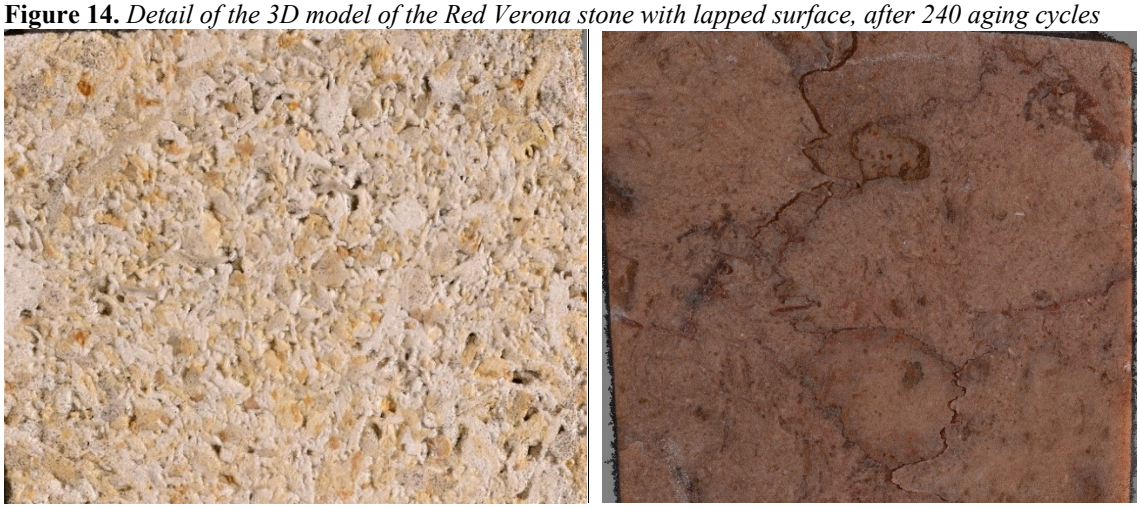

Figure 9. *Detail of the 3D models of Vicenza stone (on the left) and Brown Verona stone (on the right)*

Figure 10. *Detail of the 3D models of Botticino stone (on the left, it is possible to see the dolomite crystals) and Carrara marble (on the right)*

4. Conclusion

In this research two different photogrammetric approaches were tested for stone decay analysis:

- On site approach performed on carbonate gravestones using Structure from Motion micro-photogrammetry and a completely portable instrumentation,
- Laboratory approach by ultra-close range photogrammetry, carried out on little stone samples, that were studied under various set-ups in order to reach DEM resolutions of at least some microns.

The results underline the potentials of these innovative techniques (resolution DEM in situ approach: 50 μm; resolution DEM laboratory approach: 5 μm) which can be ideal tools for stone decay studies of carbonate rocks and determination of surface recession rates.

In particular, our results show that photogrammetry is surely a good alternative to other 3D digital techniques (LTS, augmented reality), especially for studying the stone decay and the surface topography in outdoor measurements.

In addition, the ultra-close range photogrammetry was tested to measure the recession due to the accelerated aging. Indeed, although in many cases shades and color tones are good, and the resolution can reach values even lower than 3 microns/pixel, there are still some uncertainties in the use of ultra-close range photogrammetry for a robust quantification of recession rates.

References

Al-kheder F., Al-shawabkeh Y., Haala N. (2009) Developing a documentation system for desert places in Jordan using 3D laser scanning and digital photogrammetry. *J Arch Sci*, **36**, 537-546.

Arias P., Herráez J., Lorenzo H., Ordóñez C. (2005) Control of structural problems in cultural heritage monuments using ultra close-range photogrammetry and computer methods. *Computers & Structures*, **83**, 1754-1766.

Barazzetti L., Binda L., Scaioni M., Taranto P. (2011) Photogrammetric survey of complex geometry with low cost software: Application to the 'G1' temple in Myson Vietnam. *J Cult Herit*, **12**, 253-262.

Comes R., Buna Z., Badiu I. (2014) Creation and preservation of digital cultural heritage. *J Ancient History and Archeology*, **1-2**, 50-56.

Gomes L., Bellon R. P., Silva L. (2014) 3D reconstruction methods for digital preservation of cultural heritage. *Journal of Pattern Recognition letters*.

Pavlidis G., Koutsoudis A., Arnaoutoglou F., Tsioukas V., Chamzas C. (2007) Methods for 3D digitization of cultural heritage. *J Cult Herit*, **8**, 93–98.

Remondino F., El-Hakim S. (2006) Image-based 3-D modelling: a review. *Photogram Rec*, **21**, 269–291.

Remondino F., Spera M.G., Nocerino E., Menna F., Nex F., Barsanti S.G. (2013) Dense image matching: comparisons and analyses. *Digit Herit Int Congress,* **1**, 47–54.

Salvini S., Castelli S., Massironi M., Mazzoli C., The application of SfM μ-photogrammetry to the understanding of material decay and morphology. 41st International Symposium on Archaeometry, Kalamata, 15-21 maggio 2016, Book of Abstracts, 323-324.

Tiano P., Tapete D., Matteini M., Ceccaroni F. (2008) The microphotogrammetry: a new diagnostic tool for on-site monitoring of monumental surfaces. Proceedings International Workshop 'In situ Monitoring of Monumental Surfaces', 97-106.

Yastikli N. (2007) Documentation of cultural heritage using digital photogrammetry and laser scanning, *J Cult Herit,* **8**, 423-427.

Zhang P., Arre T.J., Ide-Ektessabi A. (2015) A line scan camera-based structure from motion for high-resolution3D reconstruction. *J Cult Herit*, **16**, 656-66.

Conclusion

Carbonate rocks (limestones, marbles) are among the most commonly used building materials (both as dimension and ornamental stones), and are highly vulnerable to weathering, especially in polluted areas. This means that Cultural Heritage in Europe is increasingly under threat and decisions when managing the care of stone buildings should rely on solid knowledge of the deterioration processes and reliable prediction models of decay, also considering IPCC future scenarios of climate change.
Present day models of surface erosion for carbonate rocks are based on factors including air pollution, atmospheric CO_2 concentration, rainfall and temperature. These models tend to underestimate the rate of surface erosion in historical buildings, which is sometimes 2-3 times greater (for example, long term observation studies on the St. Paul Cathedral in London by Inkpen et al., 2012a, b, Atmospheric Environment). Therefore, prediction of stone decay and damage to heritage in a changing climate urgently require improvement on our knowledge in this research field by refining recession models for carbonate rocks, considering additional factors which have a first order effect on deterioration, but which have not been considered so far.
With this in mind, research focused on two main goals:
1) The measurement of the total stone recession in headstones from a number of Commonwealth War Graves Commission (CWGC) cemeteries located in different climatic regions in Italy and Greece, exposed for long periods of time to environmental conditions and evaluation of their control on the recession rate;
2) Accelerated ageing tests under monitored environmental conditions on a set of selected carbonate rocks in order to evaluate the effect of petrographic and textural features on recession rate.

Concerning the measurement of long term linear stone recession, in order to obtain a statistically significant number of data 11157 headstones have been surveyed and 3321 recession values collected from headstones located in 23 different CWGC cemeteries. Almost all headstones were made either of Botticino Stone or of Chiampo stone. This allowed investigating the effect of exposition to different climatic conditions on the decay of these two rock types. An attempt has been done to apply an innovative approach to the measurement of the total recession by 3D reconstruction through Structure from Motion μ-photogrammetry.
By comparing recession data with environmental climatic parameters obtained from the surface climate observing reference networks (mainly ARPA and Hellenic National Meteorological Service) the possible environmental controls on stone recession were investigated considering orientation with respect to geographical coordinates, which influences the exposition to sunlight and prevailing winds, rainfall and other climatic parameters, time. Surprisingly, results evidenced the strong influence of wind intensity and direction on total recession indicating that microclimatic conditions have a first order effect on recession that should be accounted for when formulating recession rate equations.

Considering that recession rate estimates derived from available equations are not sufficiently reliable when applied to limestones, an experimental investigation was conducted to determine the possible correlations between stone recession of different types of carbonate rocks and petrographic and textural features by a series of aging tests under controlled environmental conditions.

A set of 12 different carbonate stones have been subjected to accelerated ageing in an environmental test chamber simulating the effect of the rain wetting the two Italian cities of Bologna (pH ~ 7) and Stresa (pH ~ 6). These rocks were previously fully characterized petrographically and texturally. In particular, the grain size of calcite was determined in the different textural parts (e.g. constituted by fine-grained or coarse-grained micrite, sparitic calcite, or average grain size of bioclasts) in order to determine the control of these features on recession rate under specific environmental conditions.

Stone recession was calculated on the basis of material weight loss and measured by confocal microscopy, and positively correlated to grain size of calcite and content in clay minerals, while the effect of porosity seemed to be less relevant. Despite the different recession rate determined by differences in water composition, the influence of grain size tend to provide similar correlation coefficients suggesting that there is a constant effect of grain size on recession rate, independently from the contribution of environmental parameters. In addition, certain rock types may contain significant amounts of clay minerals, which enhance material loss during water runoff. These two observations justify the derivation of specific phenomenological coefficients (N) and their application to carbonate rocks with similar textural and mineralogical features. The effect of porosity, which resulted unclear in the present research, will be also included in such a phenomenological coefficient. The analytical setup here presented can be also considered as a guideline to the determination of such phenomenological coefficients for carbonate rocks the textural features of which do not match those of the stones here considered. Furthermore, such rock types could be also exposed to different water compositions in order to better understand stone response to specific environmental conditions characteristic of a given area under study, and reliably predict future stone recession under those specific conditions.

Bibliography

Accardo G., Giani E., Giovagnoli A. (2003) The risk map of Italian Cultural Heritage. *J archit conserv*, **2,** 41-57.

Accardo G., Altieri A., Cacace C., Giani E., Giovagnoli A. (2002) Risk map: a project to aid decision-making in the protection, preservation and conservation of Italian Cultural Heritage. *Conservation science*, **849**, 44-49.

Al-kheder F., Al-shawabkeh Y., Haala N. (2009) Developing a documentation system for desert places in Jordan using 3D laser scanning and digital photogrammetry. *J Arch Sci*, **36**, 537-546.

Amoroso G. (1995) Il restauro della pietra nell'architettura monumentale. Ed. Flaccovio, Palermo.

Amoroso G. (2002) Trattato di scienza della conservazione dei monumenti. Etica della conservazione. Degrado dei monumenti. Interventi conservativi. Ed. Alinea, Firenze.

Amoroso G., Camaiti M. (1997) Scienza dei materiali e restauro. La pietra dalle mani degli artisti e degli artisti a quelle dei chimici macromolecolari. Ed. Alinea, Firenze.

Amoroso G., Fassina V. (1983) Stone decay and conservation. Ed. Elsevier, Amsterdam.

André M.F., Phalip B. (2010) Rates of stone recession on Mediaeval monuments: some thoughts and methodological perspectives. *Cadernos Laboratorio Xeolóxico de Laxe -Coruña*, **35**, 13-40.

Anselmetti F.S., Luthi S., Eberli, G.P. (1998) Quantitative characterization of carbonate porosity by digital image analysis. *AAPG Bulletin*, **82**, 1815-1836.

Arias P., Herráez J., Lorenzo H., Ordóñez C. (2005) Control of structural problems in cultural heritage monuments using ultra close-range photogrammetry and computer methods. *Computers & Structures*, **83**, 1754-1766.

Arnold A., Zehnder K. (1990). Salt weathering on monuments. In: The conservation of monuments in the Mediterranean Basin: the influence of coastal environment and salt spray on limestone and marble. Proceedings of the 1st International Symposium, Bari, 7-10 June 1989. Ed. Grafo, Bari, pp. 31-58.

Arroyo F., Villegas-Sánchez R. (2013) The church of Saint Martin (Trujillo, Spain): study of the stone degradation. *J Cult Herit*, **14S**, e109-e112.

Bacci P., Novo A., Viarengo S. (1990) Acid deposition in coastal zone. In: The conservation of monuments in the Mediterranean Basin: the influence of coastal environment and salt spray on limestone and marble. Proceedings of the 1st International Symposium, Bari, 7-10 June 1989. Ed. Grafo, Bari, pp. 365-368.

Baedecker, P. A. (1990) Effects of acidic deposition on materials.

Baedecker P.A., Reddy M.M. (1993) The Erosion of Carbonate Stone by Acid Rain. *J Chem Educ*, **70**, 2, 104-108.

Baer N. S., Berman S. M. (1983) Marble tombstone in national cemeteries as indicators of stone damage: general methods. *J Air Pollut. Control Assoc,* **83**.

Barazzetti L., Binda L., Scaioni M., Taranto P. (2011) Photogrammetric survey of complex geometry with low cost software: Application to the 'G1' temple in Myson Vietnam. *J Cult Herit*, **12**, 253-262.

Barazzetti L., Remondino F., Scaioni M. (2010) Orientation and 3-D modelling from markerless terrestrial images: Combining accuracy with automation. *Photogramm Rec*, **25-132**, 356–381.

Bassi D., Nebelsick J.H. (2010) Components, facies and ramps: redefining upper Oligocene shallow water carbonates using coralline red algae and large foraminifera (Venetian area, northeast Italy). *Palaeogeography, Palaeoclimatology, Palaeoecology*, **295**, 258-280.

Becka F. K., Al-Mukhtara M., Rozenbaum O., Rautureau M. (2003) Characterization, water transfer properties and deterioration in tuff: Building material in the Loire valley. *Build Environ*, **38**, 1151–1162.

Behlen A., Steiger M., Dannecker W. (2008) Deposition of sulphur dioxide to building stone: the influence of the ambient concentration on the deposition velocity. *Env Geol*, **56**, 595-608.

Bell A.B., Willis K.L., Lange D.A. (1999) Mercury intrusion porosimetry and image analysis of cement-based materials. *J. Colloid Interf Sci*, **211**, 39–44.

Benavente D., García del Cura M.A., Fort R., Ordóñez S. (1999) Thermodynamic modelling of changes induced by salt pressure crystallisation in porous media of stone. *J Cryst Growth*, **204**,168 - 78.

Benchiarin S. (2007) Carbonate lithotypes employed in historical monuments: quarry materials, deterioration and restoration treatments. PhDThesis, University of Padua.

Benchiarin S., Fassina V., Molin G. (2012) Assessment of conservation treatments on Paduan Nanto Stone monuments. In: Proceedings of the 12th Congress on the Deterioration and Conservation of Stone, New York. Unpublished, http://iscs.icomos.org/pdf-files/NewYorkConf/bencetal.pdf

Bernardi A., Todorov V., Hiristova J. (2000) Microclimatic analysis in St. Stephan church, Nessebar, Bulgaria, after interventions for the conservation of frescoes. *J Cult Herit*, **1**, 281-286.

Bonazza A., Sabbioni C., Messina P., Guaraldi C., De Nuntiis P. (2009a) Climate change impact: mapping thermal stress on Carrara marble in Europe. *Sci Tot Env*, **407**, 4506-4512.

Bonazza A., Messina P., Sabbioni C., Grossi C.M., Brimblecombe P. (2009b) Mapping the impact of climate change on surface recession of carbonate buildings in Europe. *Sci Tot Env*, **407**, 2039-2050.

Borghi A., Berra V., D'Atri A., Dino G.A., Gallo L.M., Giacobino E., Martire L., Massaro G., Vaggelli G., Bertok C., Castelli D., Costa E., Ferrando S., Groppo C., Rolfo F. (2015) Stone materials used for monumental building in the historical centre of Turin (NW Italy): architectonical survey and petrographical characterization of Via Roma. In: Pereira D., Marker B.R., Kramar S., Cooper B.J., Schouenborg B.E. (Eds) Global Heritage Stone: Towards International Recognition of Building and Ornamental Stone. *Geological Society London Special Publications*, **407**, 201-218.

Bosellini A., Mutti E. e Ricci Lucchi F. (1995) Rocce e successioni sedimentarie. Ed. UTET, Torino, pp. 94-109.

Bozonnet E., Belarbi R., Allard F. (2006) Modelling air flows around buildings in urban environment. International Workshop on Energy Performance and Environmental Quality of Buildings, July 2006, Milos, Grecia.

Bravo H.A., Soto R.A., Saavedra R.M.I., Torres R.J., Granada L.M.M., Sánchez P.A. (1998) Acid rain in Mexico case: Maya monuments. *Transations on Ecology and the Environments*, **21**, 661-674.

Brimblecombe P. (1987) The Big Smoke. Ed. Methuen, London.

Brimblecombe P. (1996) *Air composition and chemistry*. Cambridge University Press.

Brimblecombe P. (2011) Environment and architectural stone. In S. Siegesmund, R. Snethlage (Eds), Stone in architecture. Properties, durability (4th ed.). Ed. Springer, Berlin, pp. 317–346.

Brimblecombe P., Grossi C.M. (2005) Aesthetic thresholds and blackening of stone buildings. *Sci Tot Env*, **349**, 175-189.

Brimblecombe P., Grossi C.M., Harris I. (2006) Climate change critical to cultural heritage, Proceeding of the International HWC – Conference, 21-24 June 2006. Ed.CRC Press, Madrid.

Brimblecombe P., Grossi C.M. (2007) Damage to Buildings from Future Climate and Pollution. *APT Bulletin*, **38-2/3**, 13-18.

Brimblecombe P., Grossi C.M. (2008) Millennium long recession of limestones facades in London. *Env Geol*, **56 -3/4**, 463-471.

Brimblecombe P., Grossi C.M. (2009) Millennium long damage to building materials in London. *Sci Tot Env*, **407**, 1354 -1361.

Brimblecombe P., Grossi C.M. (2010) Potential Damage to Modern Building Materials from 21st Century Air Pollution. *Sci World J*, **10**, 116-125.

Bugini R., Folli L. (2014) The use of "Aurisina limestone" in the Roman architecture (Milan and Lombardy). VIII Congresso Nazionale di Archeometria, Scienze e Beni Culturali: stato dell'arte e prospettive, Bologna 5 - 7 Febbraio 2014.

Bugini R., Laurenzi Tabasso M., Realini M. (2000) Rate of formation of black crusts on marble. A case study. *J Cult Herit*, **1**, 111-116.

Butlin R.N., Coote A.T., Devenish M., Huhges I.S.C., Hutchens C.M., Irving I.G., Lloyd G.O., Massey S.W., Webb A.H., Yates T.I.S. (1992) Preliminary results from the analysis of stone tablets from the National Materials Exposure Programme (NMEP). *Atmos Environ*, **26B**, 189-198.

Camuffo D., Del Monte M., Sabbioni C., Vittori O. (1982) Wetting, deterioration and visual features of stone surfaces in urban area. *Atm Env*, **16**, 9, 2253-2259.

Camuffo D. (1984) Condensation-evaporation cycles in pore and capillary systems according to the Kelvin model. *Water, Air, & Soil Pollution*, **21-1**, 151-159.

Camuffo D. (1992) Acid Rain and Deterioration of Monuments: How Old Is the Phenomenon? *Atm Env*, **26B**, 241-247.

Camuffo D. (1995) Physical weathering of stones, *Sci Tot Env*, **167**, 1-14.

Camuffo D., Sturaro G., Valentino A., Gattolin M., Enzi S., and Bernardi A. (1996) Analisi del Microclima e delle interazioni ambiente-manufatto per la conservazione della Torre di Pisa. Report to Consorzio della Torre di Pisa, Pisa.

Camuffo D., Sturaro G. (2001) The climate of Rome and its action on monument decay. *Clim Res*, **16**, 145-155.

Caneva G., Nugari M.P., Salvadori O. (2005) La biologia vegetale per i beni culturali. Ed. Nardini, Firenze.

Candigliota E., Immordino F. (2013) Telerilevamento da droni per la salvaguardia del patrimonio storico-architettonico: conoscenza, monitoraggio, emergenza. Workshop L'ENEA per la sicurezza sismica del patrimonio storico architettonico. Studi, interventi, risultati. Salone dell'Arte del Restauro e della Conservazione dei Beni Culturali e Ambientali, Ferrara 21 marzo 2013.

Cantisani E., Pecchioni E., Fratini F., Garzonio C.A., Malesani P., Molli G. (2009) Thermal stress in the Apuan marbles: Relationship between microstructure and petrophysical characteristics. *Int J Rock Mech Min*, **46**, 128-137.

Cappellaro M., Dal Farra A., De Lorenzi Pezzolo A. (2012) DRIFT characterization of the "Soft Stone of the Berici Hills" and first results of a fast method for the classification of its main varieties through Multivariate Analysis. *Sciences at Ca' Foscari*, 46-59.

Cardell-Fernández, C., Vleugels, G., Torfs, K., & Van Grieken, R. (2002). The processes dominating Ca dissolution of limestone when exposed to ambient atmospheric conditions as determined by comparing dissolution models. *Env Geol*, **43-1,** 160-171.

Cardell C., Delalieux F., Roumpopoulos K., Moropoulou A., Auger F., Van Grieken R. (2003) Salt-induced decay in calcareous stone monuments and buildings in a marine environment in SW France. *Constr Build Mater*, **17**, 165-179.

Cardell C., Benavente D., Rodríguez – Gordillo J. (2008) Weathering of limestone building material by mixed sulfate solutions. Characterization of stone microstructure, reaction products and decay forms, *Mat Char*, **59**, 1371-1385.

Carmignani L., Giglia G., Klingfield R. (1978) Structural evolution of the Apuane Alps: an exampleof continental margin deformation. *J Geol,* **86,** 487-504.

Cattaneo, A., De Vecchi, G.P., Menegazzo Vitturi, L. (1976) Le pietre tenere dei Colli Berici. *Atti Mem Accad Patav Sci Lett Arti*, **88**, 69–100.

Chabas A., Jeannette D. (2001) Weathering of marbles and granites in marine environment: petrophysical properties and special role of atmospheric salts. *Environ Geol*, **40-3**, 359 –68.

Charlson R.J., Rodhe H. (1982) Factors controlling the acidity of natural rainwater. *Nature,* **295,** 683-685.

Charola A. E. (2000) Salts in the deterioration of porous materials: an overview. *Journal of the American institute for conservation*, **39-3,** 327-343.

Cheng R.J., Hwu J.R., Kim J.T., Leu S.M. (1987) Deterioration of marble structures. The role of acid rain. *Anal Chem,* **59,** 104A-106A.

Clerici A., Meda A. (2005) Confronto tra le caratteristiche meccaniche di diversi livelli di estrazione del Botticino Classico. *Giornale di Geologia Applicata*, **2**, 307-312.

Coletti C., Cultrone G., Maritan L., Mazzoli C. (2016) Combined multi-analytical approach for study of pore system in bricks: How much porosity is there? *Mat Char*, **121**, 82-92.

Comes R., Buna Z., Badiu I. (2014) Creation and preservation of digital cultural heritage. *J Ancient History and Archeology*, **1-2**, 50-56.

Corvo F., Reyes J., Valdes C., Villaseñor F., Cuesta O., Aguilar D., Quintana P. (2010) Influence of air pollution and humidity on limestone materials degradation in historical buildings located in cities under tropical coastal climates. *Water, air, and soil pollution*, **205,** 359.

Cooke R.U. (1989) Geomorphological contribution to acid rain research: studies of stone weathering. *Geogr J*, **155**, 361-366.

Cooke R.U., Inkpen R.J., Wiggs G.F.S. (1995) Using gravestones to asses changing rates of weathering in the United Kingdom. *Earth Surf Process Landf,* **6,** 531-546.

Cornale P., Rosanò P. Eds. (1994) Le pietre tenere del vicentino: uso e restauro. Padova.

Cnudde V., Boone M.N. (2013) High-resolution X-ray computed tomography in geosciences: a review of the current technology and applications. *Earth-Sci Rev*, **123**, 1–17.

Cnudde V., Cwirzen A., Masschaele B., Jacobs P.J.S. (2009) Porosity and microstructure characterization of building stones and concretes. *Eng Geol*, **103**, 76–83.

Crawford E.C., Mortensen J.K. (2009) An ImageJ plugin for the rapid morphological characterization of separated particles and an initial application to placer gold analysis. *Computat Geosci*, **35**, 347–359.

Crnković B., Jovičić D. (1993) Dimension stone deposits in Croatia. *Rudarsko-geološko-naftni zbornik*, **5**, 139-163.

Cucchi F., Pirini Radrizzani C., Pugliese N. (1987) The carbonete stratigraphic sequence of the Karst of Trieste (Italy). *Memorie Società Geologica Italiana,* **40,** 35-44.

Cueto N., Benavente D., Martínez-Martínez J., García-del-Cura M.A. (2009) Rock fabric, pore geometry and mineralogy effects on water transport in fractured dolostones. *Eng Geol,* **107**, 1–15.

Dal Bianco B., Bertoncello R., Bouquillon A., Dran J., Milanese R., Roehrs S., Sada C., Salomon J., Voltolina S. (2008) Investigation on sol-gel silica coatings for the protection of ancient glass: interaction with glass surface and protection efficiency. *J Non-Cryst Solids*, **354**, 2983-2992.

Dal Sasso G., Maritan L., Salvatori S., Mazzoli C., Artioli G. (2014) Discriminating pottery production by image analysis: a case of Mesolithic and Neolithic pottery from Al Khiday (Khartoum, Sudan). *J Archaeol Sci*, **46**, 125-143.

De Kock T., Turmel A., Fronteau G., Cnudde V. (2017) Rock fabric heterogeinity and its influence on the petrophysical properties of a building limestone: Lede stone (Belgium) as an example. *Eng Geol*, **217**, 31-41

De La Fuente D., Vega J.M., Viejo F., Díaz I., Morcillo M. (2013) Mapping air pollution effects on atmospheric degradation of cultural heritage. *J Cult Herit*, **14**, 138-14.

De Quervain F. (1967) Technische Gesteinskunde. Lehrbücher und Monographien aus dem Gebiete der exakten Wissenschaften. *Mineralogisch-geotechnische Reihe*, **12**, 43-54.

Delalieux F., Cardell C., Todorov V., Vesselin D., Van Grieken R. (2001) Environmental conditions controlling the chemical weathering of the Madara Horseman monument, NE Bulgaria. *J Cult Herit*, **2**, 43-54.

Delalieux, F., Cardell-Fernandez, C., Torfs, K., Vleugels, G., & Van Grieken, R. (2002) Damage functions and mechanism equations derived from limestone weathering in field exposure. *Water, Air, & Soil Pollution*, **139-1,** 75-94.

Di Benedetto C., Cappelletti P., Favaro M., Graziano S.F., Langella A., Calcaterra D., Colella A. (2015) Porosity as key factor in the durability of two historical building stones: Neapolitan Yellow Tuff and Vicenza Stone. *Eng Geol*, **193**, 310-319.

Dikaiakos J. G., Tsitouris C. G., Siskos P. A., Melissos D. A., Nastos, P. (1990) Rainwater composition in Athens, Greece. *Atm Env B. Urban Atmosphere*, **24-1,** 171-176.

Doehne E. (2002) Salt weathering: a selective review. *Geological society, London, special publications*, **205-1**, 51-64.

Dolske, D. A. (1995) Deposition of atmospheric pollutants to monuments, statues, and buildings. *Sci Tot Env*, **167(1-3),** 15-31.

Dragovich D. (1981) Weathering rates on marble tombstones at a Sydney cemetery. Institute for the Rate of decay of marble in laboratory and autdoor exposure. *J Mater Civil Eng,* **1-2,** 73-85.

Dragovich D. (1987) Measuring stone wheathering in cities: surface reduction on marble monuments. *Environ Geol Water S,* **9,** 139-142.

Dragovich D. (1991) Marble weathering in an Industrial Environment, Eastern Australia, *Environ Geol Water S*, **17 -2**, 127-132.

Dubelaar C. W., Engering S., Van Hees R. P. J., Lorenz H. G., Koch R. (2003). Lithofacies and petrophysical properties of Portland Base Bed and Portland Whit Bed limestone as related to durability. *Heron,* **48-3**, 221-229.

Dubinin M. M. (1979) Characterization of porous solids. *Society of Chemical Industry, London*, **1**.

Dunham, R. J. (1962) Classification of carbonate rocks according to depositional textures.

Esbert R.M., Díaz – Pache F., Grossi C.M., Alonso F.J., Ordaz J. (2001) Airborne particulate matter around the Cathedral of burgos (Castilla y León, Spain). *Atm Env*, **35**, 441-452.

Fassina V. (1983) L'ossidazione dell'SO_2 in atmosfera e la formazione delle croste sulle superfici lapidee. Atti del Convegno "Le piogge acide", Milano 16 apr. 1983. Ed. Franco Angeli, Milano, pp.116-133.

Fassina V., Cherido M. (1985) The Nanto stone deterioration and restoration of Loggia Cornaro in Padova. In: Preprints of the Vth Int. Congr. Deterioration and Conservation of Stone, Lausanne, pp. 313-324.

Fassina V. (1987) Influenza dell'inquinamento atmosferico sui processi di degrado dei materiali lapidei. *Bollettino d'Arte*, **41**, 19-47.

Fassina V. (1988) Environmental pollution in relation to stone decay. *Durability Build Mat*, **5**, 317-368.

Fassina V., Favaro M., Naccari A. (2002) Principal decay patterns on Venetian monuments. *Geol Soc London, Special Publications*, **205**, 381-391.

Feddema J., Meierding T. (1987) Marble weathering and air pollution in Philadelphia. *Atmos Environ,* **21-1,** 143-157.

Fitzner B., Basten D. (1994) Gesteinsporosität—Klassifizierung, meßtechnische Erfassung und Bewertung ihrer Verwitterungsrelevanz—Jahresberichte aus dem Forschungsprogramm ‘‘Steinzerfall-Steinkonservierung’’ 1992, Förderprojekt des Bundesministers für Forschung und Technologie. Verlag Ernst & Sohn, Berlin.

Folk, R.L. (1959) Practical petrographic classification of limestones. *AAPG BULL*, **43**, 1-38.

Fusi N., Martinez-Martinez J. (2013) Mercury porosimetry as a tool for improving quality of micro-CT images in low porosity carbonate rocks. *Eng Geol*, **166**, 272-282

Galan, E. (1990) Carbonate rocks; alteration and control of stone quality: some consideration. In: In: The conservation of monuments in the Mediterranean Basin: the influence of coastal environment and salt spray on limestone and marble. Proceedings of the 1st International Symposium, Bari, 7-10 June 1989. Ed. Grafo, Bari, pp. 249–254.

Galaup S., Liu Y., Cerepi A. (2012) New integrated 2D–3D physical method to evaluate the porosity and microstructure of carbonate and dolomite porous systems. *Micropor Mesopor Mat*, **154**, 175-186.

Garcia-del-Cura M.A., Benavente D., Martínez-Martínez J., Cueto N. (2011) Sedimentary structures and physical properties in travertine building stone. *Constr Build Mater*, **28**, 456-467.

Gauri K.L., Popli R., Sarma A.C. (1983) Effect of relative humidity and grain size on the reaction rates of marble at high concentrations of SO_2. *Durability Build Mat,* **1,** 209-216.

Gauri K.L., Kulshreshtha N.P., Punuru A.R., Chowdhury A.N. (1989) Rate of decayof marble in laboratory and outdoor exposure. *J Mater Civil Eng,* **1-2,** 73-85.

Geometrante R., Almesberger D., Rizzo A. (?) Characterization of the State of compression of Pietra d’Istria elements by non destructive ultrasonic technique http://www.ndt.net/article/wcndt00/papers/idn173/idn173.htm

Germinario L., Andriani G.F., Laviano R. (2015) Decay of calcareous building stone under the combined action of thermoclastism and cryoclastism: A laboratory simulation. *Constr Build Mater*, **75**, 385-394.

Giesche H. (2006) Mercury porosimetry: a general (practical) overview. *Part Syst Charact*, **23**, 9-19.

Ginevra M., Saralli M., Sedea R. (1999) Il bacino estrattivo dei Colli Berici. Assessorato alle politiche per l'ambiente, Regione del Veneto, Giunta Regionale; Quaderno n°1, Venezia.

Gislason S.R., Oelkers E.H., Eiriksdottir E.S., Kardjilov M.I., Gisladottir G., Sigfusson B., Snorrason A., Elefsen S., Hardardottir J., Torssander P., Oskarsson (2009) Direct evidence of the feedback between climate and weathering. *Earth Planet Sc Lett*, **277**, 213-222.

Giugliano M., Lonati G., Butelli P., Romele L., Tardivo R., Grosso M. (2005) Fine particulate (PM2.5–PM1) at urban sites with different traffic exposure. *Atm Env*, **39**, 2421–2431.

Godden, M. (2015). Portland's Quarries and its Stone.

Gomes L., Bellon R. P., Silva L. (2014) 3D reconstruction methods for digital preservation of cultural heritage. *Journal of Pattern Recognition letters.*

Govindaraju K. (1994) Compilation of working values and sample description for 383 geostandards. *Geostandards Newsletter*, **18** (Special Issue), 1-158.

Grandi, F. Z., Szpyrkowicz, L. (1991). Sampling and analysis of rain: methods and results of the Venice regional network. *Fresenius' journal of analytical chemistry*, **341-10,** 625-630.

Gregg S. J., Sing K. S. (1983) Adsorption, surface area, and porosity.

Groen J.C., Peffer L.A.A., Pérez-Ramírez J. (2003) Pore size determination inmodified microand mesoporous materials. Pitfalls and limitations in gas adsorption data analysis. *Micropor Mesopor Mater*, **60**, 1–17.

Grossi C.M., Brimblecombe P., Bonazza A., Sabbioni C., Zamagni J. (2006) Sulfate and carbon compounds in black crusts from the Cathedral of Milan and Tower of London. In: Proceedings of the International HWC – Conference, 21-24 June 2006. Ed.CRC Press, Madrid.

Grossi C.M., Brimblecombe P., Harris I. (2007) Predicting long term freeze-thaw risks on Europe built heritage and archaeological sites in a changing climate. *Sci Tot Env*, **377**, 273-281.

Grossi C.M., Bonazza A., Brimblecomble P., Harris I., Sabbioni C. (2008) Predicting twenty-first century recession of architectural limestone in European cities. *Env Geol*, **56**, 455-461.

Grossi C.M., Esbert R.M., Díaz Pache F., Alonso F.J. (2003) Soiling of building stones in urban environments. *Build Environ*, **38**, 147-159.

Grove C., Jerram D.J. (2011) jPOR: an ImageJ macro to quantify total optical porosity from blue-stained thin sections. *Computat Geosci*, **37**, 1850–1859.

Gruen A. (1985) Adaptative least squares correlations: a powerful matching techniques. *S Afr J Photogram Rem Sens Cartogr*, **14-3**, 175–187.

Gruen A., Baltsavias E. (1988) Geometrically constrained multiphoto matching. *Photogram Eng Rem Sens*, **54-5,** 633–641.

Guiamet P., Crespo M., Lavin P., Ponce B., Gaylarde C., Gómez de Saravia S. (2013) Biodeterioration of funeral sculpture in La Recoleta Cemetery, Buenos Aires, Argentina: Pre and Post-intervention studies. *Colloid Surface B*, **101**, 337-342.

Hällström J., Barup K., Grönlund R., Johansson A., Svanberg S., Palombi L., Lognoli D., Raimondi V., Cecchi G., Conti C. (2009) Documentation of soiled and biodeteriorated facades: a case study on the Coliseum, Rome, using hyperspectral imaging fluorescence lidars. *J Cult Herit*, **10**, 106-115.

Honeyborne D. B., Price, C. A. (1977) Air pollution and the decay of limestone. *BRE note*, **117**.

Inkpen R.J. (2013) Reconstructing past atmospheric pollution levels using gravestone erosion rates. *Area*, **45-3**, 321-329.

Inkpen R.J., Jackson J. (2000) Contrasting weathering rates in coastal, urban and rural areas in Southern Britain: preliminary investigation using gravestones. *Earth Surf Proc Land*, **25**, 229-238.

Inkpen R.J., Viles H., Moses C., Baily B. (2012a) - Modelling the impact of changing atmospheric pollution levels on limestone erosion rates in central London, 1980-2010. *Atm Env*, **61**, 476-481.

Inkpen R.J., Viles H., Moses C., Baily B., Collier C., Trudgill S.T., Cooke R.U. (2012b) Thirty years of erosion and declining atmospheric pollution at St Paul's Cathedral, London. *Atm Env*, **62**, 521-529.

Jenkins H.C. (1974) Origin of red nodular limestones (Ammonitico Rosso, Knollenkalke) in the Mediterranean Jurassic: a diagenetic model. *Spec Publ Int Assoc Sediment*, **1**, 249-271.

Johns T.C., Gregory J.M., Ingram W.J., Johnson C.E., Jones A., Lowe J.A., Mitchell J.F.B., Roberts D.L., Sexton D.M.H., Stevenson D.S., Tett S.F.B., Woodage M.J. (2003) Anthropogenic climate change for 1860 to 2100 simulated with the HadCM3 model under updated emissions scenarios. *Clim Dynam*, **20**, 583–612.

Klopfer H. (1985) Feuchte. In: Lutz P., Jenisch R., Klopfer H. et al (E ds) Lehrbuch der Bauphysik. Ed. Teubner, Stuttgart.

Kodikara J., Barbour S.L., Fredlund D.G. (1999) Changes in clay structure and behavior due to wetting and drying. In: 8th Australian-New Zealand conference on geomechanics, Australian Geomechanics, Hobart.

Köppen W (1936) Das geographische System der Klimate. In:Köppen W, Geiger R (eds) Handbuch der Klimatologie.Ed. Gebrüder Borntraeger, Berlin, pp.1−44.

Kucera V., Fitz S. (1995) Direct and indiect air pollution effects on materials including cultural monuments. *Water Air Soil Poll,* **85,** 153-165.

Kucera V., Tidblad J., Kreislova K., Knotkova D, Faller M., Reiss R., Snethlage R., Yates T., Henriksen J., Schreiner M., Melcher M., Ferm M., Lefèvre R.-A., Kobus J. (2007) UN/ECE ICP Materials Dose-response functions for the multi pollutant situation, Acid Rain – Deposition to Recovery, 249-258.

Lal Gauri K., Holdren Jr. G.C. (1981) Pollutant effects on stone monuments. *Env Sci Tech*, 386-390.

Lan T. T. N., Thoa N. T. P., Nishimura R., Tsujino Y., Yokoi M., Maeda Y. (2005) New model for the sulfation of marble by dry deposition Sheltered marble—the indicator of air pollution by sulfur dioxide. *Atm Env*, **39-5,** 913-920.

Lazzarini L., Laurenzi Tabasso M. (1986) Il restauro della pietra. Ed. CEDAM, Padova.

Lazzarini L. (2012) Pietra d'Istria: quarries, characterization, deterioration of the stone of Venice. In: Proceedings of the 12th Congress on the Deterioration and Conservation of Stone, New York. Unpublished, http://iscs.icomos.org/pdf-files/NewYorkConf/lazzarin.pdf

Laurenzi Tabasso M., Marabelli M. (1992) II degrado dei monumenti in Roma in rapporto all'inquinamento atmosferico. Ed. Betagamma, Viterbo.

Lefèvre R.A., Sabbioni C. Eds. (2010) Climate change and cultural Heritage, Proceedings of the Ravello International Workshop 14-16 maggio 2009 and Strasbourg European Master – Doctorate Course 7-11 Settembre 2009. Ed. Edipuglia, Bari.

León y León C.A. (1998) New perspectives in mercury porosimetry. *Adv Colloid Interfac*, **76**, 341-372, http://dx.doi.org/10.1016/S0001-8686(98)00052-9.

Lipfert F.W. (1989) Atmospheric damage to calcareous stones: comparison and reconciliation of recent experimental findings. *Atm Env*, **23 – 2**, 415-429.

Lisci M., Monte M., Pacini E. (2003). Lichens and higher plants on stone: a review. *International Biodeterioration & Biodegradation*, **51-1,** 1-17.

Livingston R.A., Baer N.S. (1990) Use of tombstones in investigation of deterioration of stone monument. *Environ Geol Water S,* **16-1,** 83-90.

Lonati G., Giugliano M., Butelli P., Romele L., Tardivo R. (2005) Major chemical components of PM2.5 in Milan (Italy). *Atm Env*, **39**, 1925–1934.

Lowell R. P., Germanovich L. N. (2004) Hydrothermal processes at mid-ocean ridges: Results from scale analysis and single-pass models. *Mid-Ocean Ridges*, 219-244.

Lu G., Lu G.Q.M., Xiao Z.M. (1999) Mechanical properties of porous materials. *J Porous Mat*, **6**, 359–368.

Lu P.Z., Lannutti J.J., Klobes P., Meyer K. (2000) X-ray computed tomography and mercury porosimetry for evaluation of density evolution and porosity distribution. *J Am Ceram Soc,* **83**, 518-522.

Luhmann T., Robson S., Kyle S., Harley I. (2006) Close Range Photogrammetry, Principles Methods and Applications. Ed. Whittles Publishing, Caithness.

Lundberg J., Ginés A. (2009) Rillenkarren.

Manganelli del Fà C. (2002) La porosità nei materiali lapidei naturali e artificiali.

Marchesini B., Biscontin G., Frascati S. (1972) Alterazione delle pietre tenere dei colli Berici. Atti XXVI Congresso A.T.I., Roma, 1–23.

Marquardt W., Brüggemann E., Auel R., Herrmann H., Möller D. (2001) Trends of pollution in rain over East Germany caused by changing emissions. *Tellus*, **53B**, 529-545.

Martínez-Martínez J., Benavente D., Gomez-Heras M., Marco-Castaño L., Ángeles García-del-Cura M. (2013) Non-linear decay of building stones during freeze thaw weathering processes. *Constr Build Mater*, **38**, 443-454.

Martire L. (1996). Stratigraphy, facies and synsedimentary tectonics in the Jurassic Rosso Ammonitico Veronese (Altopiano di Asiago, NE Italy). *Facies*, **35-1**, 209.

Martire L., Clari P., Lozar F., Pavia G. (2006) The Rosso Ammonitico Veronese (Middle-Upper Jurassic of the Trento Plateau): a proposal of lithostratigraphic ordering and formalization. *Riv Ital Paleontol S,* **112,** 227-250.

Massari F., Medizza F., Sedea R. (1976) L'evoluzione geologica dell'area euganea tra il Giurese superiore e l'Oligocene inferiore. *Mem Ist Geol Min Univ Padova*, **30**, 174-197.

Matthias G. (1967) Wheathering rates of Portland Arkose tombstones. *J Geol Educ,* **15,** 140-144.

Matteucci R., Russo A. (2005) The Middle Eocene siliceous sponges from Val di Chiampo (Lessini Mountains, northern Italy). *Annali dell'Università di Ferrara Mus Sci Nat*, special Volume.

McGee E. S., Mossotti, V. G. (1992) Gypsum accumulation on carbonate stone. *Atm Env B. Urban Atmosphere*, **26-2**, 249-253.

Meccheri M., Molli G., Conti P., Blasi P., Vaselli L. (2007) Carrara marble (Alpi Apuane, Italy): a geological and economical updated review. *Z Dtsch Ges Geowiss,* **158,** 719-735.

Meierding T.C. (1981) Marble tombstone weathering rates: a transect of the United States. *Phys Geogr*, **2-1**, 1-18.

Melo M.J., Bracci S., Camaiti M., Chiantore O., Piacenti P. (1999) Photodegradation of acrylic resins used in the conservation of stone. *Polym degrad Stabil*, **66**, 23-30.

Meloni P., Isola D., Carcangiu G., Bonazza A., Selbmann, Zucconi L., Manca F., Faedda R., Cocco O., Toreno G., Murru A. (2012) Weathering e vulnerabilità di materiali lapidei in contesti urbani: il cimitero storico di Cagliari. Atti del XXVIII Convegno Scienza e Beni Culturali, Ed. Arcadia Ricerche, Venezia.

Mietto P. (1988). Aspetti geologici dei Monti Berici. In "I Colli Berici-Natura e Civiltà". Ed Signum, Vicenza, pp.13-23.

Moro F., Böhni H. (2002) Ink-Bottle Effect in Mercury Intrusion Porosimetry of Cement-Based Materials. *J Colloid Interf Sci*, **246**, 135-149.

Moropoulou A., Theoulakis P., Chrysophakis T. (1995) Correlation between stone weathering and environmental factors in marine atmosphere. *Atm Env*, **29-8**, 895-903.

Moses C.A. (1996) Methods for assessing stone decay mechanisms in polluted and 'clean' environments, Northern Ireland. In: B.J. Smith, P.A. Warke (Eds), Processes of Urban Stone Decay, Ed. Donhead, 212–227.

MULTI-ASSESS (2007) Model for Multi-pollutant impact and Assessment of Threshold Levels for Cultural Heritage. Deliverable 02.

Mutlutürk M., Altindag R., Türk G. (2004) A decay function model for the integrity loss of rock when subjected to recurrent cycles of freezing – thawing and heating – cooling. *Int J Rock Mech Min*, **41**, 237-244.

Navarro C.R., Doehene E. (1999) Salt waethering: influence of evaporation rate, supersaturation and crystallization pattern. *Earth Surf Proc Land*, **24**, 191-209.

Nicholson D.T. (2001) Pore properties as indicators of breakdown mechanism in experimentally weathered limestones. *Earth Surf Proc Land*, **26**, 819-838.

O'Brien P.F., Bell E., Orr T.L.L., Cooper T.P. (1995) Stone loss rates at sites around Europe. *Sci Total Environ,* **167,** 111-121.

Olson R.A., Neubauer C.M., Jennings H.M. (1997) Damage to the pore structure of hardened portland cement paste by mercury intrusion. *J Am Ceram Soc*, **80**, 2454-2458.

O' Sullivan D.A. (1985) European concern abaut acid rain is growing. *Chem Eng News,* **63,** 12-18.

Ozga I., Bonazza A., Ait Lyazibi S., Haddab M., Ben-Ncer A., Ghedini N., Sabbioni C. (2013) Pollution impact on the ancient ramparts of the Moroccan city Sale. *J Cult Herit*, **14S**, S25-S33.

Panettiere P., Cortecci G., Dinelli E., Bencini A., Guidi M. (2000) Chemistry and sulfur isotopic composition of precipitation at Bologna, Italy. *App Geoch*, **15**, 1455-1467.

Pavlidis G., Koutsoudis A., Arnaoutoglou F., Tsioukas V., Chamzas C. (2007) Methods for 3D digitization of cultural heritage. *J Cult Herit*, **8**, 93–98.

Pel L., Huinink H., Kopinga K., Van Hees R.P.J., Adan O.C.G. (2004) Efflorescence pathway diagram: understanding salt weathering. *Constr Build Materials*, **18**, 309-313.

Pirard R., Alié C., Pirard J. (2002) Characterization of porous texture of hyperporous materials by mercury porosimetry using densification equation. *Powder Technol*, **128**, Issue 2, 242-247,

Pivko D. (2003) Natural stone in Earth's History. *Acta Geologica Universitatis Comenianae*, **58**, 73-86.

Pomerantz A., Sigmund E., Song Y.Q. (2007) Spatial heterogeinity lenght scales in carbonate rocks, *Appl Magn Reson*, **32**, 221.

Ponziani D., Ferrero E., Apollonia L., Migliorini S. (2012) Effect of temperature and humidity excursions and wind exposure on the arch of Augustus in Aosta. *J Cult Herit*, **13**, 462-468.

Pope G.A., Meierding T.C., Paradise T.R. (2002) Geomorphology's role in the study of weathering of cultural stone. *Geomorphology*, **47,** 211-225.

Rahn P.H. (1971) The weathering of tombstones and its relationship to the topography of New England. *J Geol Educ,* **19,** 112-118.

Reddy M.M. (1988) Acid rain damage to carbonate stone: A quantitative assesment based on the

aqueous geochemistry of rainfall runoff from stone. *Earth Surf Processes*, **13,** 335-354.

Reddy S.M., Roberts S.M. (2005) Surface-recession weathering of marble tombstones: new field data and constraints. *GSA*, **390**, 27-37.

Reddy M.M., Sherwood S., Doe B. (1985) Limestone and marble dissolution by acid rain. 5th Int Congress on Conservation and Deterioration of Stone, Lausanne, 517-526.

Reis S., Grennfelt P., Klimont Z., Amann M., ApSimon H., Hettelingh J. P., ... & Spranger, T. (2012). From acid rain to climate change. *Science*, **338,** 1153-1154.

Remondino F., El-Hakim S. (2006) Image-based 3-D modelling: a review. *Photogram Rec,* **21-115**, 269–291.

Remondino F., Fraser C. (2006) Digital cameras calibration methods: considerations and comparisons. Int. Arch. Photogram. Rem. Sens. Spat. Inf. Sci. **36-53**, 266–272.

Remondino F., Girardi S., Rizzi A., Gonzo L. (2009) 3DModeling of complex and detailed Cultural Heritage using multi-resolution data. *ACM J Comput Cultur Herit*, **2-1**, 20.

Remondino F., Spera M.G., Nocerino E., Menna F., Nex F., Barsanti S.G. (2013) Dense image matching: comparisons and analyses. *Digit Herit Int Congress,* **1**, 47–54.

Rijniers L.A., Pel L., Huinink H.P., Kopinga K. (2005) Salt crystallization as damage mechanism in porous building materials – a nuclear magnetic resonance study. *Magn Reson Imaging*, **23**, 273-276.

Roberts S.M. (2005) Surface-recession weathering of marble tombstones: new field data and constraints. *GSA*, **390**, 27-37.

Rodriguez-Navarro C., Doehne E. (1999) Salt weathering: influence of evaporation rate, supersaturation and crystallization pattern. *Earth Surf Proc Land*, **24**, 191-209.

Rodriguez-Navarro C., Hansen E., Sebastian E., Ginell W. S. (1997) The role of clays in the decay of ancient Egyptian limestone sculptures. *J Am Inst Conserv*, **36**, 151–63.

Rodríguez-Navarro C., Sebastián E. (1994) Técnicas de análisis del sistema poroso de materiales pétreos ornamentales: usos y limitaciones. *Ingeniería Civil*, **96**, 130–142.

Rozenbaum O. (2011) 3-D characterization of weathered building limestones by high resolution synchrotron X-ray microtomograph. *Sci Total Environ*, **409**, 1959–1966.

Rodolico F. (1953) Le pietre delle città d'Italia. Ed. Le Monnier, Firenze.

Rogora M., Mosello R., Marchetto A. (2004) Long-terms trends in the chemistry of atmospheric deposition in Northwestern Italy: the role of increasing Saharian dust deposition. *Tellus*, **56B,** 426-434.

Rossi-Manaresi R., Tucci A. (1991) Pore structure and the disruptive or cementing effect of salt crystallisation in various types of stone. *Stud Conserv*, **36**, 53-58.

Ruedrich J., Siegesmund S. (2007). Salt and ice crystallization in porous sandstones. *Env Geol*, **52-2**, 225-249.

Ruedrich J., Kirchner D., Siegesmund S. (2011). Physical weathering of building stones induced by freeze–thaw action: a laboratory long-term study. *Environmental Earth Sciences*, **63**, 1573-1586.

Sabbioni C. (1995) Contribution of atmospheric deposition to the formation of damage layers. *Sci Tot Env*, **167**, 49-55.

Sabbioni C., Brimblecombe P., Bonazza A., Grossi C.M., Harris I., Messina P. (2006a) Mapping climate change and cultural heritage. In: Proceedings of the 7th EU Conference Sauveur, 31st May-3rd June, Praga.

Sabbioni C., Cassar M., Brimblecombe P., Tidblad, Kozlowski R., Drdácký M., Saiz Jimenez C., Grøntoft T., Wainwright I., Ariño X. (2006b) Global climate change impact on built heritage and cultural landscapes. Proceedings of the International HWC – Conference, 21-24 June 2006, Ed.CRC Press, Madrid.

Sabbioni C., Cassar M., Brimblecombe P., Lefevre R.A. (2008) Vulnerability of cultural heritage to climate change. Report EU, AP/CAT.

Sabbioni C., Brimblecombe P., Cassar M. (Eds) (2010) The Atlas of Climate Change Impact on European Cultural Heritage. Ed. Anthem Press, London.

Salvini S., Sacchi B., Frediani P. (2012) Study of protectives obtained from natural resources for the conservation of stone. In: Proceedings Scienza e Beni Culturali Bressanone, 833-843.

Samara C., Tsitouridou R., Balafoutis C. (1992) Chemical composition of rain in Thessaloniki, Greece, in relation to meteorological conditions. *Atm Env B. Urban Atmosphere*, **26-3,** 359-367.

Sawdy A., Price C. (2005). Salt damage at Cleeve Abbey, England. Part II: seasonal variability of salt distribution and implications for sampling strategies. *Journal of cultural heritage*, **6-3,** 269-275.

Scherer G.W. (1999) Crystallization in pores. *Cem Concr Res,* **29**, 1347–1358.

Scherer G.W. (2004) Stress from crystallization of salt. *Cem Concr Res*, **34-9**, 1613–24.

Scherer G.W., Valenza J.J. (2004) Mechanisms of frost damage. In: Young F., Skalny J. (Eds) Materials science of concrete VII. The American Ceramic Society, Westerville, 209–246.

Schirolli P. (1997) La successione liassica nelle Prealpi Bresciane centro-occidentali (Alpi Meridionali, Italia): stratigrafia, evoluzione paleogeografico-strutturale ed eventi connessi al rifting. *Atti Ticinensi di Scienze della Terra. Serie Speciale*, **6**, 5-137

Searle D.E., Mitchell D.J. (2007) The effect of coal and diesel particulates on the weathering loss of Portland Limestone in an urban environment. *Sci Tot Envir*, **370**, 207-223.

Shushakova V., Fuller E.R. Jt, Siegesmund S. (2013) Microcracking in calcite and dolomite marble: microstructural influences and effects on properties. *Environ Earth Sci*, **69**, 1263-1279.

Siegesmund S., Snethlage R. (2014) Stone in Architecture. Ed. Springer, Berlin.

Šimunić Buršić M., Aljinović D., Cancelliere S. (2007) Kirmenjak – Pietra d'Istria: a preliminary investigation of its use in Venetian architectural heritage. *Geol Soc London Spec Publ*, **271**, 63-68.

Singh A., Agrawal M. (2007). Acid rain and its ecological consequences. *Journal of Environmental Biology*, **29-1,** 15.

Steiger M. (2005a) Crystal growth in porous materials I: the crystallization pressure of large crystals. *J Cryst Growth*, **282**, 455–469.

Steiger M (2005b) Crystal growth in porous materials II: influence of crystal size on the crystallization pressure. *J Cryst Growth*, **282**, 470–481.

Steiger M., Charola A.E. (2011) Weathering and deterioration, in S. Siegesmund, R. Snethlage (Eds.), Stone in architecture. Properties, durability (4th ed.). Ed. Springer, Berlin, pp. 227–316.

Sun W., Chen T., Chen C., Li J. (2007) A study on membrane morphology by digital image processing. *J Membrane Sci*, **305**, 93–102.

Tiano P. (2002) Biodegradation of Cultural Heritage: Decay mechanism and controls methods. Seminar article, New University of Lisbon, Department of Conservation and Restoration, 7-12.

Tiano P., Tapete D., Matteini M., Ceccaroni F. (2008) The microphotogrammetry: a new diagnostic tool for on-site monitoring of monumental surfaces. In: Proceedings International Workshop 'In situ Monitoring of Monumental Surfaces', 97-106.

Tidblad J., Kucera V., Mikhailov A.A., Henriksen J., Kreislova K., Yates T. (2001) UN ECE ICP materials: dose-response functions on dry and wet acid deposition effects over 8 years of exposure. *Water, Air, Soil Pollution*, **130**, 1457–1462.

Tidblad J. (2012) Atmospheric corrosion of metals in 2010-2039 and 2070-2099. *Atm Env*, **55**, 1-6.

Torfs K., Van Grieken R. (1997) Chemical relations between atmospheric aerosols, deposition and stone decay layers on historic buildings at the Mediterranean coast. *Atm Env*, **31**, 2179-92.

Török Á. (2003) Surface strength and mineralogy of weathering crusts on limestone buildings in Budapest. *Build Environ*, **38**, 1185-1192.

Trudgill S.T., Viles H.A., Inkpen R.J., Cooke R.U. (1989) Remeasurement of weathering rates, St Paul's Cathedral, London. *Earth Surface Proc Land*, **14**, 175-196.

Tsui N., Flatt R.J., Scherer G.W. (2003) Crystallization damage by sodium sulfate. *J Cult Herit*, 4, 109-115.

Tucci P., Morbidelli P. (2004) "Apulian marbles"of the Ostuni District (south-eastern Murge, Apulia, Italy). Identification and characterisation of ancient quarries for archaeometric purposes. *Period Mineral*, **73**, 123-140.

Tuğrul A. (2004) The effect of weathering on pore geometry and compressive strength of selected rock types from Turkey. *Eng Geol*, **75**, 215-227.

Urzì C., Brusetti L., Salamone P., Sorlini C., Stackebrandt E., Daffonchio D. (2001) Biodiversity of Geodermatophilaceae isolated from altered stones and monuments in the Mediterranean basin. *Environmental Microbiology*, **3-7,** 471-479.

Vacchiano C.D., Incarnato L., Scarfato P., Acierno D. (2008) Conservation of tuff-stone with polimeric resins. *Constr Build Mater*, **22**, 855-865.

Varotsos C., Tzanis C., Cracknell A. (2009) The enhanced deterioration of the cultural heritage monuments due to air pollution. *Env Sci Poll Res*, **16**, 590-2.

Viles H.A. (2002) Is stone decay chaotic? Reflections from studies of the limestone cultural heritage of Oxford, UK. *Geological Society of America Abstracts with programs,* **34-6,** 89.

Viles H.A. (2011) Microbial geomorphology: a neglected link between life and landscape. *Geomorphology*, **129**, 167-182.

Viles H.A., Naylor L.A., Carter N.E.A., Chaput D. (2008) Biogeomorphological disturbance regimes: progress in linking ecological and geomorphological systems. *Earth Surf Proc Landf*, **29**, 1473–1485.

Villegas-Sánchez R., Arroyo F. (2013) The cathedral of Jerez De La Frontera (Cádiz, Spain): stone degradation and conservation. *J Cult Herit*, **14S**, e113-e116.

Vocom J.E. (1979) Air pollution damage to buildings on the Acropolis. *J Air Pollut control Ass*, **29,** 333-338.

Wakefield R.D., Jones M.S. (1998) An introduction to stone colonizing micro-organisms and biodeterioration of building stone. *Q J Eng Geol*, **31**, 301-313.

Warscheid T., Braams J. (2000) Biodeterioration of stone: a review. *Int Biodeter Biodegr*, **46**, 343-368.

Webb A.H., Bawden R.J., Busby A.K., Hopkins J.N. (1992) Studies on the effects of air pollution on limestone degradation in Great Britain. *Atmos Environ,* **26B,** 165-181.

Weber, J. (1985). Natural and artificial weathering of Austrian building stones due to air pollution. In: Ve congres international sur l'alteration et la conservation de la pierre. Actes. Vth international congress on deterioration and conservation of stone. Proceedings, Lausanne, 25-27September 985. Ed. Presses polytechniques romandes, Lausanne, pp. 527-535.

Weiss S., Siegesmund S., Fuller E. R. Jr. (2002) Thermal tresses and microcracking in calcite and dolomite marbles via finite element modelling. *Geological Society London Special Publications*, **205**, 89-102

Winkler E.M. (1982) Decay of stone monuments & Buildings: the Role of Acid Rain. *Technology and Conservation*, 32-36.

Winkler E.M. (1987) Weathering and weathering rates of natural stone. *Environ Geol Water Sci*, **9**, 85–92.

Winkler, E. (2013) *Stone in architecture: properties, durability*. Ed. Springer Science & Business Media, London.

Yastikli N. (2007) Documentation of cultural heritage using digital photogrammetry and laser scanning. *J Cult Herit,* 8, 423-427.

Yerrapragada S.S., Chirra S.R., Haynes J.H., Li S., Bandyopadhyay J.K., Gauri K.L. (1996) Weathering rates of marble in laboratory and outdoor conditions. *J Environ Eng*, **122,** 856-863.

Zajieek O.T. (1985) Why isn't my rain as acidic as yours? *J Chem Educ,* **62,** 158-159.

Zanardini E., Abbruscato P., Ghedini N., Realini M., Sorlini C. (2000) Influence of atmospheric pollutants on the biodeterioration of stone. *Int Biodeter Biodegr*, **45,** 35-42.

Zhang P., Arre T.J., Ide-Ektessabi A. (2015) A line scan camera-based structure from motion for high-resolution3D reconstruction. *J Cult Herit*, **16**, 656-663.

Zehnder K., Arnold A. (1989) Crystal growth in salt efflorescence. *J Crystal Growth*, **97**,513–521.

Zendri E., Biscontin G., Kosmidis P. (2001). Effects of condensed water on limestone surfaces in a marine environment. *J Cult Herit*, **2-4**, 283-289.

Zezza F., Macrì F. (1995) Marine aerosol and stone decay. *Sci Tot Env*, **167**, 123-143.

Zdravkov B.D., Čermák J.J., Šefara M., Janků J. (2007) Pore classification in the characterization of porous materials: a perspective. *Cent Eur J Chem*, **5**, 385–395.

Zong Y., Yu X., Zhu M., Lu S. (2015) Characterizing soil pore structure using nitrogen adsorption, mercury intrusion porosimetry, and synchrotron-radiation-based X-ray computed microtomography techniques. *J Soils Sediments*,**15**, 302–312.

Acknowledgements

This thesis is dedicated to Laura, the sweetest teacher I've ever had, for teaching me independence and for turning speech therapy into a fantastic game. She was the first person to believe I would have done it. If I have achieved this goal it is also her merit.

I would like to express my special appreciation and thanks to:

My parents, who are my best confidence-boosters.

My grannies, who are always been my save fund for the leisure activities.

My dear friends widespread for Italy and the world especially Valentina, Martina, Elisa, Elettra, who in the last few weeks, have strongly supported me in the best possible way: midnight calls or food or psychiatric help or reading some drafts of this last effort.

Prof. Claudio Mazzoli who have been a good mentor for me and gave me this challenging opportunity and Prof. Matteo Massironi because of his encouragement and help.

My colleagues and all the DAB group, who shared with me this experience, and the people working in the Department of Geosciences in Padua.